By Architects. For Architects.
By Engineers. For Engineers.

Architecture
Civil and Structural Engineering
Mechanics of Materials
Building and Construction
Urban Planning and Development
Transportation Issues in Construction
Geotechnical Engineering and Engineering Geology
Designing, Operation and Service
of Construction Site Engines

# CONTENTS

# Architecture

## SUITABILITY OF REFERENCE STANDARDS TO INTEGRATE ERGONOMICS IN ARCHITECTURE: AN EMPIRICAL STUDY IN BANGLADESH

Sudipti Biswas

Military Institute of Science and Technology (MIST), Dhaka, Bangladesh

E-mail: sudipti.biswas@arch.mist.ac.bd

**Abstract**

**Introduction:** Buildings are a very important part of our lives because we spend so much time there. A primary job of an architect is to assure that the buildings we live in accommodate the human activities that take place within them. Therefore, anthropometric datasets are important tools for the architect. Unfortunately, anthropometric datasets relevant to the functions that take place in buildings are relatively scarce, even as part of the architect's academic experience. Architects mostly depend on a few reference standards that may not fit the local population. **The purpose of the research** described here is to contribute to the filling of this gap with an anthropometric dataset for the Bangladeshi population that can serve as a source of data in the field of architecture. **Methods:** Body measurements of 130 people, 66 male and 64 female, are taken at 38 different postures. The postures are selected from the reference standards and considering the local practice. Then the measurements are examined with descriptive statistics and compared with the reference standards to check the differences. **Results:** This comparison indicates that the Bangladeshi people are considerably smaller; therefore, the practiced reference standards are not appropriate for Bangladesh, and presumably South Asia. Further research is required for a comprehensive anthropometric database. The presented dataset can serve as a source of data for the design of residential and other buildings in Bangladesh as well as other South Asian countries.

**Keywords:** reference standard, anthropometry, body dimension, Bangladeshi population, architecture, ergonomics.

### Introduction

The need for consideration of human factors and ergonomics (HFE) in the design of built environment is obvious, as has been much discussed (Attaianese, 2012, 2014, 2022; Attaianese and Duca, 2012; Charytonowicz, 2000; Costa et al., 2012; Eilouti, 2021; Garneau and Parkinson, 2016; Hendrick, 2008; Olguntürk and Demirkan, 2009; Remijn, 2006). Scholars agree that integrating HFE into the design process of built environment can contribute to, among other things, sustainability (Attaianese, 2014, 2016, 2017; Attaianese and Duca, 2012; Hedge and Dorsey, 2013; Hedge et al., 2010; Radjiyev et al., 2015). Although the need is recognized, there is a relative scarcity of relevant research (Attaianese and Duca, 2012; Costa et al., 2012; Fross, 2014). There are few studies regarding HFE in the built environment, and those that have been done tend to focus on the healthcare sector (for example, Codinhoto et al., 2009; Pinto et al., 2000; Rogers et al., 2013; Springer, 2007; Villeneuve, 2000; Yeoman and Ashmore, 2018). Since good architecture accommodates different human functions expected in the built environment, thus, ergonomic considerations should logically be incorporated into every aspect of the design process. Designers do it sometimes consciously, sometimes intuitively (Fross, 2014; Fross et al., 2015). However, for effective integration of HFE into architecture, it is necessary for the architect to avail good data specific to the local context.

Despite the necessity of anthropometric database for local population, it does not always exist in reality. In the case of Bangladesh, the national building code (BNBC/MoHPW/GoB, 2021), the regulations for building construction in the Dhaka Metropolitan area (MoHPW/GoB 2008) as well as Dhaka Cantonment area (Cantonment Board, 2020) provide guidelines for building design that may contain some ergonomic considerations, although they are not explicitly mentioned. However, good architecture-relevant anthropometric data for Bangladesh simply do not exist.

The present research is an attempt to address this gap. This paper describes an anthropometric study for the Bangladeshi population aimed to determine the male and female body dimensions. Although the study covers only the Bangladeshi population, it is expected to be useful for the populations of other countries with similar anthropometric features.

*Anthropometric considerations for architecture*

Considerations for HFE in architecture differ somewhat from those of other disciplines, such as industrial design, in the way that architects must consider the space within which activities take place. For architecture, a very clear understanding of human activities for any given function is the starting point. Architectural design starts with a comprehensive understanding of human activities and the space requirements for those activities. Relevant information includes a wide range of attributes such as body dimensions, flexibility, working procedures, equipment to be used, furniture and fixtures, behavioral expectations, sensory abilities, environmental needs, etc. All these considerations require data on specific body dimensions at specific postures related to the activities to be performed. Different types of anthropometric dimensions are required to accommodate different types of human activities.

Integrating HFE into the built environment is not an easy task; it requires proper training. Usually, such training is introduced in architecture education. Scholars agree that teaching ergonomics in design school can improve performance, productivity, safety, and health in the built environment (Attaianese, 2012, 2016; Garneau and Parkinson, 2016; Olguntürk and Demirkan, 2009). The typical curriculum attempts to impart a clear understanding of ergonomic issues to the students at the early stage of the academic program. Topics covered include human activities, movements, postures, relevant body dimensions, etc. Through this training, the students can learn to generate space requirements and determine appropriate dimensions for the relevant furniture and fixtures and design the space in which the intended functions can be performed efficiently.

This study proposes that the HFE education of architects, as well as professional practice, would be enhanced if better data was available. Such data would logically include different dimensions of the human body at different postures (depending on the specific human activity) for different ages, genders, races, nationalities, etc. Although, a perfect design for the user is seldom, if ever, possible, proper considerations of relevant anthropometric data should be able to better ensure comfort and efficiency and avoid discomfort and inefficiency (Klamklay et al., 2008; Mokdad, 2002; Pentikis et al., 2002; Pheasant and Haslegrave, 2006; Sanders and McCormick, 1993).

*Anthropometric data in Bangladesh*

Unfortunately, in Bangladesh, no holistic dataset of anthropometric features is available, although several research projects have covered specific features. There are various studies on anthropometric characteristics relevant to the field of health and nutrition. A large portion of such research relates to malnutrition, particularly in women and children. Research topics that deal with anthropometric features of adults tend to involve maternal anthropometry (Karim and Mascie-Taylor, 1997; Nahar et al., 2007), nutrition (D'Souza and Tandon, 2019; Islam et al., 2004; Mitra et al., 2018; Sultana et al., 2015), age at menarche (Akter et al., 2012; Chowdhury et al., 2000; Hossain et al., 2010; Islam et al., 2017), menstrual health (Hossain et al., 2011b), hypertension (Ali et al., 2018; Choudhury et al., 2014; Chowdhury et al., 2016; Simmons et al., 2021, obesity (Bhowmik et al., 2013, 2014; Biswas et al., 2017; Flora et al., 2009; Ge et al., 2014; Hussain et al., 2013; Islam et al., 2020; Qureshi et al., 2017), diabetes (Asghar et al., 2007; Chowdhury et al., 2015; Fottrell et al., 2018; Islam et al., 2015; Siddiquee et al., 2015), and/or some other issues like gut microbiomes (Osborne et al., 2020), fatty liver diseases (Alam et al., 2014, 2019), etc. However, despite the plethora of studies in the health sector, there is a dearth of adult anthropometric data other than weight and body mass index (BMI) (Flora et al., 2009).

There are also studies that cover detailed dimensions of body parts: for example, the face of Garo women (Akhter et al., 2013), face height of Garo and non-Garo women (Tania et al., 2020), hand of Garo men and women (Asadujjaman et al., 2019), head of Garo women (Akhter et al., 2009), hand anthropometry of men (Imrhan et al., 2006, 2009), hand anthropometry of women (Razzaque et al., 2021), hand of both men and women (Hossain, 2015; Imrhan et al., 2009; Shahriar et al., 2020), various body parts of Santal men (Shah et al., 2015), arm span of Garo men and women (Hossain et al., 2011a), arm span of women (Laila et al., 2010a), forearm of women (Laila et al., 2010b), external ear anthropometry (Asadujjaman et al., 2019), upper limbs of Manipuri women (Hussain et al., 2019), etc. The limitations of these studies are that they only focus on specific body parts and/or specific tribal population in Bangladesh.

More complete studies of anthropometric features are rare. Khadem and Islam (2014) created a dataset with 37 dimensions of Bangladeshi men. Khan (2014) reported data on 37 dimensions for both men and women, and, in a recent study, Parvez et al. (2022a) prepared a dataset with 37 dimensions for male and female university students. These studies are relevant, however, more for industrial engineering and occupational therapy than for architecture. A few studies have also covered anthropometry in relation to furniture, such as classroom and library furniture (Hoque et al., 2014, Parvez et al., 2021, 2022b, 2022 c; Shah et al., 2013), hospital beds (Chakrabortty et al., 2014; Islam et al., 2013), vehicle seat (Hoque et al., 2017), etc. However, again, the relevance to architecture is limited.

In sum, the available studies are not of much use for architecture. As a consequence, the architecture schools tend to rely on a few reference standards for HFE

training (Biswas, 2022; Biswas et al., 2021) rather than robust datasets. What the available studies do indicate, though, is that anthropometric features of Bangladeshi people, such as stature, hand dimensions, and weight, are significantly different from the populations associated with published anthropometric datasets: they are generally somewhat smaller (Imrhan et al., 2009; Khadem and Islam, 2014; Parvez et al., 2022a; Shahriar et al., 2020). Therefore, blind application of reference design standards may result in inappropriate designs for Bangladesh.

## Method

The research involved taking a series of measurements of Bangladeshi men and women. The measurements were taken as a part of an academic exercise at the Department of Architecture, Military Institute of Science and Technology (MIST). The exercise was to design a small residential building. Therefore, only the measurements relevant for residential use were considered. All the participants participated in the survey voluntarily with informed consent. The exercise was approved by the academic wing of MIST.

### Participants

Measurements were taken from 130 individuals — 66 men and 64 women (Table 1). The age range was from 15 to 65 years, thus covering the range of working age population able to join the labor market. Convenience sampling fitted best to obtain the participants as it was conducted within an academic exercise. The age breakdown of participants is as follows.

### Selection of Body Dimensions

For space design, the first task is to know what body dimensions are to be considered for the activities performed and what furniture/fixtures are to be accommodated in that space. The furniture/fixtures are also related to the body dimensions at different postures. For this study, body dimensions were taken at standing, sitting in a chair, and sitting/crawling on the floor positions. The postures were selected based on the relevance for residential functions and on a review of three reference books that are commonly consulted in the practice and education of architecture. The books consulted are:

1. Time Saver Standards for Building Types (De Chiara and Callender, 1990);

2. Human Dimension & Interior Space: A Source Book of Design Reference Standards (Panero and Zelnik, 1979);

3. Architects' Data (Neufert and Neufert, 2012).

The study included 38 body dimensions that are very basic for space designing. 32 of them were derived from the reference books and 6 were added as relevant for the local context. The selected dimensions are presented in Figure. Although residential functions were the focus, the data is expected to be helpful for designing other spaces such as offices, small commercial spaces, etc.

### Data Analysis

Statistical analysis involved simple examination of the dataset through descriptive statistics. This included the mean, mode, range, standard deviation, coefficient of variation and selected percentiles. Mean values were compared with reference standards with $Z$-test and $t$-test.

For comparison, Human Dimension & Interior Space: A Source Book of Design Reference Standards (Panero and Zelnik, 1979), referred to as HD hereinafter, had preference because of its gender specific and elaborate data. Time Saver Standards for Building Types (De Chiara and Callender, 1990), referred to as TSS hereinafter, and Architects' Data (Neufert and Neufert, 2012), referred to as NAD hereinafter, mostly provide dimensions with gender-neutral figurative drawings, although NAD provides occasional gender identification in the illustrations (such as clothing, body shape, hair style, etc.).

### Limitations

This study has some limitations. The number of participants was relatively small, and it did not represent the South Asia or even Bangladesh. This study was conducted within the framework of an academic exercise in architecture education, and it was particularly oriented towards residential architecture in the local context. Additionally, state of the art measurement tools were not available for this study.

## Results and Discussion

The results are shown in Tables 2–7: both the measured dimensions and comparison to reference standards. Tables 2 and 3 provide mean, mode, range, standard deviation, reference standards and the difference between the mean and reference standard for men and women. Table 4 provides selected percentile values for both men and women. Tables 5 and 6 present comparison of different body dimensions with the reference standards and Table 7 shows comparison of different ratios with the reference standards.

A vital question is how the data reported here differs from that of reference standards. It is observed that all dimensions are smaller than the reference standards, with three exceptions — side width for women and hand length and vertical reach (standing) for men. However, these latter dimensions are slightly

Table 1. **Age distribution of the participants**

| Age (years) | 15–20 | 21–30 | 31–40 | 41–50 | 51–60 | 61–65 | Total |
|---|---|---|---|---|---|---|---|
| **Male** | 17 | 26 | 4 | 5 | 13 | 1 | 66 |
| **Female** | 10 | 20 | 8 | 13 | 10 | 3 | 64 |
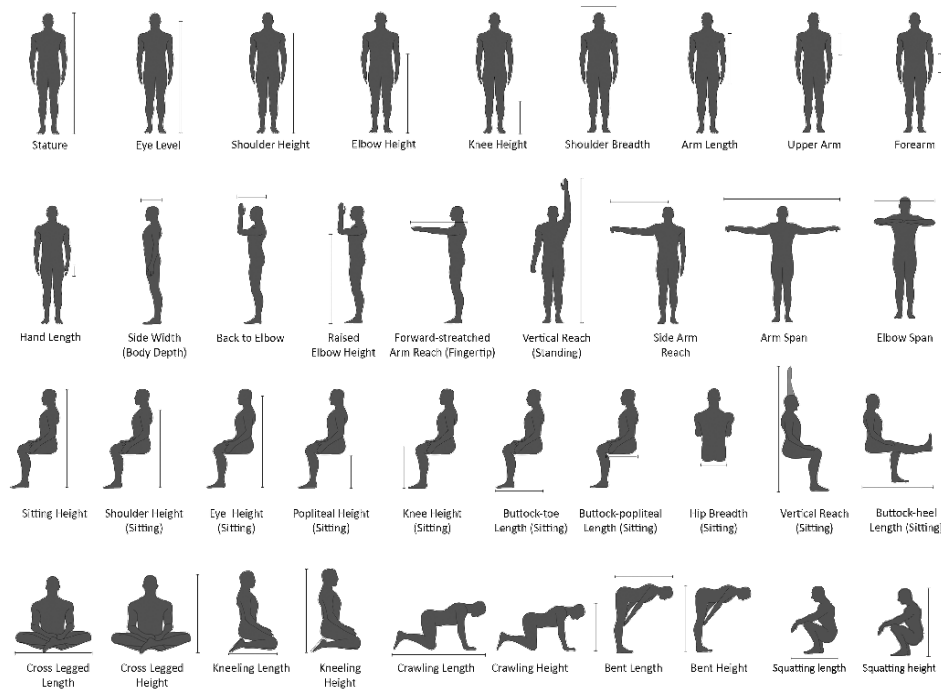
Anthropometric dimensions measured in the study

larger only when the reference is taken from the TSS as the unisex dimensions. In fact, unisex dimensions in references are generally smaller compared to the gender-specific dimensions for reasons that are not clear. The derived dataset suggests that the body dimensions are smaller than those of standard references, sometimes dramatically. Tables 5 and 6 show that most of the comparisons with reference values reach statistical significance.

The dataset is again compared with the reference standards with different ratios. Table 7 shows a comparison of all the derived dimensions and their ratios with stature and arm span for both men and women against the references. This shows that the body dimensions are considerably smaller than the reference values, $p$-value is 5.42654E-09 for men and 7.00667E-09 for women. The ratio comparison shows an interesting trend: stature ratio for men ($p$ = 0.6036852) and arm span ratio for women ($p$ = 0.07259) are strikingly similar, while stature ratio for women ($p$ = 0.02970065) and arm span ratio for men ($p$ = 0.0001983) are not that close. This may happen because proportions of different body parts may differ for different races and ethnic groups (Akhter et al., 2013; Goel and Tashakkori, 2015; Hovinga and Lerner, 2009; Hussain et al., 2019; Karmegam et al., 2011; Rossion and Michel, 2011, Tania et al., 2020).

This also indicates that a comprehensive anthropometric database is required for application in architecture and other sectors. Further studies can investigate the variations for ethnic groups and comparisons with references to find if multipliers can be used until a widespread database is prepared.

The results suggest that the reference standards are not appropriate for Bangladesh, and, presumably, for other countries in South Asia. Space design standards are vital for integrating HFE in the built environment to ensure users' comfort and health benefits; they are also essential for such architectural design considerations as functional efficiency, workability, space optimization, etc. It follows that the data presented here provides better guidance than the reference standards when one is designing for Bangladesh, or as said above, for South Asia in general.

**Conclusion**

In this article, an anthropometric dataset is presented that is specifically tailored for architectural design in Bangladesh. Considering the importance of local data, it highlights the significance of using the Bangladeshi dataset when designing for Bangladesh, rather than relying on reference standards that are relevant for other populations.

Although the focus is on architecture and Bangladesh, the data can be applied to other fields, such as product design, and to other populations, such as other countries in South Asia.

Table 2. Male anthropometric dimensions and reference standards

| SI | Derived Dimension | Male (n=66) | | | | | Male Reference | | | Unisex Reference | | |
|---|---|---|---|---|---|---|---|---|---|---|---|---|
| | | Mean | Mode | Max | Min | STDEV. | Reference Dimension | Reference Book | Ref-Mean difference | Reference Dimension | Reference Book | Ref-Mean difference |
| 1 | Stature | 169.34 | 170.00 | 183.00 | 150.00 | 7.39 | 188.6 | HD | 19.3 | 175.3 | TSS | 6.0 |
| 2 | Eye height | 158.02 | 160.00 | 173.00 | 138.00 | 7.27 | 174.2 | HD | 16.2 | - | - | - |
| 3 | Shoulder height | 141.40 | 143.00 | 159.00 | 125.00 | 7.41 | 155.7 | HD | 14.3 | - | - | - |
| 4 | Elbow height | 108.26 | 107.00 | 135.00 | 96.00 | 7.52 | 120.1 | HD | 11.8 | - | - | - |
| 5 | Knee height | 49.43 | 49.00 | 61.00 | 41.00 | 3.83 | - | - | - | 53.3 | TSS | 3.9 |
| 6 | Shoulder breadth | 43.96 | 44.00 | 54.00 | 37.50 | 3.31 | 52.6 | HD | 8.6 | 45.7 | TSS | 1.7 |
| 7 | Arm length | 75.93 | 72.00 | 90.00 | 63.00 | 4.66 | - | - | - | - | - | - |
| 8 | Upper arm | 32.00 | 30.00 | 39.00 | 22.00 | 2.70 | - | - | - | - | - | - |
| 9 | Forearm | 26.28 | 27.00 | 32.00 | 23.00 | 1.78 | - | - | - | - | - | - |
| 10 | Hand length | 18.53 | 18.00 | 21.70 | 15.00 | 1.32 | 20.5 | HD | 2.0 | 17.8 | TSS | -0.7 |
| 11 | Side width (body depth) | 24.04 | 24.00 | 35.00 | 16.00 | 3.58 | 33.0 | HD | 9.0 | 24.1 | TSS | 0.1 |
| 12 | Back to elbow | 42.36 | 41.00 | 58.00 | 34.00 | 4.08 | - | - | - | 43.2 | TSS | 0.8 |
| 13 | Raised elbow height | 131.86 | 135.00 | 156.00 | 108.00 | 8.23 | - | - | - | 137.2 | TSS | 5.3 |
| 14 | Forward-stretched arm reach (fingertip) | 78.17 | 80.00 | 90.60 | 68.00 | 4.27 | 88.9 | HD | 10.7 | 87.5 | NAD | 9.3 |
| 15 | Vertical reach (standing) | 214.73 | 220.00 | 235.00 | 191.00 | 10.81 | 224.8 | HD | 10.1 | 213.4 | TSS | -1.3 |
| 16 | Side arm reach | 88.33 | 90.00 | 101.00 | 77.00 | 4.75 | 99.1 | HD | 10.7 | - | - | - |
| 17 | Arm span | 173.52 | 174.00 | 190.00 | 154.00 | 8.48 | - | - | - | 182.9 | TSS | 9.4 |
| 18 | Elbow span | 87.49 | 94.00 | 98.90 | 69.00 | 5.83 | - | - | - | 100.0 | NAD | 12.5 |
| 19 | Sitting height | 86.58 | 86.00 | 146.00 | 73.00 | 8.35 | 96.5 | HD | 9.9 | - | - | - |
| 20 | Shoulder height (sitting) | 58.44 | 56.00 | 68.00 | 52.00 | 3.79 | 69.3 | HD | 10.9 | - | - | - |
| 21 | Eye height (sitting) | 75.18 | 74.00 | 84.00 | 64.00 | 3.73 | 86.1 | HD | 10.9 | - | - | - |
| 22 | Popliteal height (sitting) | 45.26 | 45.00 | 53.00 | 40.00 | 2.71 | 49.0 | HD | 3.7 | - | - | - |
| 23 | Knee height (sitting) | 53.42 | 55.00 | 60.00 | 45.00 | 3.13 | 59.4 | HD | 6.0 | - | - | - |
| 24 | Buttock-toe length (sitting) | 69.15 | 69.00 | 90.00 | 58.00 | 6.44 | 94.0 | HD | 24.9 | - | - | - |
| 25 | Buttock-popliteal length (sitting) | 46.72 | 46.00 | 55.00 | 39.00 | 3.31 | 54.9 | HD | 8.2 | - | - | - |
| 26 | Hip breadth (sitting) | 35.25 | 38.00 | 45.00 | 24.00 | 3.31 | 40.4 | HD | 5.1 | - | - | - |
| 27 | Vertical reach (sitting) | 130.79 | 127.00 | 143.00 | 110.00 | 6.48 | 131.1 | HD | 0.3 | - | - | - |
| 28 | Buttock-heel length (sitting) | 103.94 | 97.00 | 123.00 | 89.00 | 7.31 | 117.1 | HD | 13.2 | - | - | - |
| 29 | Cross legged length | 69.60 | 72.00 | 82.00 | 60.00 | 5.34 | - | - | - | 75.0 | NAD | 5.4 |
| 30 | Cross legged height | 83.56 | 86.00 | 100.00 | 51.00 | 6.76 | - | - | - | 87.5 | NAD | 3.9 |
| 31 | Kneeling length | 56.88 | 55.00 | 71.00 | 47.00 | 5.50 | - | - | - | 62.5 | NAD | 5.6 |
| 32 | Kneeling height | 99.08 | 105.00 | 115.00 | 86.00 | 6.76 | - | - | - | 100.0 | NAD | 0.9 |
| 33 | Crawling length | 119.60 | 121.00 | 143.00 | 100.30 | 9.69 | 147.8 | HD | 28.2 | - | - | - |
| 34 | Crawling height | 69.24 | 69.00 | 92.00 | 58.00 | 6.02 | 77.5 | HD | 8.3 | 76.2 | TSS | 7.0 |
| 35 | Bent length | 79.30 | 81.00 | 91.50 | 62.50 | 7.20 | - | - | - | - | - | - |
| 36 | Bent height | 106.02 | 101.00 | 128.80 | 90.00 | 7.81 | - | - | - | - | - | - |
| 37 | Squatting length | 82.43 | 79.00 | 111.40 | 66.00 | 12.09 | - | - | - | - | - | - |
| 38 | Squatting height | 94.91 | 95.00 | 118.00 | 84.00 | 6.35 | - | - | - | - | - | - |

Table 3. Female anthropometric dimensions and reference standards

| SI | Derived Dimension | Female (n=64) | | | | | Female Reference | | | Unisex Reference | | |
|---|---|---|---|---|---|---|---|---|---|---|---|---|
| | | Mean | Mode | Max | Min | STDEV. | Reference Dimension | Reference Book | Ref-Mean difference | Reference Dimension | Reference Book | Ref-Mean difference |
| 1 | Stature | 155.84 | 156.00 | 172.70 | 135.00 | 7.12 | 172.8 | HD | 16.96 | 175.3 | TSS | 19.46 |
| 2 | Eye height | 145.11 | 145.00 | 160.90 | 127.00 | 6.99 | 162.8 | HD | 17.69 | - | - | - |
| 3 | Shoulder height | 129.95 | 142.00 | 152.00 | 117.00 | 6.82 | 141.4 | HD | 11.45 | - | - | - |
| 4 | Elbow height | 98.98 | 98.00 | 113.00 | 86.00 | 5.26 | 110.7 | HD | 11.72 | - | - | - |
| 5 | Knee height | 45.45 | 46.00 | 53.00 | 39.50 | 3.31 | - | - | - | 53.3 | TSS | 7.85 |
| 6 | Shoulder breadth | 39.11 | 37.00 | 49.00 | 31.00 | 4.06 | 43.2 | HD | 4.09 | 45.7 | TSS | 6.59 |
| 7 | Arm length | 69.81 | 74.00 | 79.00 | 59.00 | 4.04 | - | - | - | - | - | - |
| 8 | Upper arm | 29.98 | 31.00 | 35.00 | 24.00 | 2.42 | - | - | - | - | - | - |
| 9 | Forearm | 23.59 | 23.00 | 27.00 | 20.00 | 1.56 | - | - | - | - | - | - |
| 10 | Hand length | 16.79 | 16.00 | 19.70 | 14.00 | 1.25 | - | - | - | 17.8 | TSS | 1.01 |
| 11 | Side width (body depth) | 26.70 | 30.00 | 37.00 | 20.00 | 3.58 | - | - | - | 24.1 | TSS | -2.60 |
| 12 | Back to elbow | 39.34 | 39.00 | 49.40 | 31.00 | 3.72 | - | - | - | 43.2 | TSS | 3.84 |
| 13 | Raised elbow height | 120.36 | 127.00 | 134.20 | 105.00 | 6.57 | - | - | - | 137.2 | TSS | 16.80 |
| 14 | Forward-stretched arm reach (fingertip) | 73.15 | 74.00 | 88.70 | 59.00 | 5.74 | 80.5 | HD | 7.35 | 87.5 | NAD | 14.35 |
| 15 | Vertical reach (standing) | 194.74 | 202.00 | 225.00 | 108.80 | 14.19 | 213.4 | HD | 18.66 | 213.4 | TSS | 18.66 |
| 16 | Side arm reach | 79.11 | 80.00 | 90.50 | 69.00 | 4.65 | 96.5 | HD | 17.39 | - | - | - |
| 17 | Arm span | 156.78 | 153.00 | 177.00 | 138.00 | 7.71 | - | - | - | 182.9 | TSS | 26.12 |
| 18 | Elbow span | 79.71 | 80.00 | 93.00 | 69.00 | 5.11 | - | - | - | 100.0 | NAD | 20.29 |
| 19 | Sitting height | 81.46 | 78.00 | 117.50 | 68.00 | 8.05 | 90.7 | HD | 9.24 | - | - | - |
| 20 | Shoulder height (sitting) | 55.57 | 56.00 | 64.00 | 45.00 | 3.85 | 62.5 | HD | 6.93 | - | - | - |
| 21 | Eye height (sitting) | 69.07 | 69.00 | 79.00 | 53.00 | 4.90 | 80.5 | HD | 11.43 | - | - | - |
| 22 | Popliteal height (sitting) | 42.14 | 46.00 | 53.00 | 34.40 | 4.18 | 44.5 | HD | 2.36 | - | - | - |
| 23 | Knee height (sitting) | 49.67 | 49.00 | 58.00 | 43.00 | 3.42 | 54.6 | HD | 4.93 | - | - | - |
| 24 | Buttock-toe length (sitting) | 65.13 | 67.00 | 82.20 | 49.00 | 5.90 | 94.0 | HD | 28.87 | - | - | - |
| 25 | Buttock-popliteal length (sitting) | 45.02 | 43.00 | 54.00 | 38.30 | 3.97 | 53.3 | HD | 8.28 | - | - | - |
| 26 | Hip breadth (sitting) | 36.88 | 37.00 | 46.50 | 29.90 | 3.54 | 43.4 | HD | 6.52 | - | - | - |
| 27 | Vertical reach (sitting) | 119.90 | 117.00 | 139.00 | 100.00 | 7.79 | 124.7 | HD | 4.80 | - | - | - |
| 28 | Buttock-heel length (sitting) | 98.34 | 93.00 | 122.00 | 81.80 | 7.87 | 124.5 | HD | 26.16 | - | - | - |
| 29 | Cross legged length | 65.31 | 65.00 | 114.00 | 55.50 | 10.91 | - | - | - | 75.0 | NAD | 9.69 |
| 30 | Cross legged height | 78.16 | 81.00 | 88.30 | 59.00 | 4.91 | - | - | - | 87.5 | NAD | 9.34 |
| 31 | Kneeling length | 53.98 | 53.00 | 68.00 | 41.00 | 6.37 | - | - | - | 62.5 | NAD | 8.52 |
| 32 | Kneeling height | 89.40 | 89.00 | 106.00 | 67.00 | 8.21 | - | - | - | 100.0 | NAD | 10.60 |
| 33 | Crawling length | 109.91 | 100.00 | 135.50 | 80.00 | 10.64 | - | - | - | - | - | - |
| 34 | Crawling height | 65.59 | 64.00 | 76.00 | 52.00 | 5.25 | - | - | - | 76.2 | TSS | 10.61 |
| 35 | Bent length | 73.69 | 78.00 | 88.30 | 55.00 | 7.80 | - | - | - | - | - | - |
| 36 | Bent height | 102.39 | 97.00 | 119.00 | 84.00 | 8.35 | - | - | - | - | - | - |
| 37 | Squatting length | 82.43 | 79.00 | 111.40 | 66.00 | 9.30 | - | - | - | - | - | - |
| 38 | Squatting height | 94.91 | 95.00 | 118.00 | 84.00 | 6.91 | - | - | - | - | - | - |

Table 4. Selected percentiles for male and female anthropometric dimensions and reference standards

| SI | Derived Dimension | Male (n=66) | | | | | | Female (n=64) | | | | | |
|---|---|---|---|---|---|---|---|---|---|---|---|---|---|
| | | Mean | Mode | 90th | 50th | 10th | Reference (M/Unisex) | Mean | Mode | 90th | 50th | 10th | Reference (F/Unisex) |
| 1 | Stature | 169.34 | 170.00 | 178.5 | 170.0 | 159.7 | 188.6 | 155.84 | 156 | 165.0 | 155.8 | 147.4 | 172.8 |
| 2 | Eye height | 158.02 | 160.00 | 167.0 | 159.3 | 148.3 | 174.2 | 145.11 | 145 | 155.0 | 145.0 | 137.6 | 162.8 |
| 3 | Shoulder height | 141.40 | 143.00 | 150.1 | 142.0 | 131.5 | 155.7 | 129.95 | 142 | 138.8 | 129.0 | 122.2 | 141.4 |
| 4 | Elbow height | 108.26 | 107.00 | 117.00 | 107.00 | 98.85 | 120.1 | 98.98 | 98.00 | 106.20 | 98.45 | 93.00 | 110.7 |
| 5 | Knee height | 49.43 | 49.00 | 54.00 | 49.35 | 44.55 | 53.3 | 45.45 | 46.00 | 49.35 | 45.45 | 40.48 | 53.3 |
| 6 | Shoulder breadth | 43.96 | 44.00 | 48.50 | 44.00 | 40.00 | 52.6 | 39.11 | 37.00 | 44.35 | 38.50 | 34.30 | 43.2 |
| 7 | Arm length | 75.93 | 72.00 | 81.50 | 76.00 | 70.00 | - | 69.81 | 74.00 | 74.00 | 69.90 | 64.36 | - |
| 8 | Upper arm | 32.00 | 30.00 | 35.00 | 32.00 | 29.00 | - | 29.98 | 31.00 | 33.00 | 30.00 | 27.01 | - |
| 9 | Forearm | 26.28 | 27.00 | 28.00 | 26.00 | 24.00 | - | 23.59 | 23.00 | 26.00 | 23.50 | 21.35 | - |
| 10 | Hand length | 18.53 | 18.00 | 20.00 | 18.45 | 17.00 | 20.5 | 16.79 | 16.00 | 18.30 | 17.00 | 15.20 | 17.8 |
| 11 | Side width (body depth) | 24.04 | 24.00 | 28.25 | 24.00 | 20.00 | 33.0 | 26.70 | 30.00 | 30.91 | 26.45 | 22.00 | 24.1 |
| 12 | Back to elbow | 42.36 | 41.00 | 46.00 | 42.00 | 37.50 | 43.2 | 39.34 | 39.00 | 43.00 | 39.70 | 34.37 | 43.2 |
| 13 | Raised elbow height | 131.86 | 135.00 | 140.75 | 132.05 | 123.00 | 137.2 | 120.36 | 127.00 | 129.00 | 120.75 | 111.65 | 137.2 |
| 14 | Forward-stretched arm reach (fingertip) | 78.17 | 80.00 | 83.85 | 78.00 | 72.90 | 88.9 | 73.15 | 74.00 | 80.40 | 74.00 | 67.09 | 80.5 |
| 15 | Vertical reach (standing) | 214.73 | 220.00 | 227.90 | 214.50 | 200.60 | 224.8 | 194.74 | 202.00 | 206.51 | 196.15 | 183.50 | 213.4 |
| 16 | Side arm reach | 88.33 | 90.00 | 93.15 | 88.65 | 82.40 | 99.1 | 79.11 | 80.00 | 84.70 | 79.10 | 73.12 | 96.5 |
| 17 | Arm span | 173.52 | 174.00 | 185.00 | 174.00 | 162.00 | 182.9 | 156.78 | 153.00 | 165.35 | 157.00 | 146.60 | 182.9 |
| 18 | Elbow span | 87.49 | 94.00 | 94.00 | 87.70 | 80.10 | 100.0 | 79.71 | 80.00 | 85.85 | 80.00 | 74.00 | 100.0 |
| 19 | Sitting height | 86.58 | 86.00 | 90.25 | 86.00 | 81.00 | 96.5 | 81.46 | 78.00 | 85.71 | 80.15 | 74.65 | 90.7 |
| 20 | Shoulder height (sitting) | 58.44 | 56.00 | 63.55 | 58.00 | 54.00 | 69.3 | 55.57 | 56.00 | 61.00 | 56.00 | 50.58 | 62.5 |
| 21 | Eye height (sitting) | 75.18 | 74.00 | 80.00 | 75.00 | 70.00 | 86.1 | 69.07 | 69.00 | 75.80 | 69.00 | 64.00 | 80.5 |
| 22 | Popliteal height (sitting) | 45.26 | 45.00 | 49.00 | 45.00 | 42.00 | 49.0 | 42.14 | 46.00 | 47.00 | 42.15 | 36.30 | 44.5 |
| 23 | Knee height (sitting) | 53.42 | 55.00 | 57.00 | 54.00 | 49.75 | 59.4 | 49.67 | 49.00 | 54.35 | 49.30 | 45.43 | 54.6 |
| 24 | Buttock-toe length (sitting) | 69.15 | 69.00 | 78.00 | 69.00 | 61.50 | 94.0 | 65.13 | 67.00 | 72.14 | 65.75 | 58.72 | 94.0 |
| 25 | Buttock-popliteal length (sitting) | 46.72 | 46.00 | 51.00 | 46.00 | 42.70 | 54.9 | 45.02 | 43.00 | 51.00 | 44.00 | 41.00 | 53.3 |
| 26 | Hip breadth (sitting) | 35.25 | 38.00 | 39.85 | 35.00 | 30.00 | 40.4 | 36.88 | 37.00 | 41.35 | 36.50 | 33.00 | 43.4 |
| 27 | Vertical reach (sitting) | 130.79 | 127.00 | 138.90 | 130.00 | 124.30 | 131.1 | 119.90 | 117.00 | 127.76 | 119.95 | 110.12 | 124.7 |
| 28 | Buttock-heel length (sitting) | 103.94 | 97.00 | 114.25 | 105.00 | 95.50 | 117.1 | 98.34 | 93.00 | 109.00 | 97.25 | 89.30 | 124.5 |
| 29 | Cross legged length | 69.60 | 72.00 | 76.00 | 70.10 | 61.30 | 75.0 | 65.31 | 65.00 | 71.33 | 63.80 | 57.00 | 75.0 |
| 30 | Cross legged height | 83.56 | 86.00 | 89.90 | 85.00 | 77.50 | 87.5 | 78.16 | 81.00 | 83.00 | 79.00 | 72.09 | 87.5 |
| 31 | Kneeling length | 56.88 | 55.00 | 65.00 | 56.00 | 50.50 | 62.5 | 53.98 | 53.00 | 62.00 | 54.00 | 46.18 | 62.5 |
| 32 | Kneeling height | 99.08 | 105.00 | 108.50 | 99.00 | 91.00 | 100.0 | 89.40 | 89.00 | 98.70 | 89.50 | 79.36 | 100.0 |
| 33 | Crawling length | 119.60 | 121.00 | 130.48 | 120.60 | 106.20 | 147.8 | 109.91 | 100.00 | 124.40 | 110.00 | 97.36 | - |
| 34 | Crawling height | 69.24 | 69.00 | 74.60 | 69.00 | 63.00 | 77.5 | 65.59 | 64.00 | 72.00 | 64.55 | 59.59 | 76.2 |
| 35 | Bent length | 79.30 | 81.00 | 87.00 | 81.00 | 70.05 | - | 73.69 | 78.00 | 81.97 | 75.00 | 60.60 | - |
| 36 | Bent height | 106.02 | 101.00 | 115.40 | 106.00 | 97.50 | - | 102.39 | 97.00 | 113.28 | 102.25 | 90.00 | - |
| 37 | Squatting length | 82.57 | 94.00 | 95.50 | 85.30 | 64.00 | - | 82.43 | 79.00 | 94.00 | 82.00 | 70.86 | - |
| 38 | Squatting height | 99.69 | 99.69 | 106.50 | 100.50 | 92.00 | - | 94.91 | 95.00 | 103.97 | 94.00 | 87.00 | - |

Underlined text denotes unisex references as gender specific references are not available.

Table 5. Male anthropometric dimensions compared with reference standards

| SI | Derived Dimension | Male (n=66) | | | | | Reference (M/Unisex) | Z score | p value | p<.05 |
|----|-------------------|------|------|------|------|------|----------|---------|---------|-------|
|    |                   | Mean | Mode | STDEV | CV | SEM |          |         |         |       |
| 1 | Stature | 169.34 | 170.00 | 7.39 | 0.04 | 0.91 | 188.60 | -2.61 | 0.0046 | * |
| 2 | Eye height | 158.02 | 160.00 | 7.27 | 0.05 | 0.89 | 174.20 | -2.23 | 0.0130 | * |
| 3 | Shoulder height | 141.40 | 143.00 | 7.41 | 0.05 | 0.91 | 155.70 | -1.93 | 0.0268 | * |
| 4 | Elbow height | 108.26 | 107.00 | 7.52 | 0.07 | 0.93 | 120.10 | -1.57 | 0.0577 |   |
| 5 | Knee height | 49.43 | 49.00 | 3.83 | 0.08 | 0.47 | 53.30 | -1.01 | 0.1561 |   |
| 6 | Shoulder breadth | 43.96 | 44.00 | 3.31 | 0.08 | 0.41 | 52.60 | -2.61 | 0.0045 | * |
| 7 | Arm length | 75.93 | 72.00 | 4.66 | 0.06 | 0.57 | - | - | - |   |
| 8 | Upper arm | 32.00 | 30.00 | 2.70 | 0.08 | 0.33 | - | - | - |   |
| 9 | Forearm | 26.28 | 27.00 | 1.78 | 0.07 | 0.22 | - | - | - |   |
| 10 | Hand length | 18.53 | 18.00 | 1.32 | 0.07 | 0.16 | 20.50 | -1.50 | 0.0670 |   |
| 11 | Side width (body depth) | 24.04 | 24.00 | 3.58 | 0.15 | 0.44 | 33.00 | -2.50 | 0.0061 | * |
| 12 | Back to elbow | 42.36 | 41.00 | 4.08 | 0.10 | 0.50 | 43.18 | -0.20 | 0.4200 |   |
| 13 | Raised elbow height | 131.86 | 135.00 | 8.23 | 0.06 | 1.01 | 137.16 | -0.64 | 0.2595 |   |
| 14 | Forward-stretched arm reach (fingertip) | 78.17 | 80.00 | 4.27 | 0.05 | 0.53 | 88.90 | -2.51 | 0.0060 | * |
| 15 | Vertical reach (standing) | 214.73 | 220.00 | 10.81 | 0.05 | 1.33 | 224.80 | -0.93 | 0.1756 |   |
| 16 | Side arm reach | 88.33 | 90.00 | 4.75 | 0.05 | 0.59 | 99.06 | -2.26 | 0.0120 | * |
| 17 | Arm span | 173.52 | 174.00 | 8.48 | 0.05 | 1.04 | 182.90 | -1.11 | 0.1345 |   |
| 18 | Elbow span | 87.49 | 94.00 | 5.83 | 0.07 | 0.72 | 100.00 | -2.14 | 0.0160 | * |
| 19 | Sitting height | 86.58 | 86.00 | 8.35 | 0.10 | 1.03 | 96.50 | -1.19 | 0.1174 |   |
| 20 | Shoulder height (sitting) | 58.44 | 56.00 | 3.79 | 0.06 | 0.47 | 69.30 | -2.87 | 0.0021 | * |
| 21 | Eye height (sitting) | 75.18 | 74.00 | 3.73 | 0.05 | 0.46 | 86.10 | -2.92 | 0.0017 | * |
| 22 | Popliteal height (sitting) | 45.26 | 45.00 | 2.71 | 0.06 | 0.33 | 49.00 | -1.38 | 0.0838 |   |
| 23 | Knee height (sitting) | 53.42 | 55.00 | 3.13 | 0.06 | 0.39 | 59.40 | -1.91 | 0.0281 | * |
| 24 | Buttock-toe length (sitting) | 69.15 | 69.00 | 6.44 | 0.09 | 0.79 | 94.00 | -3.86 | 0.0001 | * |
| 25 | Buttock-popliteal length (sitting) | 46.72 | 46.00 | 3.31 | 0.07 | 0.41 | 54.90 | -2.47 | 0.0068 | * |
| 26 | Hip breadth (sitting) | 35.25 | 38.00 | 3.31 | 0.09 | 0.41 | 40.40 | -1.55 | 0.0602 |   |
| 27 | Vertical reach (sitting) | 130.79 | 127.00 | 6.48 | 0.05 | 0.80 | 131.10 | -0.05 | 0.4811 |   |
| 28 | Buttock-heel length (sitting) | 103.94 | 97.00 | 7.31 | 0.07 | 0.90 | 117.10 | -1.80 | 0.0358 | * |
| 29 | Cross legged length | 69.60 | 72.00 | 5.34 | 0.08 | 0.66 | 75.00 | -1.01 | 0.1560 |   |
| 30 | Cross legged height | 83.56 | 86.00 | 6.76 | 0.08 | 0.83 | 87.50 | -0.58 | 0.2802 |   |
| 31 | Kneeling length | 56.88 | 55.00 | 5.50 | 0.10 | 0.68 | 62.50 | -1.02 | 0.1532 |   |
| 32 | Kneeling height | 99.08 | 105.00 | 6.76 | 0.07 | 0.83 | 100.00 | -0.14 | 0.4456 |   |
| 33 | Crawling length | 119.60 | 121.00 | 9.69 | 0.08 | 1.19 | 147.80 | -2.91 | 0.0018 | * |
| 34 | Crawling height | 69.24 | 69.00 | 6.02 | 0.09 | 0.74 | 77.50 | -1.37 | 0.0850 |   |
| 35 | Bent length | 79.30 | 81.00 | 7.20 | 0.09 | 0.89 | - | - | - |   |
| 36 | Bent height | 106.02 | 101.00 | 7.81 | 0.07 | 0.96 | - | - | - |   |
| 37 | Squatting length | 82.57 | 94.00 | 12.09 | 0.15 | 1.49 | - | - | - |   |
| 38 | Squatting height | 99.69 | 99.69 | 6.35 | 0.06 | 0.78 | - | - | - |   |

Underlined text denotes unisex references as gender specific references are not available.

Table 6. Female anthropometric dimensions compared with reference standards

| SI | Derived Dimension | Mean | Mode | STDEV | CV | SEM | Reference (F/Unisex) | Z score | p value | p<.05 |
|---|---|---|---|---|---|---|---|---|---|---|
| | | | | | | Female (n=64) | | | | |
| 1 | Stature | 155.84 | 156.00 | 7.12 | 0.05 | 0.88 | 172.80 | -2.38 | 0.0086 | * |
| 2 | Eye height | 145.11 | 145.00 | 6.99 | 0.05 | 0.86 | 162.80 | -2.53 | 0.0057 | * |
| 3 | Shoulder height | 129.95 | 142.00 | 6.82 | 0.05 | 0.84 | 141.40 | -1.68 | 0.0466 | * |
| 4 | Elbow height | 98.98 | 98.00 | 5.26 | 0.05 | 0.65 | 110.70 | -2.23 | 0.0129 | * |
| 5 | Knee height | 45.45 | 46.00 | 3.31 | 0.07 | 0.41 | 53.30 | -2.37 | 0.0089 | * |
| 6 | Shoulder breadth | 39.11 | 37.00 | 4.06 | 0.10 | 0.50 | 43.20 | -1.01 | 0.1568 | |
| 7 | Arm length | 69.81 | 74.00 | 4.04 | 0.06 | 0.50 | - | - | - | |
| 8 | Upper arm | 29.98 | 31.00 | 2.42 | 0.08 | 0.30 | - | - | - | |
| 9 | Forearm | 23.59 | 23.00 | 1.56 | 0.07 | 0.19 | - | - | - | |
| 10 | Hand length | 16.79 | 16.00 | 1.25 | 0.07 | 0.15 | 17.80 | -0.81 | 0.2085 | |
| 11 | Side width (body depth) | 26.70 | 30.00 | 3.58 | 0.13 | 0.44 | 24.10 | 0.73 | 0.7663 | |
| 12 | Back to elbow | 39.34 | 39.00 | 3.72 | 0.09 | 0.46 | 43.18 | -1.03 | 0.1508 | |
| 13 | Raised elbow height | 120.36 | 127.00 | 6.57 | 0.05 | 0.81 | 137.16 | -2.55 | 0.0053 | * |
| 14 | Forward-stretched arm reach (fingertip) | 73.15 | 74.00 | 5.74 | 0.08 | 0.71 | 80.50 | -1.28 | 0.1003 | |
| 15 | Vertical reach (standing) | 194.74 | 202.00 | 14.19 | 0.07 | 1.75 | 213.40 | -1.32 | 0.0942 | |
| 16 | Side arm reach | 79.11 | 80.00 | 4.65 | 0.06 | 0.57 | 96.50 | -3.74 | 0.0001 | * |
| 17 | Arm span | 156.78 | 153.00 | 7.71 | 0.05 | 0.95 | 182.90 | -3.39 | 0.0003 | * |
| 18 | Elbow span | 79.71 | 80.00 | 5.11 | 0.06 | 0.63 | 100.00 | -3.97 | 0.0000 | * |
| 19 | Sitting height | 81.46 | 78.00 | 8.05 | 0.10 | 0.99 | 90.70 | -1.15 | 0.1253 | |
| 20 | Shoulder height (sitting) | 55.57 | 56.00 | 3.85 | 0.07 | 0.47 | 62.50 | -1.80 | 0.0359 | * |
| 21 | Eye height (sitting) | 69.07 | 69.00 | 4.90 | 0.07 | 0.60 | 80.50 | -2.33 | 0.0099 | * |
| 22 | Popliteal height (sitting) | 42.14 | 46.00 | 4.18 | 0.10 | 0.51 | 44.50 | -0.56 | 0.2865 | |
| 23 | Knee height (sitting) | 49.67 | 49.00 | 3.42 | 0.07 | 0.42 | 54.60 | -1.44 | 0.0747 | |
| 24 | Buttock-toe length (sitting) | 65.13 | 67.00 | 5.90 | 0.09 | 0.73 | 94.00 | -4.89 | 0.0000 | * |
| 25 | Buttock-popliteal length (sitting) | 45.02 | 43.00 | 3.97 | 0.09 | 0.49 | 53.30 | -2.09 | 0.0183 | * |
| 26 | Hip breadth (sitting) | 36.88 | 37.00 | 3.54 | 0.10 | 0.44 | 43.40 | -1.84 | 0.0327 | * |
| 27 | Vertical reach (sitting) | 119.90 | 117.00 | 7.79 | 0.07 | 0.96 | 124.70 | -0.62 | 0.2690 | |
| 28 | Buttock-heel length (sitting) | 98.34 | 93.00 | 7.87 | 0.08 | 0.97 | 124.50 | -3.32 | 0.0004 | * |
| 29 | Cross legged length | 65.31 | 65.00 | 10.91 | 0.17 | 1.34 | - | -0.89 | 0.1872 | |
| 30 | Cross legged height | 78.16 | 81.00 | 4.91 | 0.06 | 0.60 | 75.00 | -1.90 | 0.0284 | * |
| 31 | Kneeling length | 53.98 | 53.00 | 6.37 | 1.05 | 0.78 | 87.50 | -8.86 | 0.0000 | * |
| 32 | Kneeling height | 89.40 | 89.00 | 8.21 | 0.09 | 1.01 | 62.50 | -1.29 | 0.0982 | |
| 33 | Crawling length | 109.91 | 100.00 | 10.64 | 0.10 | 1.31 | 100.00 | - | - | |
| 34 | Crawling height | 65.59 | 64.00 | 5.25 | 0.08 | 0.65 | 76.20 | -2.02 | 0.0217 | * |
| 35 | Bent length | 73.69 | 78.00 | 7.80 | 0.11 | 0.96 | - | - | - | |
| 36 | Bent height | 102.39 | 97.00 | 8.35 | 0.08 | 1.03 | - | - | - | |
| 37 | Squatting length | 82.43 | 79.00 | 9.30 | 0.11 | 1.14 | - | - | - | |
| 38 | Squatting height | 94.91 | 95.00 | 6.91 | 0.07 | 0.85 | - | - | - | |

Underlined text denotes unisex references as gender specific references are not available.

Table 7. Survey mean and reference ratio comparison

| SI | Derived Dimension | Male (n=66) | | | | | | Female (n=64) | | | | | |
|---|---|---|---|---|---|---|---|---|---|---|---|---|---|
| | | Survey Mean | Reference (M/Unisex) | Survey Mean/Stature Ratio | Reference/Stature Ratio | Survey Mean/Arm Span Ratio | Reference/Arm Span Ratio | Survey Mean | Reference (M/Unisex) | Survey Mean/Stature Ratio | Reference/Stature Ratio | Survey Mean/Arm Span Ratio | Reference/Arm Span Ratio |
| 1 | Stature | 169.34 | 188.6 | 1.00 | 1.00 | 0.98 | 1.03 | 155.84 | 172.8 | 1.0 | 1.0 | 0.99 | 0.94 |
| 2 | Eye height | 158.02 | 174.2 | 0.93 | 0.92 | 0.91 | 0.95 | 145.11 | 162.8 | 0.9 | 0.9 | 0.93 | 0.89 |
| 3 | Shoulder height | 141.40 | 155.7 | 0.83 | 0.83 | 0.81 | 0.85 | 129.95 | 141.4 | 0.8 | 0.8 | 0.83 | 0.77 |
| 4 | Shoulder breadth | 43.96 | 52.60 | 0.26 | 0.28 | 0.25 | 0.29 | 39.11 | 43.20 | 0.25 | 0.25 | 0.25 | 0.24 |
| 5 | Elbow height | 108.26 | 120.1 | 0.64 | 0.69 | 0.62 | 0.66 | 98.98 | 110.7 | 0.64 | 0.64 | 0.63 | 0.61 |
| 6 | Knee height | 49.43 | 53.3 | 0.29 | 0.28 | 0.28 | 0.29 | 45.45 | 53.3 | 0.29 | 0.31 | 0.29 | 0.29 |
| 7 | Hand length | 18.53 | 20.5 | 0.11 | 0.11 | 0.11 | 0.11 | 16.79 | 17.8 | 0.11 | 0.10 | 0.11 | 0.10 |
| 8 | Side width (body depth) | 24.04 | 33.0 | 0.14 | 0.17 | 0.14 | 0.18 | 26.70 | 24.1 | 0.17 | 0.14 | 0.17 | 0.13 |
| 9 | Back to elbow | 42.36 | 43.2 | 0.25 | 0.23 | 0.24 | 0.24 | 39.34 | 43.2 | 0.25 | 0.25 | 0.25 | 0.24 |
| 10 | Raised elbow height | 131.86 | 137.2 | 0.78 | 0.73 | 0.76 | 0.75 | 120.36 | 137.2 | 0.77 | 0.79 | 0.77 | 0.75 |
| 11 | Forward-stretched arm reach (fingertip) | 78.17 | 88.9 | 0.46 | 0.47 | 0.45 | 0.49 | 73.15 | 80.5 | 0.47 | 0.47 | 0.47 | 0.44 |
| 12 | Vertical reach (standing) | 214.73 | 224.8 | 1.27 | 1.19 | 1.24 | 1.23 | 194.74 | 213.4 | 1.25 | 1.23 | 1.24 | 1.17 |
| 13 | Side arm reach | 88.33 | 99.1 | 0.52 | 0.53 | 0.51 | 0.54 | 79.11 | 96.5 | 0.51 | 0.56 | 0.50 | 0.53 |
| 14 | Arm span | 173.52 | 182.9 | 1.02 | 0.97 | 1.00 | 1.00 | 156.78 | 182.9 | 1.01 | 1.06 | 1.00 | 1.00 |
| 15 | Elbow span | 87.49 | 100.0 | 0.52 | 0.53 | 0.50 | 0.55 | 79.71 | 100.0 | 0.51 | 0.58 | 0.51 | 0.55 |
| 16 | Sitting height | 86.58 | 96.5 | 0.51 | 0.51 | 0.50 | 0.53 | 81.46 | 90.7 | 0.52 | 0.52 | 0.52 | 0.50 |
| 17 | Shoulder height (sitting) | 58.44 | 69.3 | 0.35 | 0.37 | 0.34 | 0.38 | 55.57 | 62.5 | 0.36 | 0.36 | 0.35 | 0.34 |
| 18 | Eye height (sitting) | 75.18 | 86.1 | 0.44 | 0.46 | 0.43 | 0.47 | 69.07 | 80.5 | 0.44 | 0.47 | 0.44 | 0.44 |
| 19 | Popliteal height (sitting) | 45.26 | 49.0 | 0.27 | 0.26 | 0.26 | 0.27 | 42.14 | 44.5 | 0.27 | 0.26 | 0.27 | 0.24 |
| 20 | Knee height (sitting) | 53.42 | 59.4 | 0.32 | 0.31 | 0.31 | 0.32 | 49.67 | 54.6 | 0.32 | 0.32 | 0.32 | 0.30 |
| 21 | Buttock-toe length (sitting) | 69.15 | 94.0 | 0.41 | 0.50 | 0.40 | 0.51 | 65.13 | 94.0 | 0.42 | 0.54 | 0.42 | 0.51 |
| 22 | Buttock-popliteal length (sitting) | 46.72 | 54.9 | 0.28 | 0.29 | 0.27 | 0.30 | 45.02 | 53.3 | 0.29 | 0.31 | 0.29 | 0.29 |
| 23 | Hip breadth (sitting) | 35.25 | 40.4 | 0.33 | 0.21 | 0.20 | 0.22 | 36.88 | 43.4 | 0.37 | 0.25 | 0.24 | 0.24 |
| 24 | Vertical reach (sitting) | 130.79 | 131.1 | 0.77 | 0.70 | 0.75 | 0.72 | 119.90 | 124.7 | 0.77 | 0.72 | 0.76 | 0.68 |
| 25 | Buttock-heel length (sitting) | 103.94 | 117.1 | 0.61 | 0.62 | 0.60 | 0.64 | 98.34 | 124.5 | 0.63 | 0.72 | 0.63 | 0.68 |
| 26 | Cross legged length | 69.60 | 75.0 | 0.41 | 0.40 | 0.40 | 0.41 | 65.31 | 75.0 | 0.42 | 0.43 | 0.42 | 0.41 |
| 27 | Cross legged height | 83.56 | 87.5 | 0.49 | 0.46 | 0.48 | 0.48 | 78.16 | 87.5 | 0.50 | 0.51 | 0.50 | 0.48 |
| 28 | Kneeling length | 56.88 | 62.5 | 0.34 | 0.33 | 0.33 | 0.34 | 53.98 | 62.5 | 0.36 | 0.36 | 0.34 | 0.34 |
| 29 | Kneeling height | 99.08 | 100.0 | 0.59 | 0.53 | 0.57 | 0.55 | 89.40 | 100.0 | 0.57 | 0.58 | 0.57 | 0.55 |
| 30 | Crawling length | 119.60 | 147.8 | 0.71 | 0.78 | 0.69 | 0.81 | 109.91 | - | 0.71 | - | 0.70 | - |
| 31 | Crawling height | 69.24 | 77.5 | 0.41 | 0.41 | 0.40 | 0.42 | 65.59 | 76.2 | 0.42 | 0.44 | 0.42 | 0.42 |
| | *p*-value for paired *t*-test | 5.42654E-09 | | 0.6036852 | | 0.000198362 | | 7.00667E-09 | | 0.029700651 | | 0.072590005 | |

Underlined text denotes unisex references as gender specific references are not available.

## References

Akhter, Z., Begum, J. A., Banu, M. L. A., Alam, M., Hossain, S., Amin, N. F., Uddin, M., and Yasmin, Q. S. (2009). Stature estimation using head measurements in Bangladeshi Garo adult females. *Bangladesh Journal of Anatomy,* Vol. 7, No. 2, pp. 101–104. DOI: 10.3329/bja.v7i2.6096.

Akhter, Z, Banu, M. L. A, Alam, M. M., Hossain, S., and Nazneen, M. (2013). Photo-anthropometric study on face among Garo adult females of Bangladesh. *Bangladesh Medical Research Council Bulletin*, Vol. 39, No. 2, pp. 61–64. DOI: 10.3329/bmrcb.v39i2.19643.

Akter, S., Jesmin, S., Islam, M., Sultana, S. N., Okazaki, O., Hiroe, M., Moroi, M., and Mizutani, T. (2012). Association of age at menarche with metabolic syndrome and its components in rural Bangladeshi women. *Nutrition & Metabolism* Vol. 9, 99. DOI: 10.1186/1743-7075-9-99.

Alam, S., Gupta, U. D., Alam, M., Kabir, J., Chowdhury, Z. R., and Alam, A. K. M. K. (2014). Clinical, anthropometric, biochemical, and histological characteristics of nonobese nonalcoholic fatty liver disease patients of Bangladesh. *Indian Journal of Gastroenterology*, Vol. 33, Issue 5, pp. 452–457. DOI: 10.1007/s12664-014-0488-5.

Alam, S., Anam, K., Islam, S., Mustafa, G., Al Mamun, A., and Ahmad, N. (2019). Clinical, anthropometric, biochemical and histological character of nonalcoholic fatty liver disease without insulin resistance. *Journal of Clinical and Experimental Hepatology*, Vol. 9, No. 2, pp. 176–181. DOI: 10.1016/j.jceh.2018.06.011.

Ali, N., Mahmood, S., Manirujjaman, M., Perveen, R., Al Nahid, A., Ahmed, S., Khanum, F. A., and Rahman, M. (2018). Hypertension prevalence and influence of basal metabolic rate on blood pressure among adult students in Bangladesh. *BMC Public Health,* Vol. 18, 58. DOI: 10.1186/s12889-017-4617-9.

Asadujjaman, M., Rashid, M. H. O., and Rana, S. (2019). Anthropometric measurement of external ear and correlation with age in north regional people of Bangladesh. *Bangladesh Journal of Medical Science*, Vol. 18, No. 2, pp. 206–210. DOI: 10.3329/bjms.v18i2.40686.

Asghar, S., Hussain, A., Ali, S. M. K., Khan, A. K. A., and Magnusson, A. (2007). Prevalence of depression and diabetes: a population-based study from rural Bangladesh. *Diabetic Medicine*, Vol. 24, Issue 8, pp. 872–877. DOI: 10.1111/j.1464-5491.2007.02136.x.

Attaianese, E. (2012). A broader consideration of human factor to enhance sustainable building design. *Work,* Vol. 41, pp. 2155–2159. DOI: 10.3233/WOR-2012-1020-2155.

Attaianese, E. (2014). Human factors in design of sustainable buildings. In: Ahram, T., Karwowski W., and Marek, T. (eds.). *Proceedings of the 5th International Conference on Applied Human Factors and Ergonomics AHFE 2014,* July 19–23, 2014, Kraków, Poland. DOI: 10.54941/ahfe1001330.

Attaianese, E. (2016). Ergonomic design of built environment. *Anais do VI Encontro Nacional de Ergonomia do Ambiente Construído & VII Seminário Brasileiro de Acessibilidade Integral [= Blucher Design Proceedings, v. 2 n. 7]*, May 23–25, 2016, São Paulo, Brazil, Blucher. pp. 1–5. DOI: 10.5151/despro-eneac2016-PALAMB1.

Attaianese, E. (2017). Ergonomics of built environment i.e. how environmental design can improve human performance and well - being in a framework of sustainability. *Ergonomics International Journal*, Vol. 1, Special Issue 1, 000S1-001. DOI: 10.23880/EOIJ-16000S.

Attaianese, E. and Duca, G. (2012). Human factors and ergonomic principles in building design for life and work activities: an applied methodology. *Theoretical Issues in Ergonomics Science,* Vol. 13, Issue 2, pp. 187–202. DOI: 10.1080/1463922X.2010.504286.

Bhowmik, B., Munir, S. B., Ahmed, K. R., Siddiquee, T., Diep, L. M., Wright, E., Hassan, Z., Debnath, P. R., Mahtab, H., Azad Khan, A. K., and Hussain, A. (2014). Anthropometric indices of obesity and type 2 diabetes in Bangladeshi population: Chandra Rural Diabetes Study (CRDS). *Obesity Research & Clinical Practice,* Vol. 8, Issue 3, pp. e220–e229. DOI: 10.1016/j.orcp.2013.06.001.

Bhowmik, B., Munir, S. B., Diep, L. M., Siddiquee, T., Habib, S. H., Samad, M. A., Azad Khan, A. K., and Hussain, A. (2013). Anthropometric indicators of obesity for identifying cardiometabolic risk factors in a rural Bangladeshi population. *Journal of Diabetes Investigation,* Vol. 4, Issue 4, pp. 361–368. DOI: 10.1111/jdi.12053.

Biswas, S. (2022). Teaching ergonomics in the online studio. *Journal of Design Studio*, Vol. 4, No. 2, pp. 237–247. DOI: 10.46474/jds.1183490.

Biswas, T., Garnett, S. P., Pervin, S., and Rawal, L. B. (2017). The prevalence of underweight, overweight and obesity in Bangladeshi adults: Data from a national survey. *PloS one*, Vol. 12, No. 5, e0177395. DOI: 10.1371/journal.pone.0177395.

Biswas, S., Kundu, G. and Imam, C. A. (2021). Learning human factors/ergonomics (HFE) in architectural education: a study of studio approach in Bangladesh. *Creative Space,* Vol. 9, No. 1, pp. 29–41. DOI: 10.15415/cs.2021.91003.

BNBC/MoHPW/GoB (2021) Bangladesh National Building Code, BNBC. Government of the People's Republic of Bangladesh. Available at: http://www.dpp.gov.bd/upload_file/gazettes/39201_96302.pdf. [Date accessed September 12, 2022].

Cantonment Board (2020). Dhaka Cantonment Building Construction Rules, 2020. Government of the People's Republic of Bangladesh. [online] Available at: https://www.dpp.gov.bd/upload_file/gazettes/35221_57392.pdf [Date accessed August 24, 2022].

Chakrabortty, R. K., Asadujjaman, M., and Nuruzzaman, M. (2014). Fuzzy and AHP approaches for designing a hospital bed: a case study in Bangladesh. *International Journal of Industrial and Systems Engineering*, Vol. 17, Issue 3, pp. 315–328.

Charytonowicz, J. (2000). Architecture and ergonomics. *Proceedings of the Human Factors and Ergonomics Society Annual Meeting*, Vol. 44, Issue 33, 6-103–6–106. DOI: 10.1177/154193120004403305.

Choudhury, K. N., Mainuddin, A. K. M., Wahiduzzaman, M., and Islam, S. M. S. (2014). Serum lipid profile and its association with hypertension in Bangladesh. *Vascular Health and Risk Management*, Vol. 10, pp. 327–332. DOI: 10.2147/VHRM.S61019.

Chowdhury, M. A. B., Uddin, M. J., Haque, R., and Ibrahimou, B. (2016). Hypertension among adults in Bangladesh: evidence from a national cross-sectional survey. *BMC Cardiovascular Disorders,* Vol. 16, 22. DOI: 10.1186/s12872-016-0197-3.

Chowdhury, M. A. B., Uddin, M. J., Khan, H. M. R., and Haque, R. (2015). Type 2 diabetes and its correlates among adults in Bangladesh: a population based study. *BMC Public Health*, Vol. 15, 1070. DOI: 10.1186/s12889-015-2413-y.

Chowdhury, S., Shahabuddin, A. K. M., Seal, A. J., Talukder, K. K., Hassan, Q., Begum, R. A., Rahman, Q., Tomkins, A., Costello, A., and Talukder, M. Q. K. (2000). Nutritional status and age at menarche in a rural area of Bangladesh. *Annals of human biology,* Vol. 27, Issue 3, pp. 249–256. DOI: 10.1080/030144600282136.

Codinhoto, R., Tzortzopoulos, P., Kagioglou, M., Aouad, G., Cooper, R. (2009). The impacts of the built environment on health outcomes. *Facilities*, Vol. 27, No. 3/4, pp. 138–151. DOI: 10.1108/02632770910933152.

Costa, A. P. L., Campos, F., and Villarouco, V. (2012). Overview of ergonomics built environment. *Work,* Vol. 41, pp. 4142–4148. DOI: 10.3233/WOR-2012-0710-4142.

De Chiara, J. and Callender, J. H. (1990). *Time saver standards for building types*. 3rd edition. New York: McGraw-Hill.

D'Souza, A. and Tandon, S. (2019). Intrahousehold nutritional inequities in rural Bangladesh. *Economic Development and Cultural Change,* Vol. 67, No. 3, pp. 625–657. DOI: 10.1086/698311.

Eilouti, B. (2021). A framework for integrating ergonomics into architectural design. *Ergonomics in Design: The Quarterly of Human Factors Applications,* Vol. 31, Issue 1, pp. 4–12. DOI: 10.1177/1064804620983672.

Flora, M. S., Mascie-Taylor, C. G. N., and Rahman, M. (2009). Conicity index of adult Bangladeshi population and their socio-demographic characteristics. *Ibrahim Medical College Journal*, Vol. 3, No. 1, pp. 1–8. DOI: 10.3329/imcj.v3i1.2910.

Fottrell, E., Ahmed, N., Shaha, S. K., Jennings, H., Kuddus, A., Morrison, J., Akter, K., Nahar, B., Nahar, T., Haghparast-Bidgoli, H., Azad Khan, A. K., Costello, A., and Azad, K. (2018). Distribution of diabetes, hypertension and non-communicable disease risk factors among adults in rural Bangladesh: a cross-sectional survey. *BMJ Global Health,* Vol. 3, Issue 6, e000787. DOI: 10.1136/bmjgh-2018-000787.

Fross, K. (2014). Ergonomics in the practice of project architect on selected examples. In: Kurosu, M. (ed.). *Human-Computer Interaction. Theories, Methods, and Tools*. HCI 2014. *Lecture Notes in Computer Science*, Vol. 8510. Cham: Springer, pp. 77–85. DOI: 10.1007/978-3-319-07233-3_8.

Fross, K, Winnicka-Jasłowska, D., Gumińska, A., Masły, D., and Sitek, M. (2015). Use of qualitative research in architectural design and evaluation of the built environment. *Procedia Manufacturing,* Vol. 3, pp. 1625–1632. DOI: 10.1016/j.promfg.2015.07.453.

Garneau, C. J. and Parkinson, M. B. (2016). A survey of anthropometry and physical accommodation in ergonomics curricula. *Ergonomics,* Vol. 59, Issue 1, pp. 143–154. DOI: 10.1080/00140139.2015.1052853.

Ge, W., Parvez, F., Wu, F., Islam, T., Ahmed, A., Shaheen, I., Sarwar, G., Demmer, R. T., Desvarieux, M., Ahsan, H., and Chen, Y. (2014). Association between anthropometric measures of obesity and subclinical atherosclerosis in Bangladesh. *Atherosclerosis,* Vol. 232, Issue 1, pp. 234–241. DOI: 10.1016/j.atherosclerosis.2013.11.035.

Goel, S. and Tashakkori, R. (2015). Correlation between body measurements of different genders and races. In: Rychtář, J., Chhetri, M., Gupta, S., and Shivaji, R. (eds.). *Collaborative Mathematics and Statistics Research. Springer Proceedings in Mathematics & Statistics,* Vol. 109. Cham: Springer, pp. 7–17. DOI: 10.1007/978-3-319-11125-4_2.

Hedge, A. and Dorsey, J. A. (2013). Green buildings need good ergonomics. *Ergonomics,* Vol. 56, Issue 3, pp. 492–506. DOI: 10.1080/00140139.2012.718367.

Hedge, A., Rollings, K., and Robinson, J. (2010). "Green" ergonomics: advocating for the human element in buildings. Proceedings of the Human Factors and Ergonomics Society Annual Meeting, Vol. 54, Issue 9, pp.693–697. DOI: 10.1177/154193121005400902.

Hendrick, H. W. (2008). Applying ergonomics to systems: Some documented "lessons learned". *Applied Ergonomics,* Vol. 39, Issue 4, pp. 418–426. DOI: 10.1016/j.apergo.2008.02.006.

Hoque, M., Halder, P. K., Fouzder, P. K., and Iqbal, Z. (2017). Ergonomic design of a Bangladesh bus passenger seat. *Occupational Ergonomics,* Vol. 13, No. 3–4, pp. 157–172. DOI: 10.3233/OER-170249.

Hoque, A. S. M., Parvez, M. S., Halder, P. K., and Szecsi, T. (2014). Ergonomic design of classroom furniture for university students of Bangladesh. *Journal of Industrial and Production Engineering*, Vol. 31, Issue 5, pp. 239–252. DOI: 10.1080/21681015.2014.940069.

Hossain, Z. (2015). *Estimation of hand anthropometry among Bangladesh adults living in four different areas*. BSc Thesis. Bangladesh Health Professions Institute.

Hossain, S., Begum, J. A., and Akhter, Z. (2011a). Measurement of stature from arm-span – an anthropometric study on Garo tribal Bangladeshi females. *Bangladesh Journal of Anatomy*, Vol. 9, No. 1, pp. 5–9. DOI: 10.3329/bja.v9i1.8139.

Hossain, M. G., Islam, S., Aik, S., Zaman, T. K., and Lestrel, P. E. (2010) Age at menarche of university students in Bangladesh: secular trends and association with adult anthropometric measures and socio-demographic factors. *Journal of Biosocial Science,* Vol. 42, Issue 5, pp. 677–687. DOI: 10.1017/S0021932010000210.

Hossain, M. G., Sabiruzzaman, M., Islam, S., Hisyam, R. Z., Lestrel, P. E., and Kamarul, T. (2011b). Influence of anthropometric measures and socio-demographic factors on menstrual pain and irregular menstrual cycles among university students in Bangladesh. *Anthropological Science*, Vol. 119, Issue 3, pp. 239–246. DOI: 10.1537/ase.100903.

Hovinga, K. R. and Lerner, A. L. (2009). Anatomic variations between Japanese and Caucasian populations in the healthy young adult knee joint. *Journal of Orthopaedic Research,* Vol. 27, Issue 9, pp. 1191–1196. DOI: 10.1002/jor.20858.

Hussain, A., Azad Khan, A. K., and Bhowmik, B. (2013). Anthropometric indicators of obesity for identifying cardiometabolic risks in a rural Bangladeshi population – Chandra diabetes study. *Clinical Care,* Vol. 58, Issue 2, pp. 46–48.

Hussain, M. S. B., Bashar, F., Akhter, N., Nahid, F. A., Zobayer, M. K., Tuhin, J. (2019). Anthropometric study of correlation between the stature and selected upper limb dimensions in adult Bangladeshi Manipuri females. *International Journal of Medical Research Professionals,* Vol. 5, No. 5, pp. 72–79. DOI: 10.21276/ijmrp.2019.5.5.015.

Imrhan, S. N., Sarder, M. D., and Mandahawi, N. (2006). Hand anthropometry in a sample of Bangladesh males. In: *IIE Annual Conference*, May 20–24, 2006, Orlando, USA.

Imrhan, S. N., Sarder, M. D., and Mandahawi, N. (2009). Hand anthropometry in Bangladeshis living in America and comparisons with other populations. *Ergonomics*, Vol. 52, Issue 8, pp. 987–998. DOI: 10.1080/00140130902792478.

Islam, M. Z., Akhtaruzzaman, M., and Lamberg-Allardt, C. (2004). Nutritional status of women in Bangladesh: comparison of energy intake and nutritional status of a low income rural group with a high income urban group. *Asia Pacific Journal of Clinical Nutrition,* Vol. 13, Issue 1, pp. 61–68.

Islam, S. M. S., Alam, D. S., Wahiduzzaman, M., Niessen, L. W., Froeschl, G., Ferrari, U., Seissler, J., Rouf, H. M. A., and Lechner, A. (2015). Clinical characteristics and complications of patients with type 2 diabetes attending an urban hospital in Bangladesh. *Diabetes & Metabolic Syndrome: Clinical Research & Reviews,* Vol. 9, Issue 1, pp. 7–13. DOI: 10.1016/j.dsx.2014.09.014.

Islam, M. A., Asadujjaman, M., Nuruzzaman, M., and Hossain, M. M. (2013). Ergonomics consideration for hospital bed design: a case study in Bangladesh. *Journal of Modern Science and Technology*, Vol. 1, No. 1, pp. 30–44.

Islam, M. S., Hussain, M. A., Islam, S., Mahumud, R. A., Biswas, T., and Islam, S. M. S. (2017). Age at menarche and its socioeconomic determinants among female students in an urban area in Bangladesh. *Sexual & Reproductive Healthcare,* Vol. 12, pp. 88–92. DOI: 10.1016/j.srhc.2017.03.008.

Islam, F., Kathak, R. R., Sumon, A. H., and Molla, N. H. (2020). Prevalence and associated risk factors of general and abdominal obesity in rural and urban women in Bangladesh. *PloS one,* Vol. 15, No. 5, e0233754. DOI: 10.1371/journal.pone.0233754.

Karim, E. and Mascie-Taylor, C. G. N. (1997). The association between birthweight, sociodemographic variables and maternal anthropometry in an urban sample from Dhaka, Bangladesh. *Annals of human biology,* Vol. 24, Issue 5, pp. 387–401. DOI: 10.1080/03014469700005152.

Karmegam, K., Sapuan, S. M., Ismail, M. Y., Ismail, N., Shamsul Bahri, M. T., Shuib, S., Mohana, G. K., Seetha, P., TamilMoli, P., and Hanapi, M. J. (2011). Anthropometric study among adults of different ethnicity in Malaysia. *International Journal of the Physical Sciences*, Vol. 6, No. 4, pp. 777–788. DOI: DOI: 10.5897/IJPS10.310.

Khadem, M. M. and Islam, M. A. (2014). Development of anthropometric data for Bangladeshi male population. *International Journal of Industrial Ergonomics,* Vol. 44, Issue 3, pp. 407–412. DOI: 10.1016/j.ergon.2014.01.007.

Khan, M. M. H. (2014). *Anthropometric estimation of Bangladeshis living in three different areas*. BSc Thesis. University of Dhaka.

Klamklay, J., Sungkhapong, A., Yodpijit, N., and Patterson, P. E. (2008). Anthropometry of the southern Thai population. *International Journal of Industrial Ergonomics,* Vol. 38, Issue 1, pp. 111–118. DOI: 10.1016/j.ergon.2007.09.001.

Laila, S. Z., Begum, J. A., Ferdousi, R., Parveen, S., Husain, M. S., Holy, S. Z., and Islam, M. S. (2010a). Anthropometric measurements of the arm span and their correlation with the stature of Bangladeshi adult Muslim females. *Mymensingh Medical Journal,* Vol. 19, No. 4, pp. 561–564.

Laila, S. Z., Begum, J. A., Ferdousi, R., Parveen, S., Nurunnobi, A. M., Yesmin, F. (2010b). Anthropometric measurements of the forearm and their correlation with the stature of Bengali adult Muslim females. *Mymensingh Medical Journal,* Vol. 19, No. 3, pp. 377–381.

Mitra, D. K., Mistry, S. K., Afsana, K., and Rahman, M. (2018). Demographic, socio-economic and lifestyle determinants of under-and over-nutrition among Bangladeshi adult population: results from a large cross-sectional study. *Journal of Epidemiology and Global Health,* Vol. 8, Issues 3–4, pp. 134–142. DOI: 10.2991/j.jegh.2018.03.002.

MoHPW/GoB (2008) ইমারতনির্মাণ  বিধিমালা২০০৮ , Dhaka Imarat Nirman Bidhimala-2008 [Dhaka Metropolitan Building Construction Rules, 2008]. Government of the People's Republic of Bangladesh. Available at: https://rajuk.portal.gov.bd/sites/default/files/files/rajuk.portal.gov.bd/page/20b761b8_ab9c_4ec7_8692_0877fe834afd/DhakaImaratNirmanBidhimala-2008.pdf. [Date accessed August 24, 2022].

Mokdad, M. (2002). Anthropometric study of Algerian farmers. *International Journal of Industrial Ergonomics,* Vol. 29, Issue 6, pp. 331–341. DOI: 10.1016/S0169-8141(01)00073-7.

Nahar, S., Mascie-Taylor, C. G. N., and Begum, H. A. (2007). Maternal anthropometry as a predictor of birth weight. *Public Health Nutrition,* Vol. 10, No. 9, pp. 965–970. DOI: 10.1017/S1368980007217975.

Neufert, E. and Neufert, P. (2012). *Architects' Data*. 4th edition. Chichester: John Wiley & Sons, 583 p.

Olguntürk, N. and Demirkan, H. (2009). Ergonomics and universal design in interior architecture education. *METU Journal of the Faculty of Architecture*, Vol. 26, No. 2, pp. 123–138. DOI: 10.4305/METU.JFA.2009.2.7.

Osborne, G., Wu, F., Yang, L., Kely, D., Hu, J., Li, H., Jasmine, F., Kibriya, M. G., Parvez, F., Shaheen, I., Sarwar, G., Ahmed, A., Eunus, M., Islam, T., Pei, Z., Ahsan, H., and Chen, Y. (2020). The association between gut microbiome and anthropometric measurements in Bangladesh. *Gut Microbes,* Vol. 11, Issue 1, pp. 63–76. DOI: 10.1080/19490976.2019.1614394.

Panero, J. and Zelnik, M. (1979). *Human dimension & interior space: a source book of design reference standards*. New York: Watson-Guptill, 320 p.

Parvez, M. S., Shahriar, M. M., Tasnim, N., and Hoque, A. S. M. (2022a). An anthropometry survey of Bangladeshi university students. *Journal of Industrial and Production Engineering,* Vol. 39, Issue 2, pp. 89–108. DOI: 10.1080/21681015.2021.1963337.

Parvez, M. S., Talapatra, S., Tasnim, N., Kamal, T., and Murshed, M. (2022b). Anthropomorphic investigation into improved furniture fabrication and fitting for students in a Bangladeshi university. *Journal of The Institution of Engineers (India): Series C,* Vol. 103, Issue 4, pp. 613–622. DOI: 10.1007/s40032-022-00857-1.

Parvez, M. S., Tasnim, N., Talapatra, S., Kamal, T., and Murshed, M. (2021). Are library furniture dimensions appropriate for anthropometric measurements of university students? *Journal of Industrial and Production Engineering*, Vol. 39, Issue 5, pp. 365–380. DOI: 10.1080/21681015.2021.1998930.

Parvez, M. S., Tasnim, N., Talapatra, S., Runani, A., and Hoque, A. S. M. M. (2022c). Assessment of musculoskeletal problems among Bangladeshi university students in relation to classroom and library furniture. *Journal of The Institution of Engineers (India): Series C,* Vol. 103, Issue 3, pp. 279–292. DOI: 10.1007/s40032-021-00792-7Pentikis, J, Lopez, M. S., and Thomas, R. E. (2002). Ergonomics evaluation of a government office building. *Work,* Vol. 18, Issue 2, pp. 123–131.

Pheasant, S. and Haslegrave, C. M. (2006). *Bodyspace: Anthropometry, Ergonomics and the Design of Work*. Boca Raton: CRC press, 352 p.

Pinto, M. R., De Medici, S., Van Sant, C., Bianchi, A., Zlotnicki, A., Napoli, C. (2000). Technical note: Ergonomics, gerontechnology, and design for the home-environment. *Applied Ergonomics,* Vol. 31, Issue 3, pp. 317–322. DOI: 10.1016/S0003-6870(99)00058-7.

Qureshi, N. K., Hossain, T., Hassan, M. I., Akter, N., Rahman, M. M., Sultana, M. M., Ashrafuzzaman, S. M., and Latif, Z. A. (2017). Neck circumference as a marker of overweight and obesity and cutoff values for Bangladeshi adults. *Indian Journal of Endocrinology and Metabolism,* Vol. 21, Issue 6, pp. 803–808. DOI: 10.4103/ijem.IJEM_196_17.

Radjiyev, A., Qiu, H., Xiong, S., and Nam, K. H. (2015). Ergonomics and sustainable development in the past two decades (1992–2011): Research trends and how ergonomics can contribute to sustainable development. *Applied Ergonomics*, Vol. 46, Part A, pp. 67–75. DOI: 10.1016/j.apergo.2014.07.006.

Razzaque L, Ashrafuzzaman M and Hakim M (2021) Study of Age-Related Finger Span and Hand Grip Strength of Adult Female Garment Workers in Bangladesh. *Chattagram Maa-O-Shishu Hospital Medical College Journal,* Vol. 20, Issue 1, pp. 62–66.

Remijn, S. L. M. (2006). Integrating ergonomics into the architectural design processes: tools for user participation in hospital design. In: Proceedings of the International Ergonomics Association 16th world congress on ergonomics, 2006, p. e14.

Available at: https://www.ergos.eu/inhoud/uploads/2013/01/paper_user_centered_hospital_design.pdf. [Date accessed June 12, 2022].

Rogers, B., Buckheit, K., and Ostendorf, J. (2013). Ergonomics and nursing in hospital environments. *Workplace Health & Safety,* Vol. 61, Issue 10, pp. 429–439. DOI: 10.1177/216507991306101003.

Rossion, B. and Michel, C. (2011). An experience-based holistic account of the other-race face effect. In: Calder, A. J., Rhodes, G., Johnson, M. H., Haxby, J. V. (eds.). *The Oxford Handbook of Face Perception*. Oxford: Oxford University Press, pp. 215–244. DOI: 10.1093/oxfordhb/9780199559053.013.0012.

Sanders, M. S. and McCormick, E. J. (1993). *Human factors in engineering and design*. 7th edition. New York: McGraw Hill, 704 p.

Shah, M. R. I., Anwar, S., Mondal, D. K., Yesmin, S., and Ahmed, S. (2015). Anthropometry of the nose: a comparative study between adult male Santhals and Bengalis in Bangladesh. *Mediscope,* Vol. 2, No. 2, pp. 28–32. DOI: 10.3329/mediscope.v2i2.25407.

Shah, R. M., Bhuiyan, M. A. U., Debnath, R., Iqbal, M., and Shamsuzzoha, A. (2013). Ergonomics issues in furniture design: a case of a tabloid chair design. In: Azevedo, A. (ed.). *Advances in Sustainable and Competitive Manufacturing Systems*. Lecture Notes in Mechanical Engineering. Heidelberg: Springer, pp. 91–103. DOI: 10.1007/978-3-319-00557-7_8.

Shahriar, M. M., Parvez, M. S., and Lutfi, M. (2020). A survey of hand anthropometry of Bangladeshi agricultural farm workers. *International Journal of Industrial Ergonomics*, Vol. 78, 102978. DOI: 10.1016/j.ergon.2020.102978.

Siddiquee, T., Bhowmik, B., Karmaker, R. K., Chowdhury, A., Mahtab, H., Azad Khan, A. K., and Hussain, A. (2015). Association of general and central obesity with diabetes and prediabetes in rural Bangladeshi population. *Diabetes & Metabolic Syndrome: Clinical Research & Reviews,* Vol. 9, Issue 4, pp. 247–251. DOI: 10.1016/j.dsx.2015.02.002.

Simmons, S. S., Hagan, J. E. Jr., and Schack, T. (2021). The influence of anthropometric indices and intermediary determinants of hypertension in Bangladesh. *International Journal of Environmental Research and Public Health,* Vol. 18, Issue 11, 5646. DOI: 10.3390/ijerph18115646.

Springer, T. (2007). *Ergonomics for healthcare environments*. Knoll Workplace Research. New York: Knoll.

Sultana, T., Karim, M. N., Ahmed, T., and Hossain, M. I. (2015). Assessment of under nutrition of Bangladeshi adults using anthropometry: can body mass index be replaced by mid-upper-arm-circumference? *PloS one*, Vol. 10, No. 4, e0121456. DOI: 10.1371/journal.pone.0121456..

Tania, I. J., Zaman, F., Morium, U., Akter, M., and Rashid, S. (2020). Anthropometric study of facial height among tribal (Garo) and non-tribal Bangladeshi female of Greater Mymensingh district in Bangladesh. *Journal of Current and Advance Medical Research,* Vol. 7, No. 1, pp. 36–39. DOI: 10.3329/jcamr.v7i1.46428.

Villeneuve, J. (2000). The contribution of ergonomics to the design of hospital architecture. *Proceedings of the Human Factors and Ergonomics Society Annual Meeting,* Vol. 44, Issue 26, pp. 189–196. DOI: 10.1177/154193120004402615.

Yeoman, P. and Ashmore, N. (2018). Moving from pedagogical challenge to ergonomic challenge: Translating epistemology into the built environment for learning. *Australasian Journal of Educational Technology,* Vol. 34, No. 6. DOI: 10.14742/ajet.4502.

# ПРИГОДНОСТЬ СТАНДАРТОВ ДЛЯ ИНТЕГРАЦИИ ЭРГОНОМИКИ В АРХИТЕКТУРЕ: ЭМПИРИЧЕСКОЕ ИССЛЕДОВАНИЕ В БАНГЛАДЕШЕ

Судипти Бисвас

Военный институт науки и технологий (MIST), Дакка, Бангладеш

E-mail: sudipti.biswas@arch.mist.ac.bd

**Аннотация**

**Введение:** Здания — важная часть нашей жизни, потому что мы проводим в них очень много времени. Основная задача архитектора состоит в обеспечении соответствия зданий, в которых мы живем, происходящей в них человеческой деятельности. Поэтому антропометрические данные — важный инструмент для архитектора. К сожалению, антропометрические данные, относящиеся к функциям, выполняемым в зданиях, относительно скудны даже в рамках академического опыта архитектора. Архитекторы в основном полагаются на несколько стандартов, которые могут не соответствовать местному населению. **Цель описанного здесь исследования** — внести вклад в восполнение этого пробела с помощью составления справочных антропометрических таблиц для населения Бангладеш, которые могут служить источником данных в области архитектуры. **Методы:** Антропометрические показатели 130 человек, 66 мужчин и 64 женщин, были измерены в 38 различных позах. Позы выбраны из стандартов и с учетом местной практики. Затем измерения были исследованы с помощью описательной статистики и подверглись сравнению со стандартами для проверки различий. **Результаты:** Сравнительный анализ показывает, что показатели населения Бангладеш значительно меньше; следовательно, применяемые стандарты не подходят для Бангладеш и, предположительно, Южной Азии. Для создания всеобъемлющей антропометрической базы данных необходимы дальнейшие исследования. Представленные измерения могут служить источником данных для проектирования жилых и других зданий в Бангладеш, а также в других странах Южной Азии.

**Ключевые слова:** стандарт, антропометрия, параметры тела, население Бангладеш, архитектура, эргономика.

# CHARACTERISTICS AND SIGNIFICANCE OF THE WORK
# OF RUSSIAN ARCHITECTS IN THE CITY OF NIKŠIĆ IN MONTENEGRO,
# THE END OF THE 19th AND THE FIRST HALF OF THE 20th CENTURY

Vladimir Bojković

University of Montenegro, Podgorica, Montenegro

E-mail: bojkovicv@gmail.com

**Abstract**

**Introduction**: During its long and dramatic history, Montenegro has had close political, economic, and cultural ties with Russia. However, in the context of architecture, the connections between these two countries are the least known and explored. **Purpose of the study:** The present study aims to present for the first time some of the most significant achievements made by Russian architects in the city of Nikšić in Montenegro in the period between the end of the 19th and the first half of the 20th century to a wider professional audience. We present two cases: the project of the Cathedral Church of Saint Basil of Ostrog, which was designed by the architect Mikhail Timofeevich Preobrazhensky, and the project of the Upper Ostrog Monastery, the most significant achievement of the architect Vladimir N. Sukurenko. **Methods:** The methodological approach required classification and comparison of archival materials through the processes of synthesis, analysis, and deduction. Based on the guidelines of the Law on the Protection of Cultural Property of Montenegro, we formed criteria that were used to evaluate the work of the aforementioned architects. The criteria are sorted into three groups. The first group involves building characteristics, where we evaluate authenticity and integrity, degree of preservation, uniqueness, and rarity. In the second group, covering the significance of the building, we assess the historical and scientific significance, archaeological significance, architectural and artistic significance, and technical significance. Finally, in the third group of criteria, we study the age of the buildings, social and economic importance, environmental and landscape importance. **Results**: Based on our criteria, we find that the Cathedral Church of Saint Basil of Ostrog is a symbol and the most important spatial element of the identity of the city of Nikšić, while the Upper Ostrog Monastery, one of the most important sanctuaries in orthodox Christianity, represents the pinnacle of the construction and architectural process.

**Keywords:** Mikhail Timofeevich Preobrazhensky, Vladimir N. Sukurenko, Nikšić, Montenegro.

## Introduction
### Cathedral Church of Saint Basil of Ostrog

In 1883, the ruler of Montenegro Prince Nikola decided to start building a new, modern city in the place of Nikšić, after liberation from the Ottoman Empire. He entrusted the project of building the future city to the engineer and architect Josip Šilović Slade from Trogir (Croatia). In March of the same year, the architect Slade came to what was then Nikšić to record the existing situation and then create a regulatory plan (Fig. 1).

Although Slade's plan foresaw the development of the city up to around 10,000 inhabitants, according to his system of street development it was quite possible, with minor changes, to expand the city several times, and still keep it functional in terms of infrastructure (Maksimović, 1961).

Slade presumed that the core of the future city would be a large quadrangular square and four smaller ones in other areas connected by wide radially directed streets. One of these smaller squares would later become an ideal urban element to reach the future Cathedral Church of Saint Basil of Ostrog (Fig. 2).

Already in 1885, Prince Nikola came to Nikšić to see how the implementation of the regulatory plan was going. At the same time, this was also an opportunity to announce to the citizens of Nikšić a plan for the construction of a church dedicated to Saint Basil of Ostrog in honor of the Montenegrin and Herzegovinian warriors who died for liberation from the Turks in the wars of 1875–1880.

The following year, a commission was formed with a task to determine a suitable place for the church. With the expert consultation of Slade, it was decided
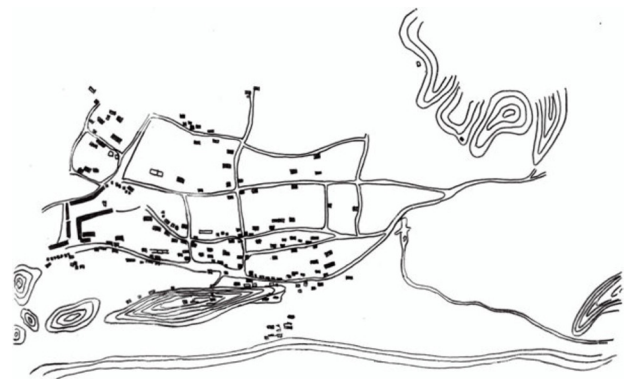


Fig. 1. Urban form of the city of Nikšić before the adoption of the regulatory plan, Vladimir Bojković
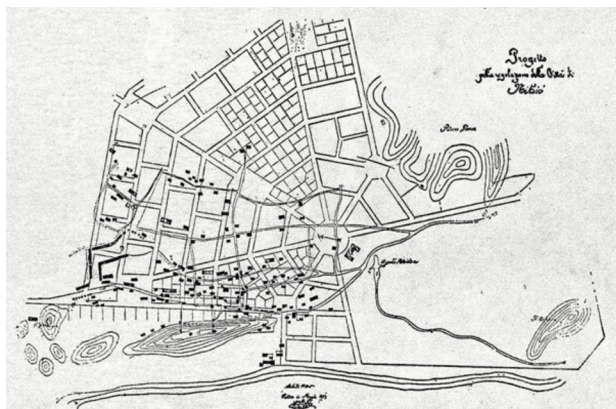
Fig. 2. First regulatory plan of the city of Nikšić,
1883, architect Josip Šilović Slade

that the small hill Petrova Glavica would be the most suitable location. At the foot of the hill, according to the regulatory plan, a smaller square was planned, so choosing this location was quite natural. The hill was 16 m high, and it was necessary to slightly level it in order to obtain the necessary space. The leveling took several years to complete, mostly due to the famine years, where all the necessary money was directed towards the food for the population and not towards the construction. At the end of this stage, the hill was 12 m high (Fig. 3).

The Holy Synod of the Russian Orthodox Church entrusted the task of designing the church to the famous architect of sacred buildings Mikhail Timofeevich Preobrazhensky (1854–1930). Preobrazhensky came to Nikšić in 1891 and after surveying the designated location, made sketches and drafts of ideas for how the temple could look

like. The following year, the final plan for the construction of the temple was presented to the prince. Certain changes were made regarding the bell tower because the prince insisted that it be done in the traditional form called preslica. In the period of 1892–1895, the necessary materials for the construction were collected, the stone blocks to be used were processed, and the works finally started on July 4, 1895.

The construction was completed on August 10, 1899, but the consecration of the church took place a year later, on August 15, 1900. It is worth noting that there were no incidents during the construction in that none of the workers were injured, although it was the first time that a project of that large scale occurred in Montenegro.

*Exterior of the church*

The entrance to the church can be reached from the north and south sides by a driveway. From the west side, directly from Duke Šako Petrović Square, the main entrance of the church can be reached by a monumental staircase with a total of 65 steps. The staircase is wide, spacious, and bordered by a fence made of large hewn stone blocks. The staircase is separated by three resting plateaus decorated with pine trees (Fig. 4).

On the main plateau, where the church is located, on the left and right sides, there are stone benches for resting and a fountain made of finely processed stone. On the eastern side of the plateau, on the left and right sides of the church, there are paved paths that lead from the foot of the hill Petrova Glavica, i.e., Duke Šako Petrović Square, to the plateau. Adjacent to the church, on its northern and southern sides, there are memorials to Stojan Kovačević and Novak
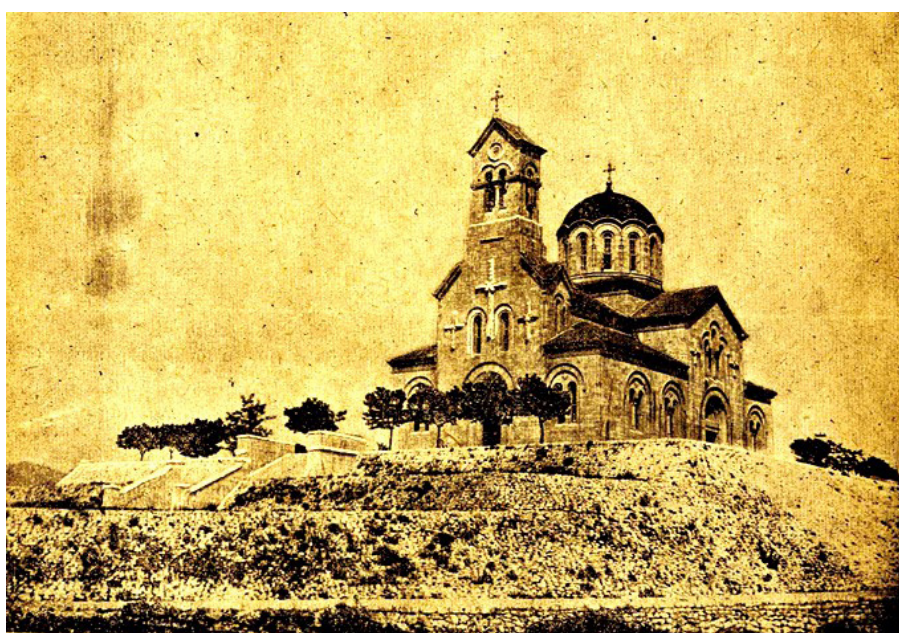


Fig. 3. One of the first photos of the church, private archive

Vladimir Bojković — Pages 19–33

CHARACTERISTICS AND SIGNIFICANCE OF THE WORK OF RUSSIAN ARCHITECTS IN THE CITY
OF NIKŠIĆ IN MONTENEGRO, THE END OF THE 19th AND THE FIRST HALF OF THE 20th CENTURY

Fig. 4. Aerial photo of the church, taken from
the monography "Saborna crkva Svetog Vasilija
Ostroškog u Nikšiću 1900–2010, publisher Saborna
crkva Svetog Vasilija Ostroškog-Nikšić, 2010"

Ramov, erected in 1955. The plateau in front of the church is not paved but only filled with gravel. The gravel is also used on the resting plateaus between the approach stairs (Fig. 5).

The hill itself is paved with hewn stone on the sides. The impression is that the hill together with the church on its top represents a unique and harmonious whole. The church is 23 m wide, 33 m long and 34 m high (Fig. 6).

The width to length ratio corresponds to the golden ratio, which also supports the harmonious impression. The church has three doors, the main one on the west side, one side door on the north and south sides. The door can be reached by 10 steps. The main door has a height of 3.90 m and a width of 1.92 m. The side door has a height of 3.90 m and a width of 2.0 m. The doors are carved and decorated with rich ornamentation of vertical rectangles with crosses. Above the main entrance, the stonecutter Stanko Lepetić carved an inscription in old Slavic language, translated as follows:

"This holy temple, dedicated to the name of Saint Basil of Ostrog the Wonderworker, and in memory of the Orthodox Montenegrin and Herzegovinian warriors, who died for their faith and homeland, was built by the pious Lord Nikola Petrović Njegoš, Prince of Montenegro, in the summer of 1885" (Dašić, 1989).

The church is three-nave, built of white hewn stone blocks from local quarries by well-trained local craftsmen as well as craftsmen from Italy and Dalmatia.

The central part of the church, together with the dome is 11 m high and 8.60 m wide. On the top is a gilded apple, 60 cm in diameter, and on it is a 2 m high gilded cross. On the cube there are 12 side windows with a height of 3.9 m and a width of 80 cm. The dome is covered with a copper cover.

The bell tower is 14 m high and is also covered with a copper cover on the gable roof. On the top is a gilded apple with a diameter of 30 cm and 1.6 m high cross.

On the north and south sides there are lancets, and on the east and west there are double lancets. There is also a clock on the bell tower, which was donated in 1929 by the watchmaker Pavle Pantelić from Zemun (Serbia). In the belfry there are five bells, which were donated by Prince Petar Karađorđević and which were cast in the famous workshop of Pietro Colbachini in Bassano, Italy.

Not counting the openings on the dome, the church has ten windows, eight of which are double lancets with a height of 3.65 m and a width of 90 cm. The two triple lancets have openings, each 90 cm wide and 3.65 m high, except for the middle opening with a height of 4.70 m (Fig. 7).

The apse is three-sided and with one double lancet. The cordon cornice vertically divides the wall of the apse into two unequal parts.

*Interior of the church*

The interior of the church is harmonious. The white stone from which it was built has acquired



Fig. 5. Main facade of the church, photo by Duško
Tasić, taken from http://www.mojacrnagora.com/

21
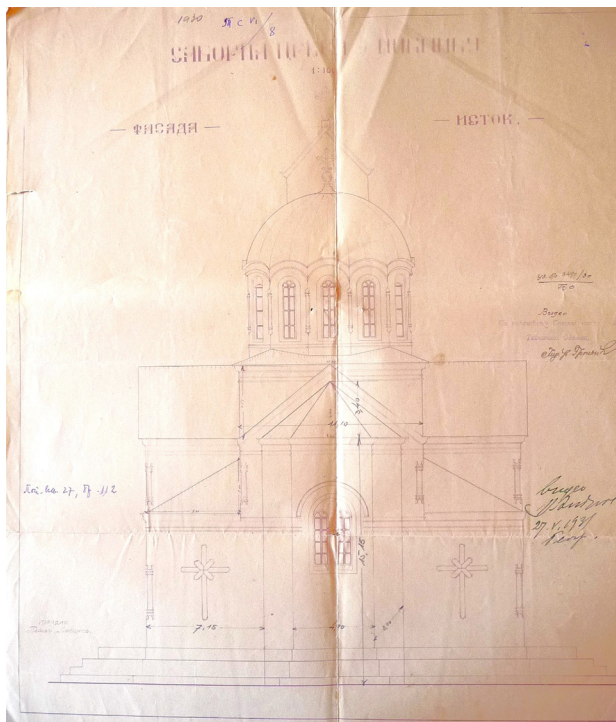
Fig. 6. East facade of the church, city archive of Nikšić

a special patina in the interior. The floor of the church is paved with white octagonal and pale red quadrangular stone slabs. The triple nave of the church is divided by four massive square columns connected by arcades that carry the central dome (Fig. 8). The columns are 1.30 m wide and over 5 m high. Like the church, they were made of finely carved and processed white granite from local quarries.

Originally, Prince Nikola had the idea to carve the names of all 3,098 Montenegrin and Herzegovinian fighters into the pillars, but finally the names were embroidered on silk in gilded frames displayed on the side walls (Glas Crnogorca, 1900).

Over time, the silk embroidered with the warriors' names will be replaced by 35 copper plates placed on the south and north interior walls of the church.

Upon entering the church, right above the main entrance, in the gallery space, there is a choir at a height of 7.65 m. It can be reached by a winding, steep staircase that also leads to the bellfry. The dome is raised on the vaults of four columns to the iconostasis, which at the same time closes the altar in the main nave. There are two rooms to the side of the altar.

The iconostasis is built of white and green marble. It is 8 m high in the middle and 8.5 m wide. The side doors have a height of 3.15 m and a width of 90 cm. The central doors have a height of 3.35 m and a width of 1.3 m. Above them, there are 12 icons 80 cm high and 34 cm wide, then three larger icons 1 m high and 41 cm wide, then an icon of the Last

Supper, and finally a cross. The icons were made in Russia and were a gift from the Synod of the Russian Orthodox Church. The doors were made by the famous craftsman Vasilije Đinovski. The iconostasis itself was a gift from the Greek Andreas Syggros.

The special beauty of the interior space is given by the chandeliers. The largest of them, which starts from the top of the dome, is particularly notable for its rich ornamentation. The four chandeliers were a gift from the Italian Queen Jelena of Savoy, daughter of Prince Nikola (Fig. 9).

The chandeliers came from the old royal court in Caserta. They were brought and installed by a special envoy, the court architect Artur Flores (Šakotić, 1996).

It is interesting that the interior of the church is not frescoed. In June 1899, Prince Nikola invited the famous Serbian painter Uroš Predić to paint the interior, however, due to the scope of the work, the artist did not agree to this job (Onogošt, 1899).



Fig. 7. Details of the windows and church bell tower, private archive
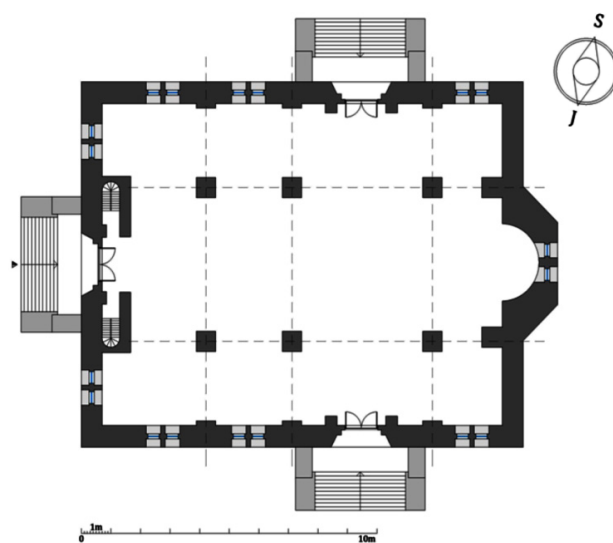


Fig. 8. Ground floor of the church, Vladimir Bojković

Vladimir Bojković — Pages 19–33

CHARACTERISTICS AND SIGNIFICANCE OF THE WORK OF RUSSIAN ARCHITECTS IN THE CITY
OF NIKŠIĆ IN MONTENEGRO, THE END OF THE 19th AND THE FIRST HALF OF THE 20th CENTURY

Fig. 9. Interior of the church, Vladimir Bojković

*Spatial context in which the Cathedral of Saint Basil of Ostrog was built*

Dr. Josip Šilović Slade was an expert consultant in the commission that was supposed to determine the location where the future temple would be built. The architect Slade, as the author of the first regulatory plan of the city of Nikšić, first proposed that the cathedral be built on the central city square. However, this proposal was not adopted. After this, the architect Slade proposed that the Petrova Glavica hill be the place of construction. This elevation proved to be ideal for several reasons. If we look at the regulatory plan of the city of 1883, it becomes evident that the elevation is located on the axis of the street that connects two planned squares, the main, larger square and the secondary, smaller one. It was logical that some significant and representative building should appear on this highly baroque arrangement of urban elements. On the other hand, the elevation itself allows for an excellent position that further emphasizes the object on it, making it more noticeable. In this way, the temple will become the most important reference point of the city and, therefore, its symbol. The consequence of this dominant positioning of the temple is that it becomes one of the main elements of the spatial identity and recognition of the city of Nikšić.

The spatial identity of the city can be best seen in the example of the city silhouette. In the case of Nikšić, the temple is its most significant element. However, the negative consequences of the so-called transition period in the late 20th century when

the devastation of space occurred did not bypass the silhouette of the city, and what is more, they are most noticeable on it.

The city silhouette, at first glance, can hide everything that makes the city less beautiful. However, once it begins, the process of space devastation rarely takes place without showing itself in every visual representation of the city. The city silhouette is perhaps the most pronounced form of the city's physical structure, its most visible representation, and as such represents a particularly significant part of the city's urban image and identity.

"The silhouette of the physical structure of the city, first of all, is the expression of a series of individual and predominant units, which are combined with the morphology of the terrain in each given example of the city. Focal central units in a group or individually placed on the terrain of the agglomeration give the macro form of the urban fabric, the silhouette" (Radović, 2009).

The city silhouette, as a special visual sensation and experience, can be experienced anew every time depending on the aspect from which it is observed, at the place and on the time of the day when it is observed. In this regard, we can distinguish between the silhouette of the city observed by day and by night. In both cases, the temple of Saint Basil of Ostrog, regardless of the visible devastation, still remains a dominant element of the spatial identity of the city of Nikšić (Fig. 10).

*Social context of the time in which the Cathedral Church of Saint Basil of Ostrog was built*

The Cathedral Church of Saint Basil was built in a specific time. After liberation from Turkish rule, a small town like Nikšić was at the time needed time to recover from the long-lasting wars. The city needed a symbol that would infuse new energy and encourage the development in a better and more beautiful direction. Hence, it is not surprising that



Fig. 10. Relationship between the city focal points, Vladimir Bojković

Prince Nikola decided, precisely at the request of the citizens of Nikšić, to build a new temple in this city after many years of occupation. Since both Montenegrin and Herzegovinian warriors gave their lives for the liberation of the city, the temple was built in their honor, thus preserving their sacrifice from oblivion.

As for the church construction, it should be taken into account that Nikšić was quite impoverished due to constant warfare. The famine years did not allow the continuous construction of the temple because the money used for the construction was used to procure food for the population. The Russian Orthodox Church played a significant role in this regard since the temple was mostly built from contributions collected by believers in Russia.

The cathedral church has almost always had a great importance in the life of the city. This importance was only marginalized in the period of socialist organization since the end of World War II until the mid-1980s.

The dominant position of the church in the urban structure of the city and its role as one of the most important city points, made it always present in the minds of the citizens of Nikšić. We should not forget that today all the most important religious holidays are celebrated in this temple, which continuously confirms its anthropo-sociological role. If we look at the temple exclusively as a monument to the fallen fighters in the liberation wars, it seems that in this respect their memory is somewhat lost, or rather relegated to the background compared to the role that the temple plays in the everyday life of the city. In the life of the city of Nikšić, the cathedral has always had a special place. During religious holidays, the building is the main place of gathering and celebration, which makes its social importance more than evident (Fig. 11).

In terms of the formation of the spatial, architectural and urban identity of the city of Nikšić, the Cathedral Church is the most important benchmark of the city. The significance of the building in the formation of the city silhouette is also great, given that it is a building that, due to its position, can be seen from all approaches to the city.

In the end, we can state that the Cathedral Church of Saint Basil of Ostrog contributes to the recognizability and identity of Nikšić, both spiritually and spatially.

### Architect Vladimir N. Sukurenko (?–1976) and the Upper Ostrog Monastery

In the first half of the 20th century, Montenegro experienced dramatic social, political, and economic changes. The Balkan wars and World War I left great consequences for the then undeveloped country. After World War I, according to the state statistics, Montenegro had 175,000 inhabitants, which is significantly less than 240,000 inhabitants in 1910 and indicates the loss of many of them (Politika, 1921).

Vladimir Bojković — Pages 19–33

CHARACTERISTICS AND SIGNIFICANCE OF THE WORK OF RUSSIAN ARCHITECTS IN THE CITY
OF NIKŠIĆ IN MONTENEGRO, THE END OF THE 19th AND THE FIRST HALF OF THE 20th CENTURY

Fig. 11. One of the Great Processions dedicated
to Saint Basil of Ostrog, www.eparhija.me

By the decision of the Great National Assembly of Podgorica in 1918, Montenegro became part of the Kingdom of Yugoslavia, thus losing its independence and eventually becoming part of the county of Zeta in 1922, and then part of the province of Zeta (Zeta banovina) from 1929 to 1941. The province of Zeta, in addition to the territory of Montenegro, also included parts of Serbia, Croatia, and Bosnia and Herzegovina. The seat of the banovina was in the Montenegrin city of Cetinje.

The Kingdom of Yugoslavia in 1918–1941 was an underdeveloped, agrarian country with a very low level of industrialization. Agricultural production was primitive, trade and banking were undeveloped, and the industry began to develop significantly only in the mid-1930s (Bakić, 2004).

The degree of development of the banovinas that made up the Kingdom of Yugoslavia was different. One of the most underdeveloped banovinas was the Zeta banovina. About 80% of the total number of inhabitants were rural people who engaged in agriculture and animal husbandry in a primitive way using hand tools and wooden ploughs. The arable land occupied only 22% of the territory, so agricultural production was accompanied by poverty and hunger (Babović Raspopović, 2002).

The fact that in 1930 only Podgorica had slightly more than 10,000 inhabitants and only a few cities had more than 4,000 inhabitants shows that the process of deagrarization was very slow in the Zeta banovina (Rastoder, 2011).

An indicator of the underdevelopment of the Zeta banovina is the underdeveloped traffic network. Two-thirds of the territory of the banovina were roadless, the sections were not connected to each other, and the traffic connection with other banovinas was not satisfactory either (Babović Raspopović, 2002).

The social and economic conditions that existed in the Kingdom of Yugoslavia and also in its provinces were also reflected in the architecture and urban planning, which played a significant role in the formation of the Yugoslav state and national identity. The state did not have a clearly defined construction policy (Toševa, 2012).

In the complex social circumstances and pronounced differences between banovinas, it was very difficult to implement a unified construction policy that had to be adapted to real circumstances (Toševa, 2012).

The work of the Ministry of Construction of the Kingdom of Yugoslavia, as the highest state institution in the field of architecture and urban planning, was organized throughout the country through the activities of construction directorates that worked on projects for the areas under their jurisdiction (Toševa, 1999).

Based on this brief review of social, political, and economic circumstances, we conclude that the conditions for the work of an architect were quite difficult.

*Work of the architect Vladimir N. Sukurenko in the city of Nikšić*

After 1918, as part of the Russian emigration, a significant number of Russian architects and engineers came to the Kingdom of Yugoslavia, where they found employment in various ministries, directorates, and administration. In the beginning, Russian engineers and architects, as foreigners, could not establish a permanent employment relationship but were engaged on a part-time basis. After the Union of Russian Engineers in the Kingdom of Yugoslavia intervened with the competent authorities, they were generally equal in terms of competence with their Yugoslav colleagues. The state law prohibiting the employment of foreign labor was not applied to Russian engineers and architects (Milenković, 1995).

The engineer and architect Vladimir N. Sukurenko was among the Russian emigrants that came to the Zeta province.

Presently, very little is known about the life of the architect Sukurenko, even his year of birth is still unknown. It is assumed that he left Montenegro in 1945, when he went to Tunisia, where he worked on the dome project of the Orthodox Church of the

Ascension of Christ. He lived in Tunisia until 1970 and spent the last years of his life in the St. Raphael nursing home in France, where he died in 1976 (Martinović, 2022).

Thanks to the pioneering work of the art historian Slađana M. Žunjić, who was the first to systematically and thoroughly research the architecture of Montenegro in the period of 1918–1941 in her PhD thesis, we can learn more about the work of the architect Vladimir N. Sukurenko (Žunjić, 2019).

For the first time, the architect Vladimir N. Sukurenko was mentioned as the head of the Construction Section in Nikšić by the decree of the Minister of Construction, which approved public practice in the field of construction engineering in the territory of the Kingdom of Yugoslavia (Službeni glasnik Zetske oblasti, 1926).

Several buildings in Nikšić were built according to the projects of the architect Vladimir N. Sukurenko, namely: Home of the Craftsmen's Association, Home of the First Nikšić Singing Society "Zahumlje", Home of the Women's Society "Kosovka Djevojka", and it is assumed that the architect Sukurenko is the author of the National Health Center in Nikšić (Fig. 12). The work of the architect Sukurenko on the restoration and reconstruction of the Upper Ostrog Monastery after the great fire of 1923, is particularly significant. The research presented in this paper deals with this building.

*Upper Ostrog Monastery*

The Upper Ostrog Monastery was built in the 17th century in a cave on the cliffs of Ostrog mountain (900 m altitude). The upper monastery had two small churches the church of the Holy Cross and the Church of Saint Basil of Ostrog. It is believed that the first Church of the Holy Cross was built by the hieromonk Isailo, and the second Church of Saint Basil of Ostrog was built around 1656. They were modest buildings, without a recognizable sacral
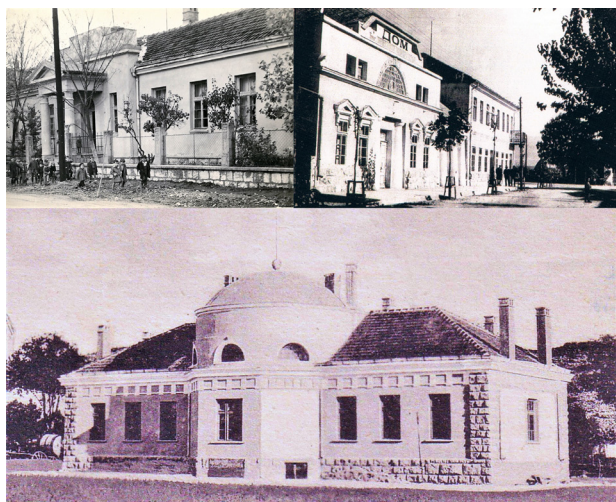


Fig. 12. Some works by the architect Vladimir
N. Sukurenko in the city of Nikšić, private archive

form (Fig. 13). Only the cross on the west side of the roof indicated that it was a place of worship for a liturgical ceremony (Martinović, 2022).

After the fire in 1923, the architect Sukurenko designed and built a completely new upper monastery. The central element of the building is the powerful bell tower, which asymmetrically but harmoniously divides the facade composition into two parts. The bell tower is visually divided into three proportional clearly distinguished parts. The first part has an entrance, a tall door, which can be reached from the path that pilgrims use to reach the relics of Saint Basil of Ostrog located in the far-right part of the building. Above the entrance, there is an arched opening, two rectangular and one square windows arranged in an unusual rhythm. The second part of the bell tower has one narrower, arched window. The third part of the bell tower has large arched openings on three sides through which the bells of the monastery can be seen. The bell tower ends with a pyramidal roof with a cross on its top (Fig. 14).

To the left of the bell tower, there is a smaller facade area that ends with a cornice and a stone terrace fence at the height of the second part of the bell tower. In this part of the building, the architect Sukurenko again applied an unusual rhythmic distribution of rectangular windows. Above this part of the building there is a steep cliff, after which comes a terrace carved into the mountain cliff (Fig. 15).

To the right of the bell tower, the architect Sukurenko applied a calmer way of treating the facade by distributing arched openings. This part of the building is visually divided into three parts. The first part is located along the path leading to the relics of the saint, and on it there are three rectangular openings, above which there is a cornice half the height of the first part of the bell tower. The second part of this part of the facade is decorated with four arched windows for the monks' cells, above which there is a cornice with a stone fence of the terrace, which can be accessed from the three cells located in the third part of this side of the building. On the main facade above the entrance there is also an inscription about the renovation of the monastery (Fig. 16).

Diagonally from the entrance to the bell tower is the Church of the Holy Cross with two square openings.

This unique building is a real masterpiece of the construction of that time and overall of the architectural approach applied by the architect Vladimir N. Sukurenko.

**Methods**

Based on the guidelines of the Law on the Protection of Cultural Property of Montenegro, we formed criteria that were used to evaluate the buildings of the Russian architects Preobrazhensky and Sukurenko. The criteria are sorted into three

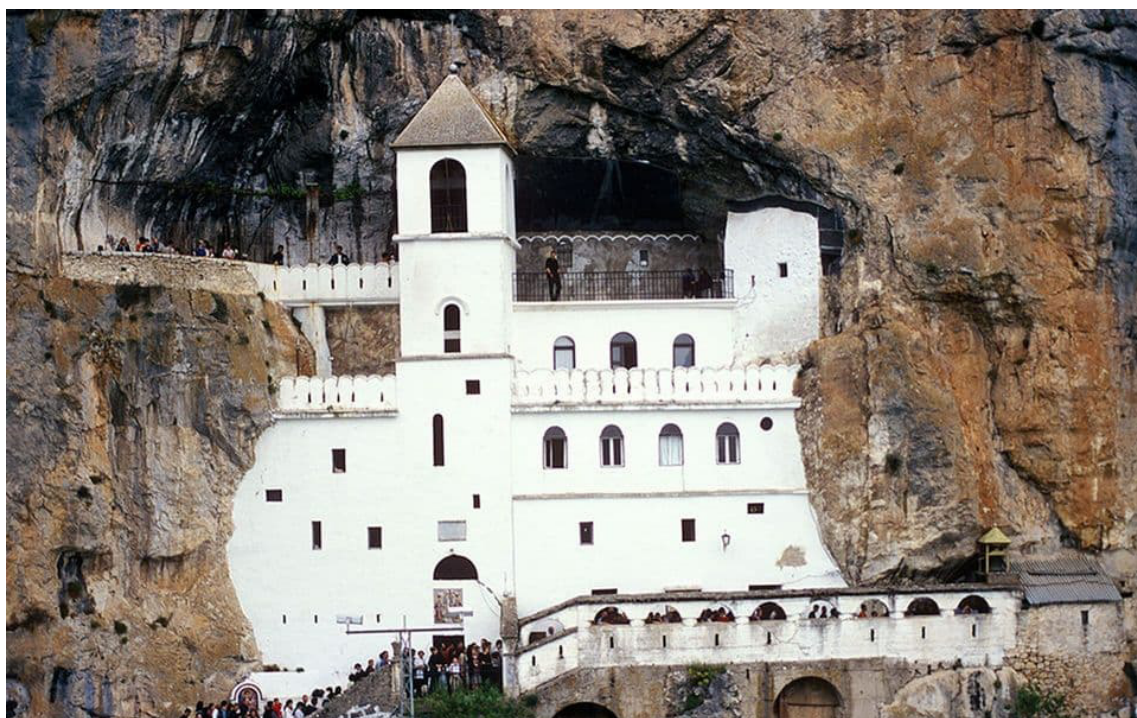Fig. 13. Upper Ostrog Monastery, 1890, private archive



Fig. 14. Photo of the Upper Ostrog Monastery by Lazar Pejović

Fig. 15. Photo of the Ostrog Upper Monastery at night, private archive

groups. The first group involves such building characteristics as authenticity and integrity, degree of preservation, uniqueness, and rarity. In the second group, covering the significance of the building, we assess the historical and scientific significance, archaeological significance, architectural and artistic significance, and technical significance. The third group of criteria covers the age of the building, social and economic importance, environmental and landscape importance.

*A. Building characteristics*

In this group of criteria, the following building features were considered:

*Authenticity and integrity*: determined through the degree of presence of original and primary forms or phenomena determined from the point of view of the natural or cultural environment in which the object is located or in which it was created.

*Degree of preservation*: determined through its completeness, the level of preservation,

endangerment or degradation, in relation to the state of the object at the time of the establishment of the protection of the cultural property, taking into account the interventions, which were later legally carried out on the property.

*Uniqueness and rarity*: determined through the representativeness of the object in its kind, originality in relation to a certain area or time, typicality or specificity of the object or phenomenon, rarity, as well as through historical, geographical, architectural or other specificities, characteristics or peculiarities. The rarity of an object is determined through the quantity in relation to the type, occurrence, processes, natural or architectural form of the object in a certain space and time.

*B. Building significance*

The general significance of the building was evaluated through the following:

*Historical and scientific significance*: expressed through the possibility of documenting, among other
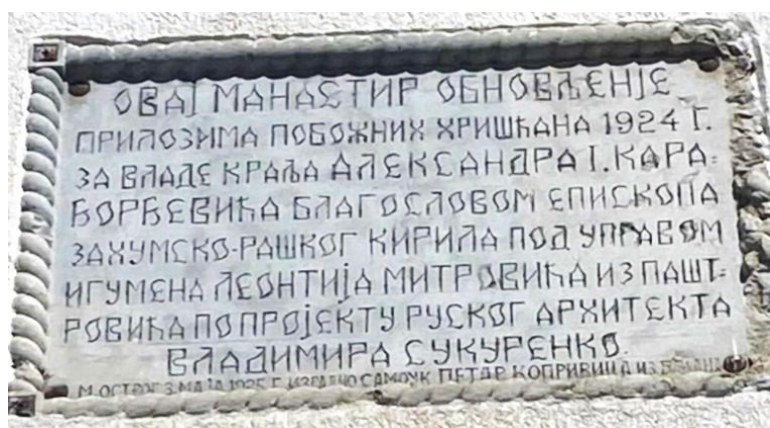


Fig. 16. Photo of the restoration plaque, private archive

Vladimir Bojković — Pages 19–33

CHARACTERISTICS AND SIGNIFICANCE OF THE WORK OF RUSSIAN ARCHITECTS IN THE CITY
OF NIKŠIĆ IN MONTENEGRO, THE END OF THE 19th AND THE FIRST HALF OF THE 20th CENTURY

things, the connection of the building with a historical figure or a significant event in history. Scientific significance is expressed through the possibility of applying fundamental scientific disciplines, as well as the degree of role and importance of a certain building in the interpretation and development of a certain scientific discipline.

*Archaeological significance*: expressed by the value and age of the building from the point of view of archaeology and its criteria.

*Architectural and artistic significance*: expressed through the value of the building, through belonging to a certain architectural style, to its original variety and original architectural expression from a certain period and method of construction. Artistic significance is expressed through the presence of exceptional artistic or aesthetic value, which is reflected in the quality of processing, quality of materials, proportions, composition, value of details, value of construction.

*Technical significance*: is the value expressed through the art of skill, the importance of tools and knowledge of production that has developed historically and which enables action on the environment for the purpose of acquiring material goods, as well as the uniqueness and peculiarity of the methods that were applied in some work, craft, art.

*C. Other criteria*

In addition to the aforementioned groups of criteria, the value of the buildings designed by the architects Preobrazhensky and Sukurenko was also examined through the following characteristics:

*Age of the building*: determined through its importance in relation to the time of creation and duration of the building.

*Social and economic importance*: is the value expressed through the possibility of using the property for cultural, health, recreational, touristic and other purposes, which do not contradict with the essential characteristics of the building.

*Environmental and landscape importance*: observed in the relationship of the form with other parts of the whole, the meaning in the structure and vision of the city, buildings or groups of buildings, which is part of the whole or the area. Landscape significance is the value expressed in the vision of the city or the area by the degree of attractiveness of the atmosphere and the visual unity of the whole.

### Results

### Cathedral Church of Saint Basil of Ostrog

*A. Building characteristics:*

*Authenticity and integrity*: The Cathedral Church of Saint Basil of Ostrog is the main and largest city church in Nikšić. It stands out for its architectural values; it is the dominant element of the city silhouette. Since it is dedicated to the Montenegrin and Herzegovinian freedom fighters who died during the war with the Ottoman Empire, this building has a memorial role, so we can conclude that its authenticity and integrity are still present today.

*Degree of preservation*: The Cathedral Church of Saint Basil of Ostrog has preserved all elements of physical recognition from the moment of construction completion until today. We conclude that the preservation criterion is also met.

*Uniqueness and rarity*: The Cathedral Church of Saint Basil of Ostrog in Nikšić is the largest church building of the end of the 19th and the beginning of the 20th century built in Montenegro. At the same time, this is the largest memorial church dedicated to fighters for freedom against the Ottoman occupation. In addition to the indisputable architectural value given by the project of the architect Preobrazhensky, this building is unique in terms of its construction method and its contribution to the wider urban context of the city of Nikšić. We can conclude that the criterion of uniqueness and rarity is also met.

*B. Building significance*:

*Historical and scientific significance*: The Cathedral Church in Nikšić has a great historical significance not only because the names of the Montenegrin and Herzegovinian heroes fallen in the period of 1875–1880 are inscribed on its walls, which is very important to historians, essential for the study of the relationship between Montenegro and Russia, as well as for documenting the development of the city of Nikšić. Based on the above, we can state that the Cathedral Church fulfills the criteria of historical and scientific significance.

*Archaeological significance*: In the context of archaeology and its criteria, this building has no archaeological significance.

*Architectural and artistic significance*: At the time of its construction, the church was the largest building of its kind in the country. It is also a unique building that was built on an elevation that was additionally reinforced with subwalls. In addition to the exterior architecture, the Cathedral Church is also characterized by a valuable interior architecture. We can conclude that the criterion of architectural and artistic significance is also met.

*Technical significance*: The building was built from hewn stone from local quarries using simple tools. The stone has an exceptional finish, above all due to the skills of both local and international stonecutters, primarily those who came from Italy. Taking into account the possibilities of the time and the large construction undertaking that ultimately resulted in an object of exceptional construction quality, we can state that this object has technical significance.

*C. Other criteria*:

*Age of the building*: The Cathedral Church in Nikšić was built in 1900, and its construction lasted five years. For 123 years, this relatively well-preserved building has been a part of the collective memory

of the citizens of Nikšić, so we can state that this building fulfills the criterion of the age of the building.

*Social and economic importance*: Every year on May 12, the Great Procession is held in Nikšić, dedicated to Saint Basil of Ostrog. Several tens of thousands of visitors from all over Montenegro and neighboring countries visit Nikšić on that day. A few days before and after the procession, a large number of pilgrims affects the economic situation in the city. During all major Christian holidays, citizens visit the church, which becomes a place of spiritual gathering and socialization. We conclude that the building has social and economic importance too.

*Environmental and landscape importance*: In addition to its architectural and artistic significance, the Cathedral Church has environmental significance, which is reflected in the specific spatial solution for its location. The location is leveled on three plateaus and decorated with lush pine vegetation, which made it possible to achieve a specific environmental composition. The building is one of the most recognizable buildings and one of the main landmarks in the urban landscape of Nikšić. We conclude that the building has environmental and landscape importance.

### Upper Ostrog Monastery

*A. Building characteristics*:

*Authenticity and integrity*: The Ostrog Monastery is the largest Orthodox shrine in Montenegro and one of the most important Orthodox shrines in the world. With its location, architecture, and spiritual significance, it has confirmed its authenticity and integrity for centuries.

*Degree of preservation*: Until today, the Ostrog Monastery has preserved almost all elements of recognition, therefore they meet the criterion of the degree of preservation.

*Uniqueness and rarity*: The uniqueness of the Ostrog Monastery stems from its spiritual dimension, given that it houses the relics of Saint Basil of Ostrog. The uniqueness and rarity of the building are also reflected in its location, the monastery complex consists of two units, the Lower Monastery and the Upper Monastery, which is built on an almost vertical cliff of Ostrog mountain. With the project of the Upper Monastery, the architect Sukurenko managed to successfully connect nature and the building into a unique and harmonious whole.

*B. Building significance*:

*Historical and scientific significance*: The Ostrog Monastery fulfills the criterion of historical significance both because of its role in the history of the people, not only in this region but also beyond, through the centuries of its existence, and because of the possibility of historical research related to the records in the archives that refer to this monastery. Archaeological research could be important considering the location, artefacts from the Paleolithic period were found near the building. We can conclude that the Ostrog Monastery, especially the Upper Monastery, has great historical and scientific significance.

*Archaeological significance*: Findings of prehistoric artefacts from the Paleolithic era and traces of medieval buildings in the area of the Lower Monastery, along with the fact that no archaeological research has been carried out, indicate that the location and monastery itself have archaeological significance.

*Architectural and artistic significance*: The Ostrog Monastery has two parts: Upper and Lower Monastery. This paper dealt exclusively with the Upper Monastery whose main characteristic is its location. The Upper Monastery was built along a vertical picturesque rock at an altitude of 900 m. The interior of the Upper Monastery stands out with frescoes of artistic value, while the treasury contains valuable icons and objects. Based on the above, we conclude that the Upper Monastery has architectural and artistic significance

*Technical significance*: In terms of technical significance, the Upper Monastery stands out since it was built against a rock on rather inaccessible terrain.

*C. Other criteria*:

*Age of the building*: The Upper Monastery was built in 1665, and the Lower Monastery was built in 1820. Considering the age and degree of preservation, we can conclude that this cultural asset fulfills the criterion of the age of the building.

*Social and economic importance*: The Ostrog Monastery has been of social and economic importance for many years, considering that it is one of the most visited Orthodox Christian shrines in the world. As a result, the monastery influences the development of the region, primarily by developing infrastructure connections with Nikšić and Danilovgrad. Religious and cultural tourism can be the backbone of the development of this region. It should be noted that the monastery is visited, in large numbers, by both Roman Catholic Christians and Muslims, which confirms the social importance of the monastery.

*Environmental and landscape importance*: In terms of environmental importance, it is clear that the complex consisting of the Lower and Upper monasteries with all the associated monastery land represents a harmonious whole with the special genius loci. The plateau on which the Lower Monastery is located, together with Ostrog Mountain in which the Upper Monastery is built, forms a unique visual entity that is easy to notice, especially from the main road connecting the country's two largest cities Podgorica and Nikšić. The monastery gives a unique visual experience of the landscape both during the day and at night due to specific lighting.

Vladimir Bojković — Pages 19–33

CHARACTERISTICS AND SIGNIFICANCE OF THE WORK OF RUSSIAN ARCHITECTS IN THE CITY
OF NIKŠIĆ IN MONTENEGRO, THE END OF THE 19th AND THE FIRST HALF OF THE 20th CENTURY

**Conclusion**

Numerous historical data speak of the century's old connections between Russia and Montenegro, which confirm the great familiarity of the two Slavic nations with each other. In the last few decades, it has only begun to be determined in detail, in the field of architecture and urban planning, to what extent Russian architects contributed to the formation of architectural heritage in Montenegro. The aim of this work was to present perhaps the two most significant achievements that Russian architects designed and built in Montenegro, the Cathedral Church of Saint Basil of Ostrog in the very center of the city of Nikšić and the Upper Monastery of Ostrog near the city of Nikšić.

Considering the defined criteria of the building characteristics, on the basis of which we determine the building value, and which are fully fulfilled, we can conclude that the Cathedral Church of Saint Basil of Ostrog in Nikšić represents an exceptional architectural achievement of the architect Preobrazhensky. With this building, the architect made a great contribution to the architectural heritage of the city as well as to its morphology and spatial identity. The value of this building is reflected in the cultural and spiritual life of the citizens of not only Nikšić but also of Montenegro (Table 1).

The Ostrog Monastery has represented a unique, spiritual center and place of pilgrimage in a long historical period. In addition to records in literature and historiography, its importance has become part of the collective consciousness in an area that in many ways exceeds the state boundaries of Montenegro, making this unique building internationally recognized (Table 2).

It seems that the architects Preobrazhensky and Sukurenko understood the specifics and circumstances of the time in which they worked during their stay in Montenegro and with a personal touch designed recognizable objects that are essential elements of the spatial architectural identity not only of the city of Nikšić but also of Montenegro.

The fact that significant Russian artists are still present in the city of Nikšić with their works in the 21st century is evidenced by the sculpture of the Holy Mother, which was gifted to Montenegro in 2003 by the great Russian sculptor Vyacheslav Mikhailovich Klikov (1939–2006). The sculpture is located on Duke Šako Petrović Square, in front of the Cathedral Church of Saint Basil of Ostrog (Fig. 17).

Table 1. **Evaluation of the Cathedral Church of Saint Basil of Ostrog**

| Building | Authenticity and integrity: | Degree of preservation: | Uniqueness and rarity: | Historical and scientific | Archaeological | Architectural and artistic | Technical | Age of the building | Social and economic importance | Environmental and landscape importance |
|---|---|---|---|---|---|---|---|---|---|---|
| Cathedral Church of Saint Basil of Ostrog | + | + | + | + | - | + | + | + | + | + |
| Eligibility criteria | A. Building characteristics | | | B. Building significance: | | | | C. Other criteria: | | |

Table 2. **Evaluation of the Upper Ostrog Monastery**

| Building | Authenticity and integrity: | Degree of preservation: | Uniqueness and rarity: | Historical and scientific | Archaeological | Architectural and artistic | Technical | Age of the building | Social and economic importance | Environmental and landscape importance |
|---|---|---|---|---|---|---|---|---|---|---|
| Upper Ostrog Monastery | + | + | + | + | + | + | + | + | + | + |
| Eligibility criteria | A. Building characteristics | | | B. Building significance: | | | | C. Other criteria: | | |

Fig. 17. The sculpture of the Holy Mother by the sculptor Vyacheslav Mikhailovich Klikov, mitropolija.com

**References**

Babović Raspopović, S. (2002). *Kulturna politika u Zetskoj banovini 1929-1941*. Beograd: Godišnjak za društvenu politiku, 271 p.

Bakić, J. (2004). *Ideologije jugoslovenstva između srpskog i hrvatskog nacionalizma 1918-1941*. Zrenjanin: Gradska narodna biblioteka "Žarko Zrenjanin", 291 p.

Dašić, M. (1989). *Oporuke i zadužbina kralja Nikole*. Pobjeda br.8561, Titograd, 18 p.

Glas Crnogorca, no. 33, 1900., 5p.

Maksimović, M. (1961). *Prvi regulacioni plan Nikšića*. Komuna br.9, Beograd, 42 p.

Martinović, S. (2022). *Tvorac Ostroške Božje kuće, Istorija graditeljstva na tlu Crne Gore: Vladimir Sukurenko.* Podgorica: Pobjeda od 03.4.2022.

Milenković, T. (1995). *Ruski inženjeri emigranti u Srbiji 1919-1941.godine*. Beograd: PINUS Zapisi 2, 63-64, 70 p.

Onogošt, no. 8, 1899., 4p.

Politika, 15. septembar, 1921., 21p.

Radović, R. (2009). *Forma grada, osnove, teorija i praksa*. Beograd: Građevinska knjiga, 90 p.

Rastoder, Š. (2011). *Crna Gora u XX vijeku*. Podgorica: CANU, 345 p.

Službeni glasnik Zetske oblasti od 13.3.1926., 2p.

Šakotić, V. (1996). *Nikšić u knjaževini (kraljevini) Crnoj Gori. Nikšić:* Centar za informativnu djelatnost, 115 p.

Toševa, S. (2012). *Arhitektonsko odeljenje Ministarstva građevina Kraljevine Jugoslavije i njegov uticaj na razvoj graditeljstva u Srbiji između dva svetska rata. PhD teza.* Univerzitet u Beogradu.

Toševa, S. (1999). *Arhitektonsko odeljenje Ministarstva građevina u periodu između dva svetska rata.* Beograd: Nasleđe II, 172 p.

Žunjić, S. (2019). *Arhitektura u Crnoj Gori 1918-1941. godine. PhD teza.* Univerzitet u Beogradu.

Vladimir Bojković — Pages 19–33

CHARACTERISTICS AND SIGNIFICANCE OF THE WORK OF RUSSIAN ARCHITECTS IN THE CITY
OF NIKŠIĆ IN MONTENEGRO, THE END OF THE 19th AND THE FIRST HALF OF THE 20th CENTURY

# ОСОБЕННОСТИ И ЗНАЧЕНИЕ ТВОРЧЕСТВА РУССКИХ АРХИТЕКТОРОВ В ГОРОДЕ НИКШИЧ В ЧЕРНОГОРИИ В КОНЦЕ XIX – ПЕРВОЙ ПОЛОВИНЕ XX ВЕКА

Владимир Бойкович

Университет Черногории, Подгорица, Черногория

E-mail: bojkovicv@gmail.com

**Аннотация**

**Введение:** на протяжении своей долгой и драматической истории Черногория имела тесные политические, экономические и культурные связи с Россией. Однако в контексте архитектуры связи между этими двумя странами наименее известны и изучены. **Цель исследования:** цель настоящей работы — впервые представить широкой профессиональной аудитории некоторые из наиболее значительных достижений, созданных русскими архитекторами в городе Никшич в Черногории в конце XIX – первой половине XX века. В качестве предмета анализа рассматриваются проект соборного храма Василия Острожского, выполненный архитектором Михаилом Тимофеевичем Преображенским, и проект Верхнего Острожского монастыря, наиболее значительного достижения архитектора Владимира Сукуренко. **Методы:** методологический подход предполагал классификацию и сравнение архивных материалов через процессы синтеза, анализа и дедукции. Основываясь на положениях Закона о защите культурных ценностей Черногории, мы сформировали критерии, которые использовались для оценки работ вышеупомянутых архитекторов. Критерии разделены на три группы. Первая группа включает в себя характеристик здания, где мы оцениваем аутентичность и целостность, степень сохранности, уникальность и редкость. Во второй группе, относящейся к значимости здания, мы оцениваем историческую и научную значимость, археологическую значимость, архитектурно-художественную значимость и техническую значимость. Наконец, в третьей группе критериев мы оцениваем возраст здания, социально-экономическую значимость, а также значимость с точки зрения окружающей среды и ландшафта. **Результаты**: с учетом предложенных критериев сделан вывод о том, что соборный храм Василия Острожского является символом и важнейшим пространственным элементом идентичности города Никшич, а Верхний Острожский монастырь, одна из важнейших святынь ортодоксального христианства, представляет собой вершину строительного и архитектурного процесса.

**Ключевые слова:** Михаил Тимофеевич Преображенский, Владимир Сукуренко, Никшич, Черногория.

# HABERMAS MODEL AND AESTHETIC PREFERENCE EVALUATION OF HOUSE FACADES: INSIGHTS FROM ERBIL CITY

Nura B. Hamad*, Salahaddin Y. Baper

College of Engineering, University of Salahaddin, Erbil, Iraq

*Corresponding author's e-mail: architnura.1@gmail.com

**Abstract:**
**Introduction:** Architecture is a discipline distinguished through diversity, message transmission, and communication. **Purpose of the study:** A notable phenomenon has been noticed in Erbil: most of the units in the typical housing complexes started to redesign or change the facade characteristics. These changes were the result of the psychological trait of aesthetic preference. This study aims to analyze aesthetic preference parameters to identify communicative action using the Habermas model of communicative action. The analysis of the effective factors contributed to the understanding of these changes. **Methods:** The methodology of this study combines case study formal analysis and a proper questionnaire survey. A statistical analysis of the obtained results was used to formulate research objectives. **Results:** Five parameters derived from the theoretical framework (unity, scale, color, proportion, and balance) serve as elements and principles of design that affect the aesthetics. As a result, the study concludes that unity, proportion, and balance are the main factors to create a pleasing aesthetic appearance on the house facades.

**Keywords:** communicative action, aesthetic preferences, diversity, residential complex, facade house, design principle.

## Introduction

The aesthetic value of a building's facade refers to the visual appeal and overall design of the building's exterior. It encompasses the beauty and artistry of a building, as well as its ability to evoke emotions and feelings in those who experience it. The built environment of humans should not only respond to physical comfort criteria but also aim to promote the psychological well-being of communities by promoting people's happiness and encouraging communication in society (Prieto and Oldenhave, 2021). Communicative action is seen as a fundamental aspect of human social interaction and is in contrast with strategic or instrumental action, which is focused on achieving specific goals or outcomes. Communicative action, as developed by German philosopher Jürgen Habermas, refers to a theory of social action and communication in which individuals engage in a process of mutual understanding and agreement-seeking through language and discourse (Bolton, 2005). In the context of architecture, communicative action can be applied to the design of buildings and spaces to facilitate communication and interaction between people. This can include using shared spaces and places where people can get together, as well as adding cultural and symbolic elements that help people feel like they belong and understand each other (Sharlamanov and Jovanoski, 2014). Aesthetics can play an important role in increasing communicative action between humans and their surroundings. The design of a building or space can influence the way people feel, behave, and interact

with one another (Prieto and Oldenhave, 2021). For example, the use of natural light and views can create a sense of connection to the outdoors, and the use of natural materials such as wood and stone can create a sense of warmth and comfort. Art and other cultural elements can also help the people who live in a building feel like they have a shared identity and understand each other better (Ferwati and Mandour, 2008). The aesthetic of a building can be influenced by a variety of factors, including the historical and cultural context in which it was built, the architect's style and design philosophy, the elements and principles of design, and the functional requirements of the building.

In architecture, elements and design principles are used to make buildings that function well and look good. Design elements like line, shape, form, texture, value, and color are used to make a building of good appearance. The principles of design, such as balance, contrast, emphasis, movement, pattern, proportion, and unity, are used to create a sense of harmony and coherence in the overall design of a building (Han et al., 2021). Every building's visual appeal is just as important as its structural stability and quality of materials because it is the first thing that people notice when they walk into a space. Attitudes about aesthetics in the present day draw from historical examples but have evolved (Sagaonkar and Narkhede, 2018). A more aesthetic appearance of a house facade attracts humans and facilitates communication between them (Rezapour et al., 2017). In Iraq, particularly in Erbil, in the second half of the 20th century, aesthetic architecture began

to take place, especially after the development of the economy and increase in population, and residential complex projects gained more attention (Board of Investment, 2020). But after some time, the house dwellers start changing their facades inside the complex, as humans have an instinctive interest in aesthetics. Many factors contributed to this shift, including climate considerations, the environment, human desires and beliefs, psychological needs, technological development, and building quality (Ghomeishi, 2021). Typical Houses are built with repetition, reducing diversity and communication between humans and their surroundings. The goal of this study is to use the Habermas model of communicative action to analyze aesthetic preference parameters of the house facades based on the factors that contributed to this change. This study used exploratory mixed methods, both qualitative and quantitative, including a questionnaire survey and case study analysis to develop a framework for evaluating an effective factor that contributes to greater community action.

### Theoretical Framework

#### Jürgen Habermas and Communicative Action:

The model of communicative action is seen as a process in which participants exchange not just information, but also understandings, justifications, and valid arguments. The success of communicative action depends on the quality of the arguments presented and the level of mutual understanding and agreement reached (Smulders et al., 2008).

Jürgen Habermas developed a theory of communicative action. The most influential author of the second generation of the Frankfurter school of sociology, in the beginning of the 1970s he started developing his social theory, above all dedicated to analyzing communication (Bolton, 2005; Sharlamanov and Jovanoski, 2014). Habermas argued that communication can be divided into two types: strategic action, which is aimed at achieving a specific goal or outcome, and communicative action, which is aimed at reaching mutual understanding and agreement (Sharlamanov and Jovanoski, 2014), as shown on Fig 1.

#### Communication in Architecture

The architectural process encompasses various communicative actions within distinct subject sectors, including social, educational, regulatory, and creative realms (Tarasova and Markova, 2018). Each of these domains entails its unique set of activities. Communicative architecture necessitates the involvement of multiple stakeholders who share information, responsibilities, and resources. The evaluation of architectural aesthetics is contingent upon the perceptions of individuals within the contextual living environment. Hence, the communicative process becomes an information interaction among participants involved in architectural events and processes across social, educational, regulatory, and creative domains (Tarasova and Markova, 2018).

#### Building Facades as Communicative Elements

Building facades serve as a form of communicative action conveying information and ideas about the building and its occupants to observers (Sharlamanov and Jovanoski, 2014). The design and materials employed in a building facade can communicate diverse messages, such as the building's function, the social standing of its inhabitants, and the cultural or historical context of its construction. Thomas Herzog emphasizes the role of the facade in conveying messages, suggesting that the human eye perceives various codes from the building, leading to a feedback loop of understanding (Bolton, 2005).

The initial impression is profoundly shaped by exterior elements, encompassing materials, shape, color, texture, as well as design principles and elements. An individual's visual satisfaction with the facade creates a lasting connection between humans and their built environment (Akalin et al., 2009; Sharlamanov and Jovanoski, 2014). There is a direct positive relationship between urban space, represented by building facades, and communicatve action (Rezapour et al., 2017). This relation is a dynamic interplay that significantly influences the urban experience. The city townscape, with its architectural diversity, infrastructure, and open spaces, provides the canvas for this complex interaction. Building facades, as the external faces of structures, play a pivotal role in shaping the visual identity of the city (Ghomeishi, 2021).

They serve as communicative surfaces that convey information about a building's purpose, style, and historical context to its human inhabitants and



Fig. 1. Types of social action (Source: Sharlamanov and Jovanoski, 2014, Designed by Author)

visitors. In return, humans actively engage with the city, navigating its streets, interacting with building facades, and forming communities within this urban framework. The aesthetics and functionality of building facades can greatly affect the overall character of the townscape, influencing human perceptions, behaviors, and emotions (Ghomeishi, 2021).

The success of communicative action through facades relies on how effectively they engage and resonate with people, ultimately shaping the way individuals experience and interact with the city. Thus, the city townscape, building facades, communicative action, and humans are intricately linked, with each element influencing and being influenced by the others, ultimately contributing to the vitality and identity of urban environments.

*Factors Influencing Communicative Action in Architecture*

Multiple factors contribute to the manifestation of communicative action in architecture, including environmental conditions, cultural and historical contexts, amenities, economic development, and the building's immediate context (Rezapour et al., 2017). Aesthetic considerations and creativity also play crucial roles in this context (Aysha Jennath and Nidhish, 2015). Creativity in architectural design is a potent tool for architects and designers to express their unique vision and imbue houses with aesthetic value (Han et al., 2021), as shown on Fig 2.

Creativity in architecture is closely intertwined with communication, representing a means to create a distinct and meaningful expression of a house and its occupants (Baper, 2001). It is important to distinguish between creativity and aesthetics, as creativity significantly influences the design process and its outcomes, while aesthetics often serves as the defining characteristic of architectural products (Han et al., 2021).

In light of the multifaceted nature of architectural communicative action and its complex determinants, this research paper focuses on the role of aesthetics as a fundamental factor contributing to communicative action within architectural contexts.

*Erbil House Facades as a Case Study*

The architectural facade of a building gives the first impression of its style, materials, and details. It is also frequently the most decorative or detailed part (Akalin et al., 2009). Erbil is the capital of the Kurdistan Regional Government (KRG) in Iraq and one of the country's largest cities. It is one of the world's oldest cities as well, dating back to at least 2300 BCE (UNESCO, 2014). Previously, Erbil was rich in vernacular architecture with local materials; then, after technological development, the western style penetrated local culture. Architecture in Erbil has entered a new era, which can be seen in house facades (Ahmed and Baper, 2022). Facade is not only a reflection of the architectural character of a region but also a representation of local cultural, social, climatic, political and economic circumstances. (F. H. Abdullah. et al,, 2016). The figures below show examples of various facade designs in Erbil. The implementation of a facade design may differ depending on environmental, social, and cultural elements, the designer's conceptions, political views, and economic and historical importance (Askari and Dola, 2009). According to Abdel-Aziz and Shuqair (2014), a house facade has three primary zones: a foundation that ties the building to the earth, a middle zone with openings, and a roof zone that connects the building to the sky through its silhouette. Building facades combine a variety of aspects resulting from the arrangement of the roof, openings, materials, architectural details, and the most important element, the design idea (Abdel-Aziz and Shuqair, 2014). Economic development of the population in Erbil resulted in increased attention to housing complexes; several projects have been built around Erbil with differences in size, designs, and location. However, after a while, habitants began to change the facades of the houses due to several factors including: the development of technologies and new materials, quality of the building, climate consideration, desire, and beliefs, physiological needs, user identity, environment, aesthetic improvement, increased property value, maintenance and repair, as well as energy efficiency. The most effective factor was aesthetic improvement as shown in Fig. 3.

Analyzing house facades provides useful information and a great understanding of aesthetic appearance (Askari and Dola, 2009). The facades of the houses in Erbil city witnessed great development. The styles used are modern, contemporary, and neoclassical (Ahmed, 2022). The elements concentrated on facades are openings (entrance and windows, ornamentation, columns, and composition
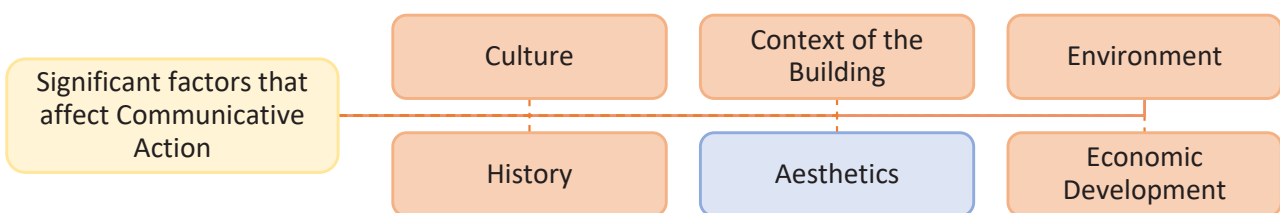


Fig. 2. Factors that affect CA (source: Han et al., 2021, Baper.,2021, Aysha Jennath and Nidhish, 2015, designed by Author)
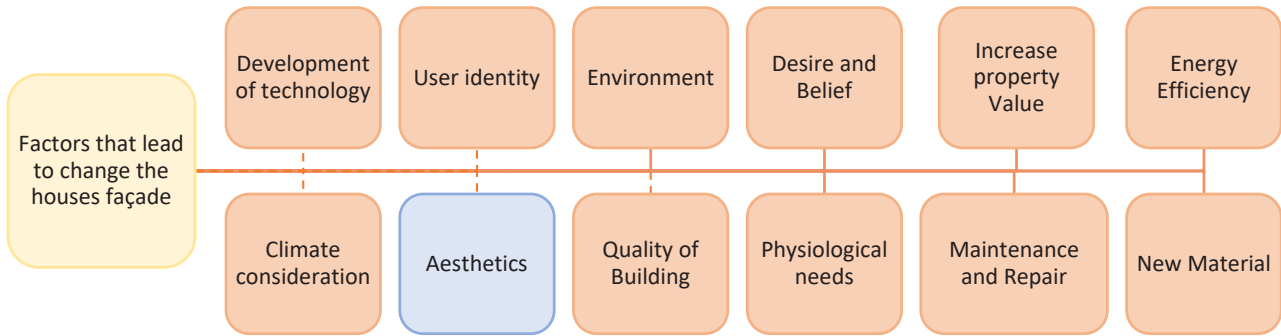
Fig. 3. Factors that lead to alternating the house facade( Designed by Author)

of masses). There are also principles of design, the scale of physical property, proportion, color, unity, and balance. According to (F. H. Abdullah. et al,, 2016)"facade is the first and most impacting connection between humans and the built environment, the outer shell of a building is not only a reflection of the architectural character of a region but also a representation of local cultural, social, climatic, political and economic circumstances". This is the result obtained via observation and is also true for the selected case studied. The figure below shows a level of alternation, a case of Italian City 2 complex in Erbil. The Figs. 4 and 5 shows a level of alternation, a case of Italian City 2 complex in Erbil. The line of the houses along the street was altered: the concept of the typical housing units starts disappearing. This is happening because aesthetic appeal can be a significant motivating factor for inhabitants of a residential complex to alter their home facades. The appearance of a person's home can represent his or her personality, ideals, and social standing. Aesthetic enhancements to the home's exterior can be viewed as a method for residents to express themselves, distinguish their home from others, and communicate a sense of pride and ownership (Salih, 2019).

*Factors Affecting Aesthetic Value of House Facades*

The exterior facade of a building, frequently referred to as the frontage, encompasses the architectural design and detailing of the building's front aspect. This brings about considerations related to the materials employed, the arrangement of windows and doors, and the integration of decorative elements. Additionally, the facade extends to encompass roofing and other exterior features, such as porches and balconies (Majid, 2022).

The house facade comprises two distinct categories of components: physical and nonphysical. Physical components are tangible elements that constitute the building's exterior and include aspects such as openings, mass geometry, articulation type, materials, arches, ornaments, porches, balconies, lighting, and fencing (Fig. 6).

On the other hand, nonphysical components pertain to elements and principles of design. Elements of design in architecture serve as fundamental building blocks utilized by architects in their creative endeavors. These elements encompass line, shape, form, space, texture, color, light, volume, and functionality (Ferwati and Mandour, 2008).

Principles of design in architecture pertain to how the elements of design are organized and employed to craft a coherent and aesthetically pleasing architectural design. Architects utilize these principles as guiding criteria for their design decisions, thereby creating visually captivating and functional designs. A comprehension and effective application of these principles empower architects to fashion buildings that seamlessly combine beauty



Figs. 4 and 5. House facade alternation (source: captured by author)
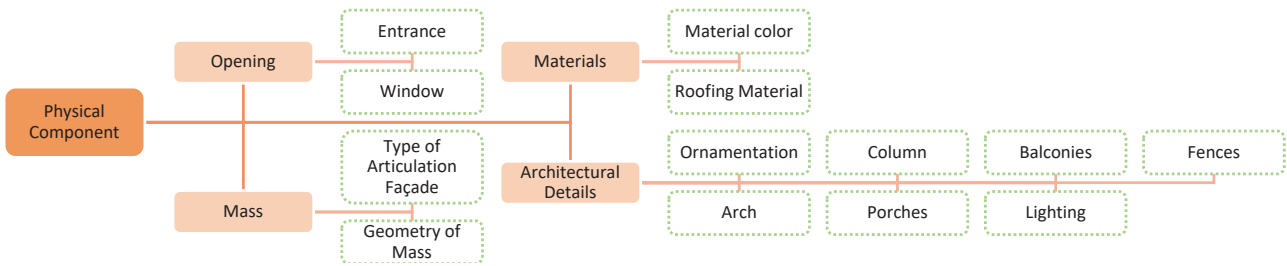
Fig. 6. Physical components of a building (Source: Designed by Author)
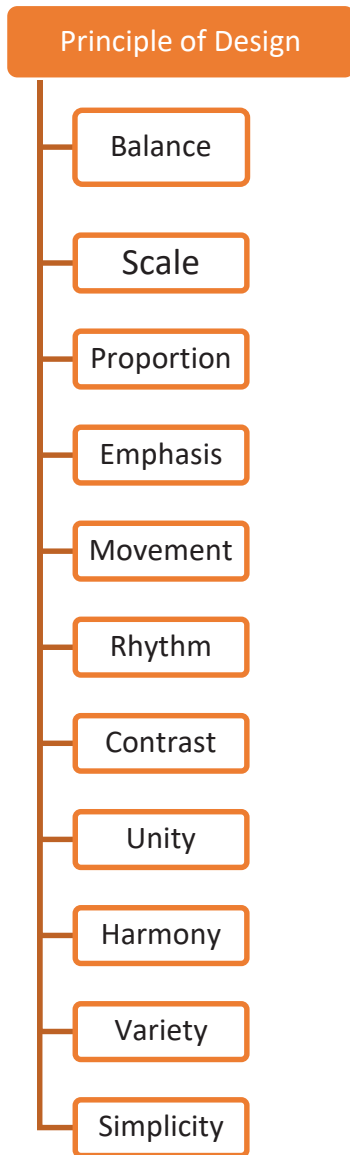


Fig. 7. Principles of design (source: Designed by Author)
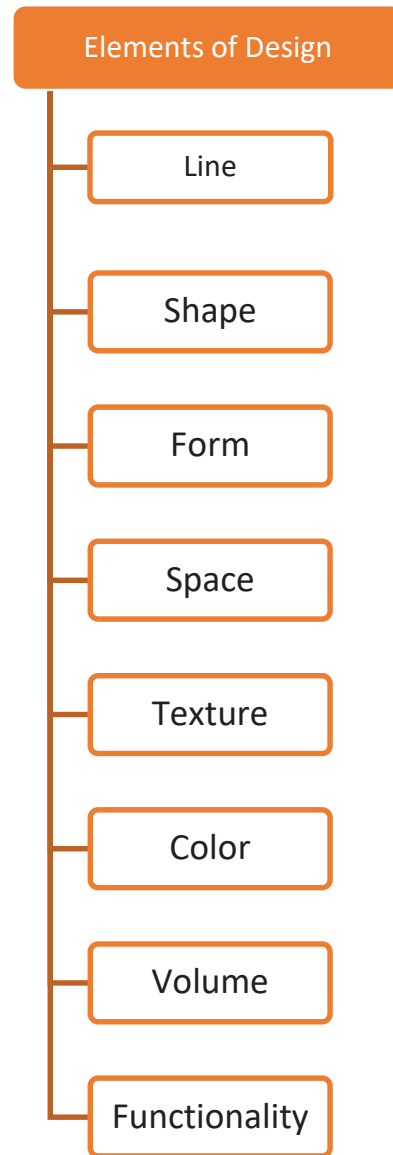


Fig. 8. Elements of design (source: Designed by Author)

and functionality. Examples of principles of design in architecture include balance, scale, proportion, emphasis, movement, rhythm, contrast, unity, harmony, variety, and simplicity (Pirhadi et al., 2017) are shown on Figs. 7 and 8.

In the context of facade aesthetics, numerous design elements and principles exert their

influence. This paper underscores the most pivotal factors contributing to the aesthetic value of facades, including unity, scale, color, proportion, and balance (Ferwati and Mandour, 2008). These elements and principles (Fig. 9) play a leading role in shaping the visual appeal and overall impression of building exteriors, making them
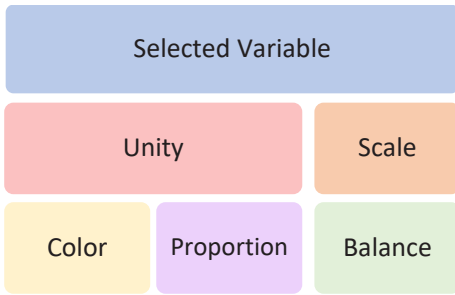
Fig. 9. Design variable (source: Designed by Author)

crucial considerations in architectural design and the assessment of facade aesthetics.

**Materials and Methods**

This paper employs a mixed-method approach, integrating both quantitative and qualitative methodologies, to comprehensively investigate the correlations and implications of aesthetic appearance in house facades. The initial methodology entails an analysis of case studies, delving into the repercussions of aesthetic preferences on house facades within Erbil. The subsequent method involves the implementation of a questionnaire survey, chosen as the primary research strategy for acquiring quantifiable data from the designated populace (individuals with a background in the field of architecture) to substantiate the research framework. The sequential progression of research methodology steps is visually represented in Fig. 10.

*Case Study*

The focal point of this study centers on the house facades within residential complexes situated in Erbil. For the purpose of case selection, eight distinct cases were chosen, employing specific criteria: zone location, land value, style approach, building quality, number of floors, project status, allowance for alternations, percentage of reconstruction, and

societal popularity. These criteria were meticulously devised based on a comprehensive review of pertinent literature and insightful discussions with real estate experts in Erbil. The chosen case studies, namely Royal City, English Village, Dream City, Italian City 2, Gunjan City, Zen City, Erbil Gate Complex, and Hiwa City, are delineated in the Appendix.

*Questionnaires*

A comprehensive distribution of 300 questionnaires was administered to individuals possessing a background in architecture, encompassing both architecture students and professionals in Erbil. Out of these, 217 questionnaires were effectively completed and returned, reflecting a notable response rate of 72.3 %. The collected dataset underwent meticulous analysis using the Social Package for Soft Sciences (SPSS). Consequently, the examination yielded outcomes from 217 respondents, with 53.9% of participants identifying as male and 46.1% as female.

**Results and Discussion**

*Evaluation of the Factors Affecting the Aesthetic Value of the House Facade*

In relation to the primary factors influencing aesthetic preference in house facades, the data indicate that 25.1% of the respondents acknowledged the impact of the design principle of Unity, while 22.3% attributed this effect to Proportion. Furthermore, Scale received an average agreement of 15.3%, while both Balance and Color garnered an average agreement of 18.4% as presented in table 1 the respondents notably associated the aesthetic preference of house facades with elements and principles of design. These findings affirm the alignment of the study's focus on house facades as visually prominent aspect of a building's structure with the perspectives of the participants concerning matters of aesthetic preference for house facades.
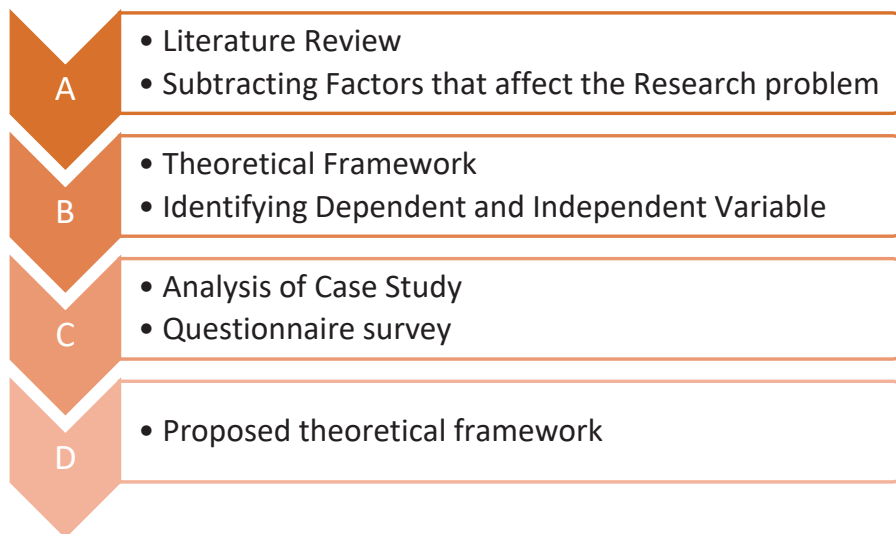


Fig. 10. Research Methodology (Source: Designed by Author).

Table 1. **Descriptive analysis Factors that affect aesthetics**

| Variable | Responses | |
|---|---|---|
| | N | Percent |
| Unity | 89 | 25.1 % |
| Proportion | 79 | 22.3 % |
| Scale | 54 | 15.3 % |
| Balance | 65 | 18.4 % |
| Color | 65 | 18.4 % |
| Other | 2 | 0.6 % |
| Total | 354 | 100.0 % |

*Analysis of Case Studies*

The case study approach aligns with one of its formal definitions, characterized as "an empirical study that investigates a contemporary phenomenon within its real-life setting, particularly when the boundaries between the phenomenon and its context are not immediately distinct". To achieve an in-depth comprehension of the phenomenon of facade alteration, a selection of case studies was undertaken in Erbil based on the aforementioned criteria. The analysis encompassed nine distinct cases through a meticulous examination of facade designs, with the aim of identifying the principal elements contributing to the aesthetic value of houses, thereby aiding in the development of a theoretical model. The characteristics of each selected case study presented in Table 2.

*Common Characteristics of Selected Case Studies*
• The selected case studies employed both modern and neo-classical architectural styles.
• Incorporating a larger entrance gate and windows contributes to a visually appealing exterior appearance for houses.
• The rhythmic arrangement of windows on the facade significantly influences preferences for aesthetic value.
• The inclusion of large-scale columns at the facade's forefront adds a sense of grandeur and aesthetic value.
• Skillful utilization of appropriate ornamentation scale enhances the impressive look of the house facade and creates a feeling of splendour.
• The use of uniform colors enhances the aesthetic value of the house facade by fostering a sense of unity.
• Textures like natural stone, brick, or concrete, characterized by rough surfaces, are favored over materials like aluminum or steel, as they infuse vitality into the facade.
• Imposing regularity in the composition of elements contributes to the aesthetic value conveyed by the facade.

*Factors Analysis*
*Proposed Theoretical Model*
As a result of the analysis of the case study and questionnaire survey, this theoretical model was figured out, which represents five parameters consisting of scale, balance, color, proportion, and unity. The first parameter, Scale, has two dimensions,

Table 2. **Characteristics of the housing complexes ("cities")**

| Name of Complex | Characteristics |
|---|---|
| *Royal City* | One of the most luxuriant housing complexes in Erbil: the house facades reflect unity, harmony and rhythm between a facade and its constituent parts; the modern and neo-classical styles give the city a diverse look, it is balancing between solid and void, by using dark and light colors. |
| *English Village* | English Village is one of the cities with minimum alternation; with classical style, "form follows function" reflected in the facade, small- and large-scale of openings, the facade looks unbalanced to the human eye; the city has light colors and the minimum proportion between the whole and the parts. |
| *Dream City* | The city has modern, classical, contemporary, and neo-classical styles, with unity reflected between all parts in the facade; the facades use symmetrical and asymmetrical balance; with light and dark homogenous colors, the facades are designed proportionally; large-scale openings and architectural detail are reflected in the design. |
| *Italian City 2* | This city was almost completely changed from its basic company design; it has modern, classical, and neo-classical design, unity between all parts reflected in the facades, large-scale openings and architecture detail, harmony and rhythm between facades and their constituent parts; light and dark color available, balancing between solid and void; symmetrical and asymmetrical balance in facades. |
| *Ganjan City* | Ganjan City was one of the diverse cities of house design type in size and style; what was selected for our case was classical style, reflecting unity between all parts, proportional and harmonious design, large-scale openings, solid fences reflect the privacy in contrast with the other selected cities; symmetrical balance reflected in facades. |
| *Zen City* | This city has both classical and modern design, symmetrical and asymmetrical balance in the facades; houses were designed in a proportional way which reflects harmony and rhythm; large- and small-scale openings were seen in the facades; unity between solid and void. |
| *Erbil Gate* | This city has both neo-classical and modern styles, facades with large-scale openings; houses focus on architectural detail and ornamentation, a symmetrical balance, unity of the whole in the facades; all physical properties with design elements are proportional; light and dark color used in the facades. |
| *Hewa City* | This city of neo-classical style with architectural details seen very strongly in the facade, balancing between the solid and void; symmetrical balance in the facade design and unity between all parts create an aesthetic appearance; large-scale openings; the facade design is proportional, which reflects harmony and rhythm between the facades and their constituent parts. |

namely 1) emphasis on the elements of design, 2) scale of openings. The second parameter, Balance, has two factors 1) symmetry/ asymmetry and 2) balance between solid and void. Color has two factors: 1) dark and light color and 2) homogeneiety of color. Proportion has three factors such as 1) the golden ratio, 2) unity and simplicity. The last parameter of unity has two factors: 1) harmony and rhythm, 2) regularity. The proposed conceptual framework is presented in Fig. 11.

*Multiple Regression Analysis*

Multiple regression analyses were conducted to test the changing average between the selected parameters. The formula of multiple regression was employed to determine the variance of each component of the aesthetic appearance parameter. The independent variables were five variable parameters of 1) scale, 2) unity, 3) color, 4) proportion, and 5) balance; the dependent variable was the communicative action in the house facade. Due to that a regression model was created to determine the relationships between variables.

• The application of the golden ratio is consistently observed on the facade.

• Arranging columns symmetrically contributes to an air of royalty and grandeur.

• Introducing symmetrical balance to the facade unifies its appearance.

• Implementing proportion between shapes and masses on the facade has a positive impact.

• The use of light colors on the facade creates visual balance and comfort for viewers.

• Facades painted with dark colors evoke a sense of power and dominance.

• Emphasizing the entrance porch fosters a welcoming and regal ambiance on the facade.

• Incorporating steel fences in the yard establishes a connection between the interior and exterior spaces.

As shown in Table 3, the first parameter, scale ($\beta = 0.090$, $p = 0.994$), showed no significant effect on communicative action within the house facade. However, the balance parameter demonstrated a relationship with communicative action, with an average of 30% ($\beta = 0.232$, $p = 0.000$), signifying a positive and significant association. This parameter corresponds to 0.307 change in communicative action on the house facade. Conversely, the color parameter with values ($\beta = -0.010$, $p = -0.887$) exhibited a negative and significant change in communicative action. Meanwhile, proportion with values of ($\beta = 0.148$, $p = 0.020$) and unity with
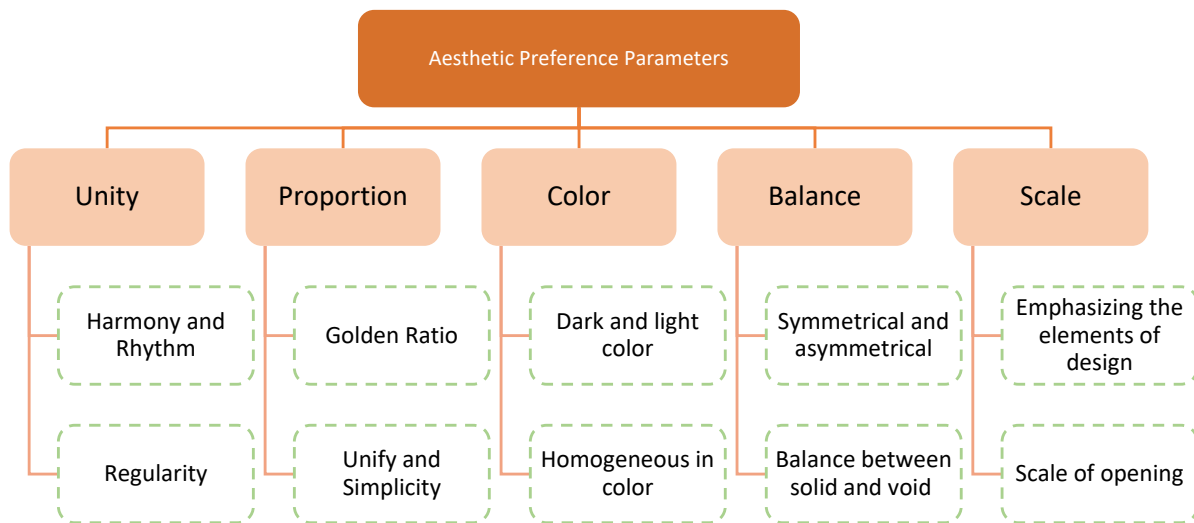


Fig. 11. Proposed theoretical framework (Source: Designed by Author)

Table 3. **Multiple regression analysis**

| Coefficients | | | | | | | |
|---|---|---|---|---|---|---|---|
| Model | | | | T | Sig. | Collinearity statistics | |
| | B | Std. error | Standardized β | | | Tolerance | VIEW |
| (Constant) | 1.256 | 0.206 | | 6.112 | 0.000 | | |
| Scale | 0.090 | 0.056 | 0.090 | -0.010 | 0.994 | 0.681 | 1.469 |
| Unity | 0.307 | 0.071 | 0.350 | 4.328 | 0.000 | 0.386 | 2.592 |
| Color | -0.010 | 0.069 | -0.010 | -0.142 | -0.887 | 0.499 | 2.006 |
| Proportion | 0.148 | 0.063 | 0.172 | 2.347 | 0.020 | 0.470 | 2.129 |
| Balance | 0.232 | 0.061 | 0.275 | 3.839 | 0.000 | 0.494 | 2.026 |

values of ($β$ = 0.307, $p$ = 0.000) both displayed a positive relationship with communicative action in the house facade. As a result, balance, unity, and proportion emerged as the main influential factors impacting communicative action. The presented model represents the outcome of multiple regression analysis, indicating the extent of change in communicative action due to these factors.

*Equation 1 multi-regression equation*

Communicative action = $β^1$ + $β1$ Scale + $β2$ Balance+ $β3$ Color+ $β4$ Proportion+ $β5$ Unity+ $ε$

$β$ = constant

$ε$ = standard error

Communicative action = 1.256 + 0.09 Scale + 0.232 Balance – 0.010 Color+ 0.148 Proportion+ 0.307 Unity+ 0.20

**Conclusion**

In conclusion, this research paper delved into the intricate relationship between aesthetics and communicative action (CA) on house facades, guided by Jürgen Habermas's model. CA, as a vital aspect of connecting humans with their built environment, is influenced by numerous factors, including the environment, culture, history, contextual elements, psychosocial factors, and aesthetics. The interplay between aesthetic appearance and CA is a complex one, where each can both influence and be influenced by the other in multifaceted ways.

Aesthetic appearance serves as a potent tool in fostering CA, as it can effectively convey codes and meanings about a building. Conversely, CA can exert its influence on aesthetic appearance by shaping the design's messages and meanings, thereby influencing its visual representation. Particularly in residential complexes, where residents often have a profound emotional attachment to their homes,

_____

[1] The beta coefficient is the degree of change in the outcome variable for every 1-unit of change in the predictor variable.

aesthetic improvements to house facades serve as a means for self-expression, differentiation, and a source of pride and ownership. Well-maintained and visually appealing homes contribute to the desirability of a community, making it more attractive.

Through a comprehensive analysis that included case studies in Erbil and a questionnaire survey, this research identified key effective factors influencing the creation of aesthetic appearances in house facades. Elements and design principles such as unity, proportion, scale, color, and balance emerged as pivotal in enhancing aesthetic appeal. Among these, balance, unity, and proportion stood out as primary and influential factors in shaping CA in building design. Architects and designers can harness these elements thoughtfully to craft building facades that are not only visually appealing but also functional, effectively communicating messages to the public.

In summary, this study underscores the reciprocity of the relationship between aesthetic appearance and CA, with each element capable of influencing and molding the other. The interplay of communicative and aesthetic facets in design is crucial for conveying information, meaning, and visual appeal, ensuring a harmonious integration of function and aesthetics in our built environment.

## References

Ahmed, L. S. and Baper, S. Y. (2022). Place branding assessment through factors affecting iconic value in Erbil city of Iraq. *International Transaction Journal of Engineering,Management, & Applied Sciences & Technologies,* Vol. 13, No. 12, pp. 1–12. DOI: 10.14456/ITJEMAST.2022.236.

Akalin, A., Yildirim, K., Wilson, C., and Kilicoglu, O. (2009). Architecture and engineering students' evaluations of house façades: Preference, complexity and impressiveness. *Journal of Environmental Psychology,* Vol. 29, Issue 1, pp. 124–132. DOI: 10.1016/j.jenvp.2008.05.005.

Askari, A. H. and Dola, K. B. (2009). Influence of building façade visual elements on its historical image: case of Kuala Lumpur City, Malaysia. *Journal of Design and Built Environment,* Vol. 5, pp. 49–59.

Aysha Jennath, K. and Nidhish, P. J. (2015). Aesthetic judgement and visual impact of architectural forms: a study of library buildings. *Procedia Technology*, Vol. 24, pp. 1808–1818. DOI: 10.1016/j.protcy.2016.05.226.

Baper, S. Y. (2001). Communicative action in architecture. *Iraqi Journal of Architecture,* Issue 2, pp. 120–135.

Board of Investment (2020). *List of licensed projects in Kurdistan region.* Erbil: Board of Investment. https://gov.krd/boi-en/publications/licensed-projects/ [Access date:2021/11/16]

Bolton, R. (2005). *Habermas's theory of communicative action and the theory of social capital*. Williamstown: Center for Environmental Studies, Williams College*,* 39 p.

F. H. Abdullah. et al,, 2016. Defining Issue of Thermal Comfort Control through Urban Mosque Façade Design. Procedia - Social and Behavioral Sciences , Volume 234, p. 416 – 423.

Ferwati, M. S. and Mandour, M. A. (2008). Proportions and human scale in Damascene courtyard houses. *International Journal of Architectural Research Archnet-IJAR,* Vol. 2, Issue 1, pp. 247–263. DOI: 10.26687/archnet-ijar.v2i1.185.

Ghomeishi, M. (2021). Aesthetic preferences of laypersons and its relationship with the conceptual properties on building façade design. *Journal of Asian Architecture and Building Engineering,* Vol. 20, Issue 1, pp. 12–28. DOI: 10.1080/13467581.2020.1782209.

Han, J., Forbes, H., and Schaefer, D. (2021). An exploration of how creativity, functionality, and aesthetics are related in design. *Research in Engineering Design,* Vol. 32, Issue 3, pp. 289–307. DOI: 10.1007/s00163-021-00366-9.

Majid, Z. K. (2022). Exterior façade design and its impact on boosting business and attracting customers in retail sectors. *Journal of Design, Business & Society,* Vol. 8, Issue 1, pp. 69–86. DOI: 10.1386/dbs_00033_1.

Pirhadi, M., and Tavakoli, F. (2017). The study of the concept of aesthetics in architecture derived from the ideas of Jörg Kurt Greuther. *International Journal of Urban and Civil Engineering,* Vol. 4, No. 5, pp. 397–418

Prieto, A. and Oldenhave, M. (2021). What makes a façade beautiful? Architects' perspectives on the main aspects that inform aesthetic preferences in façade design. *Journal of Facade Design and Engineering,* Vol. 9, No. 2, pp. 21–46. DOI: 10.7480/jfde.2021.2.5540.

Rezapour, M., Bahrainy, S. H., Tabibian, M. (2017). Analysis and assessment of communicative action indicators and variables; a case of Tehran city. *Space Ontology International Journal,* Vol. 6, Issue 4, pp. 49–58.

Sagaonkar, K. and Narkhede, P. G. (2018). Aesthetics in architecture – a historical study. *International Journal of Engineering Research,* Vol. 7, Special Issue 1, pp. 63–65. DOI: 10.5958/2319-6890.2018.00022.3.

Salih, A. B. M. (2019). The characters of the form in the vernacular architecture. A comparative study of the form's characters of facades of individual houses and commercial buildings in the City of Baghdad after 2003–Zayoona district as a case study. *Journal of Engineering,* Vol. 25, No. 7, pp. 145–164. DOI: 10.31026/j.eng.2019.07.09.

Sharlamanov, K. and Jovanoski, A. (2014). Analysis of theory of communicative action. *Journal of Language, Individual & Society,* Vol. 8, pp. 365–371.

Smulders, F., Lousberg, L., and Dorst, K. (2008). Towards different communication in collaborative design. *International Journal of Managing Projects in Business,* Vol. 1, Issue 3, pp. 352–367. DOI: 10.1108/17538370810883819.

Tarasova, I. and Markova, Ye. (2018). *Communication in architectural practice and theory with reference to city of Ekaterinburg. IOP Conference Series: Materials Science and Engineering,* Vol. 451, 012174. DOI: 10.1088/1757-899X/451/1/012174.

UNESCO (2014). *Erbil Citadel*. [online] Available at: https://whc.unesco.org/en/list/1437/ [Aceess Date: 2014/6/21]

Appendix

Table 1. **Table of Case studies** (source: author)

| Name of Complex | Case 1 | Case 2 | Case 3 |
|---|---|---|---|
| Royal City |  |  |  |
| English Village |  |  |  |
| Dream City |  |  |  |
| Italian City 2 |  |  |  |
| Ganjan City |  |  |  |
| Zen City |  |  |  |

| Name of Complex | Case 1 | Case 2 | Case 3 |
|---|---|---|---|
| Erbil Gate |  |  |  |
| Hewa City Zone A |  |  |  |

# МОДЕЛЬ ХАБЕРМАСА И ОЦЕНКА ЭСТЕТИЧЕСКИХ ПРЕДПОЧТЕНИЙ В ФАСАДАХ ДОМОВ: ОПЫТ ГОРОДА ЭРБИЛЬ

Нура Б. Хамад*, Салахаддин Ю. Бапер

Инженернsq колледж, Университет Салахаддин, Эрбиль, Ирак

*E-mail: architnura.1@gmail.com

**Аннотация:**
**Введение:** Архитектура — это дисциплина, отличающаяся разнообразием, передачей сообщений и коммуникацией. **Цель исследования**: В Эрбиле было замечено примечательное явление: большинство строений в типичных жилых комплексах были перепроектированы или претерпели изменения характеристик фасада. Эти изменения стали результатом психологической черты эстетических предпочтений. Целью данного исследования является анализ параметров эстетических предпочтений для выявления коммуникативного действия с использованием модели коммуникативного действия Хабермаса. Анализ действующих факторов способствовал пониманию указанных изменений. **Методы**: Методология данного исследования сочетает в себе формальный анализ тематического исследования и надлежащее анкетирование. Статистический анализ полученных результатов был использован для формулирования задач исследования. **Результаты**: Пять параметров, выведенных из теоретической основы (единство, масштаб, цвет, пропорция и баланс), служат элементами и принципами дизайна, влияющими на эстетику. В результате исследования делается вывод, что единство, пропорция и баланс являются основными факторами создания приятного эстетического вида фасадов домов.

**Ключевые слова:** коммуникативное действие, эстетические предпочтения, многообразие, жилой комплекс, фасадный дом, принцип проектирования.

# Civil Engineering

# EVALUATION OF BASALT FIBER REINFORCED ROLLER COMPACTED CONCRETE CONTAINING COAL POWDER FOR PAVEMENT

Sadik Alper Yildizel*, Kemal Armagan

Karamanoğlu Mehmetbey University, Engineering Faculty, Karaman, Türkiye

*Corresponding author's e-mail: sayildizel@kmu.edu.tr

**Abstract**

**Introduction**: The utilization of colored roller compacted concrete (RCC) for pavements in order to mitigate the urban heat island effect is a popular approach: increasing solar reflectance can reduce the effect. The paper explores the possibility of applying the reverse mechanism for regions with cold climates. The **purpose of the study** was to evaluate the mechanical, durability and solar reflectance properties of roller compacted concrete with coal powder (CP) and basalt fiber (BF) additives for pavement. **Methods:** an UV-Vis-NIR spectrophotometer was utilized for the albedo measurements. Consistency of the specimens was determined with Vebe consistometer. Compressive, flexural, and splitting tensile strengths were recorded at 7, 28 and 90 days. Frost resistance of the specimens was also investigated. **Result:** The combined utilization of 5% CP and 0.5% BF showed great performance for the roller compacted concrete pavements. Furthermore, the obtained albedo values also have the potential to increase the ambient temperature in cold climates.

**Keywords:** coal powder, basalt fiber, albedo, concrete, roller compacted concrete.

## Introduction

One of the most widely used forms of carbon is coal, which was produced in the United States alone to the tune of 756.2 million tons in 2018 (Masi et al., 2021). In addition to being used for the production of thermal energy, city heating, and coal chemical conversion (Ren et al., 2022), coal currently meets 41% of the world's electricity needs (Xu et al., 2022). Along with providing heat for the wallboard, aluminum, and cement industries, significant amounts of coal are also used in metallurgical processes, gasification, the cement industry, and as a source of activated carbon and many other common and industrial chemicals (Dai and Finkelman, 2018).

Basalt fibers (BF) are renowned for their ability to absorb energy, to bond with the matrix, to resist mechanical and chemical properties, and to exhibit significant acoustic and thermal characteristics (Vinotha Jenifer et al., 2023). Compared to glass fibers, basalt fiber has a better tensile strength and is more affordable. In terms of resistance to fire, chemical attack, sudden load, and good strain capacity, basalt fiber outperforms carbon fiber (Meesaraganda et al., 2023). To create basalt fiber-reinforced concrete (BFRC), BF can be incorporated into concrete as chopped fibers. The impact of using BF in BFRC on compressive strength varies across studies. With a specific dosage of BF, the compressive strength increased in some studies, decreased or did not show any significant effect in others (Al-Rousan et al., 2023).

Compared to other naturally occurring surfaces like vegetation and the earth, man-made or built-up surfaces like concrete and asphalt absorb more heat from sunlight. The urban heat island (UHI) effect is caused by the air being heated by the heat stored in the pavements. Because it is light gray instead of black, concrete has a much higher initial albedo than asphalt. However, over time, due to weathering and the buildup of dirt, the albedo of concrete decreases. Albedo's typical starting value for fresh concrete is 0.35 to 0.40, and for weathered concrete it is 0.25 to 0.30 (Reza and Boriboonsomsin, 2015).

Concrete materials have high thermal inertia and they are gray in color. They absorb a lot of solar radiation and then release it into the air as sensible heat, which helps create urban heat islands. The solar reflectance of building walls, roofs, and streets — the large proportion of which are made of hardened Portland cement concrete — determines the intensity of urban heat islands. Increasing the solar reflectance, or albedo, of building and street surfaces would reduce the urban heat island effect by decreasing heat convection from these surfaces to the air (Qin et al., 2019).

Roller compacted concrete (RCC) is a zero-slump concrete that is made of sand, Portland cement, dense-graded aggregate, and water. It is typically laid out using an asphalt paver and compacted using regular vibratory roller compactors (Modarres and Hosseini, 2014). Compared to traditional concrete, RCC contains more aggregate, less cement, and

less water. To increase its densification, compaction energy must be applied (Lam et al., 2017; Meddah et al., 2014). To achieve the desired density and homogeneous surface pavement, it is placed using a standard or high-density asphalt-type paver equipment and compacted by vibratory rollers. When compared to conventional rigid pavement or asphaltic pavement, RCC can reduce the cost of pavement construction by 15% to 30% while also allowing for an earlier opening to traffic (LaHucik et al., 2017; Mohammed and Adamu, 2018).

This study explores the mechanical and durability behaviors of RCC with basalt fiber and coal powder additives. The objective was to obtain better albedo results in RCC with these additives. The main purpose of this study was to determine: (1) the mechanical properties of RCC with basalt fiber and coal powder additives; (2) the durability properties of RCC with basalt fiber and coal powder additives; (3) the effect of adding coal powder in RCC to albedo characteristic. The results of this study can provide a possibility of replacing lower albedo traditional concrete with coal powder RCC to increase UHI in urban areas.

**Methods**

In the experimental study, crushed limestone and silica sand (SS) were used as coarse aggregate (CA) and fine aggregate (FA), respectively. Organic content of the aggregates was removed after the air-drying process. Maximum aggregate size was selected as 20 mm for preventing any possible

segregation and its effects. Combined gradation curves of the aggregates are presented in Fig. 1. CEM II type (42.5R) white cement (WC) conforming to BS EN 197(British Standard Institution BSI, 2011) standard was also used. Commercially available coal powder (CP) was utilized as filler and cement replacement material. Cement replaced with CP at the ratios of 5%, 10%, 15% and 20% by the weight of cement. Chemical compositions of the CP and WC are given in Table 1. Basalt fibers (BF: 8 mm length) were utilized with the ratios of 0.25%, 0.5%, 0.75%, and 1% by volume of the mixtures. Water-to-cement ratios were selected between 0.40 and 0.44 in order to meet the requirements of ACI 207.R-11 (ACI, 2011) regarding permissible compaction and water content limits. Utilized CP, BF and WC are given in Fig. 2. According to the ASTM C1435 standard, a compactor was used to compact the mixtures in three layers at blow counts of 1000 and 1850 r/min (10 kg of surcharge). The optimal water content values of the prepared mixtures were well within the limits.

Albedo values of the specimens were measured with an UV-Vis-NIR spectrophotometer (Fig. 3). 24 mm x 24 mm x 5 mm rectangular specimens were prepared for this measurement (Fig. 4). Wavelengths between 200–2500 nm were investigated to determine albedo properties. Mean reflection percentages were measured and albedo values of each specimen were determined according to the measurement of the spectrophotometer.
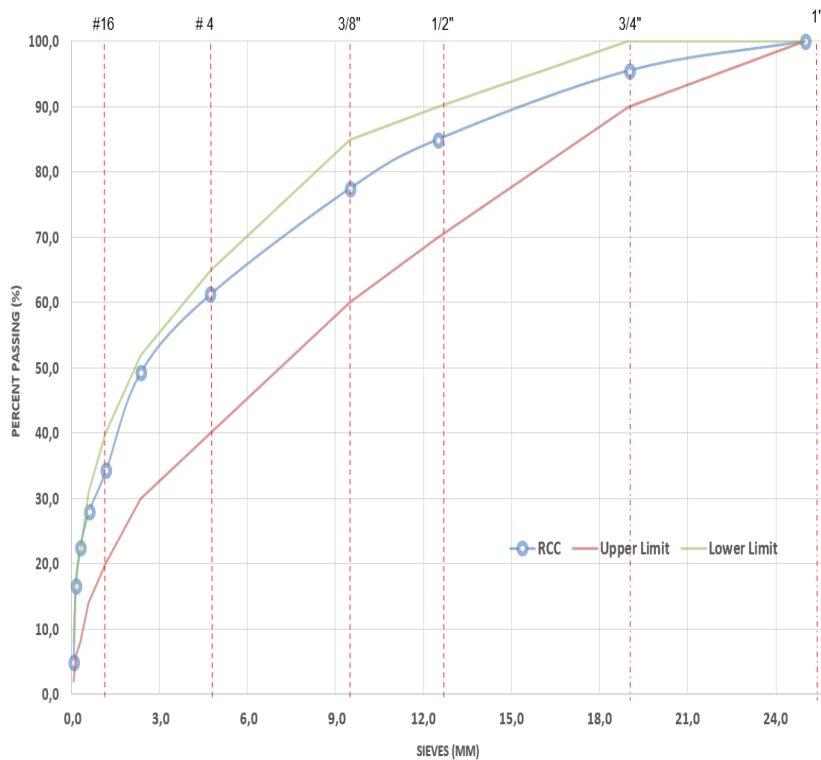


Fig. 1. Combined aggregate gradation curves

The mixtures were blended using a pan mixer (60 L) with a constant rate of 250 r/min. The consistency of all mixtures was recorded with a Vebe test device according to the ASTM C1170 (ASTM, 2014) standard. Compressive strength tests and splitting tensile tests were conducted on the 150 mm x 300 mm cylindrical specimens as per the guidance of ASTM C39 (ASTM, 2016), ASTM C496 (ASTM, 2011) for 7, 28 and 90 days, respectively. 100 mm x 100 mm x 500 mm rectangular specimens were prepared for the flexural strength test. And the loading rate kept constant at 0.9 MPa/min in accordance with ASTM C39 (ASTM, 2016). Frost resistance of the specimens (100 cycles) was also determined as per ASTM C666 (Morgan, 1991).

The albedo values of the specimens were measured at the first step during the experimental

Table 1. **Chemical ingredients of WC and CP** (provided by the supplier)

| Component (%) | WC | CP |
|---|---|---|
| $Fe_2O_3$ | 3.5 | 3.82 |
| CaO | 60.48 | 0.49 |
| $Al_2O_3$ | 4.32 | 14.47 |
| MgO | 2.37 | 0.85 |
| $SiO_2$ | - | 33.9 |
| Free CaO | 1.69 | - |
| $SO_3$ | 2.61 | - |
| $Na_2O$ | - | 0.25 |
| $K_2O$ | - | 2.32 |
| MnO | - | 0.02 |
| $TiO_2$ | - | 0.941 |



| Basalt Fiber | Coal Powder | White Cement (42.5 R) |
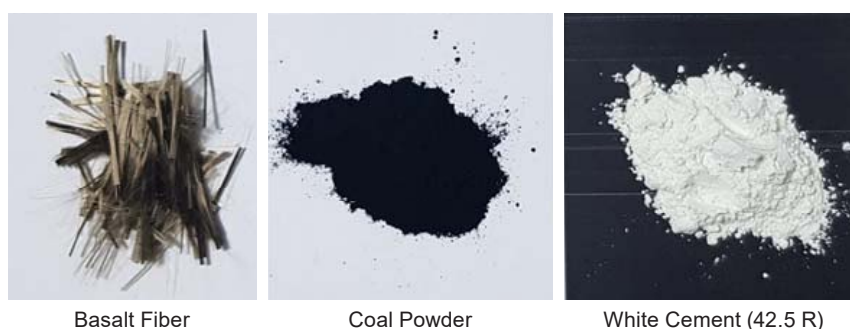
Fig. 2. Basalt fiber, coal powder and white cement

studies after 28 days of curing. Each specimen's spectral reflectance was measured three times. The mean of the three measurements was recorded. Afterwards, mechanical and durability tests were carried out. The mix design proportions and flow chart of the experimental studies are given in Table 2 and Fig. 5, respectively.

**Results and discussion**

The calculated albedo values of the prepared specimens are presented in Fig. 6. Test results vary between 0.28 and 0.16. Reference mixture with no CP and BF content showed the highest albedo of 0.28, as expected (Kaloush et al., 2008). This lowest result can be attributed to ingredients of the reference mixture since the albedo of concrete is generally correlated with the albedo of cement and aggregates (Levinson and Akbari, 2002). Albedo decreased with the increasing CP content (Emery et al., 2014). Albedo of the concrete specimens increased with the increasing water-to-cement ratios (Qin et al., 2019) due to the more possible formation of $Ca(OH)_2$ as a hydration product (Chaussadent et al., 2000). However, this phenomenon is not valid for color-incorporated concrete according to the albedo test results.

Vebe test results are presented in Fig. 7. The test results showed that Vebe time increased with the



Fig. 3. UV-Vis-NIR spectrophotometer



Fig. 4. CP added specimens

49

Table 2. **Mixture proportions**

| Mixture code | WC (kg/m³) | CP (kg/m³) | BF (%) | FA (kg/m³) | CA (kg/m³) | W/C | Optimum water content (%) |
|---|---|---|---|---|---|---|---|
| R | 270 | - | - | 750 | 1130 | 0.41 | 5.31 |
| $P_1$ | 256.5 | 13.5 | 0.25 | 750 | 1130 | 0.42 | 5.45 |
| $P_2$ | 243 | 27 | 0.5 | 750 | 1130 | 0.43 | 5.92 |
| $P_3$ | 229.5 | 40.5 | 0.75 | 750 | 1130 | 0.44 | 6.27 |
| $P_4$ | 216 | 54 | 1 | 750 | 1130 | 0.45 | 6.43 |
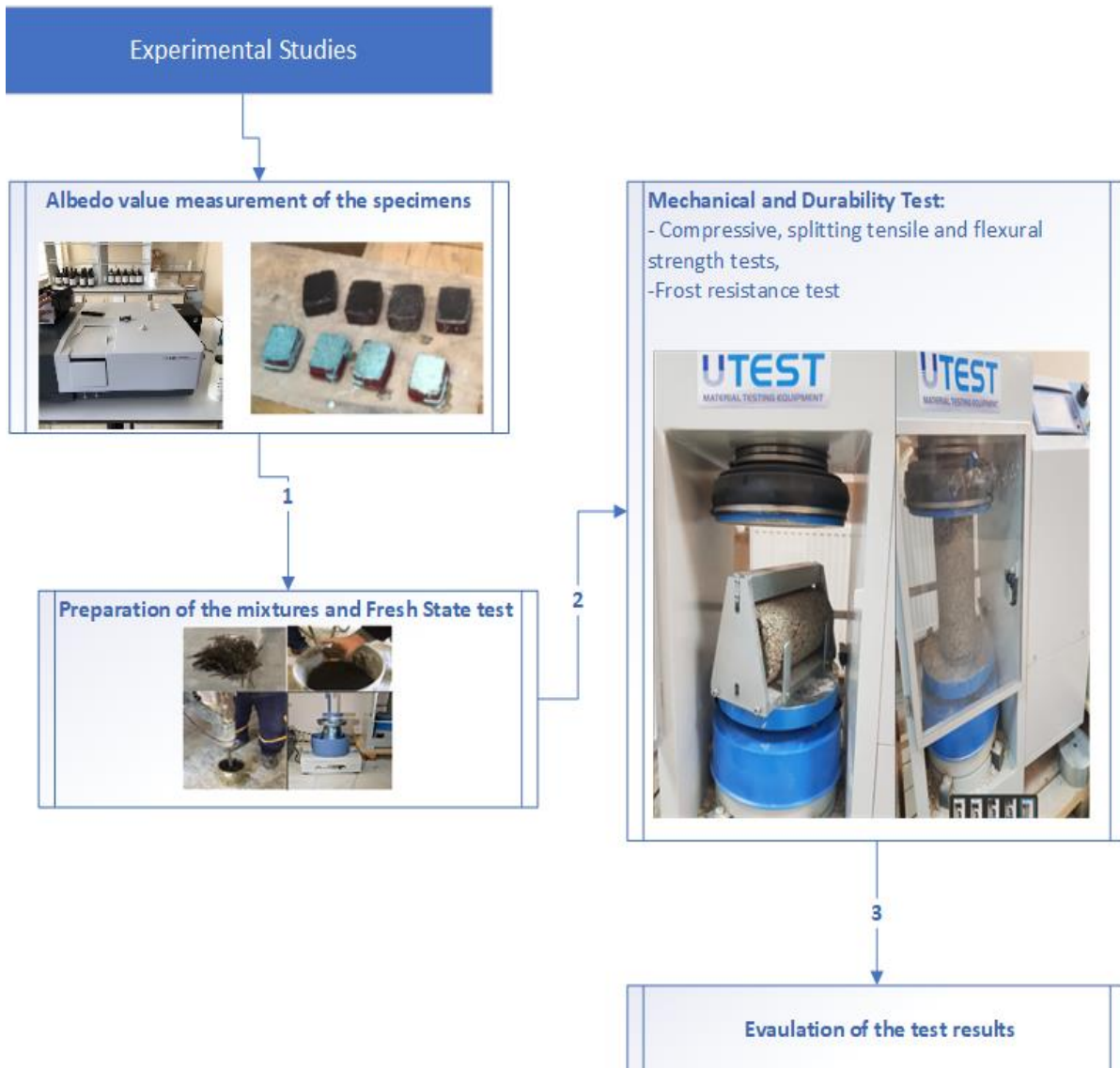


Fig. 5. Flow chart of the experimental studies

increasing CP replacement levels and BF contents. The Vebe time was 48 s for the control mix, and 69 s for the $P_4$ specimen. For such mixtures, this increase was related to the higher water absorption rate of coal powder (Argiz et al., 2018; Singh et al., 2020) and increased BF content that holds the mixture and slow aggregate settlement (Kirthika and Singh, 2018).

Compressive strength test results are presented in Fig. 8. The reported compressive strength values were calculated by the mean of the three specimens. Except $P_4$, all specimens met the requirements of ACI 325 (ACI, 2001) (min. 27.6 MPa for 28-day strength). The use of 5% CP together with the 0.25% BF was found to increase the compressive strength by 10.1% and outperformed other mixtures. The results also
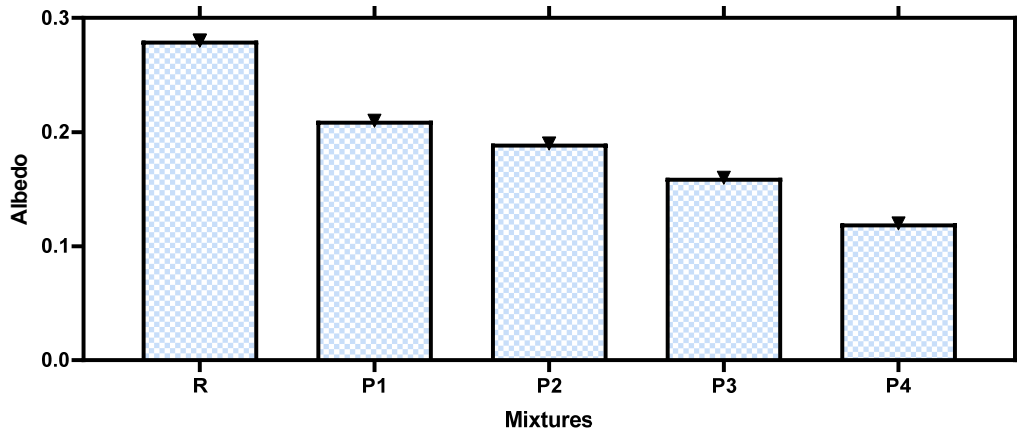
Fig. 6. Albedo values of the specimens
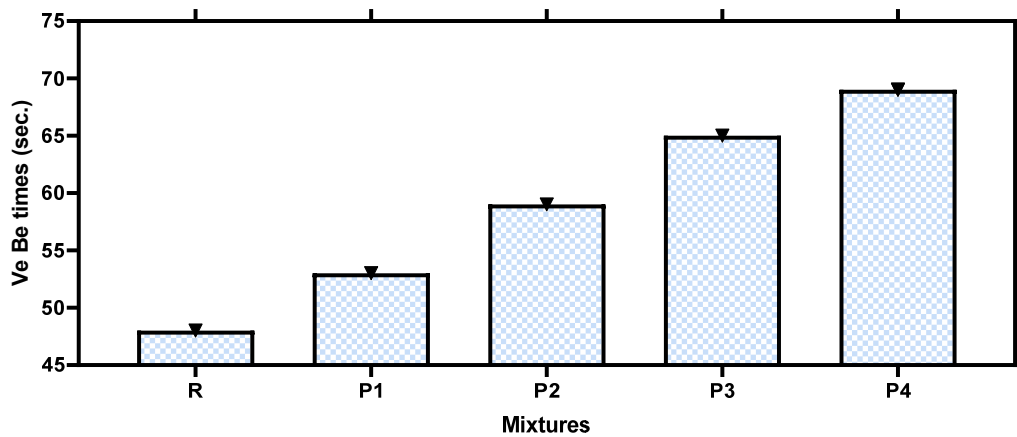


Fig. 7. Consistency of the mixtures
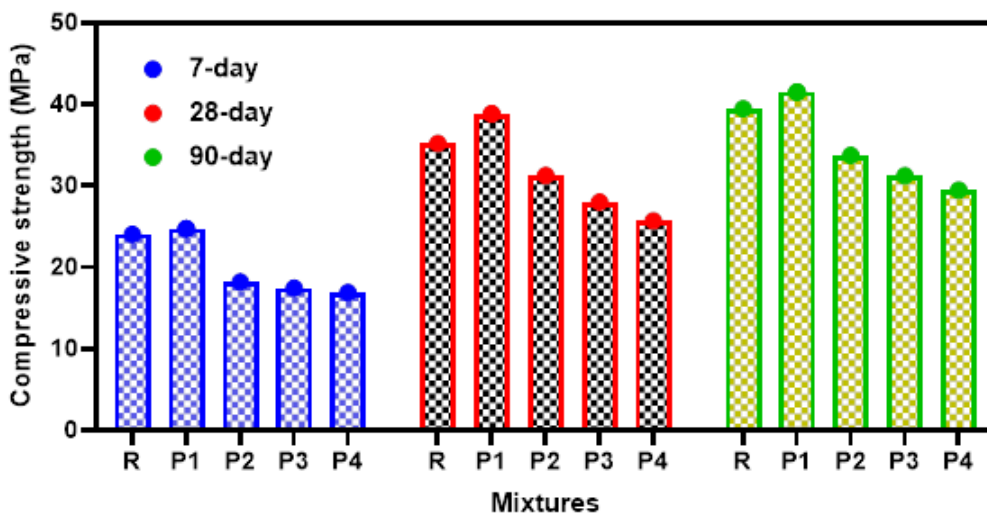


Fig. 8. Compressive strength test results

showed that increasing the CP replacement level by more than 5% reduced the compressive strength (Hesami et al., 2016). The compressive strength was reduced by approximately 50% by utilizing 20% CP and 1% BF at 28 days. This reduction is attributed to the low cement (Radović et al., 2021) and high BF

contents of $P_4$. Higher amount of BF (Liang et al., 2021) could lead to poorer interfaces between fibers and cement matrix (Algin and Ozen, 2018).

Fig. 9 shows the flexural strength test results. According to Fig. 8, the recorded flexural strength varied in the range of 3.1 and 5.34 MPa. The

combined utilization of 0.5% BF and 10% CP enhanced the flexural test results up to 20% compared to the reference mixtures at 28 days. These results also agree with the earlier studies (Haido et al., 2021; Hesami et al., 2016; Liang et al., 2021; Modarres et al., 2018), which showed that the CP replacement level of more than 10% and the BF exceeding 0.5% in volume fraction reduced the flexural strength. The flexural to compressive strength ratios at 28 days varied within the range of 14.85 and 23.1 MPa. This finding was also reported in the paper by Hesami et al. (2016), which stated that the ratios were calculated as higher values compared to the traditional concrete.

Splitting tensile strength test results are given in Fig. 10. The results show that the splitting tensile strength varied between 2.41 and 3.84 MPa. The splitting tensile to compressive strength ratios of this study were calculated within the range of 6.8% and 11.9%, which are consistent with data obtained in earlier studies (Choi and Yuan, 2005; Gaedicke,

2016). Another finding is that the splitting tensile strength decreased by increasing CP and BF content by more than 5% and 0.5%, respectively.

Compressive strength losses after 100 freezing & thawing cycles at 90 days are given in Fig. 11. The compressive strength losses of this research were measured between 4.2% and 26.7%. $P_4$ specimen performed the worst with 26.7 % strength loss. This can be attributed to the excessive BF and CP content, which hindered the connections of the cementitious materials (Yuan et al., 2020). $P_1$ showed the best performance with 5% CP and 0.5% BF content. The order of the specimens from strong to weak was obtained as $P_1 > R > P_2 > P_3 > P_4$.

**Conclusion**

In this study, coal powder added roller compacted concrete reinforced with basalt fiber was evaluated in terms of its solar reflectance, mechanical and durability properties. The combined effect of basalt fiber and coal powder was investigated as well. The main conclusion of the study can be drawn as follows:
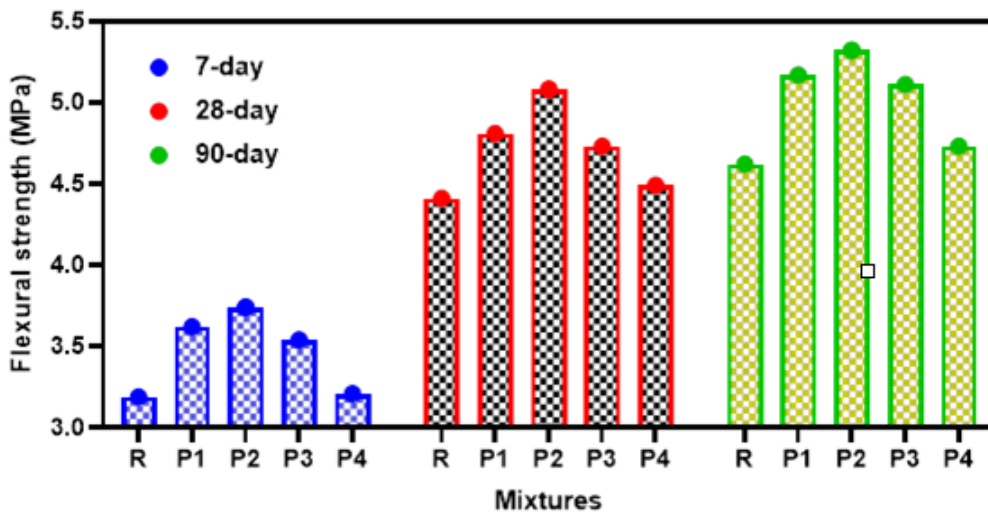


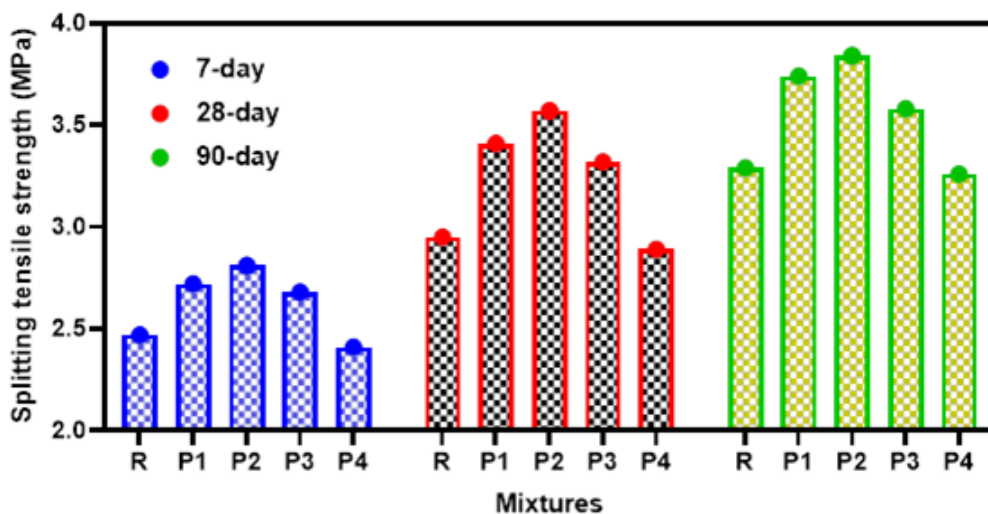Fig. 9. Flexural strength test results
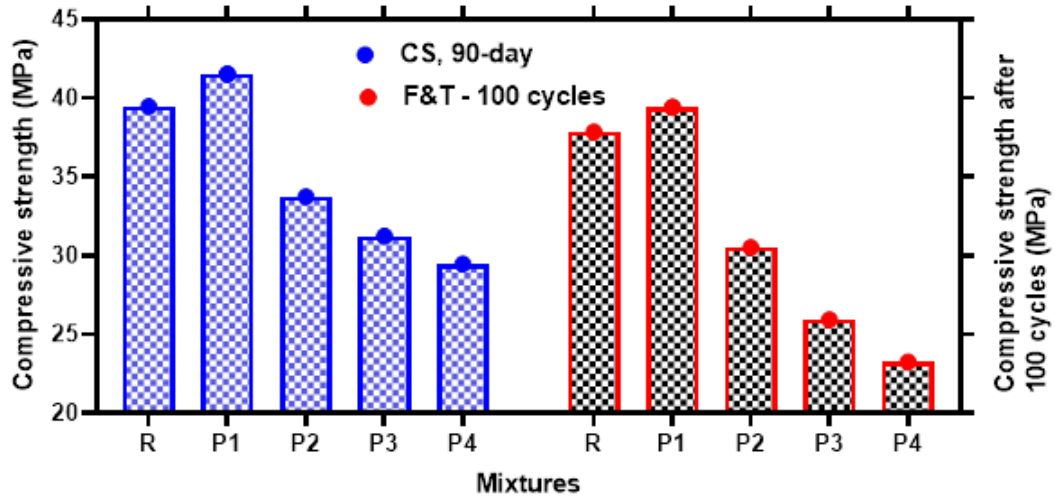


Fig. 10. Splitting tensile strength test results

Fig. 11. Compressive strength losses after 100 cycles

• Basalt fiber additives and the partial replacement of cement by coal powder produce higher optimum moisture content, Vebe times and water-to-cement ratio.

• The combination of 5% CP and 0.5% BF enhanced the mechanical properties of the roller concrete specimens.

• The potential replacement of CP in roller compacted concrete production was also investigated and the utilization of CP as cement supplementary material up to 5% can lead to a greener concrete design.

• Inclusion of 5% CP and 0.5% BF improved the frost resistance of concrete specimens after 100 cycles.

• According to the albedo within the scope of the study, future concretes can be designed to reduce or increase the urban heat island effect.

**References**

ACI (2001). ACI 325.11R-01. Accelerated techniques for concrete paving. Reported by ACI Committee 325. Farmington Hills: American Concrete Institute, USA, pp. 8-11.

ACI (2011). *ACI 207.5R-11. Report on rolller-compacted mass concrete*. Farmington Hills: American Concrete Institute, USA, pp. 6-7.

Algin, Z. and Ozen, M. (2018). The properties of chopped basalt fibre reinforced self-compacting concrete. *Construction and Building Materials*, Vol. 186, pp. 678–685. DOI: 10.1016/j.conbuildmat.2018.07.089.

Al-Rousan, E. T., Khalid, H. R., and Rahman, M. K. (2023). Fresh, mechanical, and durability properties of basalt fiber-reinforced concrete (BFRC): A review. *Developments in the Built Environment*, Vol. 14, 100155. DOI: 10.1016/j.dibe.2023.100155.

Argiz, C., Moragues, A., and Menéndez, E. (2018). Use of ground coal bottom ash as cement constituent in concretes exposed to chloride environments. *Journal of Cleaner Production*, Vol. 170, pp. 25–33. DOI: 10.1016/j.jclepro.2017.09.117.

ASTM (2011). *ASTM C496/C496M-17. Standard test method for splitting tensile strength of cylindrical concrete specimens*. ASTM International West Conshohocken, USA, pp. 3-5.

ASTM (2014). *ASTM C1170/C1170M-14. Standard test method for determining consistency and density of roller-compacted concrete using a vibrating table*. ASTM International West Conshohocken, USA, pp. 5-8.

ASTM (2016). *ASTM C39/C39M-16. Standard test method for compressive strength of cylindrical concrete specimens*. ASTM International West Conshohocken, USA, pp. 11-15.

British Standard Institution BSI (2011) 'BS EN 197-1:2011 Cement Part 1: Composition, specifications and conformity criteria for common cements', *BSI Standards Publication*, London, pp. 15–17.

Chaussadent, T., Baroghel-Bouny, V., Hornain, H., Rafai, N., and Ammouche, A. (2000). Effect of water-cement ratio of cement pastes on microstructural characteristics related to carbonation process. In: *Fifth CANMET/ACI International Conference on Durability of Concrete*, June 4–9, 2000, Barcelona, Spain.

Choi, Y. and Yuan, R. L. (2005). Experimental relationship between splitting tensile strength and compressive strength of GFRC and PFRC. *Cement and Concrete Research*, Vol. 35, Issue 8, pp. 1587–1591. DOI: 10.1016/j.cemconres.2004.09.010.

Dai, S. and Finkelman, R. B. (2018). Coal as a promising source of critical elements: Progress and future prospects. *International Journal of Coal Geology*, Vol. 186, pp. 155–164. DOI: 10.1016/j.coal.2017.06.005.

Emery, J. J., Guo, P., Stolle, D. F. E., Hernandez, J., and Zhang, L. (2014). Light-coloured grey asphalt pavements: from theory to practice. *International Journal of Pavement Engineering*, Vol. 15, Issue 1, pp. 23–35. DOI: 10.1080/10298436.2013.782402.

Gaedicke, C., Torres, A., Huynh, K. C. T., and Marines, A. (2016). A method to correlate splitting tensile strength and compressive strength of pervious concrete cylinders and cores. *Construction and Building Materials*, Vol. 125, pp. 271–278. DOI: 10.1016/j.conbuildmat.2016.08.031.

Haido, J. H., Tayeh, B. A., Majeed, S. S., and Karpuzcu, M. (2021). Effect of high temperature on the mechanical properties of basalt fibre self-compacting concrete as an overlay material. *Construction and Building Materials*, Vol. 268, 121725. DOI: 10.1016/j.conbuildmat.2020.121725.

Hesami, S., Modarres, A., Soltaninejad, M., and Madani, H. (2016). Mechanical properties of roller compacted concrete pavement containing coal waste and limestone powder as partial replacements of cement. *Construction and Building Materials*, Vol. 111, pp. 625–636. DOI: 10.1016/j.conbuildmat.2016.02.116.

Kaloush, K. E., Carlson, J. D., Golden, J. S., and Phelan, P. E. (2008). *The thermal and radiative characteristics of concrete pavements in mitigating urban heat island effects*. Skokie: Portland Cement Association, 139 p.

Kirthika, S. K. and Singh, S. K. (2018). Experimental investigations on basalt fibre-reinforced concrete. *Journal of The Institution of Engineers (India): Series A*, Vol. 99, Issue 4, pp. 661–670. DOI: 10.1007/s40030-018-0325-4.

LaHucik, J., Dahal, S., Roesler, J., and Amirkhanian, A. N. (2017). Mechanical properties of roller-compacted concrete with macro-fibers. *Construction and Building Materials*, Vol. 135, pp. 440–446. DOI: 1016/j.conbuildmat.2016.12.212.

Lam, M. N.-T., Jaritngam, S., and Le, D.-H. (2017). Roller-compacted concrete pavement made of Electric Arc Furnace slag aggregate: Mix design and mechanical properties. *Construction and Building Materials*, Vol. 154, pp. 482–495. DOI: 10.1016/j.conbuildmat.2017.07.240.

Levinson, R. and Akbari, H. (2002). Effects of composition and exposure on the solar reflectance of portland cement concrete. *Cement and Concrete Research*, Vol. 32, Issue 11, pp. 1679–1698. DOI: 10.1016/S0008-8846(02)00835-9.

Liang, N., Ren, L., Tian, S., Liu, X., Zhong, Z., Deng, Z., and Yan, R. (2021). Study on the fracture toughness of polypropylene–basalt fiber-reinforced concrete. *International Journal of Concrete Structures and Materials*, Vol. 15, 35. DOI: 10.1186/s40069-021-00472-x.

Masi, C. A., Schumacher, T. A., Hilman, J., Dulal, R., Rimal, G., Xu, B., Leonard, B., Tang, J., Fan, M., and Chien, T. Y. (2021). Converting raw coal powder into polycrystalline nano-graphite by metal-assisted microwave treatment. *Nano-Structures and Nano-Objects*, Vol. 25, 100660. DOI: 10.1016/j.nanoso.2020.100660.

Meddah, A., Beddar, M., and Bali, A. (2014). Use of shredded rubber tire aggregates for roller compacted concrete pavement. *Journal of Cleaner Production*, Vol. 72, pp. 187–192. DOI: 10.1016/j.jclepro.2014.02.052.

Meesaraganda, P. L. V., Dhar, D., and Rama Prasad Reddy, L. (2023). A study on basalt fiber reinforced concrete utilising seashells as replacement to coarse aggregate. *Materials Today: Proceedings*, in press. DOI: 10.1016/j.matpr.2023.03.033.

Modarres, A., Hesami, S., Soltaninejad, M., and Madani, H. (2018). Application of coal waste in sustainable roller compacted concrete pavement-environmental and technical assessment. *International Journal of Pavement Engineering*, Vol. 19, Issue 8, pp. 748–761. DOI: 10.1080/10298436.2016.1205747.

Modarres, A. and Hosseini, Z. (2014). Mechanical properties of roller compacted concrete containing rice husk ash with original and recycled asphalt pavement material. *Materials & Design*, Vol. 64, pp. 227–236. DOI: 10.1016/j.matdes.2014.07.072.

Mohammed, B. S. and Adamu, M. (2018). Mechanical performance of roller compacted concrete pavement containing crumb rubber and nano silica. *Construction and Building Materials*, Vol. 159, pp. 234–251. DOI: 10.1016/j.conbuildmat.2017.10.098.

Morgan, D. R. (1991), Freeze thaw durability of steel and polypropylene reinforced shotcretes: A review. In: *Durability of Concrete. Second International Conference.* August 4–9, 1991, Montreal, Canada.

Qin, Y., Zhao, Y., Chen, X., Wang, L., Li, F., and Bao, T. (2019). Moist curing increases the solar reflectance of concrete. *Construction and Building Materials*, Vol. 215, pp. 114–118. DOI: 10.1016/j.conbuildmat.2019.04.164.

Radović, A., Marinković, S.m and Savić, A. (2021). Compressive strength of green concrete with low cement and high filler content. *Gradjevinski materijali i konstrukcije*, Vol. 64, No. 2, pp. 93–108. DOI: 10.5937/grmk2102093r.

Ren, L.-F., Li, Q.-W., Xiao, Y., Hao, J.-C., Yi, X., Zou, L., and Li, Z.-B. (2022). Critical parameters and risk evaluation index for spontaneous combustion of coal powder in high-temperature environment. *Case Studies in Thermal Engineering*, Vol. 38, 102331. DOI: 10.1016/j.csite.2022.102331.

Reza, F. and Boriboonsomsin, K. (2015). Pavements made of concrete with high solar reflectance. In: Pacheco-Torgal, F., Labrincha, J. A., Cabeza, L. F., and Granqvist, C.-G. (eds.). *Eco-efficient Materials for Mitigating Building Cooling Needs: Design, Properties and Applications*. Woodhead Publishing, USA, pp. 37–62. DOI: 10.1016/B978-1-78242-380-5.00003-0.

Singh, N., Shehnazdeep, and Bhardwaj, A. (2020). Reviewing the role of coal bottom ash as an alternative of cement. *Construction and Building Materials*, Vol. 233, 117276. DOI: 10.1016/j.conbuildmat.2019.117276.

Vinotha Jenifer, J., Brindha, D., Annie Sweetlin Jebarani, J. P., Venkadapriya, S., and Pandieswari, M. (2023). Mechanical and microstructure properties of copper slag based basalt fiber reinforced concrete. *Materials Today: Proceedings*, in press. DOI: 10.1016/j.matpr.2023.03.505.

Xu, H., Ni, X., Su, X., Xiao, B., Luo, Y., Zhang, F., Weng, C., and Zheng, Q. (2022). Experimental investigation on the application of the coal powder as fuel in a rotating detonation combustor. *Applied Thermal Engineering*, Vol. 213, 118642. DOI: 10.1016/j.applthermaleng.2022.118642.

Yuan, Y., Zhao, R., Li, R., Wang, Y., Cheng, Z., Li, F., and Ma, Z. J. (2020). Frost resistance of fiber-reinforced blended slag and Class F fly ash-based geopolymer concrete under the coupling effect of freeze-thaw cycling and axial compressive loading. *Construction and Building Materials*, Vol. 250, 118831. DOI: 10.1016/j.conbuildmat.2020.118831.

# ОЦЕНКА БАЗАЛЬТО-ВОЛОКОННОГО АРМИРОВАННОГО УПЛОТНЕННОГО КАТКОМ БЕТОНА С ДОБАВЛЕНИЕМ УГОЛЬНОЙ ПЫЛИ ДЛЯ ДОРОЖНЫХ ПОКРЫТИЙ

Садик Альпер Йылдизель*, Кемаль Армаган

Университет Караманоглу Мехметбей, инженерный факультет, Караман, Турция

*E-mail: sayildizel@kmu.edu.tr

**Аннотация**

**Введение**: Использование цветного уплотненного катком бетона (УКБ) для дорожных покрытий с целью смягчения эффекта городского острова тепла является популярным подходом: увеличение отражения солнечной энергии может уменьшить эффект. В статье исследуется возможность применения обратного механизма для регионов с холодным климатом. Целью исследования была оценка механических и прочностных свойств, а также свойств отражения солнечной энергии УКБ с добавлением угольной пыли (УП) и базальтового волокна (БВ) для дорожных покрытий. **Методы:** для измерения альбедо использовался спектрофотометр UV-Vis-NIR. Консистенцию образцов определяли на консистометре Вебе. Прочность на сжатие, изгиб и раскалывание регистрировали через 7, 28 и 90 дней. Также была исследована морозостойкость образцов. **Результат:** Сочетание 5% УП и 0,5% БВ показало отличные характеристики для бетонных дорожных покрытий, уплотненных катком. Кроме того, полученные значения альбедо также могут повысить температуру окружающей среды в холодном климате.

**Ключевые слова:** угольная пыль, базальтовое волокно, альбедо, бетон, уплотненный катком бетон.

# RITZ METHOD IN THE DISCRETE APPROXIMATION
# OF DISPLACEMENTS FOR SLAB CALCULATION

Vladimir Vasilyevich Karpov, Evgeny Anatolyevich Kobelev*, Aleksandr Matveyevich Maslennikov,
Aleksandr Nikolayevich Panin

Saint Petersburg State University of Architecture and Civil Engineering,
4 Vtoraya Krasnoarmeyskaya St., Saint Petersburg, Russia

*Corresponding author's e-mail: evgeny.kobelev@gmail.com

**Abstract**

**Introduction**: The FEM reduces the problem of structural analysis for various building structures to the formation and solution of a system of linear algebraic equations. For this purpose, there are techniques available for obtaining FE stiffness and flexibility matrices where the main structural deformation characteristics are taken into account. However, the FEM can also be considered as a special case of the Ritz method in the discrete approximation of the required functions. In the functional of full potential deformation energy with regard to the considered structure, all adopted stress-strain state characteristics are taken into account.

Since it is difficult or impossible to find continuous approximation functions both in the classic version of the Ritz method and in the Bubnov–Galerkin method for some types of edge restraint in such building structures as beams, slabs, or shells, it is possible to use the Ritz method in the discrete approximation of the required functions (by analogy with the FEM). This paper presents a method of such calculations using slab calculations as an example. It is shown that, due to introducing some notations (operators), the process of finding the coefficients of the system of linear algebraic equations creates no difficulties and is easily programmable. The proposed method is not an alternative to the FEM, which is the most effective numerical method for the calculation of complex three-dimensional building structures.

**Purpose of the study:** We aimed to create a method for calculating slabs by the Ritz method in the discrete approximation of the deflection function for edge restraint cases when it is difficult or impossible to find continuous approximation functions in the classic version of the Ritz method and the Bubnov–Galerkin method. **Methods:** Based on the application of the Ritz variational method in the discrete approximation of displacements for slab calculation, all the basic relations for rectangular finite elements with 12 degrees of freedom are obtained, and an algorithm for forming the coefficients of the system of linear algebraic equations is developed. **Results:** For the first time, the solution by the Ritz method in the discrete approximation of slab displacements is obtained for the case when two edges of the slab are rigidly restrained and other two edges are free. In this case, the correct solution of the above problem is possible only with the use of the proposed method and FEM. For the test problem, we performed a comparison of the results of the calculation using the proposed method with the results using the classic Ritz method, which showed their very close agreement. The accuracy of the obtained results was assessed.

**Keywords:** Ritz method, functional of full potential deformation energy, discrete approximation of displacements, slab, deflection function, finite element, Hermite polynomials.

## Introduction

In the early 1940s, the finite element method (FEM) was developed by utilizing the idea of the mesh method. This method originated from structural mechanics and the theory of elasticity, and was later comprehended by mathematicians who often call this method variational-difference, thus emphasizing its mathematical nature. Thanks to the works of Argyris (1961), Clough (1960), Courant (1943), Hrennikoff (1941), Zienkiewicz (1975) and others, this method has been widely used in calculations of various components of building constructions, buildings, and structures (Ilyin et al., 1990; Postnov and Kharkhurim, 1974; Trushin, 2018).

When slabs are calculated with the use of the FEM, generalized displacements $q_i$ are introduced for each FE. Based on the type of potential deformation energy of the slab (plate), the stiffness matrix $[K]$ is found. If we introduce a vector of nodal displacements for FE $\{q\} = \{q_1, q_2, \ldots, q_{12}\}$ and a vector of nodal forces $\{R\}$, based on the expression for work of external forces, then the relationship between these vectors according to Postnov et al. (1987) will have the following form: $\{R\} = [K]\{q\}$. In the work by Postnov et al. (1987), the expressions for the coefficients of the matrix $[K]$ are not given due to their cumbersomeness. In contrast to the FEM, the convergence of the solution by the Ritz method was proved (Mikhlin, 1970).

Since building structures are quite diverse and have different configurations and characteristics, different types of finite elements (FE) were developed (Auricchio et al., 2016, Bishay et al.,

Farias et al., 2018, Zienkiewicz et al., 2013). Various works (Gander and Wanner, 2012; Li et al., 2014; Nwoji et al., 2017; Qu et al., 2013; Xue et al., 2021; Weinan and Yu, 2018) address the improvement of variational methods for the calculation of plates and shells and the development of modern computing systems based on them.

In construction practice, slabs having two opposite sides free are often used. When calculating such structures by the Ritz method in its classic version, it is impossible to find continuous approximation functions in this direction. Therefore, this paper proposes to use the Ritz method in the discrete approximation of displacement functions. The purpose of this study is to extend the scope of application of the Ritz method in solving new problems and develop a programming-friendly algorithm to calculate the coefficients of a system of linear algebraic equations.

*Discrete approximation of the deflection function*

Let us divide the area $D\{0 \leq x \leq a, 0 \leq y \leq b\}$ occupied by the middle plane of the slab into rectangular parts $D_{j,i}\{j = 1, 2, ..., m; i = 1, 2, ..., n\}$. Then we denote the points of intersection of these lines by $z_{j,i}$ (Fig. 1). Then we denote the area $D_{j,i}$ limited by points $z_{j,i}$, $z_{j,i+1}$, $z_{j+1,i}$, $z_{j+1,i+1}$ (nodal points) by $e_{j,i}$. Let us also denote the area $D$ division interval in the direction of axis $Ox$ by $h_x = \dfrac{a}{m}$ and in the direction of axis $Oy$ — by $h_y = \dfrac{b}{n}$. The total number of the area $D$ division points (nodal points $z_{j,i}$) will be $(m+1)(n+1) = mn + m + n + 1$, including internal nodal points $((m-1)(n-1) = mn - m - n + 1)$, and boundary nodal points $(2(m-1) + 2(n-1) + 4 = 2m + 2n)$.

By analogy with the FEM, we will call the area $e_{j,i}$ a finite element (FE). The deflection function $W(x,y)$ and its partial derivatives $W'_x(x,y)$ and $W_y(x,y)$ will be considered unknown functions. To approximate these functions on the entire area $D$, we will first construct them on partial areas $D_{j,i}$, i.e., on FE $e_{j,i}$, ensuring continuity and differentiability of the obtained approximation of the required functions on the entire area $D$.

We will calculate the values of the required functions $W$, $W'_x$, $W'_y$ at each nodal point $z_{j,i}$, considering those values unknown parameters. To approximate the required functions on FE $e_{ji}$, we will use third-degree splines (Ilyin et al., 1990) in the form of orthogonal Hermite polynomials (Korn and Korn, 1974). The most convenient form of such polynomials was described by Postnov and Kharkhurim (1974). From one-dimensional polynomials of variables $x$ and $y$, *two-dimensional functions of variables x and y* $\varphi_k^{ji}(x, y)$ *are formed*, and unknown functions $W(x,y)$, $W'_x(x,y), W'_y(x,y)$ on FE $e_{j,i}$ are presented as the sum of products of unknown numerical parameters (values of the required functions at nodal points) and

known approximation functions $\varphi_k^{ji}(x, y)$. On other FE, this approximation is considered to be equal to zero.

Since at each nodal point $z_{ji}$ there will be three unknown numerical parameters, then FE $e_{ji}$ will have 12 degrees of freedom.

The FE are connected to one another at the FE nodes. Let us necessitate the compatibility of vertical displacements $W(x,y)$ and rotation angles $W'_x(x,y), W'_y(x,y)$ at the nodal points for the FE adjacent to the node.

On FE $e_{j,i}$, let us denote the following:

$$W_{j,i} = W_1^{j,i}, \; W_{j,i+1} = W_2^{j,i}, \; W_{j+1,i} = W_3^{j,i},$$
$$W_{j+1,i+1} = W_4^{j,i}, \; \left(W_{j,i}\right)_x = W_5^{j,i},$$
$$\left(W_{j,i+1}\right)'_x = W_6^{j,i}, \; \left(W_{j+1,i}\right)'_x = W_7^{j,i}, \; \left(W_{j+1,i}\right)'_x = W_7^{j,i},$$
$$\left(W_{j+1,i+1}\right)'_x = W_8^{j,i}, \qquad (1)$$
$$\left(W_{j,i}\right)'_y = W_9^{j,i}, \; \left(W_{j,i+1}\right)'_y = W_{10}^{j,i}, \; \left(W_{j+1,i}\right)'_y = W_{11}^{j,i},$$
$$\left(W_{j+1,i+1}\right)'_y = W_{12}^{j,i}.$$

Therefore, the deflection function $W(x,y)$ on FE $e_{j,i}$ can be represented as follows:

$$W(x,y)|_{e_{j,i}} = \sum_{k=1}^{12} W_k^{j,i} \phi_k^{j,i}(x,y), \qquad (2)$$

and on other FE, this function is taken equal to zero.

On the entire area $D$, $W(x,y)$ is determined as $W_{m,n} = \sum_{j=0}^{m-1}\sum_{i=0}^{n-1}\sum_{k=1}^{12} W_k^{j,i} \phi_k^{j,i}(x,y)$. Each node will have three unknown parameters. In total, there will be $3(m+1)(n+1) = 3mn + 3m + 3n + 3$ unknown parameters.

To approximate the required functions, Hermite polynomials (Postnov and Kharkhurim, 1974) are used in the FEM. On FE $e_{j,i}$, they take the following form (in the common coordinate system $xOy$)

$$E_{01}^j(x) = \frac{h_x^3 - 3h_x\left(x - x_j\right)^2 + 2\left(x - x_j\right)^3}{h_x^3},$$

$$E_{02}^j(x) = \frac{3h_x\left(x - x_j\right)^2 - 2\left(x - x_j\right)^3}{h_x^3}, \qquad (3)$$

$$E_{11}^j(x) = \frac{h_x^2\left(x - x_j\right) - 2h_x\left(x - x_j\right)^2 + \left(x - x_j\right)^3}{h_x^2},$$

$$E_{12}^j(x) = \frac{-h_x\left(x - x_j\right)^2 + \left(x - x_j\right)^3}{h_x^2}.$$

By substituting $x$ with $y$, $h_x$ with $h_y$, $j$ with $i$, we can obtain $E_{01}^i(y)$, $E_{02}^i(y)$, $E_{11}^i(y)$, $E_{12}^i(y)$.

Let us introduce the following notations (Postnov and Kharkhurim, 1974):
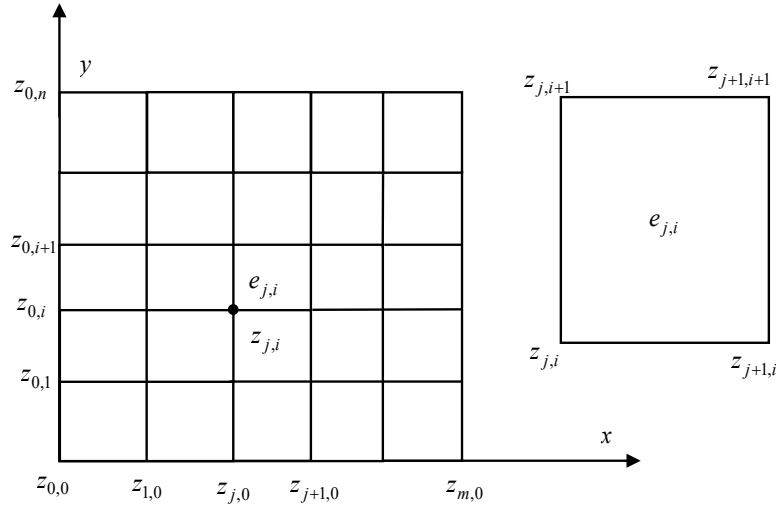
$$\phi_1^{j,i}(x,y) = E_{01}^j(x) \cdot E_{01}^i(y),$$

Fig. 1. Area $D$ divided into FE

$$\phi_2^{j,i}(x,y) = E_{01}^j(x) \cdot E_{02}^i(y),$$
$$\phi_3^{j,i}(x,y) = E_{02}^j(x) \cdot E_{01}^i(y),$$
$$\phi_4^{j,i}(x,y) = E_{02}^j(x) \cdot E_{02}^i(y),$$
$$\phi_5^{j,i}(x,y) = E_{11}^j(x) \cdot E_{01}^i(y),$$
$$\phi_6^{j,i}(x,y) = E_{11}^j(x) \cdot E_{02}^i(y),\qquad (4)$$
$$\phi_7^{j,i}(x,y) = E_{12}^j(x) \cdot E_{01}^i(y),$$
$$\phi_8^{j,i}(x,y) = E_{12}^j(x) \cdot E_{02}^i(y),$$
$$\phi_9^{j,i}(x,y) = E_{01}^j(x) \cdot E_{11}^i(y),$$
$$\phi_{10}^{j,i}(x,y) = E_{01}^j(x) \cdot E_{12}^i(y),$$
$$\phi_{11}^{j,i}(x,y) = E_{02}^j(x) \cdot E_{11}^i(y),$$
$$\phi_{12}^{j,i}(x,y) = E_{02}^j(x) \cdot E_{12}^i(y).$$

The values of Hermite polynomials at the nodal points $z_{j,i}$, $z_{j,i+1}$, $z_{j+1,i}$, $z_{j+1,i+1}$ are 0 or 1. The values of the derivatives of $E_{01}^j(x)$ and $E_{02}^j(x)$ with respect to $x$ and first-order derivatives of $E_{01}^i(y)$ and $E_{02}^i(y)$ with respect to $y$ at nodal points are also equal to 0 or 1.

Each internal nodal point $z_{j,i}$ belongs to four FE (Fig. 2).

The order of numbering at the nodes of functions $W$, $W_x'$, $W_y'$ is shown in Fig. 2 by numbers. *Let us describe in detail the $W(x,y)$ approximation on each FE adjacent to the node $z_{j,i}$.* Below are the expressions $W(x,y)$ and approximating functions in formula (2) for each of the four FEs that have a common node $z_{j,i}$ (Fig. 2).

On FE $e_{j,i}$, in expansion (2), there will be expression $W(x,y)|_{e_{j,i}} = \sum\limits_{k=1}^{12} W_k^{j,i} \phi_k^{j,i}(x,y)$, $W(z_{j,i})$ denoted by $W_1^{j,i}$ and, therefore, function $\phi_1^{j,i}(x,y)$, $W_x'(z_{j,i}) - W_5^{j,i}$ and $\phi_5^{j,i}(x,y)$, $W_y'(z_{j,i}) - W_9^{j,i}$ and

$\phi_9^{j,i}(x,y)$, variation limits $x$ and $y$ will be $x_j \leq x \leq x_{j+1}$, $y_i \leq y \leq y_{i+1}$.

On FE $e_{j,i-1}$, in expansion (2), there will be expression $W(x,y)|_{e_{j,i-1}} = \sum\limits_{k=1}^{12} W_k^{j,i-1} \phi_k^{j,i-1}(x,y)$, $W(z_{j,i})$ denoted by $W_2^{j,i-1}$ and, therefore, function $\phi_2^{j,i-1}(x,y)$, $W_x'(z_{j,i}) - W_6^{j,i-1}$ and $\phi_6^{j,i-1}(x,y)$, $W_y'(z_{j,i}) - W_{10}^{j,i-1}$ and $\phi_{10}^{j,i-1}(x,y)$, variation limits $x$ and $y$ will be $x_j \leq x \leq x_{j+1}$, $y_{i-1} \leq y \leq y_i$.

On FE $e_{j-1,i}$, in expansion (2), there will be expression $W(x,y)|_{e_{j-1,i}} = \sum\limits_{k=1}^{12} W_k^{j-1,i} \phi_k^{j-1,i}(x,y)$, $W(z_{j,i})$ denoted by $W_3^{j-1,i}$ and, therefore, function $\phi_3^{j-1,i}(x,y)$, $W_x'(z_{j,i}) - W_7^{j-1,i}$ and $\phi_7^{j-1,i}(x,y)$, $W_y'(z_{j,i}) - W_{11}^{j-1,i}$ and $\phi_{11}^{j-1,i}(x,y)$, variation limits $x$ and $y$ will be $x_{j-1} \leq x \leq x_j$, $y_i \leq y \leq y_{i+1}$.

On FE $e_{j-1,i-1}$, in expansion (2), there will be expression $W(x,y)|_{e_{j-1,i-1}} = \sum\limits_{k=1}^{12} W_k^{j-1,i-1} \phi_k^{j-1,i-1}(x,y)$, $W(z_{j,i})$ denoted by $W_4^{j-1,i-1}$ and, therefore, function $\phi_4^{j-1,i-1}(x,y)$, $W_x'(z_{j,i}) - W_8^{j-1,i-1}$ and $\phi_8^{j-1,i-1}(x,y)$, $W_y'(z_{j,i}) - W_{12}^{j-1,i-1}$ and $\phi_{12}^{j-1,i-1}(x,y)$, variation limits $x$ and $y$ will be $x_{j-1} \leq x \leq x_j$, $y_{i-1} \leq y \leq y_i$.

*Method of obtaining algebraic equations*

The functional of full potential deformation energy with regard to a rigid slab has the following form:

$$E_s = \frac{D}{2} \int\limits_0^a \int\limits_0^b \left[ \left( \frac{\partial^2 W}{\partial x^2} + \frac{\partial^2 W}{\partial y^2} \right)^2 + \right.$$

$$\left. +2(1-\mu)\left( \left( \frac{\partial^2 W}{\partial x \partial y} \right)^2 - \frac{\partial^2 W}{\partial x^2} \frac{\partial^2 W}{\partial y^2} \right) - 2\frac{q}{D} W \right] dx dy, \quad (5)$$
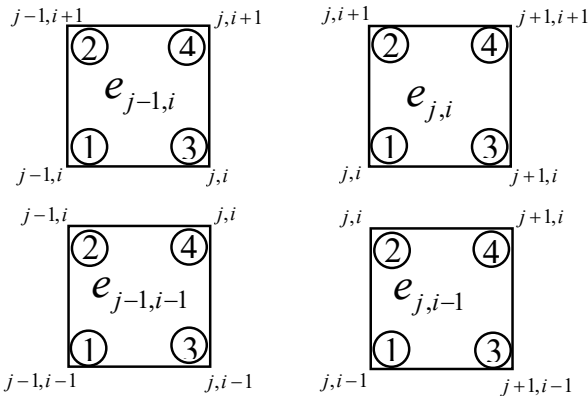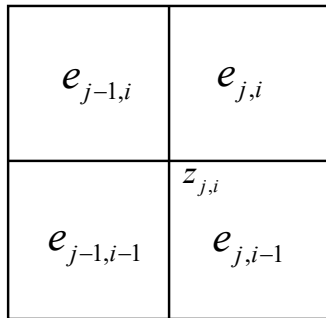
59

Fig. 2. FE adjacent to the node $z_{j,i}$

where $D = \dfrac{Eh^3}{12\left(1-\mu^2\right)}$ — cylindrical stiffness of the slab;

$E$ — elasticity modulus;

$h$ — slab height;

$\mu$ — Poisson's ratio;

$W$ — slab deflection function;

$q$ — transverse load;

$a, b$ — slab dimensions in plan view.

The boundary conditions corresponding to the type of slab contour fixing are also specified. All this (the functional and boundary conditions) constitutes the variational problem to be solved.

On the entire area $D$ occupied by the slab, the $W(x, y)$ approximation will have the following form:

$$W_{m,n}\left(x,y\right) = \sum_{j=0}^{m-1}\sum_{i=0}^{n-1}\sum_{k=1}^{12} W_k^{j,i}\phi_k^{j,i}\left(x,y\right). \qquad (6)$$

To find the unknown parameters $W_k^{j,i}$, we substitute expression (6) into expression (5), and then find the derivatives of the functional $E_s\left(W_{m,n}\left(x,y\right)\right)$ with respect to the unknown parameters at each internal nodal point of the area $D$ and equate them to 0. Each node will have three unknown parameters.

Thus, we obtain the following:

$$\frac{\partial E_s\left(W_{m,n}\right)}{\partial W\left(z_{j,i}\right)} = 0, \quad \frac{\partial E_s\left(W_{m,n}\right)}{\partial W_x'\left(z_{j,i}\right)} = 0, \quad \frac{\partial E_s\left(W_{m,n}\right)}{\partial W_y'\left(z_{j,i}\right)} = 0, \quad (7)$$

when $j = 1, 2, ..., m-1;\ i = 1, 2, ..., n-1$.

Since there will be $(m-1)(n-1)$ internal nodal points, then there will be $3(m-1)(n-1) = 3mn - 3m - 3n + 3$ such equations.

The missing equations can be obtained using the boundary conditions.

Since each internal nodal point $z_{j,i}$ belongs to four FE at once, then each equation in (7) will contain four summands, according to the number of FE adjacent to the nodal point $z_{j,i}$.

Thus, the system of equations (7) can be written as follows:

$$\frac{\partial E_s\left(e_{j,i}\right)}{\partial W_1{}^{j,i}} + \frac{\partial E_s\left(e_{j,i-1}\right)}{\partial W_2{}^{j,i-1}} + \frac{\partial E_s\left(e_{j-1,i}\right)}{\partial W_3{}^{j-1,i}} +$$

$$+ \frac{\partial E_s\left(e_{j-1,i-1}\right)}{\partial W_4{}^{j-1,i-1}} = 0,$$

$$\frac{\partial E_s\left(e_{j,i}\right)}{\partial W_5{}^{j,i}} + \frac{\partial E_s\left(e_{j,i-1}\right)}{\partial W_6{}^{j,i-1}} + \frac{\partial E_s\left(e_{j-1,i}\right)}{\partial W_7{}^{j-1,i}} +$$

$$+ \frac{\partial E_s\left(e_{j-1,i-1}\right)}{\partial W_8{}^{j-1,i-1}} = 0, \qquad (8)$$

$$\frac{\partial E_s\left(e_{j,i}\right)}{\partial W_9{}^{j,i}} + \frac{\partial E_s\left(e_{j,i-1}\right)}{\partial W_{10}{}^{j,i-1}} + \frac{\partial E_s\left(e_{j-1,i}\right)}{\partial W_{11}{}^{j-1,i}} +$$

$$+ \frac{\partial E_s\left(e_{j-1,i-1}\right)}{\partial W_{12}{}^{j-1,i-1}} = 0.$$

In equations (8), the functional $E_s$ is considered only on those FE that are adjacent to the internal node $z_{j,i}$ since the derivatives of the functional of other FE with respect to $W\left(z_{j,i}\right), W_x'\left(z_{j,i}\right), W_y'\left(z_{j,i}\right)$ will be 0.

*Formation of the coefficients of the system of linear algebraic equations*

The derivatives of functional (5) are taken with respect to the unknown parameters in each internal node of the area $D$.

At each nodal point, e.g., $z_{j,i}$ the three unknown parameters are the deflection value $W$, the value $W_x'$, and the value $W_y'$. Hence, the derivatives of the functional are taken with respect to the parameter $W$, parameter $W_x'$, parameter $W_y'$, and these derivatives are equated to 0 (Ritz method procedure). We obtain three equations at each internal node. There are four FE adjacent to the node $z_{j,i}$ each of which has the specified parameters in the common node $z_{j,i}$. Therefore, there will be four terms in each equation, which are derivatives of $E_s$ with respect to the corresponding parameter included in each FE (see (8)).

The four FE adjacent to the node $z_{j,i}$ contain nine nodal points of the area ($z_{j,i}, z_{j+1,i}, z_{j,i+1}, z_{j,i-1}, z_{j-1,i}, z_{j-1,i-1}, z_{j-1,i+1}, z_{j+1,i+1}, z_{j+1,i-1}$). Therefore, in each of the three equations, there will be nine parameters of values $W$, nine parameters of values $W_x'$, and nine parameters of values $W_y'$, i.e., in each equation, there will be 27 terms and, accordingly, 27 coefficients,

the values of which must be determined to solve the system of linear algebraic equations (SLAE), which is obtained after applying the described method to the initial variational problem.

For convenience of further transformations, we introduce the following notations (operators), based on the type of functional (5):

$$FW(f_1, f_2, \alpha, \beta) =$$

$$= \phi_{f_1xx}^{\alpha,\beta} \phi_{f_2xx}^{\alpha,\beta} + \phi_{f_1xx}^{\alpha,\beta} \phi_{f_2yy}^{\alpha,\beta} + \phi_{f_1yy}^{\alpha,\beta} \phi_{f_2xx}^{\alpha,\beta} + \phi_{f_1yy}^{\alpha,\beta} \phi_{f_2yy}^{\alpha,\beta} +$$

$$+2(1-\mu)\left( \phi_{f_1xy}^{\alpha,\beta} \phi_{f_2xy}^{\alpha,\beta} - \frac{1}{2} \phi_{f_1xx}^{\alpha,\beta} \phi_{f_2yy}^{\alpha,\beta} - \frac{1}{2} \phi_{f_1yy}^{\alpha,\beta} \phi_{f_2xx}^{\alpha,\beta} \right),$$

$$A_1^{j,i} = \int_{x_j}^{x_{j+1}} dx \int_{y_i}^{y_{i+1}} (\ ) dy, \quad A_2^{j,i} = \int_{x_j}^{x_{j+1}} dx \int_{y_{i-1}}^{y_i} (\ ) dy,$$

$$A_3^{j,i} = \int_{x_{j-1}}^{x_j} dx \int_{y_i}^{y_{i-1}} (\ ) dy, \quad A_4^{j,i} = \int_{x_{j-1}}^{x_j} dx \int_{y_{i-1}}^{y_i} (\ ) dy,$$

$$B_1^{j,i} = A_1^{j,i} \left( \phi_1^{j,i} \right) + A_2^{j,i} \left( \phi_2^{j,i-1} \right) +$$

$$+ A_3^{j,i} \left( \phi_3^{j-1,i} \right) + A_4^{j,i} \left( \phi_4^{j-1,i-1} \right),$$

$$B_2^{j,i} = A_1^{j,i} \left( \phi_5^{j,i} \right) + A_2^{j,i} \left( \phi_6^{j,i-1} \right) +$$

$$+ A_3^{j,i} \left( \phi_7^{j-1,i} \right) + A_4^{j,i} \left( \phi_8^{j-1,i-1} \right), \quad (9)$$

$$B_3^{j,i} = A_1^{j,i} \left( \phi_9^{j,i} \right) + A_2^{j,i} \left( \phi_{10}^{j,i-1} \right) +$$

$$+ A_3^{j,i} \left( \phi_{11}^{j-1,i} \right) + A_4^{j,i} \left( \phi_{12}^{j-1,i-1} \right).$$

Now all three equations of system (8) can be written as follows:

$$\sum_{k=1}^{12} \left[ A_1^{j,i} \left( W_k^{j,i} FW(k,1,j,i) \right) + \right.$$

$$+ A_2^{j,i} \left( W_k^{j,i-1} FW(k,2,j,i-1) \right) +$$

$$+ A_3^{j,i} \left( W_k^{j-1,i} FW(k,3,j-1,i) \right) +$$

$$\left. + A_4^{j,i} \left( W_k^{j-1,i-1} FW(k,4,j-1,i-1) \right) \right] = \frac{q}{D} B_1^{j,i},$$

$$\sum_{k=1}^{12} \left[ A_1^{j,i} \left( W_k^{j,i} FW(k,5,j,i) \right) + \right.$$

$$+ A_2^{j,i} \left( W_k^{j,i-1} FW(k,6,j,i-1) \right) +$$

$$+ A_3^{j,i} \left( W_k^{j-1,i} FW(k,7,j-1,i) \right) +$$

$$\left. + A_4^{j,i} \left( W_k^{j-1,i-1} FW(k,8,j-1,i-1) \right) \right] = \frac{q}{D} B_2^{j,i}, \quad (10)$$

$$\sum_{k=1}^{12} \left[ A_1^{j,i} \left( W_k^{j,i} FW(k,9,j,i) \right) + \right.$$

$$+ A_2^{j,i} \left( W_k^{j,i-1} FW(k,10,j,i-1) \right) +$$

$$+ A_3^{j,i} \left( W_k^{j-1,i} FW(k,11,j-1,i) \right) +$$

$$+ A_4^{j,i} \left( W_k^{j-1,i-1} FW(k,12,j-1,i-1) \right) = \frac{q}{D} B_3^{j,i}.$$

These equations ensure continuity of the approximation of functions $W(x,y)$ and $W_x'(x,y), W_y(x,y)$ on four FE adjacent to the node $z_{j,i}$.

We will denote the values of the parameters $w_x'$ at the nodal points by $wx$, but it is necessary to add 4 to the indices of the parameter $w$, and, correspondingly, we will denote the values of the parameters $w'_y$ at the nodal points by $wy$, but it is necessary to add 8 to the indices of $w$.

The first equation of system (10) can now be written in the following form:

$$a_1^{j,i} w_{j,i} + a_2^{j,i} w_{j+1,i} + a_3^{j,i} w_{j,i+1} + a_4^{j,i} w_{j,i-1} + a_5^{j,i} w_{j-1,i} +$$

$$+ a_6^{j,i} w_{j-1,i-1} + a_7^{j,i} w_{j-1,i+1} + a_8^{j,i} w_{j+1,i+1} +$$

$$+ a_9^{j,i} w_{j+1,i-1} + a_{10}^{j,i} wx_{j,i} + a_{11}^{j,i} wx_{j+1,i} + \ldots$$

$$+ a_{18}^{j,i} wx_{j+1,i-1} + a_{19}^{j,i} wy_{j,i} + a_{20}^{j,i} wy_{j+1,i} + \ldots$$

$$+ a_{27}^{j,i} wy_{j+1,i-1} = \frac{q}{D} B_1^{j,i}.$$

The first nine coefficients $a_1^{j,i} - a_9^{j,i}$ are basic and are as follows:

$$a_1^{j,i} = A_1^{j,i} \left( FW(1,1,j,i) \right) + A_2^{j,i} \left( FW(2,2,j,i-1) \right) +$$

$$+ A_3^{j,i} \left( FW(3,3,j-1,i) \right) + A_4^{j,i} \left( FW(4,4,j-1,i-1) \right),$$

$$a_2^{j,i} = A_1^{j,i} \left( FW(3,1,j,i) \right) + A_2^{j,i} \left( FW(4,2,j,i-1) \right),$$

$$a_3^{j,i} = A_1^{j,i} \left( FW(2,1,j,i) \right) + A_3^{j,i} \left( FW(4,3,j-1,i) \right),$$

$$a_4^{j,i} = A_2^{j,i} \left( FW(1,2,j,i-1) \right) + A_4^{j,i} \left( FW(3,4,j-1,i-1) \right),$$

$$a_5^{j,i} = A_3^{j,i} \left( FW(1,3,j-1,i) \right) + A_4^{j,i} \left( FW(2,4,j-1,i-1) \right),$$

$$a_6^{j,i} = A_4^{j,i} \left( FW(1,4,j-1,i-1) \right),$$

$$a_7^{j,i} = A_3^{j,i} \left( FW(2,3,j-1,i) \right),$$

$$a_8^{j,i} = A_1^{j,i} \left( FW(4,1,j,i) \right),$$

$$a_9^{j,i} = A_2^{j,i} \left( FW(3,2,j,i-1) \right).$$

The parameter $w$ has an index that changes from 1 to 4, and the value of $f_1$ in the operator $FW(f_1, f_2, \alpha, \beta)$ for that parameter changes as well. For the parameter $wx$, the index $f_1$ will change from 5 to 8. Hence, the coefficients $a_{10}^{j,i} - a_{18}^{j,i}$ are obtained from the corresponding coefficients $a_1^{j,i} - a_9^{j,i}$ by adding 4 to the corresponding value of $f$. Similarly, to obtain the coefficients $a_{19}^{j,i} - a_{27}^{j,i}$, we need to add 8 to the value $f_1$ in the corresponding coefficients $a_1^{j,i} - a_9^{j,i}$. In this case, in the first equation of system (10), the parameter $f_2$ in the operator $FW(f_1, f_2, \alpha, \beta)$ changes from 1 to 4. In the second equation of system (10), this parameter changes from 5 to 8, and in the third equation of system (10), $f_2$ changes from 9 to 12.

The second and third equations of system (10) can be briefly written in the following form:

$$b_1^{j,i} w_{j,i} + b_2^{j,i} w_{j+1,i} + b_3^{j,i} w_{j,i+1} + b_4^{j,i} w_{j,i-1} + b_5^{j,i} w_{j-1,i} +$$

$$+ b_6^{j,i} w_{j-1,i-1} + b_7^{j,i} w_{j-1,i+1} + b_8^{j,i} w_{j+1,i+1} + b_9^{j,i} w_{j+1,i-1} +$$

$$b_{10}^{j,i} wx_{j,i} + b_{11}^{j,i} wx_{j+1,i} + \dots + b_{18}^{j,i} wx_{j+1,i-1} +$$

$$+ b_{19}^{j,i} wy_{j,i} + b_{20}^{j,i} wy_{j+1,i} + \dots + b_{27}^{j,i} wy_{j+1,i-1} = \frac{q}{D} B_2^{j,i}.$$

$$c_1^{j,i} w_{j,i} + c_2^{j,i} w_{j+1,i} + \dots + c_9^{j,i} w_{j+1,i-1} + c_{10}^{j,i} wx_{j,i} +$$

$$+ c_{11}^{j,i} wx_{j+1,i} + \dots + c_{18}^{j,i} wx_{j+1,i-1} + c_{19}^{j,i} wy_{j,i} +$$

$$+ c_{20}^{j,i} wy_{j+1,i} + \dots + c_{27}^{j,i} wy_{j+1,i-1} = \frac{q}{D} B_3^{j,i}.$$

To obtain the coefficients $b_1^{j,i} - b_{27}^{j,i}$, we need to add 4 to the value $f_2$ in the corresponding expressions of the coefficients $a_1^{j,i} - a_{27}^{j,i}$, and to obtain the coefficients $c_1^{j,i} - c_{27}^{j,i}$, we need to add 8 to the value $f_2$ in the corresponding expressions of the coefficients $a_1^{j,i} - a_{27}^{j,i}$. Thus, the algorithm for calculating the coefficients of the system of linear algebraic equations (SLAE) of the method for the discrete approximation of the initial functions can be presented in the form of Table, which will make it easy to design a program for their calculation with a computer.

When we moving to a new nodal point $z_{j,i}$, its coordinates $x_j$ and $y_i$ change. That is why these values should be changed in the expressions of the approximation of the functions $\varphi_k^{ji}(x, y)$ (4). Correspondingly, the coefficients of system (10) should be changed too. All these changes are carried out in a cycle with respect to variables $j, i$ and do not pose any difficulties.

*Calculation examples*

As an example of the use of the considered method for slab calculation, let us find the deflection of a square slab with side $a$, which is under the uniformly distributed transverse load $q$. Let us assume that the slab has rigid restraint along the contour, therefore, on the contour, $w = 0, w'_x = 0, w'_y = 0$. The area $D\{0 \le x \le a; 0 \le y \le a\}$ is divided into four FE (Fig. 3). Due to the symmetry of the problem, at the node $z_{1,1}$, the first-order derivatives with respect to $x$ and $y$ will

be equal to 0. Only the deflection at the node $z_{1,1}$ remains unknown.

In this case, the approximation $W(x, y)$ at each of the four FE will have the following form:

$$\left( h_x = \frac{a}{2}, h_y = \frac{a}{2} \right)$$

On FE $e_{1,1}$: $W(x, y) = w_1^{1,1} \phi_1^{1,1}(x, y)$,

where $\frac{a}{2} \le x \le a, \frac{a}{2} \le y \le a$,

On FE $e_{1,0}$: $W(x, y) = w_2^{1,0} \phi_2^{1,0}(x, y)$,

where $\frac{a}{2} \le x \le a, 0 \le y \le \frac{a}{2}$,

On FE $e_{0,1}$: $W(x, y) = w_3^{0,1} \phi_3^{0,1}(x, y)$,

where $0 \le x \le \frac{a}{2}, \frac{a}{2} \le y \le a$,

On FE $e_{0,0}$: $W(x, y) = w_4^{0,0} \phi_4^{0,0}(x, y)$,

where $0 \le x \le \frac{a}{2}, 0 \le y \le \frac{a}{2}$.

Here, $w_1^{1,1}, w_2^{1,0}, w_3^{1,0}, w_4^{0,0}$ are $w(z_{1,1})$.

The equation for finding $w(z_{1,1})$ will have the following form:

$$\frac{\partial f(e_{1,1})}{\partial w_1^{1,1}} + \frac{\partial f(e_{1,0})}{\partial w_2^{1,0}} + \frac{\partial f(e_{0,1})}{\partial w_3^{0,1}} + \frac{\partial f(e_{0,0})}{\partial w_4^{0,0}} = 0.$$

The compact form of this equation will be as follows (with the $D$ multiplier omitted):

$$w(z_{1,1}) \left[ A_1^0 (FW(1,1,1,1)) + A_2^0 (FW(2,2,1,0)) + \right.$$

$$\left. + A_3^0 (FW(3,3,0,1)) + A_4^0 (FW(4,4,0,0)) \right] = \frac{q}{D} B_1^0,$$

where

$$A_1^0 (\;) = \int_{a/2}^{a} dx \int_{a/2}^{a} (\;)dy, \; A_2^0 (\;) = \int_{a/2}^{a} dx \int_{0}^{a/2} (\;)dy,$$

$$A_3^0 (\;) = \int_{0}^{a/2} dx \int_{a/2}^{a} (\;)dy, \; A_4^0 (\;) = \int_{0}^{a/2} dx \int_{0}^{a/2} (\;)dy,$$

$$B_1^0 = A_1^0 (\phi_1^{1,1}) + A_2^0 (\phi_2^{1,0}) + A_3^0 (\phi_3^{0,1}) + A_4^0 (\phi_4^{0,0}).$$

Since there is one unknown parameter $w(z_{1,1})$ in the resulting equation, then the equation can be written in the following form:

### Algorithm for calculating the SLAE coefficients for the slab

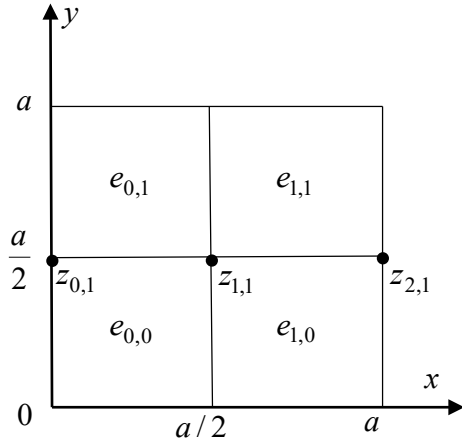| Coefficient No. | Coefficient type | | |
|---|---|---|---|
| | $a_1^{j,i} - a_{27}^{j,i}$ | $b_1^{j,i} - b_{27}^{j,i}$ | $c_1^{j,i} - c_{27}^{j,i}$ |
| 1–9 | Basic $1 \le f_1 \le 4; 1 \le f_2 \le 4$ | $1 \le f_1 \le 4$ $f_2 = f_2 + 4$ | $1 \le f_1 \le 4$ $f_2 = f_2 + 8$ |
| 10–18 | $1 \le f_2 \le 4$ $f_1 = f_1 + 4$ | $f_1 = f_1 + 4$ $f_2 = f_2 + 4$ | $f_1 = f_1 + 4$ $f_2 = f_2 + 8$ |
| 19–27 | $1 \le f_2 \le 4$ $f_1 = f_1 + 8$ | $f_1 = f_1 + 8$ $f_2 = f_2 + 4$ | $f_1 = f_1 + 8$ $f_2 = f_2 + 8$ |

Fig. 3. Square slab divided into four FE

$$w\left(z_{1,1}\right)\cdot A = \frac{q}{D} B_1^0.$$

Let us calculate the integrals in the corresponding expressions.

Then we express the functions $\phi_1^{1,1}(x,y), \phi_2^{1,0}(x,y), \phi_3^{0,1}(x,y), \phi_4^{0,0}(x,y)$, using (4):

$$\phi_1^{1,1} = \frac{\left(a/2\right)^3 - 3\frac{a}{2}\left(x - a/2\right)^2 + 2\left(x - a/2\right)^3}{\left(a/2\right)^3} \times$$

$$\times \frac{\left(a/2\right)^3 - 3\frac{a}{2}\left(y - a/2\right)^2 + 2\left(y - a/2\right)^3}{\left(a/2\right)^3},$$

$$\phi_2^{1,0} = \frac{\left(a/2\right)^3 - 3\frac{a}{2}\left(x - a/2\right)^2 + 2\left(x - a/2\right)^3}{\left(a/2\right)^3} \times$$

$$\times \frac{3\frac{a}{2}y^2 - 2y^3}{\left(a/2\right)^3}, \qquad (11)$$

$$\phi_3^{0,1} = \frac{3\frac{a}{2}x^2 - 2x^3}{\left(a/2\right)^3} \cdot \frac{\left(a/2\right)^3 - 3\frac{a}{2}\left(y - a/2\right)^2 + 2\left(y - a/2\right)^3}{\left(a/2\right)^3},$$

$$\phi_4^{0,0} = \frac{3\frac{a}{2}x^2 - 2x^3}{\left(a/2\right)^3} \cdot \frac{3\frac{a}{2}y^2 - 2y^3}{\left(a/2\right)^3}.$$

The derivatives of the function $\phi_1^{1,1}(x,y)$ will take the following form:

$$\phi_{1xx}^{1,1} = \frac{-6\frac{a}{2} + 12\left(x - a/2\right)}{\left(a/2\right)^3} \times$$

$$\times \frac{\left(a/2\right)^3 - 3\frac{a}{2}\left(y - a/2\right)^2 + 2\left(y - a/2\right)^3}{\left(a/2\right)^3},$$

$$\phi_{1yy}^{1,1} = \frac{\left(a/2\right)^3 - 3\frac{a}{2}\left(x - a/2\right)^2 + 2\left(x - a/2\right)^3}{\left(a/2\right)^3} \times$$

$$\times \frac{-6\frac{a}{2} + 12\left(y - a/2\right)}{\left(a/2\right)^3},$$

$$\phi_{1xy}^{1,1} = \frac{-6\frac{a}{2}\left(x - a/2\right) + 6\left(x - a/2\right)^2}{\left(a/2\right)^3} \times$$

$$\times \frac{-6\frac{a}{2}\left(y - a/2\right) + 6\left(y - a/2\right)^2}{\left(a/2\right)^3}.$$

Then we calculate the integrals:

$$\int_{a/2}^{a} dx \int_{a/2}^{a} \left[ \left(\phi_{1xx}^{1,1}\right)^2 + 2\phi_{1xx}^{1,1} \cdot \phi_{1yy}^{1,1} + \left(\phi_{1yy}^{1,1}\right)^2 + \right.$$

$$\left. 2(1-\mu)\left( \left(\phi_{1yy}^{1,1}\right)^2 - \phi_{1xx}^{1,1} \cdot \phi_{1yy}^{1,1} \right) \right] dy = \frac{47,177}{a^2},$$

$$\int_{a/2}^{a} dx \int_{a/2}^{a} \phi_1^{1,1}(x,y) dy = \frac{a^2}{16}.$$

Other integrals are calculated in the same way. Thus, we obtain the following:

$$B_1^0 = \frac{a^2}{4}, \quad A = \frac{188,697}{a^2},$$

and, therefore, $w\left(z_{1,1}\right) = 0,00132 \frac{a^4 q}{D}$.

For comparison, let us find the deflection of the slab under consideration using the Ritz method in the continuous approximation of $W(x,y)$ in the following form:

$$W(x,y) = w_1 \sin^2 \pi \frac{x}{a} \sin^2 \pi \frac{y}{a}.$$

By substituting this expression into functional (5), we find the derivative of the functional with respect to $w_1$ and equate it to 0. As a result, we obtain the following equation:

$$\frac{\partial E_s}{\partial w_1} = D \int_0^a dx \int_0^a \left[ w_1 \left( 4\left(\frac{\pi}{a}\right)^4 \cos^2 2\pi\frac{x}{a} \sin^4 \pi\frac{y}{a} + \right. \right.$$

$$+4\left(\frac{\pi}{a}\right)^4 \sin^4 \pi\frac{x}{a} \cos^2 2\pi\frac{y}{a} +$$

$$\left. +2\cdot 4\left(\frac{\pi}{a}\right)^4 \cos 2\pi\frac{x}{a} \sin^2 \pi\frac{y}{a} \sin^2 \pi\frac{x}{a} \cos 2\pi\frac{y}{a} \right) +$$

$$+2(1-\mu) w_1 \left( \left(\frac{\pi}{a}\right)^4 \sin^2 2\pi\frac{x}{a} \sin^2 2\pi\frac{y}{a} - \right.$$

$$\left. \left. -4\left(\frac{\pi}{a}\right)^4 \cos 2\pi\frac{x}{a} \sin^2 \pi\frac{x}{a} \sin^2 \pi\frac{y}{a} \cos 2\pi\frac{y}{a} \right) \right] -$$

63

$$-\frac{q}{D}\sin^2\pi\frac{x}{a}\sin^2\pi\frac{y}{a}\Bigg]dy=0. \qquad (12)$$

Whence it follows that: $w_1 = w\big(z_{1,1}\big)=0,00128\dfrac{qa^4}{D}$.

The exact solution of this problem is known:

$$W\left(\frac{a}{2},\frac{a}{2}\right)=0,00126\frac{qa^4}{D}.$$

Thus, the solution obtained by the Ritz method in the continuous approximation of the deflection $W(x,y)$ differs from the exact one by 1.6%, and the solution obtained in the discrete approximation differs from the exact one by 4.6%.

The discrete approximation of the deflection is reasonable when the boundary conditions are such that it is difficult or impossible to find an approximation of the deflection by functions that are continuous over the entire area.

Now, in the example under consideration, let us change the slab edge restraint conditions Let us assume that at $y=0$ and $y=a$, the edge is rigidly restrained, and at $x=0$, $x=a$, it is free. Therefore, at the nodes $z_{1,1}, z_{0,1}, z_{2,1}$ (see Fig. 2), the deflection will not be 0. Moreover, at the nodes $z_{0,1}$ and $z_{2,1}$, $w'_x$ will not be equal to 0, but $w'_y$ at these nodes will be equal to 0 due to symmetry. Thus, $w(z_{1,1}), w(z_{0,1}), w(z_{2,1}), w'_x(z_{0,1}), w'_x(z_{2,1})$ will be the sought parameters. Let us express the $W(x,y)$ approximation in this case for each of the four FE.

$$W(x,y)\Big|_{e_{1,1}}=$$
$$=w_1^{1,1}\phi_1^{1,1}(x,y)+w_3^{1,1}\phi_3^{1,1}(x,y)+w_7^{1,1}\phi_7^{1,1}(x,y),$$

$$W(x,y)\Big|_{e_{1,0}}=$$
$$=w_2^{1,0}\phi_2^{1,0}(x,y)+w_4^{1,0}\phi_4^{1,0}(x,y)+w_8^{1,0}\phi_8^{1,0}(x,y),$$

$$W(x,y)\Big|_{e_{0,1}}=$$
$$=w_3^{0,1}\phi_3^{0,1}(x,y)+w_1^{0,1}\phi_1^{0,1}(x,y)+w_5^{0,1}\phi_5^{0,1}(x,y),$$

$$W(x,y)\Big|_{e_{0,0}}=$$
$$=w_2^{0,0}\phi_2^{0,0}(x,y)+w_4^{0,0}\phi_4^{0,0}(x,y)+w_6^{0,0}\phi_6^{0,0}(x,y).$$

Here

$$w_1^{1,1}, w_2^{1,0}, w_3^{0,1}, w_4^{0,0} — w(z_{1,1}),\ w_3^{1,1}, w_4^{1,0} — w(z_{2,1}),$$
$$w_1^{0,1}, w_2^{0,0} — w(z_{0,1}),$$
$$w_7^{1,1}, w_8^{1,0} — w'_x(z_{2,1}),\ w_5^{0,1}, w_6^{0,0} — w'_x(z_{0,1}).\ 1$$

The functions $\phi_e^{\alpha,\beta}$ at $\alpha$ equal to 0 or 1 and $\beta$ equal to 0 or 1 have form (4).

Let us denote the following:

$$w(z_{1,1})=w_{1,1},\ w(z_{2,1})=w_{2,1},\ w(z_{0,1})=w_{0,1},$$
$$w'_x(z_{2,1})=wx_{2,1},\ w'_x(z_{0,1})=wx_{0,1}.$$

Now we can write the following:

$$W(x,y)\Big|_{e_{1,1}}=w_{1,1}\phi_1^{1,1}+w_{2,1}\phi_3^{1,1}+wx_{2,1}\phi_7^{1,1},$$

$$W(x,y)\Big|_{e_{1,0}}=w_{1,1}\phi_2^{1,0}+w_{2,1}\phi_4^{1,0}+wx_{2,1}\phi_8^{1,0},$$

$$W(x,y)\Big|_{e_{0,1}}=w_{1,1}\phi_3^{0,1}+w_{0,1}\phi_1^{0,1}+wx_{0,1}\phi_5^{0,1},$$

$$W(x,y)\Big|_{e_{0,0}}=w_{0,1}\phi_2^{0,0}+w_{1,1}\phi_4^{0,0}+wx_{0,1}\phi_6^{0,0}.$$

There will be one internal point $z_{1,1}$, therefore, there will be one equation:

$$\frac{\partial E_s\big(e_{1,1}\big)}{\partial w_{1,1}}+\frac{\partial E_s\big(e_{1,0}\big)}{\partial w_{1,1}}+\frac{\partial E_s\big(e_{0,1}\big)}{\partial w_{1,1}}+\frac{\partial E_s\big(e_{0,0}\big)}{\partial w_{1,1}}=0.$$

By using the previously adopted notations (operators) and functional (5), we can write this equation as follows:

$$w_{1,1}A_1^0\big(FW(1,1,1,1)\big)+w_{2,1}A_1^0\big(FW(3,1,1,1)\big)+$$
$$+wx_{2,1}A_1^0\big(FW(7,1,1,1)\big)+w_{1,1}A_2^0\big(FW(2,2,1,0)\big)+$$
$$+w_{2,1}A_2^0\big(FW(4,2,1,0)\big)+wx_{2,1}A_2^0\big(FW(8,2,1,0)\big)+$$
$$+w_{1,1}A_3^0\big(FW(3,3,0,1)\big)+w_{0,1}A_3^0\big(FW(1,3,0,1)\big)+$$
$$wx_{0,1}A_3^0\big(FW(5,3,0,1)\big)+w_{1,1}A_4^0\big(FW(4,4,0,0)\big)+$$
$$+w_{0,1}A_4^0\big(FW(2,4,0,0)\big)+wx_{0,1}A_4^0\big(FW(6,4,0,0)\big)=$$
$$=\frac{q}{D}B_1^0.$$

Having calculated the corresponding integrals, we reduce this equation to the following form:

$$a_1w_{1,1}+a_2w_{2,1}+a_3w_{0,1}+a_4wx_{2,1}+a_5wx_{0,1}=\frac{q}{D}a_b,$$

where

$$a_1=188,576\frac{1}{a^2},\quad a_2=-46,35\frac{1}{a^2},\quad a_3=-46,35\frac{1}{a^2},$$

$$a_4=16,811\frac{1}{a^2},\quad a_5=-16,811\frac{1}{a^2},\quad a_6=\frac{a^2}{4}.$$

Another four equations are obtained from the boundary conditions at the edge at $x=0$, $x=a$.. Since these edges are free, the moment and transverse force must be 0 here, which means that at $x=0$, $x=a$, the second-order derivative of the deflection $w''_{xx}$ and the third-order derivative $w'''_{xxx}$ must be 0. Thus, we obtain the following conditions:

$$w''_{xx}\big(z_{2,1}\big)=0,\ w'''_{xxx}\big(z_{2,1}\big)=0,\ w''_{xx}\big(z_{0,1}\big)=0,$$

$$w'''_{xxx}\big(z_{0,1}\big)=0.$$

And, therefore,

$$w''_{xx}\big(z_{2,1}\big)\Big|_{e_{1,1}}=0,\ w'''_{xxx}\big(z_{2,1}\big)\Big|_{e_{1,1}}=0,$$

$$w''_{xx}\big(z_{0,1}\big)\Big|_{e_{0,1}}=0,\ w'''_{xxx}\big(z_{0,1}\big)\Big|_{e_{0,1}}=0.$$

The missing four equations take the following form:

$$\frac{\partial^2 W}{\partial x^2}\Bigg|_{e_{1,1}}=w_1^{1,1}\frac{24}{a^2}-w_3^{1,1}\frac{24}{a^2}+w_7^{1,1}\frac{8}{a}=0,$$

$$\frac{\partial^3 W}{\partial x^3}\Bigg|_{e_{1,1}}=w_1^{1,1}\frac{96}{a^3}-w_3^{1,1}\frac{96}{a^3}+w_7^{1,1}\frac{24}{a^2}=0,$$

$$\frac{\partial^2 W}{\partial x^2}\bigg|_{e_{0,1}} = -w_3^{0,1}\frac{24}{a^2} + w_1^{0,1}\frac{24}{a^2} - w_5^{0,1}\frac{8}{a} = 0,$$

$$\frac{\partial^3 W}{\partial x^3}\bigg|_{e_{0,1}} = w_3^{0,1}\frac{96}{a^3} - w_1^{0,1}\frac{96}{a^3} + w_5^{0,1}\frac{24}{a^2} = 0.$$

Here

$$w_1^{1,1} = w_{1,1}, w_3^{1,1} = w_{2,1}, w_7^{1,1} = wx_{2,1},$$

$$w_3^{0,1} = w_{1,1}, w_1^{0,1} = w_{0,1}, w_5^{0,1} = wx_{0,1}.$$

The same equations are obtained if we use the following conditions:

$$w_{xx}''\left(z_{2,1}\right)\big|_{e_{1,0}} = 0,\ w_{xxx}'''\left(z_{2,1}\right)\big|_{e_{1,0}} = 0,\ w_{xx}''\left(z_{0,1}\right)\big|_{e_{0,0}} = 0,$$

$$w_{xxx}'''\left(z_{0,1}\right)\big|_{e_{0,0}} = 0.$$

Thus, to find the unknown parameters $w_{1,1}, w_{2,1}, w_{0,1}, wx_{2,1}, wx_{0,1}$, we have five equations:

$$-\frac{24}{a^2}w_{1,1} + \frac{24}{a^2}w_{0,1} - \frac{8}{a}wx_{0,1} = 0,$$

$$\frac{96}{a^3}w_{1,1} - \frac{96}{a^3}w_{0,1} + \frac{24}{a^2}wx_{0,1} = 0,$$

$$\frac{24}{a^2}w_{1,1} - \frac{24}{a^2}w_{2,1} + \frac{8}{a}wx_{2,1} = 0,$$

$$\frac{96}{a^3}w_{1,1} - \frac{96}{a^3}w_{2,1} + \frac{24}{a^2}wx_{2,1} = 0,$$

$$\frac{188,576}{a^2}w_{1,1} - \frac{46,35}{a^2}w_{2,1} - \frac{46,35}{a^2}w_{0,1} + \frac{16,811}{a^2}wx_{2,1} -$$

$$-\frac{16,811}{a^2}wx_{0,1} = \frac{a^2 q}{4D}.$$

If we add the first and third equations, we will obtain $wx_{0,1} = wx_{2,1}$, and if we subtract the fourth equation from the second equation, we will obtain $w_{0,1} = w_{2,1}$. The equality $w_x'\left(z_{0,1}\right) = w_x'\left(z_{2,1}\right)$ is possible only if these derivatives are 0. Therefore, since $w\left(z_{0,1}\right) = w\left(z_{2,1}\right)$, then $w\left(z_{1,1}\right) = w\left(z_{0,1}\right) = w\left(z_{2,1}\right)$. Given all this, based on the last equation, we obtain the following:

$$\frac{188,576}{a^2}w_{1,1} - \frac{96,7}{a^2}w_{1,1} = \frac{a^2 q}{4D},$$

therefore, $w_{1,1} = 0,0026\dfrac{a^4 q}{D}.$

By analyzing the obtained solution, we can conclude that the slab in this case deforms axisymmetrically, i.e., the deformation along the $x$ axis is constant. In this case, the calculation for the deformation of the slab can be replaced by the calculation for the deformation of a beam of length $a$, rigidly fixed at the ends at $y = 0$, $y = a$. The equation of equilibrium of the beam will have the following form:

$$W^{\mathrm{IV}} = \frac{q}{EI},$$

and the general solution can be written as follows:

$$W\left(x\right) = \frac{q}{EI}\frac{y^4}{24} + c_1\frac{y^3}{6} + c_2\frac{y^2}{2} + c_3 y + c_4.$$

Based on the boundary conditions at $y = 0$, $y = a$, $W = 0$, $W' = 0$, we will obtain:

$$c_3 = 0,\ c_4 = 0,\ c_1 = -\frac{qa}{2EI},\ c_3 = \frac{qa^2}{12EI}.$$

Therefore, the deflection of the beam under consideration can be expressed by the following function:

$$W\left(x\right) = \frac{q}{EI}\left(\frac{y^4}{24} - \frac{a}{12}y^3 + \frac{a^2}{24}y^2\right),$$

and at $y = \dfrac{a}{2}$, the deflection will have the following form:

$$W\left(\frac{a}{2}\right) = 0,0026\frac{a^4 q}{EI}.$$

**Conclusion**

The system of linear algebraic equations obtained in the above examples contains 27 x 3 = 81 coefficients. And only the first nine coefficients are basic. Other coefficients can be found by recurrence relations based on these nine coefficients (see Table). Thus, due to the introduction of some notations (operators) $FW$, $A_k^{ji}$, $B_k^{ji}$, the process of finding the coefficients of the system of resolving algebraic equations is very simple and convenient for programming.

The proposed method of slab calculation by the Ritz method in the discrete approximation of displacements cannot serve as an alternative to the FEM, but it is very convenient for the calculation of relatively simple components of building structures, such as beams, slabs, and shells. However, the calculation of complex three-dimensional structures is possible only with the FEM.

**References**

Argyris, J. (1961). Energy theorems and structural analysis. Part 1. In: Filin, A. P. (ed.). *Modern methods for calculating complex statically indeterminate systems*. Leningrad: Sudpromgiz, pp. 37–255.

Auricchio, F., Beirão da Veiga, L., Kiendl, J., Lovadina, C., and Reali, A. (2016). Isogeometric collocation mixed methods for rods. *Discrete and Continuous Dynamical Systems - Series S*, Vol. 9, Issue 1, pp. 33–42. DOI: 10.3934/dcdss.2016.9.33.

Bishay, P. L., Sladek, J., Sladek, V., and Gao, X. W. (2017). Analysis of elastic media with voids using a mixed-collocation finite-element method. *Journal of Engineering Mechanics*, Vol. 143, Issue 4, 04016119. DOI: 10.1061/(ASCE)EM.1943-7889.000119.

Clough, R. W. (1960). The finite element method in plane stress analysis. *Proceedings of the American Society of Civil Engineers*, Vol. 23, pp. 345–378.

Courant, R. (1943). Variational methods for the solution of problems of equilibrium and vibrations. *Bulletin of the American Mathematical Society*, Vol. 49, No. 1, pp. 1–23. DOI: 10.1090/S0002-9904-1943-07818-4.

Farias, A. M., Devloo, P. R. B., Gomes, S. M., and Durán, O. (2018). An object-oriented framework for multiphysics problems combining different approximation spaces. *Finite Elements in Analysis and Design*, Vol. 151, pp. 34–49. DOI: 10.1016/j.finel.2018.08.002.

Gander, M. J. and Wanner, G. (2012). From Euler, Ritz, and Galerkin to modern computing. *SIAM Review*, Vol. 54, Issue 4, pp. 627–666. DOI: 10.1137/100804036.

Hrennikoff, A. (1941). Solution of problems of elasticity by the framework method. *Journal of Applied Mechanics*, Vol. 8, Issue 4, pp. A169–A175. DOI: 10.1115/1.4009129.

Ilyin, V. P., Karpov, V. V., and Maslennikov, A. M. (1990). *Numerical methods for solving problems of structural mechanics*. Minsk: Vysheishaya Shkola, 349 p.

Korn, G. and Korn, T. (1974). *Mathematical handbook (for scientists and engineers)*. Moscow: Nauka, 832 p.

Li, R., Wang, B., and Li, P. (2014). Hamiltonian system-based benchmark bending solutions of rectangular thin plates with a corner point supported. *International Journal of Mechanical*

*Sciences*, Vol. 85, pp. 212–218. DOI: 10.1016/j.ijmecsci.2014.05.004.

Mikhlin, S. G. (1970). *Variation methods in mathematical physics*. 2nd edition. Moscow: Nauka, 512 p.

Nwoji, C. U., Mama, B. O., Ike, C. C., and Onah, H. N. (2017). Galerkin-Vlasov method for the flexural analysis of rectangular Kirchhoff plates with clamped and simply supported edges. *IOSR Journal of Mechanical and Civil Engineering (IOSR-JMCE)*, Vol. 14, Issue 2, pp. 61–74. DOI: 10.9790/1684-1402016174.

Postnov, V. A. and Kharkhurim, I. Ya. (1974). *The finite element method in ship structural analysis*. Leningrad: Sudostroenie, 344 p.

Postnov, V. A., Rostovtsev, D. M., Suslov, V. P., and Kochanov, Y. P. (1987). *Ship structural mechanics and theory of elasticity. Vol. 2. Bending and stability of rods, rod systems, plates and shells*. Lenindrad: Sudostroenie, 416 p.

Qu, Y., Chen, Y., Long, X., Hua, X., and Meng, G. (2013). A modified variational approach for vibration analysis of ring-stiffened conical-cylindrical shell combinations. *European Journal of Mechanics - A/Solids*, Vol. 37, pp. 200–215. DOI: 10.1016/j.euromechsol.2012.06.006.

Trushin, S. I. (2018). Structural mechanics: finite element method. Moscow: INFRA-M, 305 p.

Weinan, E. and Yu, B. (2018). The Deep Ritz method: a deep learning-based numerical algorithm for solving variational problems. *Communications in Mathematics and Statistics*, Vol. 6, Issue 1, pp. 1–12. DOI: 10.1007/s40304-018-0127-z.

Xue, X.-Y., Du, D.-W., Sun, J.-Y., and He, X.-T. (2021). Application of variational method to stability analysis of cantilever vertical plates with bimodular effect. *Materials*, Vol. 14, Issue 20, 6129. DOI: 10.3390/ma14206129.

Zienkiewicz, O. (1975). *The finite element method in engineering science*. Moscow: Mir, 541 p.

Zienkiewicz, O. C., Taylor, R. L., and Fox, D. D. (2013). *The finite element method for solid and structural mechanics*. 7th edition. Oxford: Butterworth-Heinemann, 672 p.

# МЕТОД РИТЦА ПРИ ДИСКРЕТНОЙ АППРОКСИМАЦИИ ПЕРЕМЕЩЕНИЙ ДЛЯ РАСЧЕТА ПЛИТ

Владимир Васильевич Карпов, Евгений Анатольевич Кобелев\*, Александр Матвеевич Масленников, Александр Николаевич Панин

Санкт-Петербургский государственный архитектурно-строительный университет
2-ая Красноармейская ул., 4, Санкт-Петербург, Россия

\*E-mail: evgeny.kobelev@gmail.com

**Аннотация**
**Введение**: МКЭ сводит задачу расчета самых различных строительных конструкций к формированию и решению системы линейных алгебраических уравнений. Для этого существуют методики получения матриц жесткости и податливости КЭ, в которых учитываются основные характеристики деформирования конструкции. Но МКЭ можно рассматривать и как частный случай метода Ритца при дискретной аппроксимации искомых функций. В функционале полной потенциальной энергии деформирования рассматриваемой конструкции учитываются все принятые характеристики напряженно-деформированного состояния. Так как для некоторых видов закрепления краев таких строительных конструкций как балка, плита или оболочка сложно или невозможно подобрать непрерывные аппроксимирующие функции как в классическом варианте метода Ритца, так и методе Бубнова – Галеркина, то (по аналогии с МКЭ) можно использовать метода Ритца при дискретной аппроксимации искомых функций. В работе на примере расчета плиты дается методика проведения таких расчетов. Показано, что введением некоторых обозначений-операторов процесс нахождения коэффициентов системы линейных алгебраических уравнений не вызывает затруднений и легко программируется. Предлагаемая методика не является альтернативой МКЭ, который является наиболее эффективным численным методом для расчета сложных трехмерных строительных конструкций. **Целью работы** было создание методики расчета плит методом Ритца при дискретной аппроксимации функции прогибов для случаев закрепления краев, когда сложно или невозможно подобрать непрерывные аппроксимирующие функции в классическом варианте метода Ритца и методе Бубнова – Галеркина. **Методы:** На основе применения вариационного метода Ритца при дискретной аппроксимации перемещений для расчета плит получены все основные соотношения для прямоугольных конечных элементов с 12 степенями свободы и разработан алгоритм формирования коэффициентов системы линейных алгебраических уравнений. **Результаты:** Впервые получено решение методом Ритца при дискретной аппроксимации перемещений плиты для случая, когда два края плиты жестко защемлены, а другие два края свободны. При этом корректное решение указанной задачи возможно только по предлагаемой методике и МКЭ. Для тестовой задачи было выполнено сравнение результатов расчета по предлагаемой методике с результатами при использовании классического метода Ритца, которое показало их весьма близкое совпадение. Оценена точность полученных результатов.

**Ключевые слова:** метод Ритца, функционал полной потенциальной энергии деформации, дискретная аппроксимация перемещений, плита, функция прогиба, конечный элемент, многочлены Эрмита.

# ADOBE BRICKS TO HOLLOW SANDCRETE BLOCK WALLING IN TROPICAL BUILDING CONSTRUCTION: MATERIAL IMPACT ON SUSTAINABLE INDOOR THERMAL COMFORT ATTAINMENT

Sule Adeniyi Olaniyan*

Ladoke Akintola University of Technology, Ogbomoso, Nigeria

*Corresponding author's e-mail: saolaniyan@lautech.edu.ng

**Abstract**

**Introduction**: Tropical climate is characterized by high temperature, the consequence of which induces indoor thermal discomfort. This is attributed to high solar gains through various elements of the building envelope, including windows, walls, and roof among others. However, in an attempt to optimize indoor thermal comfort with minimal or no recourse to mechanical installations, this study explores the roles of the walling fabrics by comparing varying thermo-physical properties of two identified masonry units in the study area of Ogbomoso, Nigeria (adobe bricks and hollow sandcrete blocks), with a view to identifying a more thermally comfortable and sustainable material option. **The methodology** involves virtual models of two similar residential buildings each composed of either adobe bricks or sandcrete blocks, as masonry units. These models were subjected to energy performance simulation analyses using DesignBuilder software, over a 12-month cycle period, to experience year-round differential thermal conditions. Through the observed comparative annual heat loads as experienced in the models, the results show improved indoor thermal comfort in the brick building (i.e., 7119.54 KWh), with heat loads being 11% lower than that of the sandcrete building (i.e., 8875.65 KWh) due to the brick walling fabric. This may be associated with the brick's lower thermal conductivity (U-Value) of 1.798 W/m²-K, compared with the sandcrete blocks' value of 1.999 W/m²-K. **Results**: In general, adobe bricks as a walling unit exhibit more thermal resistance against the harsh outdoor weather conditions than sandcrete blocks. The study is part of an ongoing effort towards reviving this partially neglected low impact material — adobe brick — with a view to attaining sustainable indoor thermal comfort as well as protect the environment in the study area.

**Keywords**: adobe brick, sandcrete block, simulation, sustainable, thermal comfort, tropics.

## Introduction

Over the past decades, architectural practice has faced a lot of challenges and transformations as our living conditions changed in different contexts considering social, technological, economic, political, and more importantly, environmental impacts. Our emerging housing typologies, in the tropical region particularly, as a consequence of our evolving patterns of living, are largely influenced by the phenomenal global environmental conditions (Altan et al., 2015). The tropical region falls between two lines of latitude, the Tropic of Cancer, 23.5 degrees north, where the sun is directly overhead at noon on June 21 (midsummer in the northern hemisphere), and the Tropic of Capricorn, 23.5 degrees south where the noon sun is directly overhead on December 21 (midsummer in the southern hemisphere). The region includes much of Central and South America, most of Africa, among others, as it is home to around 40% of the world population (Karyono, 2017; JCU, 2014). Its climate is mainly characterized by an elevated temperature and a high relative air humidity as these account for some level of indoor thermal discomfort ordinarily (Prianto and Depecker, 2003). However, buildings are required to offer sustainable, healthy and comfortable indoor environment, irrespective of the outdoor climatic conditions (Lotfabadi and Hançer, 2019). The consequence of these is the need for integration of the passive design approach (Bay and Ong, 2006). Alternatively, active energy sources such as mechanical cooling systems involving mechanical ventilation, air conditioning systems, are introduced for improved indoor thermal comfort. However, the latter often consume substantial energy among all building services (about 20–40% of the total energy needs), without which significant energy savings would have been achieved with the attendant reduced electricity costs (Kenisarin and Mahkamov, 2016; Prianto and Depecker, 2002; Raja et al., 2001).

It has been established that the building sector is responsible for around 39% of world $CO_2$-equivalent emissions. This is indicated in various submissions, including the Global Status Report for Buildings and Construction of 2019 (Ascione et al., 2021; Attoye et al., 2017). Besides, the sector is liable for about 36% of global energy consumption, 50% of extraction of raw materials, and 1/3 of drinking water consumption (Ascione et al., 2021; Lotfabadi et al., 2016; Nejat et al., 2015; World Energy Council, 2013). In this alarming scenario, the global building stock is expected to increase

Sule Adeniyi Olaniyan — Pages 68–81

ADOBE BRICKS TO HOLLOW SANDCRETE BLOCK WALLING IN TROPICAL BUILDING CONSTRUCTION:
MATERIAL IMPACT ON SUSTAINABLE INDOOR THERMAL COMFORT ATTAINMENT

and double by 2060 because of new constructions, particularly in developing countries, due to the rapid growth in population, economic activities and fast urbanization, with an attendant increase in $CO_2$ emissions (Lotfabadi, 2013). The building sector is a major energy consumer in tropical countries, apart from the industrial and transportation sectors (Prianto and Depecker, 2002). Thus, without any initiatives, suitable policies and action plans, energy demand in the construction sector could increase by 50%, with the consequent impact on global and local warming (Attoye et al., 2017; Camanzi et al., 2017; Jiang et al., 2016). This may otherwise affect the general wellbeing of the occupants. Thus, energy saving in this sector is important.

Towards such energy saving approach in building design and construction for indoor thermal comfort of the occupants in the tropical area, various attempts have been made by various researchers. Givoni (1976), Kwong et al. (2014), Longo et al. (2011), among others, demonstrate significant potentials of energy savings and improvements of indoor environmental quality accruable from adoption of natural ventilation. Attoye et al. (2017), Koukelli et al. (2022) as well as Quesada et al. (2012) illustrate integration of passive dynamic adaptive façade systems as the threshold between building and exterior environment to improve indoor thermal comfort (while reducing the building's energy consumption). Ascione et al. (2021) study the best trade-off among transparent envelope solutions, thermal mass of the building, and radiative characteristics of the roof. Thermo-physical properties of the materials used in the building envelope have also been studied by Pacheco-Torgal et al. (2014) as well as Pacheco-Torgal and Jalali (2011). In general, improvement of the construction methodology, energy efficiency technologies, adoption of passive design, use of renewable energy, and appropriate selection of building materials may constitute important strategies for the energy saving approach (Abanda et al., 2015) in this regard.

As a major point of departure, the focus of this study is on building materials. It examines the implications of the varying constituents of the building walling fabrics with emphasis on the locally available low impact building material, specifically adobe bricks, in place of the predominantly adopted sandcrete blocks in the study area. This is with a view to attaining more sustainable comfortable indoor thermal environment with minimal impact on the environment.

### Literature Review

Thermal comfort refers to that condition of mind, which expresses satisfaction with the thermal environment based on the heat balance of the human body (Shastry et al., 2016). This may also refer to the state of mind that expresses mental satisfaction with

the surrounding environment (Prianto and Depecker, 2003). It can be measured by both environmental and personal parameters. While the former is defined by such factors as ambient temperature, mean radiant temperature, water vapor pressure or relative humidity, and relative air velocity, the latter is defined by the clothing level or thermal resistance as well as activity or metabolic rate (Shastry et al., 2016; Prianto and Depecker, 2003). Attainment of thermal comfort is essential for the general wellbeing of occupants as a building does not only confer a spatial form to accommodate people but also acts as a device to modify an extreme outdoor environment to a moderately comfortable to keep their activities at a normal metabolic rate (Vale and Vale, 2017).

In practical dimensions, Omonijo (2017) outlines guidelines towards achieving occupants' thermal comfort in standard dwellings: adequate availability of thermal capacity in the building structure and on the interior envelope surfaces of habitable rooms; provision of additional levels of thermal insulation for exposed opaque walls and, when required, for exposed ground floor elements; proper adjustment of the window size as a function of orientation, room size, and occupant requirements, for passive solar heat gains; provision of internally insulated shutters on exposed glazing elements, for control of excess heat losses during evenings and at night; provision of controllable means for ventilation, such as adjustable trickle vents, extract fans, and/or individual heat recovery ventilators; provision of operable shading devices on the north-, east- and west-facing windows with adjustable blinds for control of excess solar heat gains. Other considerations affecting the energy requirements of buildings as highlighted by Al-ajmi and Hanby (2008) include: building location (altitude, latitude, longitude, and orientation); local weather conditions; heat transfer and storage characteristics of the building's elements, which depend on the various thermo-physical properties of the building components; windows, doors, and other openings; shading of the exterior surface; building dimensions; indoor temperature, number of occupants, lighting and building usage; primary and secondary air-conditioning systems; ventilation and infiltration. Each of these factors influences the cooling load of the building as the impact of each factor varies from building to building subject to the architectural design, building function, and material composition (Al-ajmi and Hanby, 2008).

Rapid growth in population, economic activities and general urbanization during the last decades in the tropical countries have had several environmental, economic, and social consequences, with an increase in energy consumption. More houses, schools, hospitals, roads, railways, bridges, public libraries, and other public facilities are needed to be built to accommodate people and meet the

population growth. These have raised concerns over depletion of local natural resources and supply difficulties as the building sector constitutes one of the major end users of energy (Koukelli et al., 2022; Kwong et al., 2014). Buildings account for about 15% of emissions, while transport and industry are 14 and 21%, respectively, and the remainder is emitted by other activities (Karyono, 2015, 2017; Karyono and Bachtiar, 2017). Thus, efficient and sustainable utilization of energy is essential in conserving the fast-depleting resources.

One of the main aims for sustainable development is to reduce the use of non-renewable energy resources. In view of industrialization and the expansion of modernization, urban areas have increased in size and so has the global population, with an expected annual growth of 1.8% (Mahravan and Vale, 2017). For these reasons, and to achieve sustainable growth objectives, energy saving in this sector is important. Thus, the building stock should be re-developed from the energy viewpoint. In effect, it is necessary to design comfortable buildings that do not use, or hardly use, active mechanical installations (Bastide et al., 2006). Thus, the building envelope shall be the focus of this study. The envelope constitutes the primary subsystem through which energy losses occur between indoor and outdoor environments of the building (Ascione et al., 2021). The idea is to reduce the heat transfer through it, while still ensuring comfort for the occupants. An improvement of the building envelope and the energy efficiency may reduce the ambient temperature and building's impact on the available natural resources. In this case, adequate climatic responsiveness and adaptiveness of the elements of the building envelope to extreme heat changes in an energy-efficient way can result in reduced building's energy consumption (Koukelli et al., 2022). This, therefore, gives way to comparative research work on two locally available walling elements as separate constituents (individually) of the building envelope in the study area, adobe bricks and hollow sandcrete blocks.

Brick is one of the oldest, most popular and environmentally friendly construction materials because of its durability, ease of handling, aesthetics and local availability (Abdullah et al., 2015). Adobe brick is essentially a dried mud brick, combining the natural elements of earth, water, and sun. It is an ancient building material usually made with tightly compacted sand, clay, and straw or grass mixed with moisture, formed into bricks, and naturally dried or baked in the sun without an oven or kiln (Craven, 2019). Bricks are used for exterior and interior walls, partitions, piers, footings, and other load-bearing structures (Duggal, 2008). Recipe for its construction varies according to climate, local customs, and the historical era. Many building structures of architectural significance such as the

Great Wall of China, Colosseum in Rome, pyramids in Egypt, the San Miguel Mission in Santa Fe, New Mexico, and the Taj Mahal in India, among others, were built with bricks (Craven, 2019; Phonphuak and Chindaprasirt, 2015). Introduction of chopped straw and grass to the clay mixture of the naturally sun-baked brick improves its quality and reduces distortions and cracking. The brick firing is also used to improve its strength and durability (Pacheco-Torgal, 2015; Phonphuak and Chindaprasirt, 2015). However, introduction of Portland cement in the 21$^{st}$ century led to development of masonry hollow sandcrete block, which is characterized with faster hardening and higher compressive strength (Olaniyan, 2021). Hollow sandcrete blocks are masonry units manufactured from a mixture of cement, sand, and water, and play a crucial role in the building construction. Hollow sandcrete blocks are largely used for load-bearing and non-load-bearing walls and foundations (Sholanke et al., 2015; The Constructor, 2022).

Thus, masonry hollow sandcrete blocks subsequently became an alternative to bricks, thereby leading to significant reduction in the use of the latter (Bingel and Bown, 2009; Smith et al., 2016). This development led to partial abandonment of the brick, despite its huge potentials in building energy moderation and conservation. In this context, these potentials accruable from old but partially abandoned bricks as opposed to prevailing sandcrete blocks in the tropical study area of Ogbomoso, Nigeria, are subjected to thermal performance analysis using a simulation tool, DesignBuilder. This paper, therefore, deals with optimization of building energy efficiency in the tropical city of Ogbomoso through comparative evaluations of relative thermal performance of walling fabrics, using two locally available building materials, adobe bricks and hollow sandcrete blocks. This approach attempts to reduce residential building cooling energy needs for attainment of indoor thermal comfort in the study area, by maximizing the advantages of the thermo-physical properties of the constituents of the low impact material, adobe brick. This is part of an ongoing research work as life building models will be constructed for direct validation at a later stage.

**Research Methodology**

*The Study Area: Climate and Design Implications*

Ogbomoso lies on 8° 10' north of the equator and 4° 15' east of the Greenwich Meridian. The city is situated within the derived savannah region and it is a gateway to the northern part of Nigeria from the south. It is characterized by the tropical wet and dry climates as it falls within the transition zone lying between the rainforest and the savannah, with a mean annual rainfall of about 1200 mm. The variation in the precipitation between the driest and wettest months is 178 mm. Both the highest

and lowest relative humidity occur in January (42.54%) and September (85.18%), respectively. The highest and lowest number of rainy days are recorded in July (24.70 days) and December (0.73 days), respectively. There is an average of 76.53 hours of sunshine per month as around 2323.51 hours of sunshine are counted through the year. This climate is considered to be 'Aw' according to the Köppen–Geiger climate classification. The wet season falls between April and October while the dry season is usually experienced between November and March. The dry season exhibits a typical harmattan season where high radiation cooling under clear skies at night causes temperature to fall as low as 18°C. The average lowest and highest temperatures of about 28.3 °C and 23.8 °C are usually experienced in March and August, respectively. The average temperatures vary during the year by 4.6°C (en.climate-data.org, 2022; Femi et al., 2015; Olaniyan, 2012). Below is the summary of the climatic data for Ogbomoso, the study area (Table).

The climate is characterized by high solar radiation (i.e., radiation value of over 10 KJ/m²/day for some months). This usually results in indoor thermal discomfort of the interior spaces in most parts of the year. Hence, there is the need for proper thermal analyses of the materials for the building envelope, for appropriate design interventions in the area (Olaniyan, 2012).

*Materials and Methods*

In this study, impacts of the varying walling fabrics (i.e., building materials) on attainment of sustainable indoor thermal comfort for residential buildings are examined. Virtual models of two similar residential buildings with bricks and sandcrete blocks (separately as walling components) are the objects of assessments for comparison. The two buildings represent a commonly adopted building typology (design) in the study area. While the first building type, tagged 'Sandcrete Building' (SB) is made up of a predominantly adopted masonry unit, hollow sandcrete block, the second building type, the 'Brick Building' (BB) is constructed of an age-long local building material, adobe brick (i.e., sun-baked earth block in this context). Figs. 1 and 2 give general outlooks of the structures.

The typical floor plan of either of the buildings is as shown in Fig. 3. It is a four-bedroom apartment with an approach balcony, occupying a total area of 103.85 square meters.

The wall of the Sandcrete Building is constructed of 225 mm hollow sandcrete blocks while that of the Brick Building is made of 230 mm traditional sun-baked bricks. Both structures are finished with 12 mm thick sand-cement mortar on both internal and external surfaces. As commonly found in the study area, both roofs are constructed of 0.45 mm thick long span aluminum sheets on a timber roof carcass, finished underneath with 6 mm thick

### Summary of the climatic data for Ogbomoso, the study area

| | Jan | Feb | Mar | Apr | May | Jun | Jul | Aug | Sep | Oct | Nov | Dec |
|---|---|---|---|---|---|---|---|---|---|---|---|---|
| Avg. temperature (°C) | 27.3 | 28.3 | 28.3 | 27.5 | 26.4 | 25.0 | 24.1 | 23.8 | 24.2 | 25.0 | 26.4 | 26.8 |
| Min. temperature (°C) | 21.5 | 23.1 | 24.1 | 24.1 | 23.6 | 22.6 | 21.9 | 21.5 | 21.9 | 22.3 | 22.9 | 21.4 |
| Max. temperature (°C) | 34.2 | 35.1 | 35 | 33.3 | 31.4 | 29.2 | 28.0 | 27.5 | 28.5 | 29.8 | 31.9 | 33.5 |
| Precipitation / Rainfall mm (in) | 5 (0.2) | 13 (0.5) | 40 (1.6) | 78 (3.1) | 121 (4.8) | 154 (6.1) | 175 (6.9) | 180 (7.1) | 182 (7.2) | 105 (4.1) | 13 (0.5) | 4 (0.2) |
| Humidity (%) | 43% | 50% | 62% | 73% | 79% | 83% | 84% | 85% | 85% | 83% | 71% | 50% |
| Rainy days (d) | 1 | 2 | 5 | 9 | 14 | 16 | 19 | 18 | 18 | 13 | 2 | 1 |
| Avg. sun hours (hours) | 9.2 | 8.7 | 8.0 | 7.0 | 5.6 | 4.4 | 4.2 | 3.7 | 4.2 | 5.2 | 7.3 | 9.0 |

a) (source: en.climate-data.org, 2022)

b)



Fig. 1. Illustrations of the components of the adobe brick masonry units for the Brick Building: (a) individual sun-baked brick unit; (b) typical constructed walls joined with cement-sand mortar (images adopted from: Abanda et al., 2015).
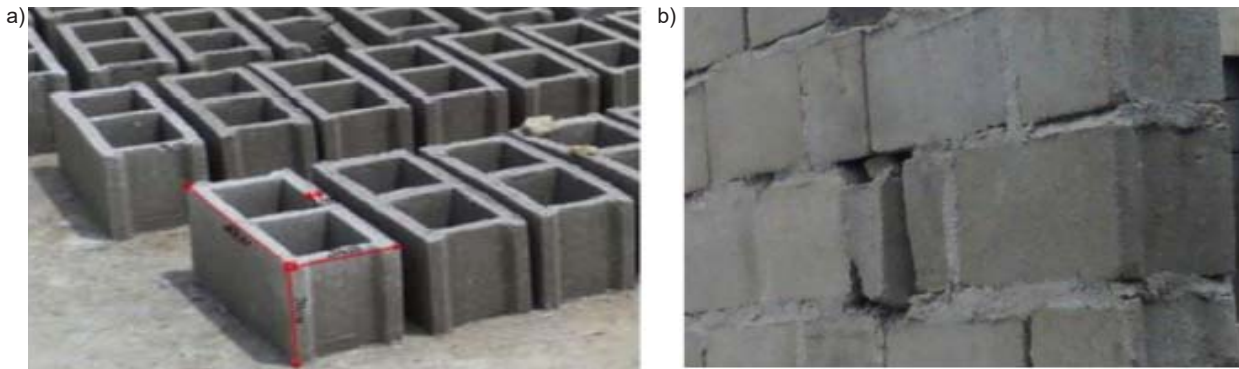
Fig. 2. Illustrations of the components of the hollow sandcrete masonry units for the Sandcrete Building:
(a) individual hollow sandcrete block unit; (b) typical constructed walls joined with cement-sand mortar
(images adopted from: Abanda et al., 2015)

asbestos ceiling sheets. The windows made of 6 mm thick clear glass are complemented with 40 mm thick wooden panel doors.

*Virtual Building Modeling and Simulation Approach*

Virtual models of the two buildings were subjected to energy performance simulation analysis. This is a powerful tool that architects, engineers, and other relevant professionals use to analyze how the form, size, orientation, and type of building systems affect overall building energy consumption. It is used to optimize building energy efficiency with respect to building input parameters (Al-ajmi and Hanby, 2008; Altan et al., 2015). This analysis is useful for informed design decisions to improve building energy performance in respect of the buildng envelope, glazing, lighting, HVAC, etc. As a modern design tool, it allows us to use the numerical simulation to analyze the influence of design elements on indoor thermal comfort for sustainable housing development (Altan et al., 2015). In many cases, few building simulations runs in the early phases of a project assist in attaining the best design solutions (Energy Design Resources, 2000).

In this study, DesignBuilder software was adopted for the building simulation work (DesignBuilder, 2021) as a typical virtual building model as illustrated in Fig. 4. The software is integrated with EnergyPlus, the US Department of Energy (DOE) third ($3^{rd}$) generation dynamic building energy simulation engine for modeling building, heating, cooling, lighting, ventilation and other energy flows. This integration within DesignBuilder allows for complete simulations within the interface, which constitutes an excellent feature for ease of simulation. DesignBuilder uses construction components to model the conduction of heat through walls, windows, roofs, ground and other opaque parts of the building envelope. In this case, the physical properties of each element have been defined for the building (DesignBuilder, 2021). These simulations are run for the whole year (i.e., 12 months) as hourly, daily and monthly results are available. Passive solar gains and indoor comfort temperature due to the alternative walling fabrics, adobe bricks and hollow sandcrete blocks (external walls and partitions) in particular, obtained through
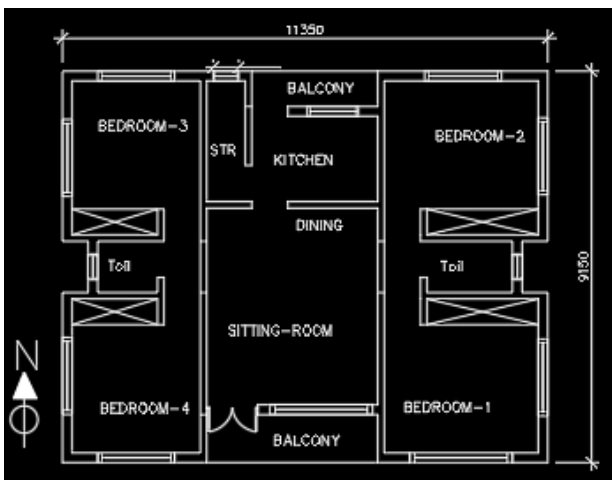


Fig. 3. Typical floor plan of the building model
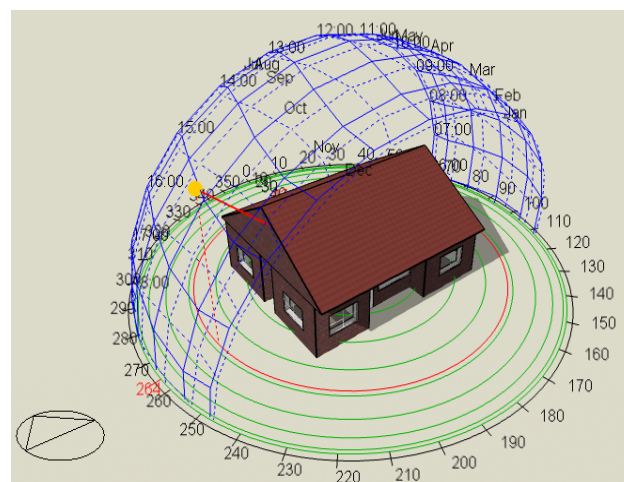


Fig. 4. Typical virtual model of the building as displayed in DesignBuilder Interface (sandcrete: U-Value (W/m²K) = 2.137; R-Value (m²-K/W) = 0.468)

Sule Adeniyi Olaniyan — Pages 68–81

ADOBE BRICKS TO HOLLOW SANDCRETE BLOCK WALLING IN TROPICAL BUILDING CONSTRUCTION: MATERIAL IMPACT ON SUSTAINABLE INDOOR THERMAL COMFORT ATTAINMENT

cooling design simulations in the study area, are the simulation output variables considered relevant for the analysis. Thus, effects of the varying walling fabrics on indoor thermal comfort are compared to establish their individual impacts with a view to making necessary recommendations for the study area.

### Results and Discussion

Arising from the geographical location of the study area in relation to the simulation output, relevant climatic data particularly, solar radiation (both direct and diffuse) is analyzed as presented in Fig. 5. It could be observed that high solar radiation values are recorded particularly between October and May, with each month experiencing almost 100 kwh/m$^2$ area of diffuse radiation. The trend is similar for direct radiation over the same period. March witnessed the highest diffuse and direct radiation values of 114.13 kwh/m$^2$ and 84.45 kwh/m$^2$, respectively. Details of this simulation output as captured directly from DesignBuilder interface are shown in Appendix I for referencing and verification. Of particular interest is the impact of this radiation data, which forms the basis for the indoor solar gains through the walling fabrics, among others.

The primary focus of this study is to establish comparative heat gains due to the walling fabrics of hollow sandcrete blocks and adobe bricks, as a basis for their respective indoor thermal comfort analyses. Comparative monthly heat gains due to the walling fabric received by the east end of indoor spaces of Bedrooms 1 and 2, by both SB and BB are as shown in Figs. 6 and 7. Details of these on a typical dry-season peak day (i.e., March 23) are as shown in Appendix.

Similarly, Figs. 8 and 9 illustrate comparative heat gains received by west end bedrooms 3 and 4.

The overall annual heat gains for the entire building through the walling fabric are illustrated graphically in Fig. 10.

From the results above, it could be observed that for every month, heat gains received by the building interior both in the east and west ends are more for the sandcrete building. Consequently, the annual heat load for the entire building due to the sandcrete blocks is 8875.65 KWh, with high values recorded in the months of March, April, and May (i.e., 791 KW/m, 788 KW/m, and 778 KW/m, respectively). This is significantly more than that of the brick building, which has the annual heat load of 7119.54 KWh, with high values also recorded in the months of March, April, and May (i.e., 726.77 KWh, 726.32 KWh, and 715.80 KWh, respectively). These are direct reflections of the components of the walling fabric.

From the foregoing, comparative annual heat loads as experienced in the building upon which indoor thermal comfort is based is 11% lower in BS (7119.54 KWh) due to the brick walling fabric. This may be associated with the brick's lower thermal conductivity (U-Value) of 1.798 W/m$^2$-K, which may even be as low as 1.5 W/m$^2$-K (Delgado and Guerrero, 2006), compared with the sandcrete block's value of 1.999 W/m$^2$-K. It should be noted that the ability of adobe brick to conduct heat depends on its moisture content, which is considered advantageous in moderate and hot climates because of the phase transition of the water. As the material dries, the water evaporates, leading to heat loss in the form of latent heat, which in turn causes the external surface temperature to decrease (Quagliarini et al., 2015).

From the thermal analyses above, adobe brick as a walling unit exhibits more thermal resistance against the harsh outdoor weather conditions to effect more thermally comfortable indoor environment. This position aligns with the findings of Martín et al. (2010) who analyzed comfort conditions inside earth buildings in Spain. It also agrees with the results obtained from several other related studies inclusive
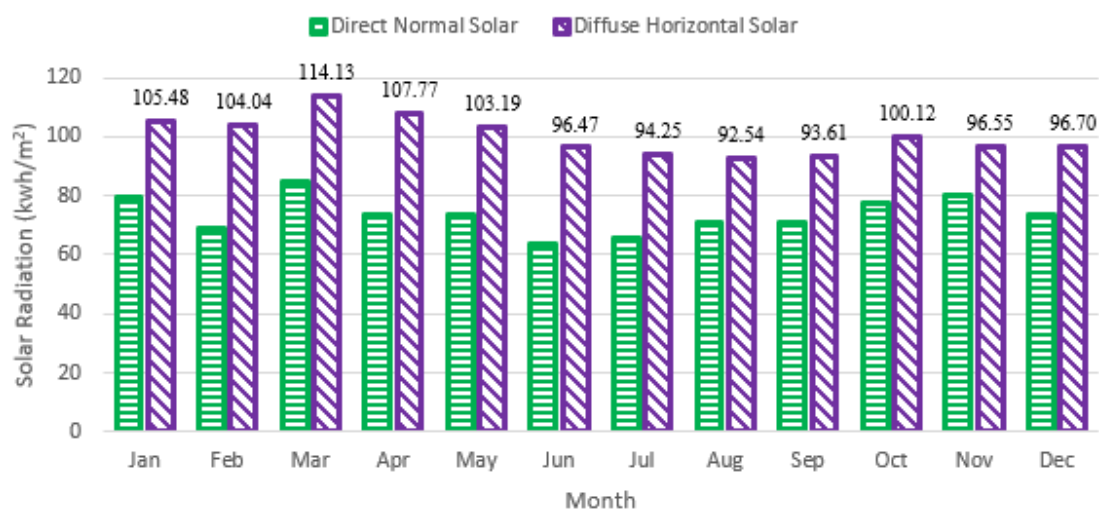


Fig. 5. Monthly solar radiation (direct and diffuse) for the study area
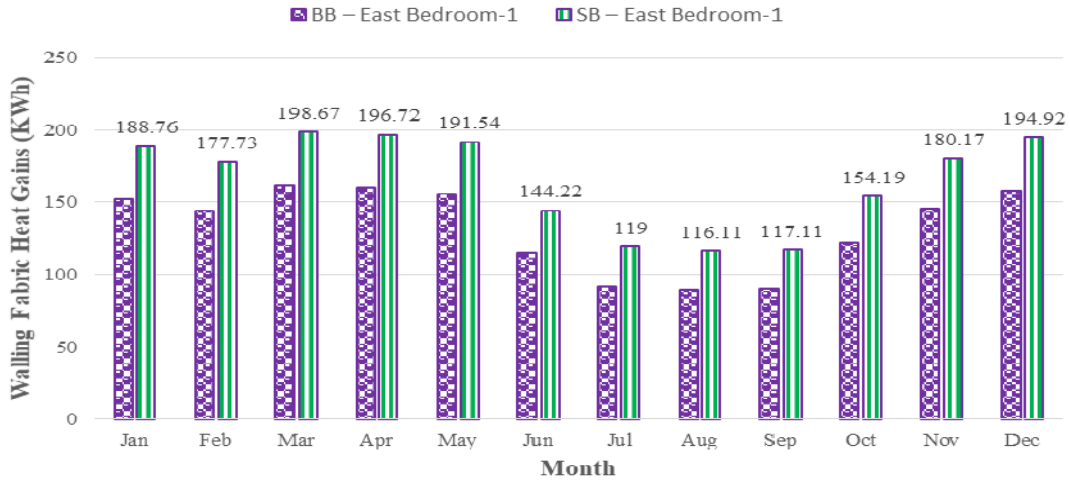
Fig. 6. Comparative monthly heat gains through the walling fabric received by east bedroom-1 for both sandcrete building and brick building
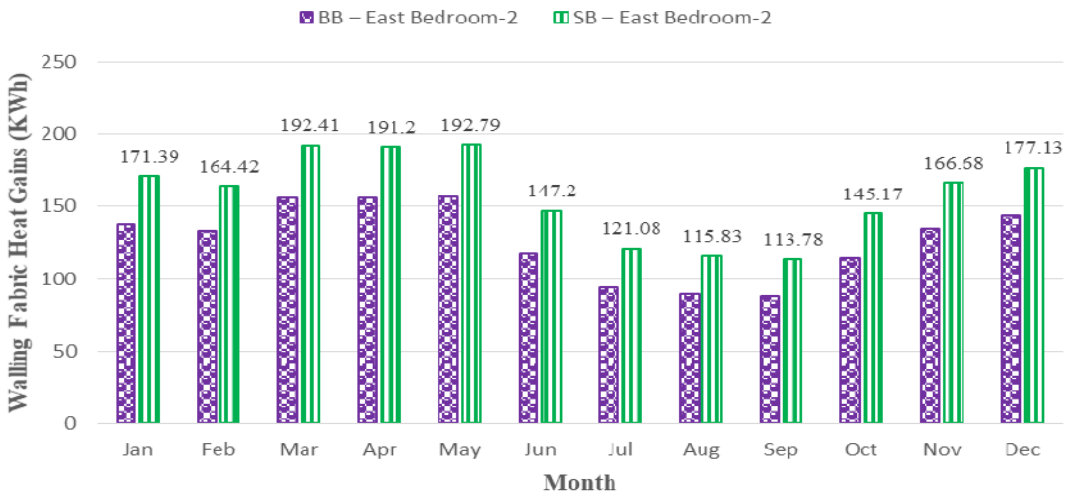


Fig. 7. Comparative monthly heat gains through the walling fabric received by east bedroom-2 for both sandcrete building and brick building
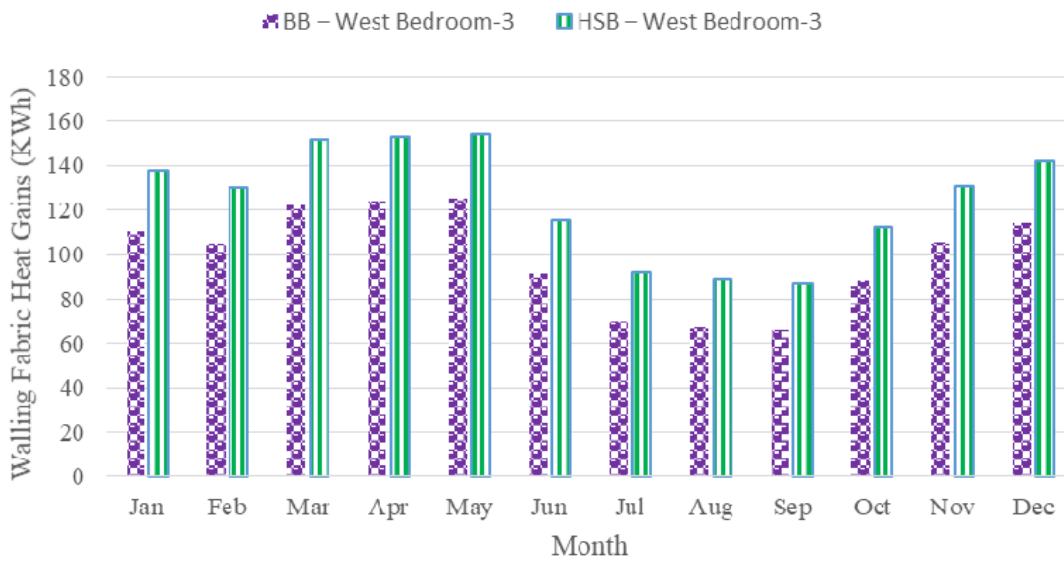


Fig. 8. Comparative monthly heat gains through the walling fabric received by west bedroom-3 for both sandcrete building and brick building
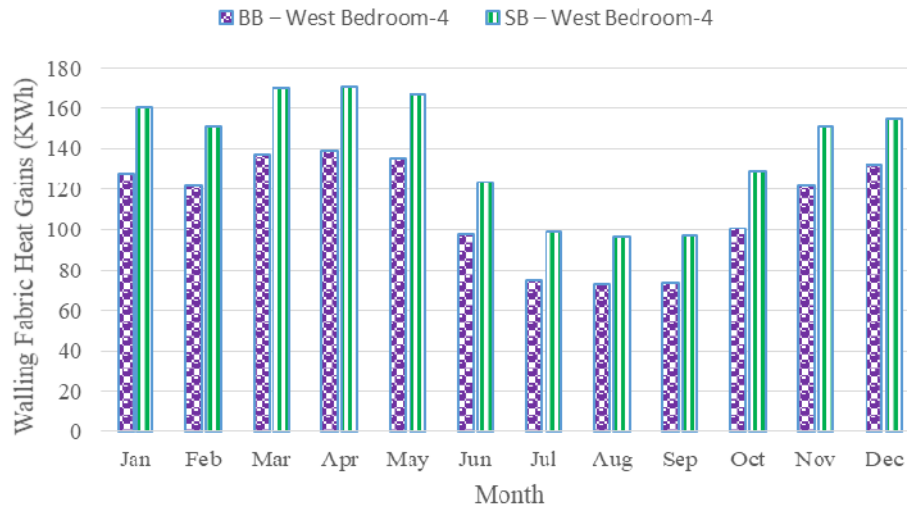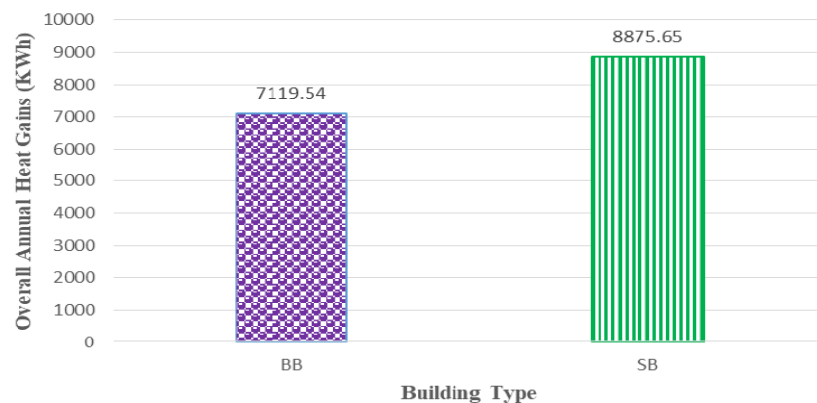
Sule Adeniyi Olaniyan — Pages 68–81

ADOBE BRICKS TO HOLLOW SANDCRETE BLOCK WALLING IN TROPICAL BUILDING CONSTRUCTION:
MATERIAL IMPACT ON SUSTAINABLE INDOOR THERMAL COMFORT ATTAINMENT



Fig. 9. Comparative monthly heat gains through the walling fabric received by west bedroom-4
for both sandcrete building and brick building



Fig. 10. Comparative annual heat gains through the walling fabrics

of Algifri et al. (1992), Chel and Tiwari (2009), Sale (1990), etc., as they all show that an adobe brick house can maintain natural indoor thermal comfort. It could therefore be demonstrated that compared with sandcrete blocks, adobe bricks provide a more comfortable indoor thermal environment in the tropical study area of Ogbomoso.

This research advances current knowledge on improving indoor comfort temperature ranges in naturally conditioned dwellings, at no extra construction costs. It also expands understanding of the thermal performance of different building residential types using conventional and alternative building materials.

*Future Research Project / Research Validation*

The simulation research approach was employed to theoretically predict the thermal roles of the components of the building fabrics (i.e., adobe bricks and hollow sandcrete blocks, in this case) and their impacts on the thermal conditions of the interior. However, the results obtained constitute the preliminary outputs, which require further validation using more empirical analysis. Thus, the

information gained from the simulation exercise will inform comparative modeling/simulation of different building propositions, using comparative building fabrics as the building envelopes (by applying combinations of different thermal insulating materials as components of the building fabrics). Through trial experimentations, the result will evolve preliminary design guidelines for the proposed responsive architectural design solution in the study area. To achieve this, full scale testing, involving thermal analysis, will be carried out over a 12-month period using three prototype models as shown in Fig. 11.

Three prototype life building models will be constructed. Each model will be 2 m x 2 m x 1.8 m. The first model will be made of the building fabric prevailing in the study area and will serve as the control model. Components of the building fabric will consist of materials for the floor, wall, window, ceiling, door, and roof. The other two models will be constructed of different low impact building materials in the study area and serve as comparative bases for building performance assessment. Data collection in respect of these is expected to last one

year. Subsequently, results of the life models will be compared with the simulated outcomes for validation and acceptability of the proposed design guidelines.

**Conclusion**

Tropical region is characterized by harsh outdoor weather conditions. However, the primary role of a building is to shield the interior from the impacts of such outdoor climatic elements. This is usually achieved through adoption of any available fabrics of building envelope. This is usually supported with additional mechanical installations such as fans, air-conditioners, etc. for indoor thermal comfort attainment. However, the rising energy costs, coupled with undesirable carbon emissions associated with such active installations have necessitated the need for more research on possible adoption of more low impact building materials available in the study area. Consequently, this study has demonstrated, with regard to the indoor thermal comfort attainment, that the partially abandoned locally available building material, adobe brick, as a walling fabric is more

suitable than the predominantly adopted hollow sandcrete blocks in the study area. This is with a view to minimizing building construction impacts on the environment for overall sustainable utilization of the available limited resources. Therefore, wherever it is practically possible, adoption of adobe bricks as an enclosing material in the tropical city of Ogbomoso and its environment should be encouraged for inexpensive residential apartments. This is an attempt to revive an age-long partially abandoned locally available material for overall sustainable construction purposes. It should be emphasized that this result is part of an ongoing research work as life building models are to be constructed for direct validation of the results at a later stage.

**Funding**

Fig. 11. Illustrations of the proposed prototype life building models

**References**

Abanda, H., Tah, J. H. M., and Elambo Nkeng, G. (2015). Earth-block versus sandcrete-block houses: embodied energy and $CO_2$ assessment. In: Pacheco-Torgal, F., Lourenço, B. P., Labrincha, J. A., Kumar, S., and Chindaprasirt, P. (eds.). *Eco-efficient Masonry Bricks and Blocks. Design, Properties and Durability*. Cambridge: Woodhead Publishing, pp. 481–514. DOI: 10.1016/B978-1-78242-305-8.00022-X.

Abdullah, M. M. A., Ibrahim, W. M. W., and Tahir, M. F. M. (2015). The properties and durability of fly ash-based geopolymeric masonry bricks. In: Pacheco-Torgal, F., Lourenço, B. P., Labrincha, J. A., Kumar, S., and Chindaprasirt, P. (eds.). *Eco-efficient Masonry Bricks and Blocks. Design, Properties and Durability*. Cambridge: Woodhead Publishing, pp. 273–287. DOI: 10.1016/B978-1-78242-305-8.00012-7

Al-ajmi, F. F. and Hanby, V. I. (2008). Simulation of energy consumption for Kuwaiti domestic buildings. *Energy and Buildings*, Vol. 40, Issue 6, pp. 1101–1109. DOI: 10.1016/j.enbuild.2007.10.010.

Algifri, A. H., Bin Gadhi, S. M., and Nijaguna, B. T. (1992). Thermal behaviour of adobe and concrete houses in Yemen. *Renewable Energy*, Vol. 2, Issue 6, 597–602. DOI: 10.1016/0960-1481(92)90024-W.

Altan, H., Gasperini, N., Moshaver, S., and Frattari, A. (2015). Redesigning terraced social housing in the UK for flexibility using building energy simulation with consideration of passive design. *Sustainability*, Vol. 7, Issue 5, pp. 5488–5507. DOI: 10.3390/su7055488.

Ascione, F., Bianco, N., Iovane, T., Mastellone, M., and Mauro, G. M. (2021). The evolution of building energy retrofit via double-skin and responsive façades: A review. *Solar Energy*, Vol. 224, pp. 703–717. DOI: 10.1016/j.solener.2021.06.035.

Attoye, D. E., Aoul, K. A. T., and Hassan, A. (2017). A review on building integrated photovoltaic façade customization potentials. *Sustainability*, Vol. 9, Issue 12, 2287. DOI: 10.3390/su9122287.

Bastide, A., Lauret, P., Garde, F., and Boyer, H. (2006). Building energy efficiency and thermal comfort in tropical climates: Presentation of a numerical approach for predicting the percentage of well-ventilated living spaces in buildings using natural ventilation. *Energy and Buildings*, Vol. 38, Issue 9, pp. 1093–1103. DOI: 10.1016/j.enbuild.2005.12.005.

Bay, J.-H. and Ong, B.-L. (2006). *Tropical sustainable architecture: social and environmental dimensions*. London: Routledge, 310 p.

Bingel, P., and Bown, A. (2009). Sustainability of masonry in construction. In: Jamal M. Khatib (eds.) Woodhead Publishing Series in Civil and Structural Engineering, Sustainability of Construction Materials. Woodhead Publishing, pp. 82-119. DOI: 10.1533/9781845695842.82.

Camanzi, L., Alikadic, A., Compagnoni, L., and Merloni, E. (2017). The impact of greenhouse gas emissions in the EU food chain: A quantitative and economic assessment using an environmentally extended input-output approach. *Journal of Cleaner Production*, Vol. 157, pp. 168–176. DOI: 10.1016/j.jclepro.2017.04.118.

Chel, A. and Tiwari, G. N. (2009). Performance evaluation and life cycle cost analysis of earth to air heat exchanger integrated with adobe building for New Delhi composite climate. *Energy and Buildings*, Vol. 41, Issue 1, pp. 56–66. DOI: 10.1016/j.enbuild.2008.07.006.

Craven, J. (2019). *All about adobe - sustainable and energy efficient*. ThoughtCo. [online]. Available at: thoughtco.com/what-is-adobe-sustainable-energy-efficient-177943 [Date accessed June 15, 2022].

Delgado, M. C. J. and Guerrero, I. C. (2006). Earth building in Spain. *Construction and Building Materials*, Vol. 20, Issue 9, pp. 679–690. DOI: 10.1016/j.conbuildmat.2005.02.006.

DesignBuilder (2021). An online based simulation software acquired as an annual package via: https://designbuilder.co.uk [Date accessed 01 November, 2021].

Duggal, S. K. (2008). *Building materials*. 3rd edition. New Delhi: New Age International Publishers, 525 p.

En.climate-data.org (2022). *Ogbomosho climate (Nigeria)*. [online] Available at: https://en.climate-data.org/africa/nigeria/oyo/ogbomosho-525/ [Date accessed May 12, 2022].

Energy Design Resources (2000). *Building simulation*. [online] Available at: https://datacenters.lbl.gov/sites/default/files/Design%20Brief_Chiller%20Efficiency.pdf [Date accessed October 17, 2021].

Femi, A. B., Khan, T. H., Ahmad, A. S. B. H., and Bin Udin, A. (2015). Impact of tertiary institutions on house rental value in developing city. *Procedia - Social and Behavioral Sciences*, Vol. 172, pp. 323–330. DOI: 10.1016/j.sbspro.2015.01.371.

Givoni, B. (1976). *Man, climate and architecture*. 2nd edition. London: Applied Science Publishers Ltd., 483 p.

Jiang, W., Liu, J., and Liu, X. (2016). Impact of carbon quota allocation mechanism on emissions trading: An agent-based simulation. *Sustainability*, Vol. 8, Issue 8, 826. DOI: 10.3390/su8080826.

JCU (2014). *State of the Tropics. A report prepared by* James Cook University, Townsville (Australia), p. 462

Karyono, T. H. (2015). Predicting comfort temperature in Indonesia, an initial step to reduce cooling energy consumption. *Buildings*, Vol. 5, Issue 3, pp. 802–813. DOI: 10.3390/buildings5030802.

Karyono, T. H. (2017). Climate change and the sustainability of the built environment in the humid tropic of Indonesia. In: Karyono, T. H., Vale, R., and Vale, B. (eds.). *Sustainable Building and Built Environments to Mitigate Climate Change in the Tropics.* Cham: Springer, pp. 9–25. DOI: 10.1007/978-3-319-49601-6_2

Karyono, T. H. and Bachtiar, F. (2017). Adapting city for frequent floods: a case study of Jakarta, Indonesia, In: Karyono, T. H., Vale, R., and Vale, B. (eds.). *Sustainable Building and Built Environments to Mitigate Climate Change in the Tropics.* Cham: Springer, pp. 103–111. DOI: 10.1007/978-3-319-49601-6_8.

Kenisarin, M. and Mahkamov, K. (2016). Passive thermal control in residential buildings using phase change materials. *Renewable and Sustainable Energy Reviews*, Vol. 55, pp. 371–398. DOI: 10.1016/j.rser.2015.10.128.

Koukelli, C., Prieto, A., and Asut, S. (2022). Kinetic solar envelope: performance assessment of a shape memory alloy-based autoreactive façade system for urban heat island mitigation in Athens, Greece. *Applied Sciences*, Vol. 12, Issue 1, 82. DOI: 10.3390/app12010082.

Kwong, Q. J., Adam, N. M., and Sahari, B. B. (2014). Thermal comfort assessment and potential for energy efficiency enhancement in modern tropical buildings: A review. *Energy and Buildings*, Vol. 68, Part A, pp. 547–557. DOI: 10.1016/j.enbuild.2013.09.034.

Longo, T. A., Melo, A. P., and Ghisi, E. (2011). Thermal comfort analysis of a naturally ventilated building. In: *Proceedings of Building Simulation 2011, 12th Conference of International Building Performance Simulation Association*, 14–16 November, 2011, Sydney, Australia, pp. 2004–2010.

Lotfabadi, P. (2013). The impact of city spaces and identity in the residents' behavior. *Humanities and Social Sciences Review*, Vol. 2, No. 3, pp. 589–601

Lotfabadi, P., Alibaba, H. Z., and Arfaei, A. (2016). Sustainability; as a combination of parametric patterns and bionic strategies. *Renewable and Sustainable Energy Reviews*, Vol. 57, pp. 1337–1346. DOI: 10.1016/j.rser.2015.12.210.

Lotfabadi, P. and Hançer, P. (2019). A comparative study of traditional and contemporary building envelope construction techniques in terms of thermal comfort and energy efficiency in hot and humid climates. *Sustainability*, Vol. 11, Issue 13, 3582. DOI: 10.3390/su11133582.

Mahravan, A. and Vale, B. (2017). The sustainable portion of gross domestic product: a proposed social ecological economic indicator for sustainable economic development. In: Karyono, T. H., Vale, R., and Vale, B. (eds.). *Sustainable Building and Built Environments to Mitigate Climate Change in the Tropics*. Cham: Springer, pp. 53–69. DOI: 10.1007/978-3-319-49601-6_5.

Martín, S., Mazarron, F. R., and Cañas, I. (2010). Study of thermal environment inside rural houses of Navapalos (Spain): the advantages of reuse buildings of high thermal inertia. *Construction and Building Materials*, Vol. 24, Issue 5, pp. 666–676. DOI: 10.1016/j.conbuildmat.2009.11.002.

Nejat, P., Jomehzadeh, F., Taheri, M. M., Gohari, M., and Majid, M. Z. A. (2015). A global review of energy consumption, $CO_2$ emissions and policy in the residential sector (with an overview of the top ten $CO_2$ emitting countries). *Renewable and Sustainable Energy Reviews*, Vol. 43, pp. 843–862. DOI: 10.1016/j.rser.2014.11.066.

Olaniyan, S. A. (2012). Optimizing thermal comfort for tropical residential designs in Nigeria: how significant are the walling fabrics? In: *2nd Conference "People and Buildings"*, September 18, 2012, London, UK.

Olaniyan, S. A. (2021). Pore structure as a determinant of flexibility in sustainable lime-cement mortar composites. *European Journal of Engineering and Technology Research*, Vol. 6, Issue 6, pp. 113–122. DOI: 10.24018/ejeng.2021.6.6.2598.

Omonijo, A. G. (2017). Assessing seasonal variations in urban thermal comfort and potential health risks using Physiologically Equivalent Temperature: A case of Ibadan, Nigeria. *Urban Climate*, Vol. 21, pp. 87–105. DOI: 10.1016/j.uclim.2017.05.006.

Pacheco-Torgal, F. (2015). Introduction to eco-efficient masonry bricks and blocks. In: Pacheco-Torgal, F., Lourenço, P. B., Labrincha, J. A., Kumar, S., and Chindaprasirt, P. (2014). *Eco-efficient masonry bricks and blocks: design, properties and durability*. Cambridge: Woodhead Publishing, pp. 1–10. DOI: 10.1016/B978-1-78242-305-8.00001-2.

Pacheco-Torgal, F. and Jalali, S. (2011). *Eco-efficient construction and building materials*. London: Springer, 247 p. DOI: 10.1007/978-0-85729-892-8.

Pacheco-Torgal, F., Lourenco, P. B., Labrincha, J., Chindaprasirt, P., & Kumar, S. (2014). *Eco-efficient Masonry Bricks and Blocks: Design, Properties and Durability* (1st ed., Vol. 55). Elsevier Science. https://doi.org/10.1016/C2014-0-02158-2

Phonphuak, N. and Chindaprasirt, P. (2015). Types of waste, properties, and durability of pore-forming waste-based fired masonry bricks. In: Pacheco-Torgal, F., Lourenço, P. B., Labrincha, J. A., Kumar, S., and Chindaprasirt, P. (2014). *Eco-efficient masonry bricks and blocks: design, properties and durability*. Cambridge: Woodhead Publishing, pp. 103–127. DOI: 10.1016/B978-1-78242-305-8.00006-1.

Prianto, E. and Depecker, P. (2002). Characteristic of airflow as the effect of balcony, opening design and internal division on indoor velocity: A case study of traditional dwelling in urban living quarter in tropical humid region. *Energy and Buildings,* Vol. 34, Issue 4, pp. 401–409. DOI: 10.1016/S0378-7788(01)00124-4.

Prianto, E. and Depecker, P. (2003). Optimization of architectural design elements in tropical humid region with thermal comfort approach. *Energy and Buildings*, Vol. 35, Issue 3, pp. 273–280. DOI: 10.1016/S0378-7788(02)00089-0.

Quagliarini, E., D'Orazio, M., and Lenc, S. (2015). The properties and durability of adobe earth-based masonry blocks. In: Pacheco-Torgal, F., Lourenço, P. B., Labrincha, J. A., Kumar, S., and Chindaprasirt, P. (2014). *Eco-efficient masonry bricks and blocks: design, properties and durability*. Cambridge: Woodhead Publishing, pp. 361–378. DOI: 10.1016/B978-1-78242-305-8.00016-4.

Quesada, G., Rousse, D., Dutil, Y., Badache, M., and Hallé, S. (2012). A comprehensive review of solar facades. Opaque solar facades. *Renewable and Sustainable Energy Reviews*, Vol. 16, Issue 5, pp. 2820–2832. DOI: 10.1016/j.rser.2012.01.078.

Raja, I. A., Nicol, J. F., McCartney, K. J., and Humphreys, M. A. (2001). Thermal comfort: use of controls in naturally ventilated buildings. *Energy and Buildings*, Vol. 33, Issue 3, pp. 235–244. DOI: 10.1016/S0378-7788(00)00087-6.

Saleh, M. A. E. (1990). Adobe as a thermal regulating material. *Solar & Wind Technology*, Vol. 7, Issue 4, pp. 407–416. DOI: 10.1016/0741-983X(90)90025-W.

Shastry, V., Mani, M., and Tenorio, R. (2016). Evaluating thermal comfort and building climatic response in warm-humid climates for vernacular dwellings in Suggenhalli (India). *Architectural Science Review*, Vol. 59, Issue 1, pp. 12–26. DOI: 10.1080/00038628.2014.971701.

Sholanke, A. B., Fagbenle, O. I., Aderonmu, A. P., and Ajagbe, M. A. (2015). Sandcrete block and brick production in Nigeria - prospects and challenges. *International Journal of Environmental Research*, Vol. 1, No. 4, pp. 1–17.

Smith, A. S., Bingel, P., and Bown, A. (2016). Sustainability of masonry in construction. *Sustainability of Construction Materials (Second Edition)*, pp. 245–282. DOI: 10.1016/B978-0-08-100370-1.00011-1.

The Constructor (2022). *Sandcrete block manufacturing and testing*. [online] Available at: https://theconstructor.org/building/sandcrete-block-manufacturing-testing/25382/ [Date accessed June 9, 2022].

Vale, R. and Vale, B. (2017). Introduction: the tropics: a region defined by climate. In: Karyono, T. H., Vale, R., and Vale, B. (eds.). *Sustainable Building and Built Environments to Mitigate Climate Change in the Tropics.* Cham: Springer, pp. 1–6. DOI: 10.1007/978-3-319-49601-6_1.

World Energy Council (2013). *World Energy Resources: 2013 Survey*. London: World Energy Council, 468 p.

**Appendix:** Simulation Output for Direct and Diffuse Solar Radiations in the Study Area
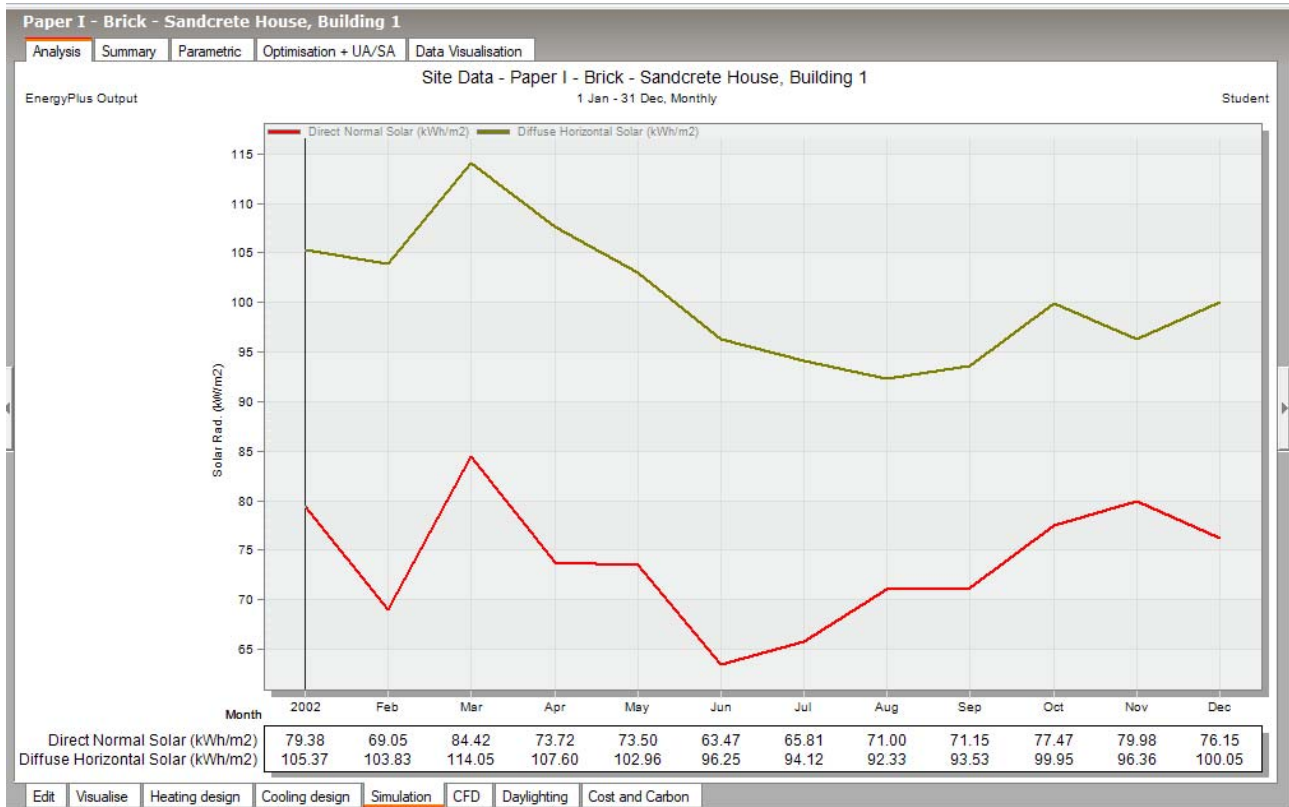
# САМАН ВМЕСТО ПУСТОТЕЛЫХ ПЕСКОБЕТОННЫХ БЛОКОВ СТЕН В ТРОПИЧЕСКОМ СТРОИТЕЛЬСТВЕ: ВЛИЯНИЕ МАТЕРИАЛОВ НА ДОСТИЖЕНИЕ УСТОЙЧИВОГО ТЕПЛОВОГО КОМФОРТА В ПОМЕЩЕНИИ

Суле Адении Оланиян

Технологический университет Ладок Акинтола, Огбомошо, Нигерия

E-mail: saolaniyan@lautech.edu.ng

**Аннотация**

**Введение**: Тропический климат характеризуется высокой температурой, вследствие чего возникает тепловой дискомфорт в помещении. Это объясняется высоким притоком солнечной энергии через различные элементы ограждающих конструкций здания, включая, среди прочего, окна, стены и крышу. Тем не менее, в попытке оптимизировать тепловой комфорт в помещении с минимальным использованием механических приборов или вообще без них в этом исследовании анализируется роль стеновых материалов путем сравнения различных теплофизических свойств двух идентифицированных кладочных блоков в исследуемой зоне Огбомошо, Нигерия — саманного кирпича и пустотелых блоков из пескобетона — с целью определить более термически комфортный и устойчивый вариант материала. **Методика** включает в себя виртуальные модели двух одинаковых жилых домов, каждый из которых состоит либо из саманного кирпича, либо из пескобетонных блоков в качестве каменной кладки. Эти модели были подвергнуты анализу энергетических характеристик с использованием программного обеспечения DesignBuilder в течение двенадцатимесячного цикла, чтобы рассмотреть круглогодичные дифференциальные температурные условия. Благодаря наблюдаемым сравнительным годовым тепловым нагрузкам, полученным в моделях, результаты показывают улучшение теплового комфорта внутри кирпичного здания (т.е. 7119,54 кВтч), причем тепловые нагрузки на 11 % ниже, чем у здания из пескобетона (т. е. 8875,65 кВтч) за счет кирпичной облицовки. Это может быть связано с более низкой теплопроводностью кирпича (U-значение) 1,798 Вт/м$^2$-К по сравнению со значением пескобетонных блоков в 1,999 Вт/м$^2$-К. **Результаты**: В целом, саман в качестве стенового блока демонстрирует бо́льшую термическую устойчивость к суровым погодным условиям, чем пескобетонные блоки. Исследование является частью продолжающейся работы по возрождению такого частично забытого экологичного материала, как саманный кирпич, с целью достижения устойчивого теплового комфорта в помещениях, а также для защиты окружающей среды в исследуемой зоне.

**Ключевые слова:** саман, пескобетонные блоки, моделирование, экологичность, тепловой комфорт, тропики.

# FREE VIBRATION MODELING IN A FUNCTIONALLY GRADED HOLLOW CYLINDER USING THE LEGENDRE POLYNOMIAL APPROACH

Rabab Raghib[1]*, Ismail Naciri[1], Hassna Khalfi[1], Lahoucine Elmaimouni[1], Jiangong Yu[2], Abdelmajid Bybi[3], Mustapha Sahal[1]

[1]Ibn Zohr University, Polydisciplinary Faculty of Ouarzazate, BP.638, 45000 Ouarzazate, Morocco
[2]School of Mechanical and Power Engineering, Henan Polytechnic University, Jiaozuo 454003, China
[3]Mohammed V University in Rabat, Higher School of Technology in Salé, Materials, Energy and Acoustics Team (MEAT), Morocco

*Corresponding author's e-mail: rababraghib97@gmail.com

**Abstract**

**Introduction**: The building industry is under increasing pressure to maximize performance while reducing the costs and the environmental impact. To solve this problem, a new type of materials, i.e., functionally graded materials (FGMs), are proposed. These materials have the advantage of being able to withstand harsh environments without losing their properties. **Purpose of the study:** The paper aims to further extend the understanding of the propagation modes and characteristics of guided waves in FGM cylinders with infinite lengths. In the course of the study, we analyzed a cylindrical shell composed of three annular layers, each separated by a gradient layer across the wall thickness. A modeling tool based on the Legendre orthogonal polynomial method is proposed in the paper. **Methods:** The method applied results in an eigenvalue/eigenvector problem. The boundary conditions are integrated into the constitutive equations of guided wave propagation. The phase velocity and normalized frequency dispersion curves are calculated. Besides, the displacement distributions and stress field profiles for a functionally graded cylinder with various graded indices in both modes (axisymmetric and symmetric) are calculated and discussed. The results show a constant fluctuation of effective FGM material. **Results:** It was found that the phase velocity curves of the same mode decrease as the exponents of the power law increase. In addition, the boundary conditions have a greater impact on the normal stresses. The accuracy and effectiveness of the improved orthogonal polynomial method are demonstrated through a comparison of the exact solution obtained by an analytical-numerical method and our numerical results.

**Keywords:** guided waves, Legendre polynomial method, functionally graded materials (FGMs), dispersion curves.

## Introduction

Material structures are becoming more complex and delicate due to recent scientific advancements in materials. Functionally graded materials (FGMs) have emerged as a result of exciting developments in engineering and material processing. FGMs are created in order to achieve higher levels of performance. In fact, FGMs are a class of composite materials with graded structure and characteristics changing spatially in the thickness direction. These materials have a graded interface rather than a sharp interface between two dissimilar materials. The purpose of choosing graded materials, particularly at the interface between layers, is to reduce inter-laminar stress discontinuities. These can occur around the edges of laminates due to material incompatibility across the interface. The interface between two layers in FGM is typically seen as having seamless bonding, with properties that progressively change based on their thickness. The properties of FGM change continuously from one surface to another due to the effective monotonic variation in the volume fraction of the constituent phases. That enables the elimination of stress discontinuity in most

searches, including layered structures made of two materials. The primary advantage of these materials is their ability to adjust specific thermomechanical properties through a continuous spatial distribution, resulting in increased resistance to interfacial failure (Yang and Liu, 2020). Another advantage is their ability to withstand various external factors such as temperature or thickness gradients while maintaining their structural integrity (Gong et al., 1999).

Due to their graded properties in several dimensions, many researchers have focused greater attention on FGMs, utilizing a variety of techniques and mathematical approaches. Among those, the finite element method has become the most widely used for their structural analysis. Wang and Pan (2011) used the three-dimensional finite element method to investigate the behavior of FGM multiferroic composites under different types of loads. Hedayatrasa et al. (2014) used the time-domain spectral finite element method based on Chebyshev Lagrangian expansion to numerically describe the characteristics of elastic wave propagation in 2D FGMs. Using an analytical method, Gong et al. (1999) investigated the effects of the constituent volume

fraction on various structures of FG shells. Other researchers applied the same method to investigate elastic waves in an FG cylinder (Han et al., 2002) and an FG piezoelectric cylinder (Han and Liu, 2003). Furthermore, higher-level modeling techniques such as the Legendre polynomial series approach were developed to improve its accuracy. Some researchers also studied guided wave dispersion curves and displacement distributions in FGM plates (Lefebvre et al., 2001) and radially graded cylinders (Elmaimouni et al., 2005). This approach was further developed to explain the behavior of guided waves in more complex structures, including thermoelastic (Yu et al., 2010) and viscoelastic FGM plates (Yu et al., 2012) as well as functionally graded piezoelectric-piezomagnetic plates (Zhang et al., 2018). Liu et al. (2021) relied on the modified couple stress theory to examine the Lamb wave propagation properties in a small-scale functionally graded piezoelectric plate. Several other methods were utilized to analytically solve the wave equations in FGMs (Ashida et al., 2022; Bezzie & Woldemichael, 2021; Bian et al., 2022; Radman et al., 2023; Velhinho & Rocha, 2011; Wang et al., 2022).

The study of elastic wave propagation and dispersion is essential in the most diverse applications and domains like earthquake engineering, architecture and non-destructive testing (Yilmaz et al., 2020). The use of ultrasonic guided waves represents a rapid, effective, and delicate non-destructive testing method commonly employed for various engineering materials. Zhang et al. (2022b) explored the influence of polarization variation on phonon modes and phason modes in the quasi-periodic direction. Based on the Legendre polynomial method, Li et al. (2022) studied the propagation of longitudinal axisymmetric guided waves in a full-length bonding resin bolt, which is a bilayer structure. Zhang et al. (2022a) analyzed the propagation of generalized thermo-elastic waves in bars with a rectangular cross-section. Naciri et al. (2019) investigated the numerical vibrational characterization of an annular piezoelectric disc resonator partially covered with electrodes to express the mechanical displacement components as well as the electric potential.

In this perspective, the current research intends to provide an analytical framework to investigate wave propagation properties in a composite functionally graded (FG) structure made of stainless steel (SS) and silicon nitride (SN). In particular, it aims to numerically analyze wave propagation in a three-layered (SS/SN/SS) FGM cylinder. For this purpose, the volume fraction distribution is used to confirm that Young's modulus, Poisson's ratio, and the density of FGM cylinders vary gradually in the radial direction. Mathematical equations are converted into a complex eigenvalue and eigenvector problem,

enabling the calculation of dispersion curves for normalized frequencies and phase velocity. The numerical results enable the evaluation of dispersion curves for longitudinal, torsional, and flexural modes. We also studied displacement distributions and stress field profiles to reveal and extend our understanding of the characteristics of guided waves in FG materials. The results of our comprehensive model are in line with the theoretical numerical results found in literature.

**Methods**

In this paper, the Legendre orthogonal polynomial method is proposed to model guided wave propagation in a multi-layered functionally graded hollow cylinder. In fact, the propagation of guided waves and their physical properties still remain an essential tool in several application domains, such as: non-destructive testing and evaluation (NDT&E) (Yilmaz et al., 2020) and structural health monitoring (SHM) (Wang et al., 2020). In this case, the acoustic waves are reflected when they encounter changes in the characteristic properties or geometry of materials, caused by specific phenomena, e.g., corrosion, discontinuities, welds, etc., thus making it possible to localize defects and providing information about their nature. This simplifies testing over long distances and prevents the need to scan the entire structure. Thanks to this method, it is possible to inspect even hard-to-reach areas without having to remove the insulation material in certain cases (Huang et al., 2020). This study represents a crucial step for non-destructive evaluation (NDE) of material properties and, therefore, for better understanding of its potential applications in manufacturing and quality control. The scope of this research could be expanded to encompass numerous other applications, including aeronautics, biomechanics, biomedicine, and automotive. Besides, FGMs are suitable for aerospace applications due to their ability to withstand extremely high thermal gradients. FGMs were first created for the aerospace sector. Their use has since expanded to cover components of rocket engines, heat exchangers, turbine wheels, turbine blades, space shuttles, and other machines (Ghatage et al., 2020).

*Basic equation*

In this section, a hollow FGM cylinder with infinite length is used to describe the problem as a part of the three-dimensional linear elasticity theory with various material parameters (Poisson's ratio $v$, density $\rho$, and Young's modulus $E$) varying in the radial direction, where $a$ and $b$ are the inner and outer radius, respectively. Let us also introduce such values as $H$, which is the thickness, and $R$, which is the average surface radius of the cylinder, with $H = b - a$ and $R = (a + b) / 2$ as shown in Fig. 1.

The problem will be solved in a cylindrical coordinate system $(r, \varphi, z)$, where $r$, $\varphi$, and $z$ are
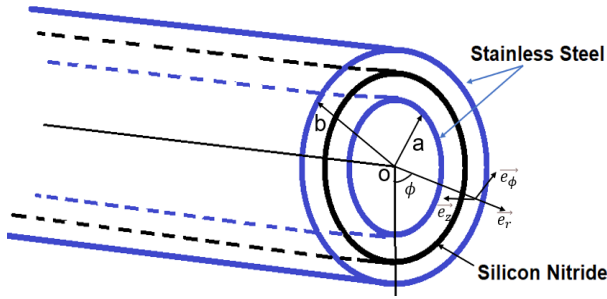
Fig. 1. FGM cylindrical structure with the (SS/SN/SS) configuration

the radial, circumferential, and axial directions, respectively. As the first assumption, the propagation of the acoustic waves is considered throughout the z-axis.

The usual approach is to start from an infinitesimal element in an infinite elastic isotropic solid with density $\rho$. In this case, a change of variable is proposed to solve the wave equations for circular cylinders:

$$q_1 = k\,r, \ q_2 = \varphi, \ q_3 = k\,z,$$

where $k$ is the wave number.

The following equations can be used to represent the law of variation of stiffness $C_{ij}^{(M)}$ and density $\rho^{(M)}$ as a polynomial with degree $L$:

$$C_{ij}^{(M)}\left(q_1\right) = C_{ij}^{(0)} + C_{ij}^{(1)}\left(\frac{q_1}{kH}\right)^1 + C_{ij}^{2}\left(\frac{q_1}{kH}\right)^2 +$$

$$+\ldots\ldots + C_{ij}^{L}\left(\frac{q_1}{kH}\right)^L; \qquad (1.a)$$

$$\rho^{(M)}\left(q_1\right) = \rho^{(0)} + \rho^{(1)}\left(\frac{q_1}{kH}\right)^1 + \rho^{(2)}\left(\frac{q_1}{kH}\right)^2 +$$

$$+\ldots\ldots + \rho^{(L)}\left(\frac{q_1}{kH}\right)^L, \qquad (1.b)$$

where:

$C_{ij}^{(M)}\left(q_1\right)$, $i, j = 1, 2, \ldots 6$ are the ordinary elastic constants of the space constituting the cylinder at the point $M\left(q_1\right)$.

$\rho^{(M)}\left(q_1\right)$ is the density of the structure at the point $M\left(q_1\right)$.

In FGM hollow cylinders, the radial variation of material properties is considered progressive (Elmaimouni, 2005). As a result, material characteristics may be described in terms of $q_1$. Using the Einstein summation convention, Eq. 1.b can be expressed as follows:

$$\begin{cases} C_{ij}^{(M)}\left(q_1\right) = C_{ij}^{(l)}\left(\dfrac{q_1}{kH}\right)^l \\[2mm] \rho^{(M)}\left(q_1\right) = \rho^{(l)}\left(\dfrac{q_1}{kH}\right)^l \end{cases} l = 0, 1, 2, \ldots L, \quad (2)$$

where:

$C_{ij}^{(l)}$ and $\rho^{(l)}$ are the coefficients of a polynomial with degree $l$.

In a cylindrical coordinate system, the relationship between the deformation tensors and the displacement components for an elastic medium was described by Zhang et al. (2022a):

$$\begin{cases} \varepsilon_{rr} = \dfrac{\partial u_1}{\partial q_1} & \varepsilon_{\varphi z} = \dfrac{1}{2}\left(\dfrac{\partial u_2}{\partial q_3} + \dfrac{1}{q_1}\dfrac{\partial u_3}{\partial q_2}\right) \\[3mm] \varepsilon_{\varphi\varphi} = \dfrac{u_1}{q_1} + \dfrac{1}{q_1}\dfrac{\partial u_2}{\partial q_2}, & \varepsilon_{rz} = \dfrac{1}{2}\left(\dfrac{\partial u_1}{\partial q_3} + \dfrac{\partial u_3}{\partial q_1}\right) \\[3mm] \varepsilon_{zz} = \dfrac{\partial u_3}{\partial q_3} & \varepsilon_{r\varphi} = \dfrac{1}{2}\left(\dfrac{1}{q_1}\dfrac{\partial u_1}{\partial q_2} + \dfrac{\partial u_2}{\partial q_1} - \dfrac{u_2}{q_1}\right) \end{cases} ,(3)$$

where $u_1$, $u_2$ and $u_3$ are the components of mechanical displacement in the radial, circumferential, and axial directions, respectively.

According to the three-dimensional theory of elasticity, Hooke's law describes the properties of both homogeneous and inhomogeneous materials. For each layer, the stress-strain expressions can be represented as follows (Elmaimouni, 2005):

$$\begin{cases} T_{rr} = C_{11}^{l}\left(\dfrac{q_1}{kH}\right)^l \dfrac{\partial u_1}{\partial r} + C_{12}^{l}\left(\dfrac{q_1}{kH}\right)^l \left(\dfrac{u_1}{r} + \dfrac{1}{r}\dfrac{\partial u_2}{\partial \varphi}\right) + \\[3mm] \qquad + C_{13}^{l}\left(\dfrac{q_1}{kH}\right)^l \dfrac{\partial u_3}{\partial z} \\[3mm] T_{\varphi\varphi} = C_{12}^{l}\left(\dfrac{q_1}{kH}\right)^l \dfrac{\partial u_1}{\partial r} + C_{22}^{l}\left(\dfrac{q_1}{kH}\right)^l \left(\dfrac{u_1}{r} + \dfrac{1}{r}\dfrac{\partial u_2}{\partial \varphi}\right) + \\[3mm] \qquad + C_{23}^{l}\left(\dfrac{q_1}{kH}\right)^l \dfrac{\partial u_3}{\partial z} \\[3mm] T_{zz} = C_{13}^{l}\left(\dfrac{q_1}{kH}\right)^l \dfrac{\partial u_1}{\partial r} + C_{23}^{l}\left(\dfrac{q_1}{kH}\right)^l \left(\dfrac{u_1}{r} + \dfrac{1}{r}\dfrac{\partial u_2}{\partial \varphi}\right) + , (4) \\[3mm] \qquad + C_{33}^{l}\left(\dfrac{q_1}{kH}\right)^l \dfrac{\partial u_3}{\partial z} \\[3mm] T_{\varphi z} = C_{44}^{l}\left(\dfrac{q_1}{kH}\right)^l \left(\dfrac{\partial u_2}{\partial z} + \dfrac{1}{r}\dfrac{\partial u_3}{\partial \varphi}\right) \\[3mm] T_{rz} = C_{55}^{l}\left(\dfrac{q_1}{kH}\right)^l \left(\dfrac{\partial u_1}{\partial z} + \dfrac{1}{r}\dfrac{\partial u_3}{\partial r}\right) \\[3mm] T_{r\varphi} = C_{66}^{l}\left(\dfrac{q_1}{kH}\right)^l \left(\dfrac{1}{r}\dfrac{\partial u_1}{\partial \varphi} + \dfrac{\partial u_2}{\partial r} - \dfrac{u_2}{r}\right) \end{cases}$$

where $T_{ij}$ denote the components of the stress tensor and $C_{ijkl}$ denote the elastic coefficients.

By neglecting the body force, we can write the three-dimensional stress motion equations and displacement components of a linear elastic material in cylindrical coordinates as follows (Li et al., 2022):

$$\frac{\partial T_{rr}}{\partial r} + \frac{1}{r}\frac{\partial T_{r\varphi}}{\partial \varphi} + \frac{\partial T_{rz}}{\partial z} + \frac{T_{rr} - T_{\varphi\varphi}}{r} = \rho\frac{\partial^2 u_1}{\partial t^2};$$

Rabab Raghib, Ismail Naciri, Hassna Khalfi, Lahoucine Elmaimouni, Jiangong Yu, Abdelmajid Bybi, Mustapha Sahal — Pages 82–98

FREE VIBRATION MODELING IN A FUNCTIONALLY GRADED HOLLOW CYLINDER
USING THE LEGENDRE POLYNOMIAL APPROACH

$$\frac{\partial T_{r\varphi}}{\partial r} + \frac{1}{r}\frac{\partial T_{\varphi\varphi}}{\partial \varphi} + \frac{\partial T_{\varphi z}}{\partial z} + \frac{2T_{r\varphi}}{r} = \rho\frac{\partial^2 u_2}{\partial t^2}; \qquad (5)$$

$$\frac{\partial T_{rz}}{\partial r} + \frac{1}{q_1}\frac{\partial T_{\varphi z}}{\partial \varphi} + \frac{\partial T_{zz}}{\partial z} + \frac{T_{rz}}{r} = \rho\frac{\partial^2 u_3}{\partial t^2}.$$

*Boundary conditions*

The electrical and mechanical boundary conditions are embedded directly into the equations of motion, using position-dependent physical quantities $C_{ij}(q_1)$ and rectangular window functions $\pi(ka,kb)$ (Elmaimouni et al., 2005; Lefebvre et al., 2001; Naciri et al., 2019), defined according to the studied geometrical structure, in order to take into consideration the entire surface of the studied structure without the need of meshing. Thus, the cylindrical structure can be defined as follows:

$$ka \leq q_1 \leq kb, \ 0 \leq q_2 \leq 2\pi, \ -\infty \leq q_3 \leq +\infty$$

When the boundary condition of the material is taken into account, the position-dependent elastic constants and density can be obtained by the following expressions:

$$\begin{cases} C_{ij}^{(M)}(q_1) = C_{ij}^{(l)}\left(\frac{q_1}{kH}\right)^l \pi(ka,kb) \\ \rho_{ij}^{(M)}(q_1) = \rho_{ij}^{(l)}\left(\frac{q_1}{kH}\right)^l \pi(ka,kb) \end{cases}, \qquad (6)$$

where:

$\pi(ka,kb)$ is the rectangular window function defined as follows:

$$\pi(ka,kb) = \begin{cases} 1 & ka \leq q_1 \leq kb \\ 0 & \text{elsewhere} \end{cases}. \qquad (7)$$

According to Eqs. 6 and 7, the density and the elastic modulus in the outer cylinder are equal to zero. As a result, the vacuum outside the cylinder is regarded as a medium with zero impedance, which ensures that the stresses outside the cylinder are equal to zero.

*Mechanical displacements*

Since in this research guided waves are assumed to propagate in the z-direction, the components of the mechanical displacement in an orthonormal basis can be represented as follows:

$$u_1(q_1,q_2,q_3,t) = \frac{1}{\sqrt{2\pi}}e^{inq_2}e^{i(\omega t - q_3)}\sum_{m=0}^{\infty}p_m^1 Q_m(q_1); (8.a)$$

$$u_2(q_1,q_2,q_3,t) = \frac{1}{\sqrt{2\pi}}e^{inq_2}e^{i(\omega t - q_3)}\sum_{m=0}^{\infty}p_m^2 Q_m(q_1); (8.b)$$

$$u_3(q_1,q_2,q_3,t) = \frac{1}{\sqrt{2\pi}}e^{inq_2}e^{i(\omega t - q_3)}\sum_{m=0}^{\infty}p_m^3 Q_m(q_1). (8.c)$$

where n = 0, 1, 2, ... — the circumferential wave number, $\omega$ — the pulsation, $p_m^\alpha (\alpha = 1, 2 \ et \ 3)$ — the amplitudes of the polynomial $Q_m$, $\alpha = 1$ pertains to the radial direction, $\alpha = 2$ pertains to the circumferential

direction, and $\alpha = 3$ pertains to the axial direction. The polynomials $Q_m(q_1)$ can be written as follows:

$$Q_m(q_1) = \sqrt{\frac{2m+1}{kH}}P_m\left(\frac{2q_1 - (kR_2 + kR_1)}{kH}\right),$$

where:

$P_m$ is the Legendre polynomial with degree $m$,

$Q_m(q_1)$ is the complete orthonormal set in the range $ka \leq q_1 \leq kb$, which can represent any continuous function. Each of these three components of mechanical displacements is represented by a set of three functions. The functions associated with the circumferential and axial terms are expressed by exponential functions while the radial term is represented by Legendre polynomials (Yilmaz et al., 2020).

The stress tensors in Eq. 4 and the mechanical displacement in Eq. 8 can be embedded into the motion equations given in Eq. 5, and the derivatives of the rectangular window function $\pi(ka,kb)$ produce terms $\delta(q_1 = ka)$ and $\delta(q_1 = kb)$. Such formulation gives us the equation system shown below:

$$\begin{bmatrix} C_{11}^{(l)}q_1^{l+2}\frac{\partial^2 u_1}{\partial q_1^2} + (1+l)C_{11}^{(l)}q_1^{l+1}\frac{\partial u_1}{\partial q_1} + \\ +(lC_{12}^{(l)} - C_{22}^{(l)} - n^2 C_{66}^{(l)})q_1^l u_1 - \\ -C_{55}^{(l)}q_1^{l+2}u_1 - in(C_{12}^{(l)} + C_{66}^{(l)})q_1^{l+1}\frac{\partial u_2}{\partial q_1} + \\ +in(lC_{22}^{(l)} - C_{66}^{(l)} - C_{12}^{(l)})q_1^l u_2 - i(C_{13}^{(l)} + \\ +C_{55}^{(l)})q_1^{l+2}\frac{\partial u_3}{\partial q_1} - i((1+l)C_{13}^{(l)} - C_{23}^{(l)})q_1^{l+1}u_3 \end{bmatrix} \times$$

$$\times\frac{1}{(kH)^l}\pi(ka,kb) +$$

$$+\frac{1}{(kH)^l}\begin{bmatrix} C_{11}^{(l)}q_1^{l+2}\frac{\partial u_1}{\partial q_1} + C_{12}^{(l)}q_1^{l+1}u_1 + \\ +inC_{12}^{(l)}q_1^{l+1}u_2 - iC_{13}^{(l)}q_1^{l+2}u_3 \end{bmatrix} \times$$

$$\times(\delta(q_1 = ka) - \delta(q_1 = kb)) =$$

$$= -\rho^{(l)}\left(\frac{\omega}{k}\right)^2\frac{1}{(kH)^l}q_1^{l+2}u_1\pi(ka,kb); \qquad (9.a)$$

$$\begin{bmatrix} in(C_{12}^{(l)} + C_{66}^{(l)})q_1^{l+1}\frac{\partial u_1}{\partial q_1} + in(C_{22}^{(l)} + \\ +(1+l)C_{66}^{(l)})q_1^l u_1 - (n^2 C_{22}^{(l)} + \\ +(1+l)C_{66}^{(l)})q_1^l u_2 + C_{66}^{(l)}q_1^{l+2}\frac{\partial^2 u_2}{\partial q_1^2} + \\ +(1+l)C_{66}^{(l)}q_1^{l+1}\frac{\partial u_2}{\partial q_1} - C_{44}^{(l)}q_1^{l+2}u_2 + \\ +n(C_{23}^{(l)} + C_{44}^{(l)})q_1^{l+1}u_3 \end{bmatrix} \times$$

$$\times \frac{1}{(kH)^l} \pi(ka,kb) +$$

$$+ \frac{1}{(kH)^l}\left[ C_{66}^{(l)}\left( inq_1^{l+1} u_1 + q_1^{l}\,\frac{\partial u_2}{\partial q_1} - q_1^{l+1} u_2 \right) \right] \times$$

$$\times \left( \delta(q_1 = ka) - \delta(q_1 = kb) \right) =$$

$$= -\rho^{(l)}\left(\frac{\omega}{k}\right)^2 \frac{1}{(kH)^l} q_1^{l+2} u_2 \pi(ka,kb);$$

(9.b)

$$\begin{bmatrix} -i(C_{13}^{(l)} + C_{55}^{(l)})q_1^{l+2}\,\dfrac{\partial u_1}{\partial q_1} - \\[2mm] -i(C_{23}^{(l)} + (1+l)C_{55}^{(l)})q_1^{l+1} u_1 + \\[2mm] + n(C_{23}^{(l)} + C_{44}^{(l)})q_1^{l+1} u_2 + \\[2mm] + C_{55}^{(l)} q_1^{l+2}\,\dfrac{\partial^2 u_3}{\partial q_1^2} - n^2 C_{44}^{(l)} q_1^{l} u_3 - \\[2mm] - C_{33}^{(l)} q_1^{l+2} u_3 + (1+l)C_{55}^{(l)} q_1^{l+1}\,\dfrac{\partial u_3}{\partial q_1} \end{bmatrix} \times$$

$$\times \frac{1}{(kH)^l}\pi(ka,kb) +$$

$$+ \left[ -iC_{55}^{(l)} q_1^{l+2} u_1 + C_{55}^{(l)} q_1^{l+2}\,\frac{\partial u_3}{\partial q_1} \right]\frac{\partial}{\partial q_1}\pi(ka,kb) =$$

$$= -\rho^{(l)}\left(\frac{\omega}{k}\right)^2 \frac{1}{(kH)^l} q_1^{l+2} u_3 \pi(ka,kb).$$

(9.c)

Each element of Eq. 9 (a–c) was multiplied by $\frac{1}{\sqrt{2\pi}} Q_j^*(q_1) e^{-inq_2}$, with $j$ varying from 0 to infinity. The obtained equations were integrated over $j$ from 0 to infinity, over $q_1$ from $kR_1$ to $kR_2$, and over $q_2$ from 0 to $2\pi$. Thus, we can deduce the following system of equations:

$$^l A_{11}^{m,j} p_m^1 + {}^l A_{12}^{m,j} p_m^2 + {}^l A_{13}^{m,j} p_m^3 = -\eta^2\, {}^l M_j^m p_m^1;$$

$$^l A_{21}^{m,j} p_m^1 + {}^l A_{22}^{m,j} p_m^2 + {}^l A_{23}^{m,j} p_m^3 = -\eta^2\, {}^l M_j^m p_m^2; \quad (10)$$

$$^l A_{31}^{m,j} p_m^1 + {}^l A_{32}^{m,j} p_m^2 + {}^l A_{33}^{m,j} p_m^3 = -\eta^2\, {}^l M_j^m p_m^3.$$

These characteristic equations may be expressed as the product of two matrices with the following eigenvalues and eigenvectors:

$$\left[ \left( {}^l M \right)^{-1}\, {}^l A \right]_{\alpha\beta}^{m,j} p_m^\alpha = -\eta^2 p_m^\alpha. \quad (11)$$

The guided velocity is as follows: $\eta^2 = \rho V_{ph}^2$, $V_{ph} = \omega / k$.

$p_m^\alpha (\alpha = 1, 2\ and\ 3)$ is the eigenvector enabling the calculation of the displacement components and all other associated field parameters.

${}^l A_{\alpha\beta}^{m,j} (\alpha, \beta = 1,2,3)$, ${}^l M_j^m$ are the equations required to calculate all the matrix elements (more details are given in the Appendix below).

All the equations required to calculate the pertinent matrix elements are provided in the Appendix below. A three-layered FGM cylinder is examined using the suggested approach following the above derivation steps. In this regard, MATLAB software is used to numerically solve the matrix of eigenvalues and eigenvectors in Eq. 11. Finally, we point out that when the wave number $k$ and the graded index change, the eigenvalue problem is resolved using MATLAB eig function. Eigenvectors can be used to define the wave profile, and eigenvalues — to calculate the phase velocity. As a result, it is clear that the suggested approach represents an efficient way to simultaneously acquire the displacement, stress distribution and dispersion curves of an FGM cylinder.

**Results and discussion**

*Configurations of cylindrical FGM structures*

In order to verify the accuracy and effectiveness of our polynomial approach, we examined the acoustic waves in a three-layered hollow inhomogeneous cylinder made of two different materials, as discussed by Gong et al. (1999) and Han et al. (2002) and shown in Fig. 1. In our investigation, silicon nitride and stainless steel were used. FG cylinders have silicon nitride (SN) at the central surface and stainless steel (SS) on the exterior and interior. Table lists the elastic properties of stainless steel and silicon nitride required to solve the FGM frequency equation.

A computer program was developed to calculate the dispersion behavior using the preceding equation. In this case, the Voigt-type model is applied to determine the effective FGM property of two mixed materials at the $i^{th}$ layer level. It can be written as follows:

$$f^{(i)}(q_1) = f_1^{(i)} V_{m1}^{(i)}(q_1) + f_2^{(i)} V_{m2}^{(i)}(q_1);\ i = 1,2......k, \quad (12)$$

where $f^{(i)}$ is the effective material proportion of FGM and the volume fraction, $V_{mj}^{(i)}(q_1)$ is the $j^{th}$ material volume fraction with $V_{m1}^{(i)}(q_1) + V_{m2}^{(i)}(q_1) = 1$.

In case of FGM structures, the displacement and stress components should be continuous at the interfaces between the layers due to the advantages of the monotonic change in the volume fraction of the phase components, which allows the elimination of stress discontinuities. These considerations are adopted to align with those utilized by Gong et al. (1999) for validation, with position to thickness ratio $\frac{q_1}{kH}$ in the range 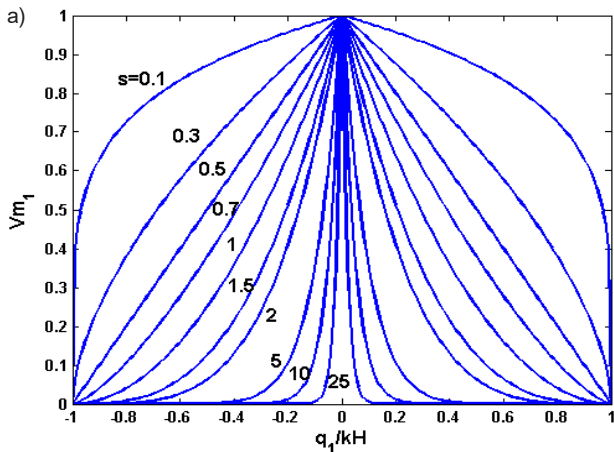from -1 to 1. Additionally, the shape of the local volume fraction is shown as a power series $S$ using the following equation in the radial direction:

$$\begin{cases} V_{m1}^{(1)}(q_1) = \left[ \left( \dfrac{q_1 - ka}{kH} \right)^2 \right]^S \\ V_{m2}^{(1)}(q_1) = 1 - V_{m1}^{(1)}(q_1) \end{cases} \quad -\dfrac{ka}{kH} \le q_1 \le 0;$$

$$\begin{cases} V_{m1}^{(2)}(q_1) = \left[ \left( \dfrac{q_1 + ka}{kH} \right)^2 \right]^S \\ V_{m2}^{(2)}(q_1) = 1 - V_{m1}^{(1)}(q_1) \end{cases} \quad 0 \le q_1 \le \dfrac{kb}{kH}. \quad (13)$$

This research examines a three-layered FGM cylinder. Here, $V_{m1}^{(i)}$ is the volume fraction of silicon nitride, and $V_{m2}^{(i)}$ is the volume fraction of stainless steel in the (SS/SN/SS) cylinder arrangement. It is assumed that the values of the gradient index $S$ vary from 0.1 to 25 for the functionally graded material along the radial direction. The variation tendency of volume fraction distribution along the radial direction significantly changed due to gradient exponents, as observed in Fig. 2. The amount of silicon nitride in the inner layer of the FGM cylinder equals 0, increasing continuously to 1 at the middle surface $\left( \dfrac{q_1}{kH} = 0 \right)$ as the gradient index $S$ rises before continually decreasing to 0 in the outer layer. As for the stainless steel volume fraction, it roughly decreases from 1 in the inner layer to 0 at the middle surface as the gradient exponent grows, and then exponentially increases to 1 at the outer surface. This proves that in the inner layer $\left( \dfrac{q_1}{kH} = -1 \right)$ and the outer layer $\left( \dfrac{q_1}{kH} = 1 \right)$, the surface is uniformly dominated by stainless steel, whereas at the middle surface $\left( \dfrac{q_1}{kH} = 0 \right)$, the silicon nitride volume fraction is dominant.

Based on Eqs. 12 and 13, we have calculated the spatial distributions of the mechanical characteristics of the FGM cylinder along the thickness direction. Figs. 3(a-c) show the variations of FGM Young's modulus, Poisson's ratio, and density for the (SS/SN/SS) configuration with the variation of the power-law exponent ($S$) across the radial direction when $S$ = 0.1, 0.3, 0.5, 1, 2, and 4. Furthermore, it is possible to calculate the stiffness coefficient $C_{ij}^{(l)}$ of order $l$ of the examined FGM based on Poisson's ratio $\nu(q_1)$, density $\rho^{(l)}$, and Young's modulus $E(q_1)$ of the silicon nitride and stainless steel volume fractions previously determined using Eq. 12. As for the numerical results, the coefficients $C_{11}^{(l)}, C_{12}^{(l)}$ and $C_{44}^{(l)}$ of the studied FGM are shown in Fig. 4. It can be observed that Poisson's ratio, density, Young's modulus, and position-dependent elastic constants $C_{ij}^{(l)}$ of the functionally graded material vary continuously along the radial direction. This research also demonstrates a significant influence of the graded index on changes in material properties in the radial direction $q_1$ when $kH = ka$.

*Dispersion curves*

The resolution of the system of equations (10) results in the dispersion curves of the propagation modes in the structure, relating the frequencies ($f$) to the wave numbers ($k$). In this context, a computer program was developed to plot the dispersion curves of cylindrical structures. We decided to express the phase velocities as a function of frequency-thickness. Moreover, the

**Stainless steel and silicon nitride material properties**

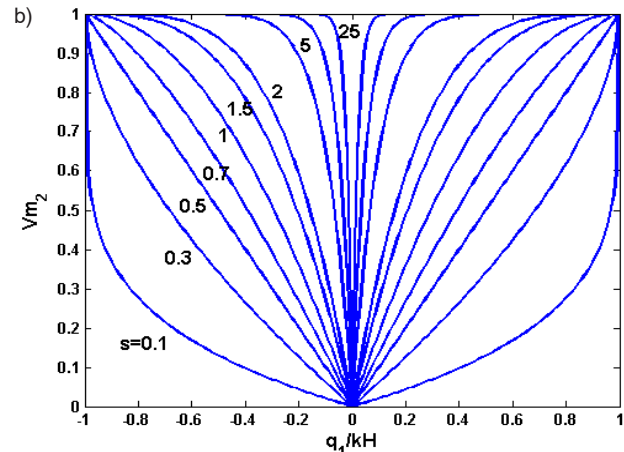| | Properties | | |
|---|---|---|---|
| | E (GPa) | ν | ρ (kg/m³) |
| Silicon nitride | 322.4 | 0.24 | 2370 |
| Stainless steel | 207.82 | 0.317 | 8166 |



Fig. 2. Variation of the volume fraction in the cylindrical layer of FGM in the radial direction with different graded index *S* values: (a) volume fraction of silicon nitride (b) volume fraction of stainless steel

numerical results are used to demonstrate how the graded index affects the convergence of dispersion curves. It provides a theoretical support for the quantitative measurement of the structural properties of the FGM cylinder by utilizing the relationship between the gradient distribution and propagation characteristics. Figs. 5 and 6 show the dispersion curves for the (SS/SN/SS) configuration of the FGM cylinder for axisymmetric (longitudinal L(0, m), torsional T(0, m)) and symmetric (F(1, m)) modes, respectively. It can be noticed that for all propagation modes for the functionally graded cylinder in the (SS/SN/SS) configuration, only the

first modes L(0,1), T(0,1) and F(0,1) did not show any cut-off frequencies.

In this section, the relationship between the guided wave phase velocity and gradient distribution is examined. Figs. 7 and 8 present the phase velocity curves of the axisymmetric ($n = 0$) and symmetric ($n = 1$) modes of the configuration (SS/SN/SS) as a function of the frequency ($f$)-thickness ($H$) product, where $H/R = 1$.

In this study, only three mode values are taken into account: 0.1, 1, and 4. Figs. 7 and 8 show that all modes are dispersive. Besides, it was found that only the first modes (the lowest modes) did not have any cut-
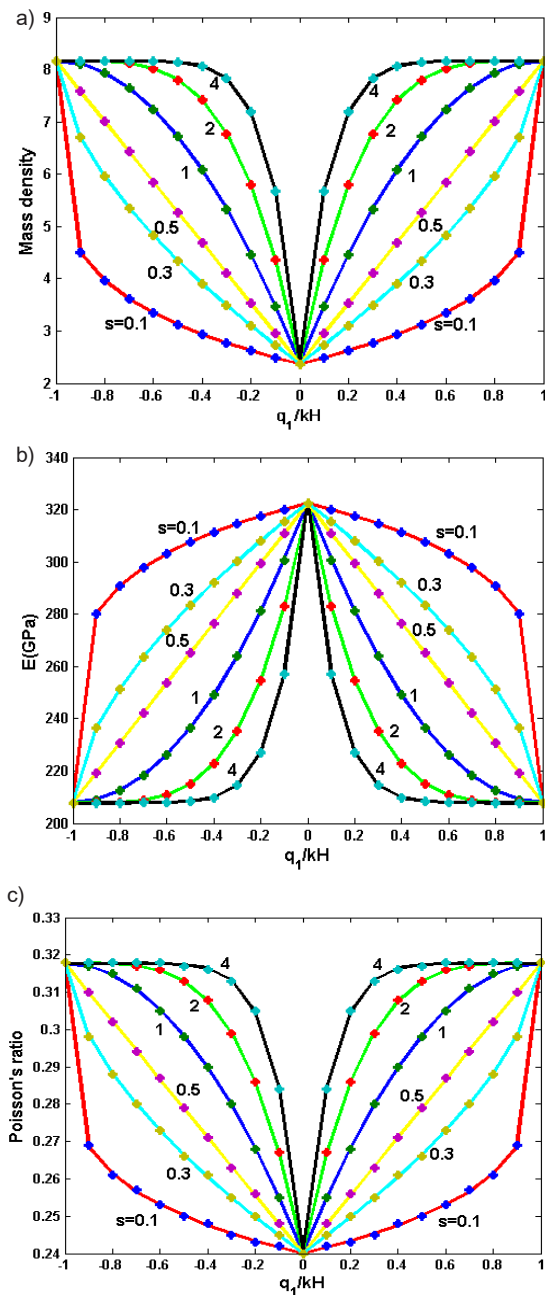


Fig. 3. Spectral variation of: (a) Poisson's ratio, (b) density, (c) Young's modulus
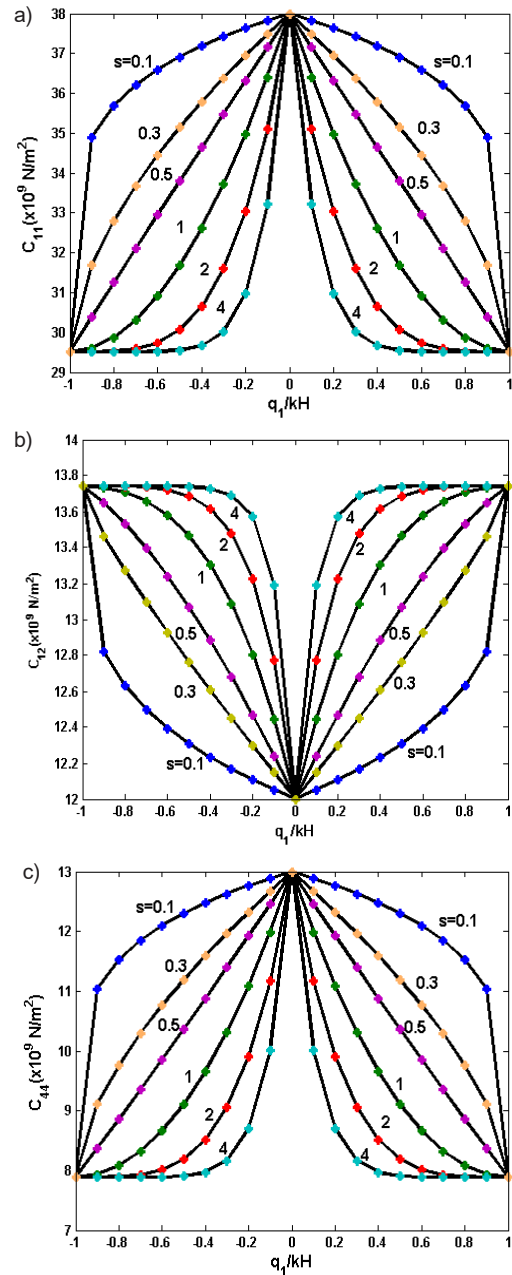


Fig. 4. Spectral variation of the stiffness coefficient $c_{ij}^{(l)}$: (a) $c_{11}^{(l)}$, (b) $c_{12}^{(l)}$, (c) $c_{44}^{(l)}$
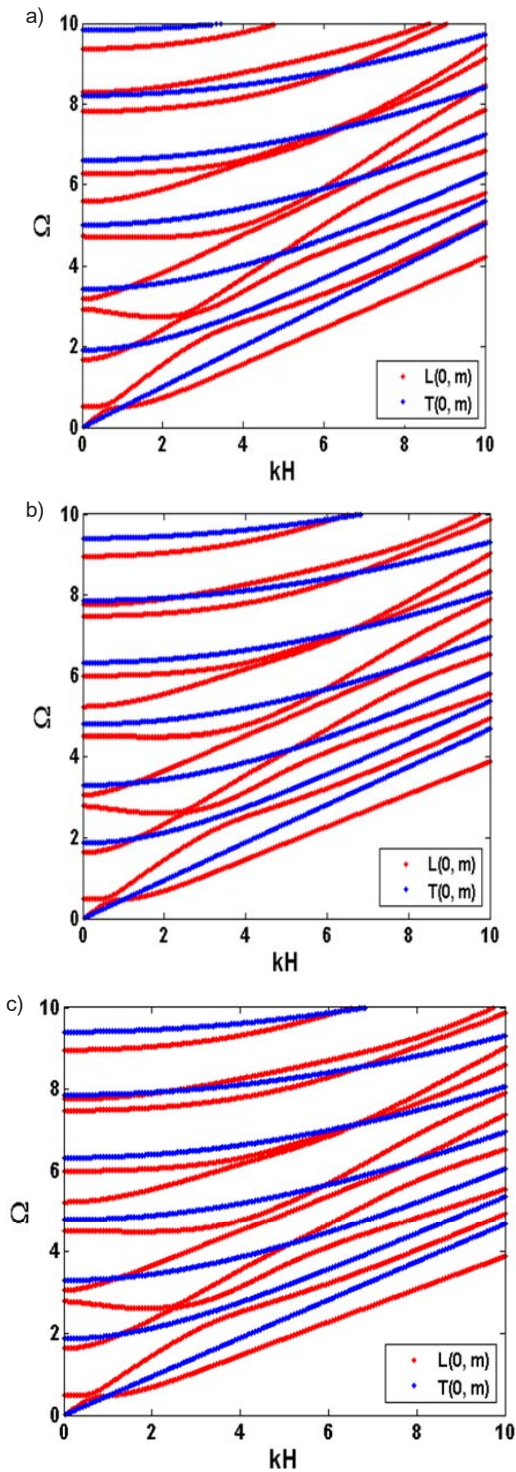
Fig. 5. Normalized frequency $\Omega = \omega H / \left(C_{44}/\rho\right)^{1/2}$ as a function of $kH$ in the hollow cylinder for longitudinal and torsional modes ($n = 0$): (a) $S = 0.1$, (b) $S = 1$, (c) $S = 4$
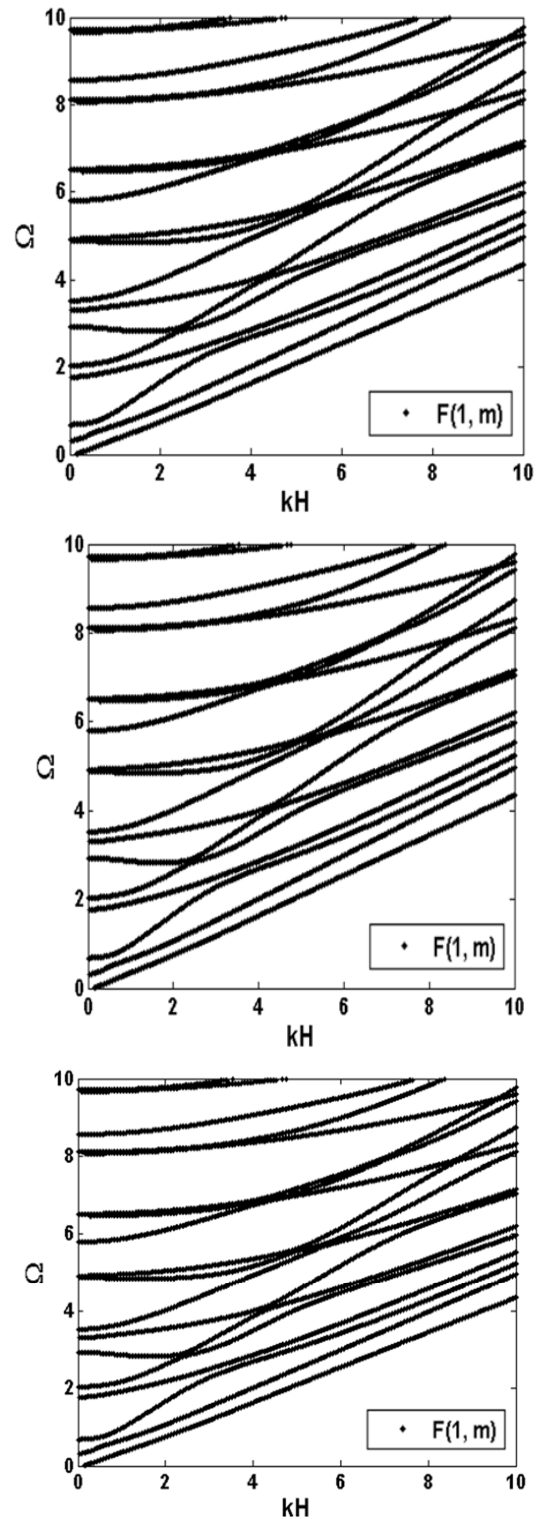
Fig. 6. Normalized frequency $\Omega = \omega H / \left(C_{44}/\rho\right)^{1/2}$ as a function of $kH$ in the FGM hollow cylinder for symmetric modes ($n = 1$): (a) $S = 0.1$, (b) $S = 1$, (c) $S = 4$

off frequency. Fundamental modes L(0,1), T(0,1), and F(0,1) are the only modes that exist at extremely low frequencies. At higher frequencies, all the fundamental modes are transformed into Rayleigh surface waves and propagate at the Rayleigh speed $\left(V_R = 2940 \text{ m/s}\right)$.

It is clear that there is a relationship between the values of the graded index and phase velocity curves for L(0, 1) and T(0, 1) modes of the three-layered FGM cylinder. Furthermore, in both figures, the effects of the graded index on the cut-off frequencies differ in propagation modes that are symmetric and axisymmetric. The graded index has a considerable effect on the

89

a)



a)



b)



b)



c)



c)



Fig. 8. Phase velocity dispersion curves as a function
of the frequency-thickness product in the hollow FGM cylinder
for flexural modes: (a) S = 0.1, (b) S = 1, (c) S = 4

Fig. 7. Phase velocity dispersion curves as a function
of the frequency-thickness product in the hollow FGM cylinder
for longitudinal and torsional modes: (a) S = 0.1, (b) S = 1,
(c) S = 4

phase velocity curves in longitudinal and torsional modes. Fig. 7a shows that the phase velocity of L(0,1) and T(0,1) modes is substantially higher than that in Figs. 7b and 7c for hollow FGM

cylinders. These results demonstrate that the phase velocities of the same mode decrease as the exponents of the power law increase. This can be explained by the fact that small values of $s$ correlate to the large volume fractions of stainless steel (Figure 2a $V_{m1}$), while the large values of $s$

correlate to the small volume fractions of silicon nitride (Fig. 2b $V_{m2}$).

*Mechanical displacements and stress distributions*

In this section, the conundrum lays in determining the profiles of the mechanical displacements and normal stresses corresponding to different normalized frequencies, through the thickness of the cylinder. Therefore, we examined the normal stresses and mechanical displacement profiles for the axisymmetric ($n = 0$) and non-axisymmetric modes ($n = 1$) in the hollow inhomogeneous functionally graded cylinder. Figs. 9 and 10 show the mechanical displacement profiles for both axisymmetric ($n = 0$) and non-axisymmetric ($n = 1$) modes, respectively. In case of longitudinal modes, the circumferential component $v$ always remains zero along the cylinder thickness, whereas the axial component dominates in the mechanical displacements. However, the axial and radial components are zero for torsional modes. In case of flexural modes, as opposed to compression and torsional modes, each component of the mechanical displacement is coupled with each and every other component.

*Stress distributions and boundary conditions*

Figs. 11 and 12 show the normal stress profiles of the hollow FGM cylinder for longitudinal modes ($n = 0$) and flexural modes ($n = 1$), respectively. As can be observed, in case of axisymmetric modes, the circumferential stresses $T_{r\varphi}$ are zero, while in case of flexural modes they are very low. In case of axisymmetric and flexural modes, it is evident that all normal stresses are zero on the inner and outer surfaces of the cylinder. This demonstrates the effectiveness of the mathematical approach employed to establish the boundary conditions. Although the elastic constants of two adjoining layers differ, it is widely known that at the interfaces, the normal stresses and displacements vary continuously from one surface to the next due to the advantages of monotonic fluctuation in the volume fraction of the component phases. All higher order modes propagate inside the cylinder, and the motion of the particles becomes more complicated. The latter is what explains why all the constraints are zero at the edges of the cylinder.

*Method validation*

In the course of the study, we investigated the dispersion curves of the guided waves propagating through the hollow inhomogeneous FGM cylinder of the (SS/SN/SS) configuration with various gradient shapes. For this purpose, a computer program using the Legendre polynomial approach based on the previous formulations was implemented
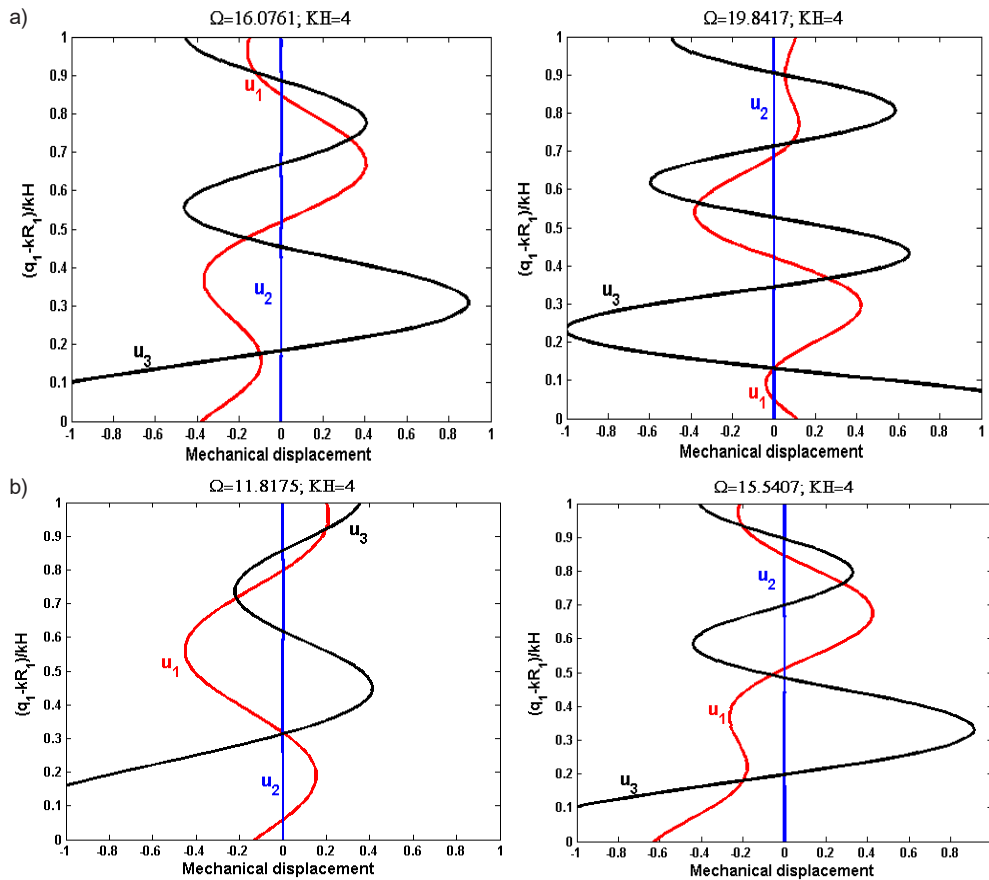


Fig. 9. Normalized mechanical displacement profiles of the hollow cylinder in case of longitudinal modes,
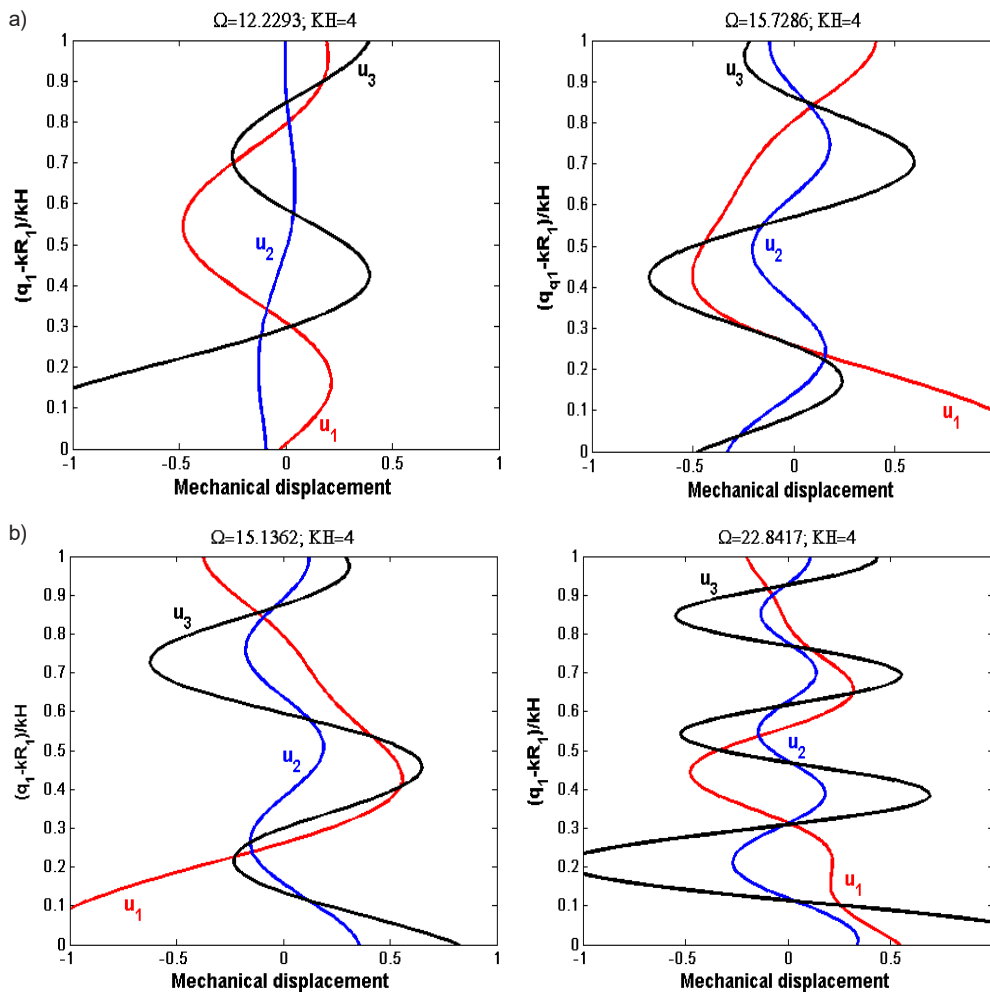$n = 0$, $H/R = 4.00$ for (SN/SS/SN): (a) $S = 1$, (b) $S = 4$

91

Fig. 10. Normalized mechanical displacement profiles of the hollow cylinder in case of flexural modes,
$n = 1$, $H/R = 4.00$: (a) $S = 1$, (b) $S = 4$

in MATLAB software. The dispersion curves of normalized frequencies and phase velocity for three layers of FGM with a cylindrical shape are completely undetermined. As shown in Fig. 13, to compare our results with the available data (Gong et. al., 1999; Hedayatrasa et al., 2014), we calculate the normalized frequencies of the hollow FGM cylinder with two layers made of stainless steel and silicon nitride. Simulations are made considering the axisymmetric mode ($n = 0$) with three different gradient index $S$ values for a specific limit when $kR = 20kH$ with truncation $M = 25$. The comparison of our results with those reported in literature by Han et al. (2002) demonstrates that our methods has a high degree of precision and reliability in addition to the theoretical and programming equation accuracy.

It is clearly observed that the results of the numerical analytical method (reported by Han et al. (2002)) are compatible with the results obtained with the use of our method. This approach can predict the behavior of an infinite-length FGM cylinder with quite a high accuracy. The comparison of our findings with those found in literature demonstrates

that our method has a high degree of accuracy and reliability.

**Conclusion**

The goal of the study was to develop a numerical approach to solve and compute the wave propagation problem in a continuous three-layered FGM cylinder, without discretizing the gradient structure. The polynomial approach considerably reduced the challenges experienced in this context and offered access to more rapid and precise numerical results. The propagation characteristics of the guided waves in three-layered FGM cylinders were determined. The obtained results showed that the variations of the material properties in the radial direction are significantly influenced by the graded index. The dispersion curves of the normalized frequencies and phase velocities are considerably impacted by the graded index due to the continuous variation of the volume fraction. The influence of the boundary conditions on the normal stresses across the radial direction of FG material was examined. Based on the simulations, it was found that the field profiles are strongly influenced by the
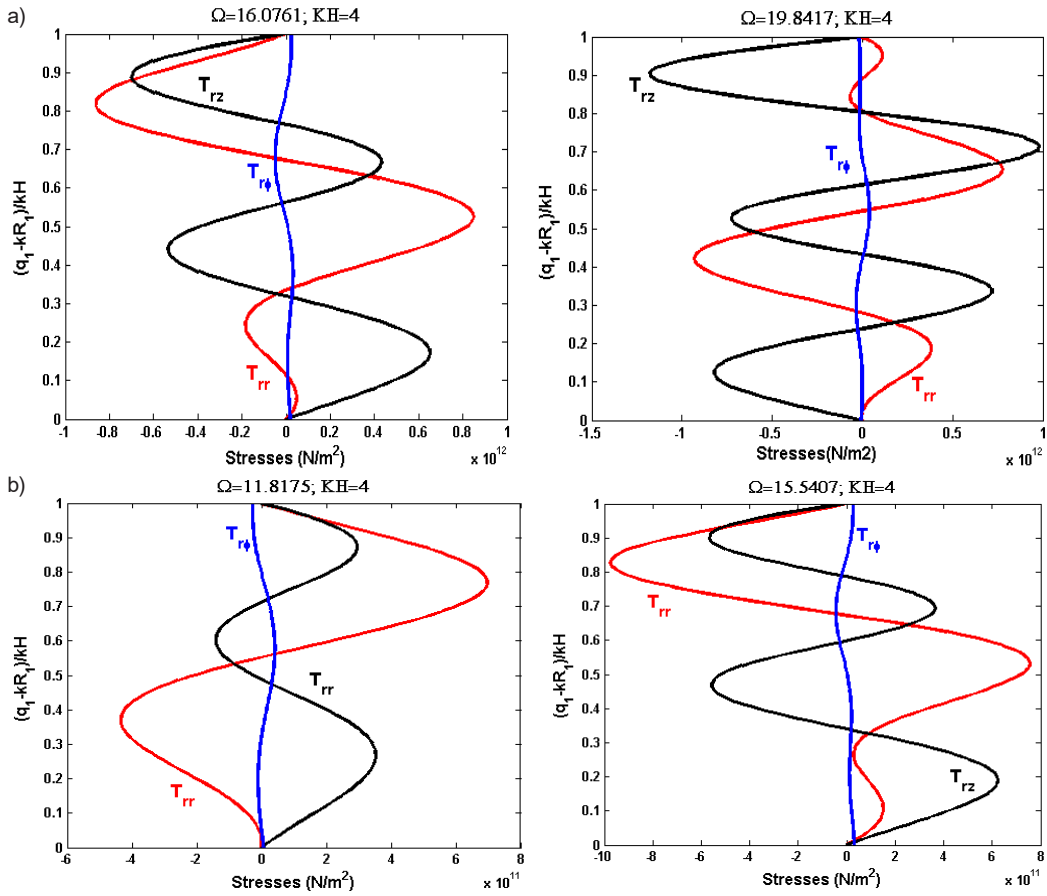
Fig. 11. Normal stress profiles for the first six modes in case of longitudinal modes ($n = 0$),
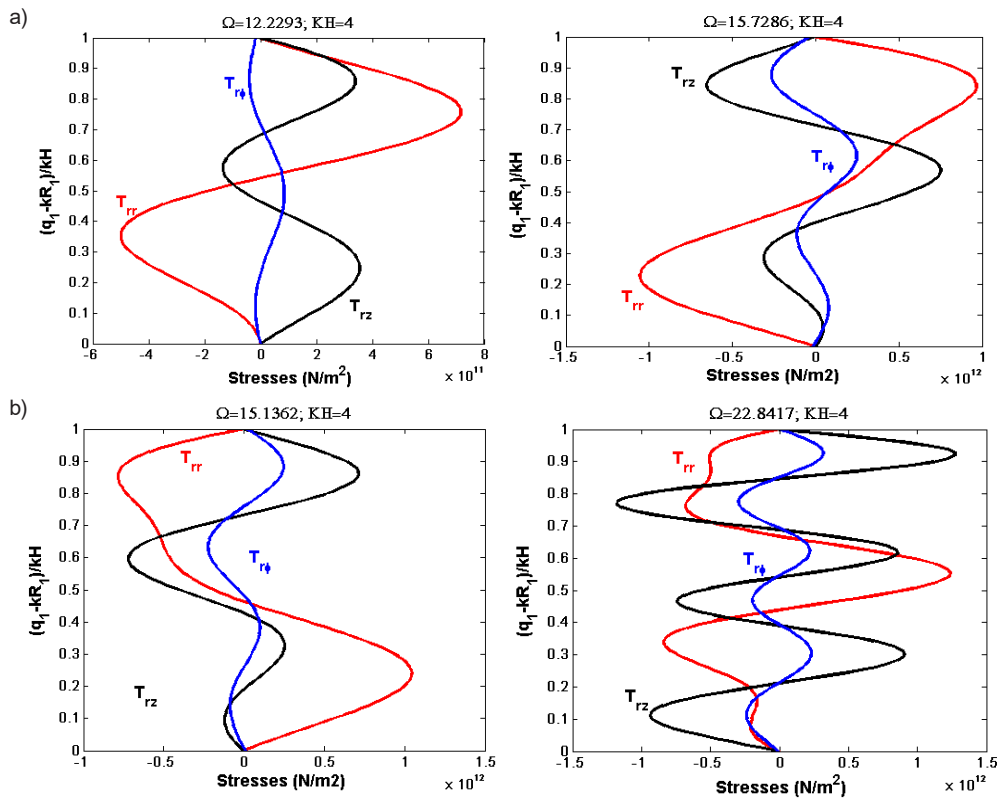$H/R = 4.00$ for (SN/SS/SN): (a) $S = 1$, (b) $S = 4$



Fig. 12. Normal stress profiles in case of flexural modes ($n = 0$), $H/R = 4.00$: (a) $S = 1$, (b) $S = 4$
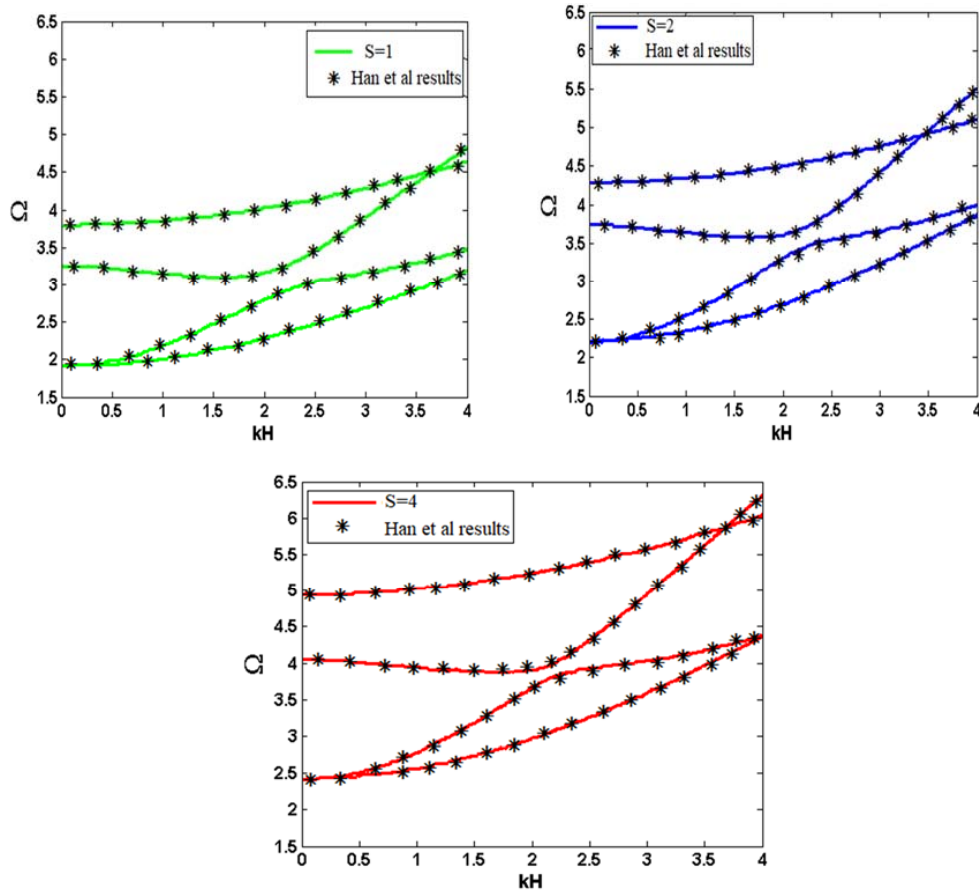
Fig. 13. Comparison for the normalized frequency using the results obtained by Han et al. (2022)
and the results obtained by the polynomial method at $n = 0$ and $R = 20H$

electrical and mechanical boundary conditions. The comparisons with the results published in literature showed that the Legendre polynomial approach can model the propagation of acoustic waves in a three-dimensional FGM cylinder. The results reveal that the current approach is extremely accurate when compared to other available reference data. All acoustic eigenmodes, regardless of their kind, can be precisely identified due to the fast convergence of the presented method.

**Appendix**

The elements required to calculate the eigenvalues and eigenvectors:

$$
{}^l A_{11}^{m,j} = \frac{1}{(kH)^l} \left\{ \begin{bmatrix} C_{11}^{(l)\,l+2} I_{m,j}^3 + (1+l) C_{11}^{(l)\,l+1} I_{m,j}^2 + \\ + (l C_{12}^{(l)} - C_{22}^{(l)} - n^2 C_{66}^{(l)})\,{}^l I_{m,j}^1 - C_{55}^{(l)\,l+2} I_{m,j}^1 \end{bmatrix} \pi(ka,kb) + \\ + \left( C_{12}^{(l)\,l+1} K_{m,j}^1 + C_{11}^{(l)\,l+2} K_{m,j}^2 \right) (\delta(q_1 = ka) - \delta(q_1 = kb)) \right\};
$$

$$
{}^l A_{12}^{m,j} = \frac{1}{(kH)^l} \left\{ \begin{bmatrix} -in(C_{12}^{(l)} + C_{66}^{(l)})^{l+1} I_{m,j}^2 + \\ + in(l C_{22}^{(l)} - C_{66}^{(l)} - C_{12}^{(l)})\,{}^l I_{m,j}^1 \end{bmatrix} \times \pi(ka,kb) + in C_{12}^{(l)\,l+1} K_{m,j}^1 (\delta(q_1 = ka) - \delta(q_1 = kb)) \right\};
$$

$$
{}^l A_{13}^{m,j} = \frac{1}{(kH)^l} \left\{ \begin{bmatrix} -i(C_{13}^{(l)} + C_{55}^{(l)})^{l+2} I_{m,j}^2 - \\ - i((1+l) C_{13}^{(l)} - C_{23}^{(l)})^{l+1} I_{m,j}^1 \end{bmatrix} \pi(ka,kb) - i C_{13}^{(l)\,l+2} K_{m,j}^2 (\delta(q_1 = ka) - \delta(q_1 = kb)) \right\};
$$

$$
{}^l A_{21}^{m,j} = \frac{1}{(kH)^l} \left\{ \begin{bmatrix} in(C_{12}^{(l)} + C_{66}^{(l)})^{l+1} I_{m,j}^2 + \\ + in(C_{22}^{(l)} + (1+l) C_{66}^{(l)})\,{}^l I_{m,j}^1 \end{bmatrix} \times \pi(ka,kb) + C_{66}^{(l)\,l+1} K_{m,j}^1 (\delta(q_1 = ka) - \delta(q_1 = kb)) \right\};
$$

$$
{}^l A_{22}^{m,j} = \frac{1}{(kH)^l} \left\{ \begin{bmatrix} -(n^2 C_{22}^{(l)} + (1+l) C_{66}^{(l)})\,{}^l I_{m,j}^1 + \\ C_{66}^{(l)\,l+2} I_{m,j}^3 + (1+l) C_{66}^{(l)\,l+1} I_{m,j}^2 - C_{44}^{(l)\,l+2} I_{m,j}^1 \end{bmatrix} \pi(ka,kb) + \\ + C_{66}^{(l)} \left( {}^l K_{m,j}^2 - {}^{l+1} K_{m,j}^1 \right) (\delta(q_1 = ka) - \delta(q_1 = kb)) \right\};
$$

$$
{}^l A_{23}^{m,j} = \frac{1}{(kH)^l} n(C_{23}^{(l)} + C_{44}^{(l)})^{l+1} I_{m,j}^1 \pi(ka,kb);
$$

$$
{}^l A_{31}^{m,j} = \frac{1}{(kH)^l} \left\{ \begin{bmatrix} -i(C_{13}^{(l)} + C_{55}^{(l)})^{l+2} I_{m,j}^2 - i(C_{23}^{(l)} + \\ + (1+l) C_{55}^{(l)})^{l+1} I_{m,j}^1 \end{bmatrix} \pi(ka,kb) - i^{l+2} K_{m,j}^1 (\delta(q_1 = ka) - \delta(q_1 = kb)) \right\};
$$

$$
{}^l A_{32}^{m,j} = \frac{1}{(kH)^l} n(C_{23}^{(l)} + C_{44}^{(l)})^{l+1} I_{m,j}^1 \pi(ka,kb);
$$

$$
{}^l A_{33}^{m,j} = \frac{1}{(kH)^l} \left\{ \begin{bmatrix} C_{55}^{(l)\,,l+2} I_{m,j}^2 - n^2 C_{44}^{(l)\,l} I_{m,j}^1 - \\ - C_{33}^{(l)\,l+2} I_{m,j}^1 + (1+l) C_{55}^{(l)\,l+1} I_{m,j}^2 \end{bmatrix} \pi(ka,kb) + C_{55}^{(l)\,l+2} K_{m,j}^2 (\delta(q_1 = ka) - \delta(q_1 = kb)) \right\};
$$

$$
{}^l M_m^j = -\frac{\rho^{(l)}}{(kH)^l} \pi(ka,kb),
$$

where:

$$
{}^l I_{m,j}^1 = \int_{kR_1}^{kR_2} Q_j^* q_1^l Q_m(q_1) dq_1 = \left\langle Q_j \middle| q_1^l \middle| Q_m \right\rangle;
$$

$$
{}^l I_{m,j}^2 = \int_{kR_1}^{kR_2} Q_j^* q_1^l \frac{\partial Q_m(q_1)}{\partial q_1} dq_1 = \left\langle Q_j \middle| q_1^l \frac{\partial}{\partial q_1} \middle| Q_m \right\rangle;
$$

$$
{}^l I_{m,j}^3 = \int_{kR_1}^{kR_2} Q_j^* q_1^l \frac{\partial^2 Q_m(q_1)}{\partial q_1^2} dq_1 = \left\langle Q_j \middle| q_1^l \frac{\partial^2}{\partial q_1^2} \middle| Q_m \right\rangle;
$$

$$
{}^l K_{m,j}^1 = \int_{kR_1}^{kR_2} Q_j^* q_1^l \frac{\partial \pi(ka,kb)}{\partial q_1} Q_m(q_1) dq_1 = \left\langle Q_j \middle| q_1^l \frac{\partial \pi(ka,kb)}{\partial q_1} \middle| Q_m \right\rangle;
$$

$$
{}^l K_{m,j}^2 = \int_{kR_1}^{kR_2} Q_j^* q_1^l \frac{\partial Q_m(q_1)}{\partial q_1} \frac{\partial \pi(ka,kb)}{\partial q_1} dq_1 = \left\langle Q_j \middle| q_1^l \frac{\partial \pi(ka,kb)}{\partial q_1} \frac{\partial}{\partial q_1} \middle| Q_m \right\rangle.
$$

95

References

Ashida, F., Morimoto, T., and Kuwahara, R. (2022). Adaptive control of an unsteady stress oscillation in a functionally graded multiferroic composite thin plate. *European Journal of Mechanics - A/Solids*, Vol. 95, 104643. DOI: 10.1016/j.euromechsol.2022.104643.

Bezzie, Y. M. and Woldemichael, D. E (2021). Effects of graded-index and Poisson's ratio on elastic-solutions of a pressurized functionally graded material thick-walled cylinder. *Forces in Mechanics*, Vol. 4, 100032. DOI: 10.1016/j.finmec.2021.100032.

Bian, P.-L., Qing, H., and Yu, T. (2022). A new finite element method framework for axially functionally-graded nanobeam with stress-driven two-phase nonlocal integral model. *Composite Structures*, Vol. 295, 115769. DOI: 10.1016/j.compstruct.2022.115769.

Elmaimouni, L., Lefebvre, J. E., Zhang, V., and Gryba, T. (2005). Guided waves in radially graded cylinders: a polynomial approach. *NDT & E International*, Vol. 38, Issue 5, pp. 344–353. DOI: 10.1016/j.ndteint.2004.10.004.

Ghatage, P. S., Kar, V. R., and Sudhagar, P. E. (2020). On the numerical modelling and analysis of multi-directional functionally graded composite structures: A review. *Composite Structures*, Vol. 236, 111837. DOI: 10.1016/j.compstruct.2019.111837.

Gong, S. W., Lam, K. Y., and Reddy, J. N. (1999). The elastic response of functionally graded cylindrical shells to low-velocity impact. *International Journal of Impact Engineering*, Vol. 22, Issue 4, pp. 397–417. DOI: 10.1016/S0734-743X(98)00058-X.

Han, X. and Liu, G. R. (2003). Elastic waves in a functionally graded piezoelectric cylinder. *Smart Materials and Structures*, Vol. 12, No. 6, pp. 962–971. DOI: 10.1088/0964-1726/12/6/014.

Han, X., Liu, G. R., Xi, Z. C., and Lam, K. Y (2002). Characteristics of waves in a functionally graded cylinder. *International Journal for Numerical Methods in Engineering*, Vol. 53, Issue 3, pp. 653–676. DOI: 10.1002/nme.305.

Hedayatrasa, S., Bui, T. Q, Zhang, C., and Lim, C. W (2014). Numerical modeling of wave propagation in functionally graded materials using time-domain spectral Chebyshev elements. *Journal of Computational Physics*, Vol. 258, pp. 381–404. DOI: 10.1016/j.jcp.2013.10.037.

Huang, S., Zhang, Y., Wei, Z., Wang, S., and Sun, H. (2020). *Theory and methodology of electromagnetic ultrasonic guided wave imaging*. Singapore: Springer, 289 p.

Lefebvre, J. E., Zhang, V., Gazalet, J., Gryba, T., and Sadaune, V. (2001). Acoustic wave propagation in continuous functionally graded plates: an extension of the Legendre polynomial approach. *IEEE Transactions on Ultrasonics, Ferroelectrics, and Frequency Control*, Vol. 48, Issue 5, pp. 1332–1340. DOI: 10.1109/58.949742.

Li, Z., Yu, J., Zhang, X., and Elmaimouni, L. (2022). Study on propagation characteristics of ultrasonic guided wave and detection of the defect in resin bolts. *Applied Acoustics*, Vol. 195, 108843. DOI: 10.1016/j.apacoust.2022.108843.

Liu, C., Yu, J., Zhang, B., Zhang, X., and Elmaimouni, L. (2021). Analysis of Lamb wave propagation in a functionally graded piezoelectric small-scale plate based on the modified couple stress theory. *Composite Structures*, Vol. 265, 113733. DOI: 10.1016/j.compstruct.2021.113733.

Naciri, I., Rguiti, A., Elmaimouni, L., Lefebvre, J.-E., Ratolojanahary, F. E, Yu, J. G., Belkassmi, Y., and El Moussati, A. (2019). Numerical modelling of vibration characteristics of a partially metallized micro electromechanical system resonator disc. *Acta Acustica united with Acustica*, Vol. 105, No. 6, pp. 1164–1172. DOI: 10.3813/AAA.919393.

Radman, A., Huang, X., and Xie, Y. M. (2013). Topology optimization of functionally graded cellular materials. Journal of Materials Science, Vol. 48, Issue 4, pp. 1503–1510. DOI: 10.1007/s10853-012-6905-1.

Velhinho A. and Rocha, L. A (2011). Longitudinal centrifugal casting of metal-matrix functionally graded composites: an assessment of modelling issues. *Journal of Materials Science*, Vol. 46, Issue 11, pp. 3753–3765. DOI: 10.1007/s10853-011-5289-y.

Wang, K., Cao, W., Xu, L., Yang, X., Su, Z., Zhang, X., and Chen, L. (2020). Diffuse ultrasonic wave-based structural health monitoring for railway turnouts. *Ultrasonics*, Vol. 101, 106031. DOI: 10.1016/j.ultras.2019.106031.

Wang, Q., Hu, S., Zhong, R., Bin, Q., and Shao, W. (2022). A local gradient smoothing method for solving the free vibration model of functionally graded coupled structures. *Engineering Analysis with Boundary Elements*, Vol. 140, pp. 243–261. DOI: 10.1016/j.enganabound.2022.04.015.

Wang, R. and Pan, E. (2011). Three-dimensional modeling of functionally graded multiferroic composites. *Mechanics of Advanced Materials and Structures*, Vol. 18, Issue 1, pp. 68–76. DOI: 10.1080/15376494.2010.519227.

Yang, Y. and Liu, Y. (2020). A new boundary element method for modeling wave propagation in functionally graded materials. *European Journal of Mechanics - A/Solids*, Vol. 80, 103897. DOI: 10.1016/j.euromechsol.2019.103897.

Yilmaz, C., Topal, S., Ali, H. Q., Tabrizi, I. E., Al-Nadhari, A., Suleman, A., and Yildiz, M. (2020). Non-destructive determination of the stiffness matrix of a laminated composite structure with lamb wave. *Composite Structures*, Vol. 237, 111956. DOI: 10.1016/j.compstruct.2020.111956.

Rabab Raghib, Ismail Naciri, Hassna Khalfi, Lahoucine Elmaimouni, Jiangong Yu, Abdelmajid Bybi, Mustapha Sahal — Pages 82–98

FREE VIBRATION MODELING IN A FUNCTIONALLY GRADED HOLLOW CYLINDER
USING THE LEGENDRE POLYNOMIAL APPROACH

Yu, J., Lefebvre, J. E., Guo, Y., & Elmaimouni, L. (2012). Wave propagation in the circumferential direction of general multilayered piezoelectric cylindrical plates. IEEE transactions on ultrasonics, ferroelectrics, and frequency control, 59(11), 2498-2508. DOI: 10.1109/TUFFC.2012.2482.

Yu, J., Wu, B., and He, C. (2010). Guided thermoelastic waves in functionally graded plates with two relaxation times. International Journal of Engineering Science, Vol. 48, Issue 12, pp. 1709–1720. DOI: 10.1016/j.ijengsci.2010.10.002.

Zhang, X., Li, Z., and Yu, J. (2018). The computation of complex dispersion and properties of evanescent Lamb wave in functionally graded piezoelectric-piezomagnetic plates. *Materials*, Vol. 11, Issue 7, 1186. DOI: 10.3390/ma11071186.

Zhang, B., Li, L. J., Yu, J. G., and Elmaimouni, L. (2022a). Generalized thermo-elastic waves propagating in bars with a rectangular cross-section. *Archive of Applied Mechanics*, Vol. 92, Issue 3, pp. 785–799. DOI: 10.1007/s00419-021-02072-3.

Zhang, B., Yu, J., Zhou, H., Zhang, X., and Elmaimouni, L. (2022b). Guided waves in a functionally graded 1-D hexagonal quasi-crystal plate with piezoelectric effect. *Journal of Intelligent Material Systems and Structures*, Vol. 33, Issue 13, pp. 1678–1696. DOI: 10.1177/1045389X211063952.

# МОДЕЛИРОВАНИЕ СВОБОДНЫХ КОЛЕБАНИЙ В ПОЛОМ ФУНКЦИОНАЛЬНО-ГРАДИЕНТНОМ ЦИЛИНДРЕ С ПОМОЩЬЮ МЕТОДА ПОЛИНОМОВ ЛЕЖАНДРА

Рабаб Рагиб[1]*, Исмаил Насири[1], Хассна Хальфи[1], Лахусин эльмаймуни[1], Цзяньгун Юй[2], Абдельмаджид Биби[3], Мустафа Сахал[1]

[1]Лаборатория ПЕТИ-ЭРМАМ, Университет Ибн-Зор, полидисциплинарный факультет Варзазата, BP.638, 45000 Варзазат, Марокко
[2]Факультет механики и энергетики, Политехнический университет Хэнаня, Цзяоцзо 454003, Китай
[3]Университет Мохаммеда V в Рабате, Высшая школа технологий Сале, группа по материалам, энергии и акустике (MEAT), Марокко

*E-mail: rababraghib97@gmail.com

**Аннотация**
**Введение**: Строительная отрасль испытывает все большее давление в связи с тем, что требуется максимизировать эксплуатационные характеристики при одновременном снижении затрат и уменьшении воздействия на окружающую среду. Для решения этой проблемы предлагается новый тип материалов, а именно функционально-градиентные материалы (ФГМ). Преимущество этих материалов в том, что они способны выдерживать жесткие условия эксплуатации без потери своих свойств. **Цель исследования:** данная работа направлена на дальнейшее расширение представлений о типах распространения и характеристиках направленных волн в цилиндрах из ФГМ с бесконечной длиной. В ходе исследования мы проанализировали цилиндрическую оболочку, состоящую из трех кольцевых слоев, каждый из которых разделен градиентным слоем по толщине стенки. В статье предлагается инструмент моделирования, основанный на методе ортогональных полиномов Лежандра. **Методы:** применяемый метод приводит к проблеме собственных значений / собственных векторов. Граничные условия интегрируются в определяющие уравнения распространения направленных волн. Рассчитаны кривые дисперсии фазовой скорости и нормированной частоты. Кроме того, рассчитываются и рассматриваются распределения перемещений и профили поля напряжений для функционально-градиентного цилиндра с различными градиентными показателями в обоих типах (осесимметричном и симметричном). Результаты демонстрируют постоянные колебания в эффективном ФГМ. **Результаты:** было обнаружено, что кривые фазовой скорости одного и того же типа распространения уменьшаются с увеличением экспоненты степенного закона. Кроме того, граничные условия оказывают большее влияние на нормальные напряжения. Точность и эффективность усовершенствованного метода ортогональных полиномов демонстрируется на примере сравнения точного решения, полученного численно-аналитическим способом, и наших численных результатов.

**Ключевые слова:** направленные, метод полиномов Лежандра, функционально-градиентные материалы (ФГМ), кривые дисперсии.

# VALORIZATION OF DREDGED SEDIMENTS FROM DAMS IN PAVEMENT DESIGN

Boumediene Serbah[1,2]*, Maghnia Asmahane Bourabah[2], Joanna Eid[3], Salima Bouchemella[4], Moussaab Hariche[5], Nabil Abou-Bekr[2], Said Taibi[6]

[1]University of Tiaret, Algeria
[2]University of Tlemcen, Algeria
[3]Ai Environnement FACÉA Group, R&D Department, Noisy-le-Grand, France
[4]University of Souk Ahras, Algeria
[5]University of Djelfa, Algeria
[6]University of Le Havre, France

*Corresponding author's e-mail: boumediene.serbah@univ-tiaret.dz

**Abstract**

**Introduction**: This study is part of research aimed at valorizing dredged sediments through the development of formulations for use in road engineering. The **purpose of the study** was to determine if the materials selected for pavement layers comply with road design standards, in particular, with specific requirements for density, grain size, plastic properties, organic matter, and mechanical performance. **Methods**: To determine the physical-chemical and mechanical characteristics of the dredged sediments obtained from samples taken from the Bakhadda dam located in western Algeria's semi-arid climate, the sediments were treated with binders in small amounts (3% lime (L), 6% cement (C)) for reuse in road construction. The study focused on the evolution of physical and mechanical characteristics of the treated sediments, including LL, PI, VBS, immediate bearing index (IBI%), UCS, tensile strength $\sigma_t$, as well as small strain modulus $E_{ss}$ and large strain modulus $E_{50}$. The **results** showed that adding lime and cement to the dredged sediments improved their strength, as evidenced by the increased compressive strength (UCS) over time for the samples containing different amounts of binders (3%L, 6%C, and 3%L + 6%C). Additionally, the effect of the water content on the mechanical properties of the formulations was demonstrated. The study showed that the strength increased when the water content decreased.

**Keywords:** valorization, dredged sediments, compaction, modulus of elasticity, UCS, tensile strength, eco-geo-material, road construction.

## Introduction

The dredged sediments from western Algeria provide a new source of materials for pavement layers. This study aims to investigate the feasibility of using raw dredged sediments as a road construction material and improving their mechanical properties. One of the methods used is to amend them with binders such as lime and cement (Hussan et al., 2022; Tribout et al., 2011; Wang et al., 2013). Large quantities of dredged sediments pose a significant challenge for their valorization in road engineering. However, these sediments from dams are ecologically sustainable and recyclable materials. The Bakhadda sediments are also advantageous because they are uncontaminated, allowing for direct reuse without any decontamination treatment. Nevertheless, the weak geotechnical properties of dredged sediments often hinder their use in road techniques due to their low resistance and durability (Larouci et al., 2021; Wang et al., 2013; Zentar et al., 2021). Therefore, we will explore potential solutions to enhance their properties and increase their potential use in road construction.

In order to overcome these limitations, it is essential to understand the criteria required for road construction materials (Association Française de Normalisation, 1992a; LCPC, SETRA, 1992, 2000) such as:

- Controlling particle size is crucial as it can affect the physical and mechanical properties of pavement layers.

- Compressive strength (UCS > 1 MPa) is an important parameter in determining the material capacity to support the circulation of construction machinery on the treated layer (Association Française de Normalisation, 1992a, 2003b; Qureshi et al., 2021; Wang et al., 2013; Zentar et al., 2021). As per the NF P11-300 standard, the recommended minimum and maximum compressive strength (UCS) is 2 to 4 MPa to ensure the bearing capacity of vehicles and 8 MPa for re-excavation of the base coat, subgrade, and sub-base layer.

- Indirect tensile strength and $E_{ss}$ modulus shall also be verified since the ($\sigma_t$, E) pair at 28, 90, and 360 days should show a minimum of mechanical material class 5. Tensile strength is a significant mechanical parameter that controls the development of tensile cracking (Gajewska et al., 2017; Jamsawang et al., 2021; LCPC, SETRA, 2000; Zentar et al., 2021).

• The minimum recommended values of Immediate bearing capacity IBI vary from layer to layer (Association Française de Normalisation, 1997, 2012; Banoune et al., 2016), which also determines the material capacity to support the weight of construction machinery on the treated layer. The CBR test is both simple and cost-effective, offering advantages that vary depending on such factors as the road class and material placement within the pavement structure (Association Française de Normalisation, 2012; Banoune et al., 2016; Hamouche and Zentar, 2018).

• The ability of treatment depends on volume swelling (LS(%) ≤ 5) and mechanical performance represented by the Brazilian tensile strength $\sigma_t$ ≥ 0.2 MPa (Association Française de Normalisation, 2015).

To achieve the target strength, dredged sediments shall be treated with a specific ratio of cement or lime. Various studies (Jamsawang et al., 2021; Tribout et al., 2011; Zentar et al., 2021) showed that cement and lime are the binders most frequently utilized in laboratory experiments aimed at reinforcing dredged sediments. Macroscopic changes in clayey soil are caused by the addition of binders at the microscopic scale, which involves interactions at that level (Eid, 2017; Jamsawang et al., 2021). The strength of sediments and hardened stabilized layer is reliant on the cement and water content. When cement is added, the formation of calcic hydrates (Banoune et al., 2016; Baston et al. 2012; Jamsawang et al., 2021; Zentar et al., 2021) can enhance the soil strength. Hussan et al. (2022), found that the increase in the unconfined compressive strength (UCS) of the soil was noted at 7, 14, and 28 days, with an increase of 10 to 15% per day following the replacement of 3% and 5% of ordinary Portland cement (OPC) with lime. the results showed that sediments treated with traditional hydraulic binders did not achieve the required UCS values for use in road layers. However, the development of a geopolymer using alkali-activated GGBS and the incorporation of 30% sediments yielded a UCS value above 2 MPa at 28, 60, 90, and 180 days. Furthermore, the addition of 5% lime and 3% granular calcium carbonate in the same mixture (geopolymer + 30% sediments) increased the UCS by up to 60% and 90%, respectively. Gajewska et al. (2017) showed that the compressive strength UCS of the tested cement-soils ranged from 0.74 to 9.19 MPa, but most of the UCS results were within the 0.74–4.00 MPa range.

In studies by Wang et al. (2012, 2013), the effects of cement and lime on Dunkirk sediments were evaluated using modified Proctor compaction and UCS tests. The researchers classified the sediments as sandy soil and concluded that 6% cement is a cost-effective and practical amount for enhancing the mechanical properties of the sediments, particularly

for use in road construction. This finding is consistent with the recommendations from the French guide on the treatment of soils with lime and/or hydraulic binders and application to the construction of pavement base layers (LCPC, SETRA, 2000). This guide divides lime stabilization into two phases: short-term reactions, which include cation exchange (studied by Baston et al. (2012), Eades and Grim (1966), Khattab et al. (2007), and Townsend (1979)), and flocculation and agglomeration. Khattab et al. (2007) also investigated the second phase, i.e., long-term pozzolanic reactions and carbonation. The fundamental parameters for designing road layers are tensile strength $\sigma_t$ and modulus E (Tribout et al., 2011; Zentar et al., 2021). Most researchers (Gajewska et al., 2017; Tribout et al., 2011; Zentar et al., 2021) observed a sharp increase in $\sigma_t$ from the beginning of the treatment, making it possible to achieve a better mechanical class, and a slow increase in modulus (E) preventing a decline in mechanical class. Gajewska et al. (2017) also found that the elastic modulus increased by 2.5 times when the cement content increased from 6 to 8%. According to Venkatarama and Gupta (2005) as well as Gajewska et al. (2017), the relationship between $\sigma_t$ and E is primarily influenced by the type and quantity of the binder used as well as the grain size distribution in the material. Interestingly, the universal correlation E = f(R) can be applied to various cement-stabilized soils regardless of their grain size.

Many Maghreb researchers (Banoune et al., 2016; Larouci et al. 2021; Loudini et al., 2020) showed the possibility of using these dredged sediments in road construction materials, which allows for better use of this natural resource. The study by Achour et al. (2014) focused on the use of fine dredged sediments in road construction. The tests showed that the chemical properties of the sediments are acceptable for use in road construction, but their bearing capacity is insufficient. To improve the mechanical properties, a mix of 1/3 fine sediments, and 2/3 dredged sand with 6% cement and 1% lime was proposed. The tests showed that the mixture meets the mechanical requirements for use in the road , subgrade and sub-base layer.

This paper discusses the technique of using dredged sediments from dams for road construction, which has several advantages such as reducing waste and cost. However, it is important to conduct specific studies for each case as sediment composition can vary depending on the dam's location and nature. The example of the Bakhadda dam is mentioned as a particular case where feasibility studies should be conducted. In our research, we examined the effect of binders on the mechanical strength parameters of the treated sediments, which will enable us to characterize the behavior of the treated sediments

in the short and long term. This will also allow us to determine their appropriate age for machinery to circulate on the treated layer and the frost resistance. In this paper, we study the possibility of valorization in pavement design with regard to the sediments dredged from a dam in western Algeria. The originality of the study is related to the fineness and high plasticity of the sediments, which requires double treatment with hydraulic binders to meet the updated recommendations and standards for pavement design.

### Material and Methods

The materials consist of a deposit of fine particles. Raw dredged sediments (RDS) were taken from the area on the upstream side (settling basin of the Bakhadda dam in north-west of Algeria), where the dredged sediments are found accumulated in remarkable quantities. The dam is located near the village of Machraa Sfa, 25 km west of Tiaret, on the upper reaches of the Mina river, a tributary of the Oued Chéliff river. This basin receives annually $38 \times 10^6$ m$^3$ of water with a specific degradation of 860 t·km$^{-2}$·year$^{-1}$ (Hallouz et al., 2018).

Due to the siltation rate of approximately 30% of its total capacity, a dredging operation was assigned to Hydrodragage-C-T-Systems, a company specializing in dredging, with a goal of removing 20 million m$^3$ of material (Fig. 1) (hydrodragage-c.t.systems, 2005). A number of identification tests were carried out on the collected sediments, making it possible to classify the sediments according to French standard NF P11-300 (Association Française de Normalisation, 1992a) and GTR 92 (LCPC, SETRA, 1992).

The RDS samples were oven-dried at 50°C for 48 hours prior to testing, with the aim of preventing any damage to the soil structure and organic matter that could potentially impact the accuracy of the test results. Then they were crushed and sieved through 5 mm sieves without any additional treatment. The set of samples was then evaluated for geotechnical properties, including specific gravity, water content, particle-size distribution, Atterberg limits, methylene blue absorption (VBS), organic matter content, calcium carbonate content (CaCO$_3$), and pH, as well as compaction properties with the immediate bearing index (IBI). These geotechnical properties allowed for the classification of the material in its natural state.

### Grain-size analysis

The particle size distribution of the RDS was analyzed by wet sieving in accordance with French standard XP-P94-041 (Association Française de Normalisation, 1995). This analysis separated the particles with dimensions greater than 80 µm by sieving, and then the fraction less than 80 µm — by sedimentation test, according to French standard NF P94-057 (Association Française de Normalisation, 1992b). Fig. 2 presents the particle size curves of the RDS, which show that the material is fine particles in almost all its composition, with nearly 32% of clay and 60% of silt, while the presence of sandy particles greater than 63 µm is the least significant (% sand ≤ 8%).

The calculation of the coefficients of uniformity (Cu = $D_{60}/D_{10}$) and curvature (C$_c$ = $d^2_{30}/(d_{10} \cdot d_{60})$) indicates that the RDS are well-graded (Cu = 16).

### Atterberg limits tests

The Atterberg limits tests of the RDS were carried out in accordance with French standard NF P94-051 (Association Française de Normalisation, 1993a). The RDS sediments exhibited a high liquidity limit of 55% and a plasticity limit of 33%, resulting in a plasticity index of 22. When plotted on the Casagrande plasticity chart (Fig. 3), the material was found to be located below the line A of equation PI = 0.73(LL − 20). This position falls outside the recommended range in terms of road engineering



Fig. 1. View of the reservoir of the Bakhadda dam and the Djebel Debbagh stationary dredger

due to a high plasticity index of PI > 20, indicating highly plastic silt.

### Other parameters

*Methylene blue test*

The methylene blue absorption (VBS) and the specific surface area (SSA) were investigated on the RDS samples according to French standard NF P94-068 (Association Française de Normalisation, 1993c). The test results indicate that the VBS and SSA are significantly high, with values of approximately 2.4 (g/100g, dry) and 50.4 ($m^2$/g), respectively. According to the Unified Soil Classification System (USCS), the RDS could be classified as silt of high plasticity, implying potential sensitivity of the tested soil to water invasion. Thus, the results suggest that the VBS is enough for accurate swelling potential estimates (Çokça, 1993; Seed et al., 1962; Yukselen and Kaya, 2008).

*Organic matter content (OM%)*

The OM content was estimated by two methods, the calcination method (CMOC) and the chemical method, according to French standards XP-P94-047 (Association Française de Normalisation, 1998), NF-EN-12879 (Association Française de Normalisation, 2000) and NF P94-055 (Association Française de Normalisation, 1993b). The sediments have organic content values ranging from 0.5 to 2.6%. Moreover, these are slightly below the maximum limit of 3% recommended by French standards NF P11-300 (Association Française de Normalisation, 1992a) and GTR 92 (LCPC, SETRA, 1992) for using them in pavement design. According to these standards, the F11 subclass refers to weak organic materials with an organic content ranging from 0.5 to 3%.

*Calcium carbonate content (CaCO$_3$%)*

The volumetric calcimeter method in accordance with French standard NF P94-048 (Association Française de Normalisation, 1996) was used to determine the percent calcium carbonate (CaCO$_3$%) content of the RDS sample. The results showed that the calcium carbonate level in the sediments is 18%, indicating the presence of a small amount of limestone (10% < CaCO$_3$% < 30%). The presence of calcium carbonate in the sediments creates hard points within the material, leading to a significant reduction in swelling, as noted in previous studies (Molnár et al., 2021).

*Specific density ($\gamma_s$)*

The specific density of the RDS determined using a pycnometer according to French-standard NF-P94-054 (Association Française de Normalisation, 1991) is 2.66 g/cm³.

*Material acidity determination (pH meter test)*

The acidity of the material was determined using the pH meter test according to NF EN ISO 10390:2022 (NF EN, 2022). The suspensions of the sediments showed an average pH value of 8.4, indicating that the sediments from Bakhadda dam exhibits an alkaline nature. Table 1 presents the geotechnical characteristics of the RDS, which initially fall under class F according to LPC-USCS, GTR 92 (LCPC, SETRA, 1992), and French standard NF P11-300 (Association Française de Normalisation, 1992a) classifications for natural materials with an organic matter content less than 3% (OM = 2.6%). The sediments contain a dominant fine fraction less than 63 µm (silt and clay), which accounts for almost 90% of the material. The sediments have a poorly-graded particle size distribution with a low density due to the lack of sand particles. The coefficient of uniformity Cu is 16, and the coefficient of curvature C$_c$ is 0.81, indicating well-graded and poorly-graded fine sediments. The particle size analysis, methylene blue value (VBS), and Atterberg limits (PI) indicate
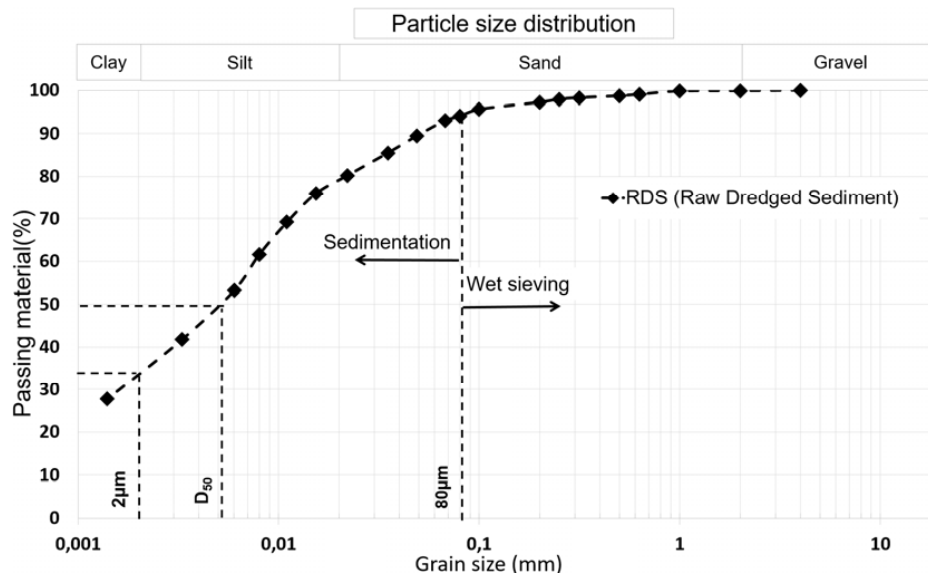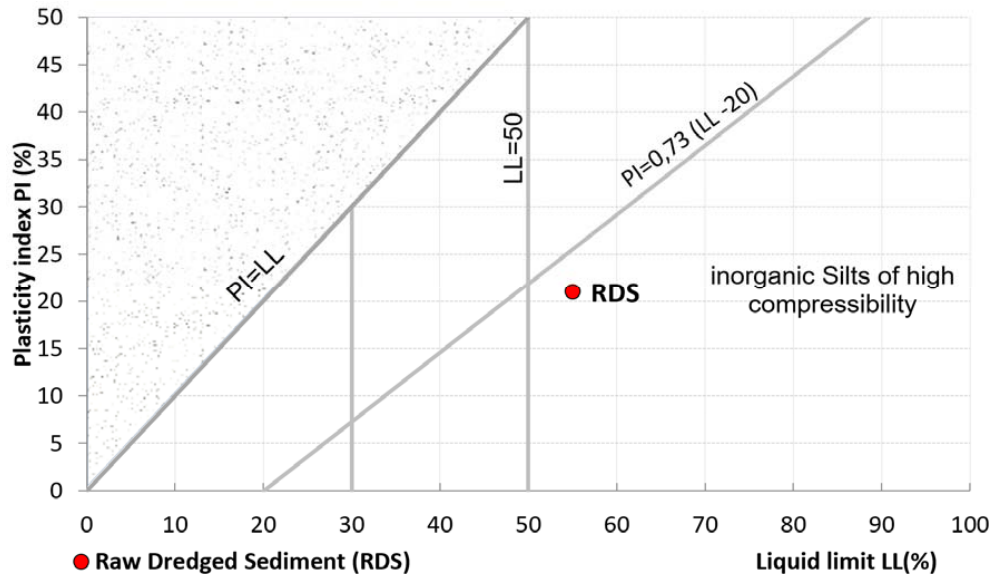


Fig. 2. Particle size distribution of the RDS

Fig. 3. Position of the RDS on the Casagrande plasticity chart

Table 1. **Characterization parameters of the Bakhadda dam RDS**

| Bakhadda dam sediment | Sand (%) | | Silt (%) | | Clay (%) | | Cu | | $C_c$ |
|---|---|---|---|---|---|---|---|---|---|
| Particle size distribution | 8 | | 60 | | 32 | | 16 | | 0.81 |
| characterization parameter | Atterberg limits | | | | | | | | |
| | LL (%) | PL (%) | IP (%) | Wn (%) | IL (%) | Ic (%) | Ac | | γs (kN/m3) |
| | 55 | 33 | 22 | 20 | −1.1 | 1.14 | 0.69 | | 26.57 |
| | VBS | | S.S.T (m²/g) | | CaCO₃ (%) | | OM (%) | | pH |
| | 2.4 | | 50.4 | | 18 | | 0 – 2.6 | | 8.4 |

that the material falls under class A2 (silty, clayey) as per the classification guide for fine soils (French-standard NF P11-300 (Association Française de Normalisation, 1992a), GTR 92 (LCPC, SETRA, 1992)).

### Compaction tests

The modified Proctor compaction test was performed on the RDS in accordance with French standard NF P94-093 (Association Française de Normalisation, 1993d) to determine the optimal water content and maximum dry density. The immediate bearing index ($IBI_{MPO}$) of the samples compacted in the CBR Mold was evaluated in accordance with French standards NF P94-078 (Association Française de Normalisation, 1997) and NF EN-13286-47 (Association Française de Normalisation, 2012).

Figs. 4, 5 show the modified compaction and IBI curves, respectively. It can be noted that the clear appearance of the peak on the compaction-bearing curve of the RDS indicates sensitivity to the water content. The $IBI_{MPO}$ at modified compaction is low, approximately 16%, indicating a low bearing capacity of the RDS, which cannot ensure the trafficability of compaction machinery on the site. In terms of the IBI, the value remained below the minimum value required for use as an alternative road material (the IBI greater

than 20%). According to GTR 92 (LCPC, SETRA, 1992) and GTS 2000 (LCPC, SETRA, 2000), the sub-base layer and base layer of pavement should have a minimum value of 35 and 45%, respectively.

### Results and Discussion

The RDS has high plasticity and swelling potential due to its fineness and was classified as Lt (MH), a highly plastic silt. The densification and bearing capacity ($γd_{MPO}$, $W_{MPO}$, $IBI_{MPO}$) were lower than the values prescribed for use in road engineering, indicating the need for prior treatment for its use in pavement layers. The RDS in its current state is not suitable for road construction and requires treatment, particularly with binders. Various mixtures of sediments, cement, and lime in different proportions were tested to meet the recommendations of French standard NF-P11-300 (Association Française de Normalisation, 1992a), GTR 92 (LCPC, SETRA, 1992), GTS 2000 (LCPC, SETRA, 2000) and Bourabah et al. (2013).

### RDS treatment with binders
#### Treatment protocol

For this study, a CPJ CEMII/A 42.5 compound Portland cement and quicklime were chosen. It is crucial to consider the added percentage of these binders, as it provides an additional fine fraction
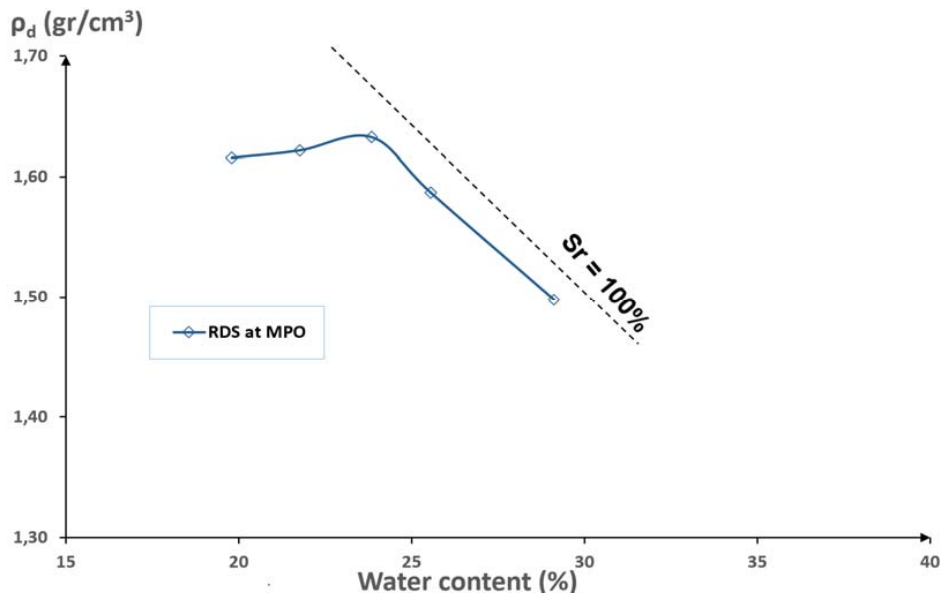
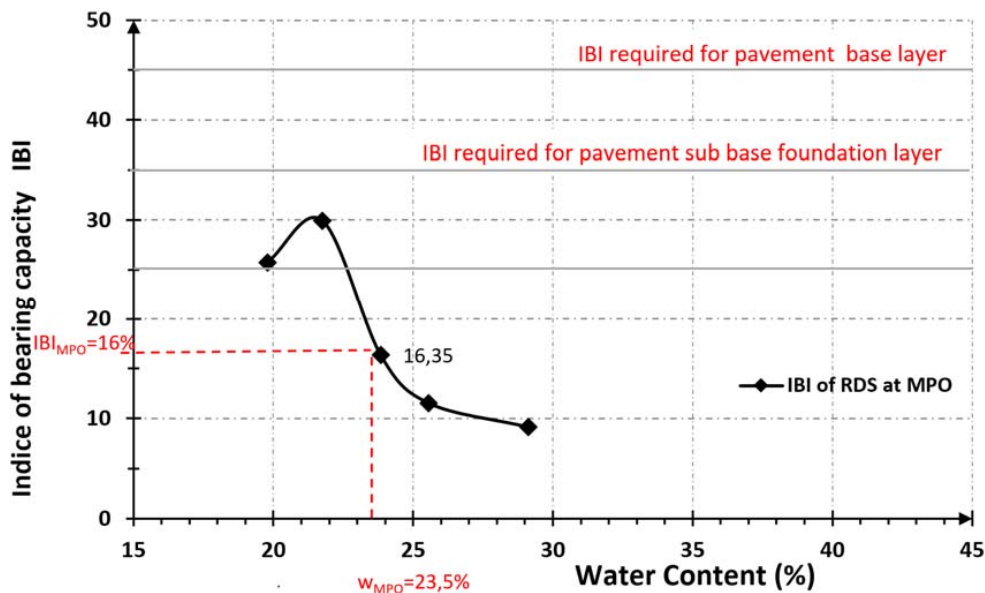Fig. 4. Compaction tests at MPO for the RDS



Fig. 5. Compaction-bearing curves (IBI) of the Bakhadda dam RDS

in the granular skeleton. Various studies were conducted on the optimum percentage of lime for different types of soils, based on pH testing (ASTM, 2006; Djelloul et al., 2017; Eades and Grim, 1966; Eid, 2017; Khattab et al., 2007; Makki-Szymkiewicz et al., 2015; Sivapullaiah et al., 2000). These studies showed that the minimum effective dosage of lime required for stabilization, called Lime fixation point (PFC), ranged from 1 to 4%. It is important to note that treating soil with a lime content equal to or greater than the PFC of the soil can ensure better homogeneity of the treatment and long-term structural resistance, regardless of the humidity conditions. Most studies (Akula et al., 2021; Baston et al. 2012; Eades and Grim 1966)

showed that the pH increases to approximately 12.45 at 25°C. The pozzolanic reaction continues with time and results in consistency changes and strength gain. In response to the release of $OH^-$, the pH of the soil increases to high alkaline pH (>10), which partially dissolves clay minerals, releasing soluble silica and alumina. C-S-H and C-A-H are strength-enhancing pozzolanic products formed by free $Ca^{2+}$ ions reacting with soluble silica and alumina (Akula et al 2021; Baston et al., 2012; Hilt and Davidson, 1960).

Khattab et al. (2007) discussed two methods proposed by Eades and Grim (1966) as well as Hilt and Davidson (1960) for determining the optimum lime percentage for FoCa soils. To activate the pozzolanic

reaction between lime and soil, a pH value of 12.4 is required for a soil-water mixture containing varying masses of lime, as suggested by Eades and Grim (1966). Adding lime to the soil increases alkalinity, which, in turn, leads to better flocculation during the pozzolanic reaction by increasing the pH value. To achieve a pH value of 12.4 or higher, 3% lime is required. The second method related to the minimum lime content ($L_m$), suggested by Hilt and Davidson (1960), involves an empirical expression given by them as the minimum lime percentage or lime fixation point in Eq. (1). The expression is as follows:

$$L_m = \frac{Clay\ content(< 2\mu m)}{35} + 1.25. \qquad (1)$$

Moreover, Khattab et al. (2007) confirmed that the treatment efficiency is excellent, sometimes reaching more than 90%, in the presence of an optimal lime percentage of 4% and optimal compaction conditions. On the one hand, it is important to note that there is a limit to the amount of cement that can be used in soil stabilization, depending on the clay content of the soil. However, GTS 2000 (LCPC, SETRA, 2000) states that adding a reasonable quantity of lime and cement (not exceeding 9%) can increase the unconfined compressive strength (UCS) of the soil and reduce volumetric shrinkage strains. Based on this analysis, the RDS was treated with 3% lime and 6% cement to improve its mechanical properties. The proposed formulations were F1 (97%RDS + 3%L), F2 (94%RDS + 6%C), and F3 (91%RDS + 6%C + 3%L) for use in road sub-base layers and/or backfills.

### RDS identification after treatment

After treatment with binders, the properties of the treated RDS (TRDS) were measured, including the soil suitability for treatment and determination of the grain size distribution curves, consistency limits, and methylene blue value for each formulation.

*Suitability for treatment based on volume swelling*

The evaluation of soil suitability for treatment is frequently carried out in accordance with French standard NF P94-100 (Association Française de Normalisation, 2015). The evaluation process includes two steps. First, the volume swelling (LS) of the soil samples immersed in water at 40°C for 7 days is determined using cylindrical specimens (ø = 5 cm, h = 5 cm), which are made with an optimal water content $W_{MPO}$ and 96% $\gamma d_{(MPO)}$ dry density by static compaction according to French standard NF P98-230-2 (Association Française de Normalisation, 1993e). The demolding of each specimen is carried out immediately after its making. Table 2 shows the results of volume swelling ($L_S$) and splitting tensile strength $\sigma_t$ (in immersion) for the formulations studied. The average value of three test specimens is taken. This value is calculated using the Eq. (2), which measures the variation in volumes $V_1$, $V_2$, and $V_0$:

$$L_S(\%) = \frac{(V_1 - V_2) - V_0}{V_0} \times 100. \qquad (2)$$

Volume $V_0$ is the initial volume of the specimen. Volumes $V_1$ and $V_2$ are measured by performing hydrostatic weighing of the test specimens both in open air and under water, while taking into account the Flexible Plastic Mesh + elastic bands. Then tensile strength $\sigma_t$ is measured through a Brazilian splitting test (BST), which involves curing the soil samples (ø = 5 cm, h = 5 cm) in water at 40°C until the 7-day crushing deadline is met. It is important to note that each recorded result is an average of three separate samples.

Table 2 shows the results of volume swelling ($L_S$) and resistance $\sigma_t$ (in immersion) for the treated sediments, based on the type of binder used. The formulations of the raw sediments treated with binders are found to be suitable for treatment, as they meet the relevant criteria (i.e., low volume swelling ($L_S$) of 5% and good development of resistance $\sigma_t > 0.25$ MPa) and can be used for the remainder of the study. Furthermore, the frost resistance is deemed satisfactory, since resistance $\sigma_t$ at the age corresponding to the first statistical appearance of freeze is greater than 0.25 MPa, as per GTS 200 (LCPC, SETRA, 2000).

*Granulometry*

The particle size distribution of the treated materials is presented in Fig. 6. It can be observed that the sediments mainly consist of the silt fraction. The particle size distribution of the sediments treated with binders shows a slightly improved granularity, compared to the curve of the raw sediments without treatment. Additionally, the values of the uniformity coefficient Cu exceed the reference value of 4, satisfying the spread particle size of the mixtures.

On the other hand, the recommended values for the curvature coefficients of the sediments treated with binders are verified according to their uniformity coefficients (Cu = 11 for cement, Cu = 10 for combined lime-cement, and Cu = 5.5 > 4 for lime), $C_c = 1.61 > 1$ and $C_c = 1.41 > 1$ for cement and combined lime cement, respectively (Table 3). They indicate that the materials generally have a well-graded character.

*Effect of treatment on the Atterberg limits*

Fig. 7 illustrates the effect of binder addition on the Atterberg limits of TRDS, revealing the following findings: adding binders significantly decreases plasticity, indicating particle flocculation.

Lime, once added to the RDS, acts on the electric charges through cation exchange, where calcium ($Ca^{++}$) cations from the lime replace exchangeable cations, such as sodium ($Na^+$), hydrogen ($H^+$), potassium ($K^+$), etc., on the soil's exchange sites. This alteration of inter-particle electric fields leads to particle flocculation and agglomeration (Cabalar et al., 2014; Townsend,

Table 2. **Results of volume swelling (L$_s$) and splitting tensile strength б$_t$ (in immersion) for the formulations studied**

| No. | Formulations studied | Volumetric swelling L$_s$ (%) | Tensile strength б$_t$ | Suitable for treatment |
|-----|----------------------|-------------------------------|------------------------|------------------------|
| 1 | 97%RDS + 3%L | 2.74 | 0.26 | adapted |
| 2 | 94%RDS + 6%C | 3.38 | 0.275 | adapted |
| 3 | 91%RDS + 6%C + 3%L | 1.66 | 0.29 | adapted |
| 4 | 100% RDS | 8.23 | 0.14 | Unsuitable |
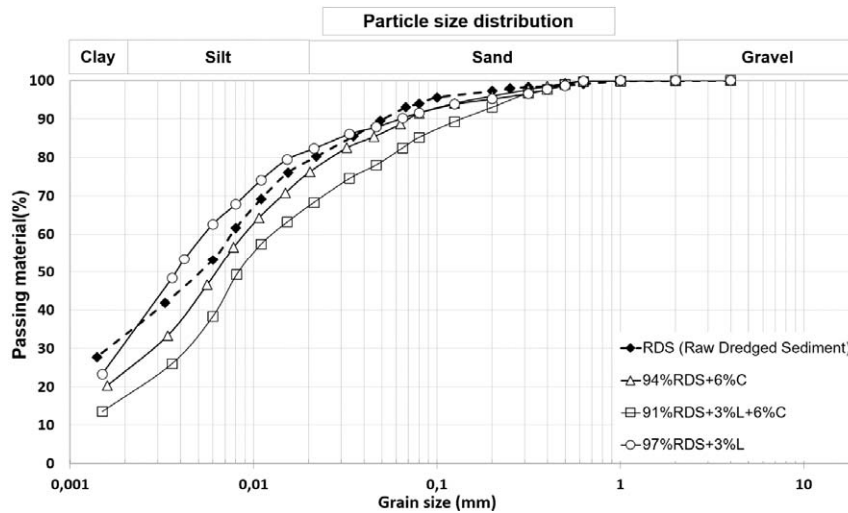


Fig. 6. Particle size distribution of the RDS and RDS treated with lime and cement

Table 3. **Influence of the addition of binder on the treated RDS**

| No. | Formulations studied | % > 63 µm | | % < 63 µm | | Cu | C$_c$ |
|-----|----------------------|-----------|---|-----------|---|----|----|
| | | Coarse sand (%) | Fine sand (%) | Silt (%) | Clay (%) | | |
| 1 | 97%RDS + 3%L | 4 | 15 | 54 | 27 | 5.5 | 0.73 |
| 2 | 94%RDS + 6%C | 3 | 21 | 60 | 16 | 11 | 1.61 |
| 3 | 91%RDS + 6%C + 3%L | 7 | 26 | 57 | 10 | 10 | 1.41 |
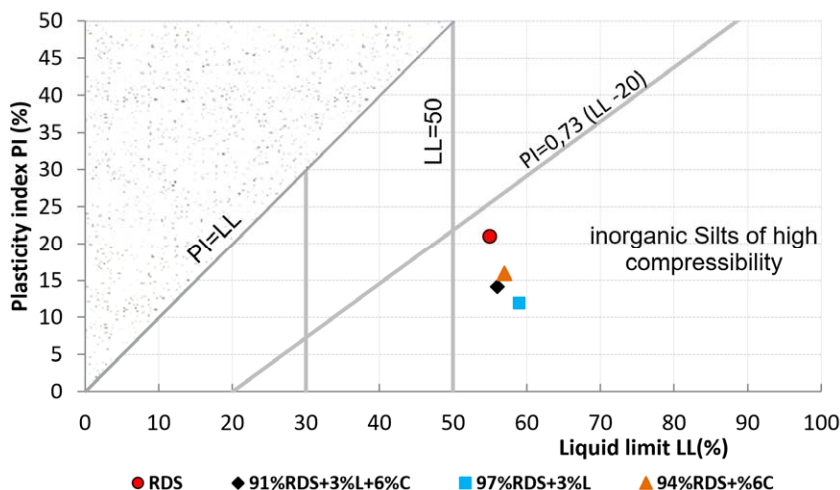


Fig. 7. Atterberg limits of the RDS and RDS with lime and cement

1979). This flocculation results in an increase in the soil plastic limit without significantly affecting its liquid limit, leading to a reduction in the plasticity index (PI). This confirms that the sediment plasticity is significantly reduced by the binder treatment. As a result, the concurrent reduction of the water content and plasticity index radically modifies the material behavior.

*Classification according to GTR 92, NF P11-300 / LPC-USCS*

Fig. 8 shows the treated material positioned in class A1 as loamy sand. The addition of binders such as 3% lime and 6% cement to the sediments reduced their plasticity, which positively influenced the flocculation of the particles.

Additionally, the identification test results showed a good reduction in the plasticity degree with a notable decrease in the plasticity index (PI = 11.89%) and the percentage of swelling-shrinkage. The plasticity index was significantly reduced, making it suitable for use as a road layer.

### Characterization of the TRDS mechanical properties

*Compaction after treatment*

Fig. 9 shows the modified Proctor optimum for the TRDS curves, while Table 4 summarizes the results of the optimum parameters ($w_{MPO}$, $\gamma_{dmax}$) and bearing tests ($IBI_{MPO}$) of the TRDS. The compaction-bearing tests showed that the modified Proctor curve of the RDS exhibited a peak shape, indicating the sensitivity to the water content enhancement.

The addition of binders (lime and cement) resulted in an increase in the optimum water content at MPO and a significant reduction in the maximum dry density. If the curing time is not allowed in the compaction test, the densification may be negatively influenced, but the immediate bearing index can be greatly improved.

It should be noted that Fleureau et al. (2002), presented the correlations between the optimal water content and maximum dry unit weight of soils compacted under modified Proctor conditions (MPO), as well as their liquid limit LL in %. The regression equations (3, 4) for these correlations are as follows:

$$W_{MPO}(\%) = 4.55 + 0.32LL - 0.0013LL^2; \qquad (3)$$

$$\gamma_{d\max}(kN/m^3) = 20.56 - 0.086LL + 0.00037LL^2. \quad (4)$$

The compactness and bearing parameters obtained at modified Proctor optimum (MPO) for the RDS are compared with those given by the correlations in Table 4. Consistency is observed between the values, despite a notable difference in the water content of approximately 6% for MPO. Good agreement is shown for the maximum dry density. Besides, the results for the treated materials in Table 4 show that the water content values for cement-treated and lime-treated sediments are approximately 4.5 and 6%, respectively, greater than the values given by the correlation.

As shown in Table 4, the maximum dry unit weight of the treated sediments $\gamma_{dmax}$ was approximately 0.7 to 1.2 kN/m³ less than the correlated values.

Concerning the IBI, adding of 6%C and 3%L to the RDS resulted in a reduction in the plasticity index, leading to an increase in the IBI (16% for RDS to 30.75%; 33.15%; 35.25% for RDS+3%L; RDS + 6%C; RDS + 3%L + %6C, respectively) (Fig. 10). These results confirm the feasibility of the beneficial reuse of treated dredged sediments in road layers.

*UCS tests on the treated RDS*

The unconfined compressive strength (UCS) test was performed according to French standard NF EN 13286-41 (Association Française de Normalisation, 2003a). The UCS was measured on the samples compacted at MPO. The samples 50 mm in diameter and 100 mm in height were compacted in a mold equipped with two pistons, upper and lower ones, to ensure homogeneous compaction. The unconfined compressive strength tests were carried out until failure. To assess reproducibility, three samples were tested for each state. Using the stress-strain curve, two parameters were derived: the secant modulus E and the unconfined compressive strength.

The secant modulus decreases with the axial strain E(ε), and the mean secant modulus $E_{50}$ (Daheur et al. 2023; Taibi et al., 2009) is defined at a strain level $\varepsilon_{50}$ corresponding to 50% of the maximum strength (Fig. 11). The results of the UCS measurements of the RDS and RDS treated with binders (lime, cement) are presented in Fig. 12. The curves show good reproducibility, but low stiffness is observed for the RDS. Three formulations of the treated sediments met the French criteria (UCS ≥ 1 MPa) according to GTS 2000 (LCPC, SETRA, 2000) to authorize the circulation of machinery on the treated layer, and the mechanical strength increased with the binder content.

The strength increased from 0.69 MPa for the RDS to 2.64, 3.72, and 3.84 MPa for 3% lime and 6% cement and their combination (3%L + 6%C), respectively. At a curing time of 90 days, the mechanical strength stabilized at 3.20, 4.13, and 4.06 MPa (Table 5).

The influence of 3% lime addition was initially weak but increased in the long term. In comparison of the treated RDS with the untreated RDS, the stiffness of the treated material and the elasticity modulus increased. Overall, the study demonstrated the feasibility of the beneficial reuse of treated dredged sediments in road layers. The values of the compressive strength of the treated materials increased with increasing curing time, as expected. The use of binders had a significant influence on the durability of this treated material, particularly on strength and modulus of elasticity. Finer particle size sediments were found to be more reactive with pozzolanic binder (lime and cement), producing higher strength in terms of mechanical properties. Overall, the study provides insights into the mechanical performance of treated sediments, with specific recommendations for their use in road construction based on their classification and performance values.
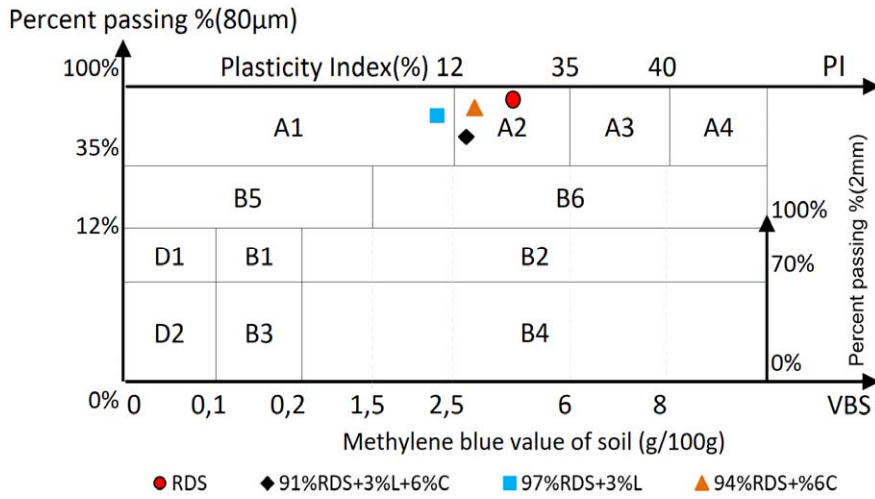
Fig. 8. Classification of the RDS according to the soil classification table of the NF P11-300 standard (Association Française de Normalisation, 1992a) (fraction 0/50 mm)
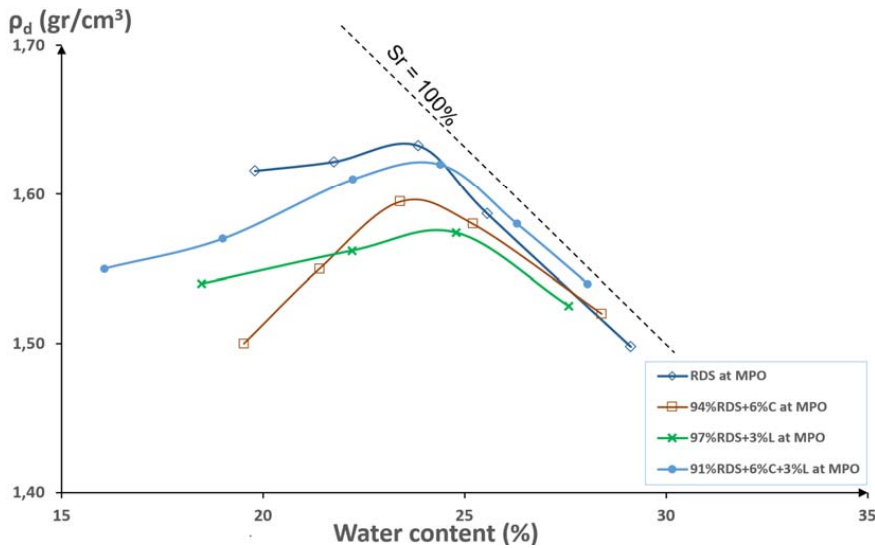


Fig. 9. Compaction tests of: RDS, RDS + 3%L, RDS + 6%C,
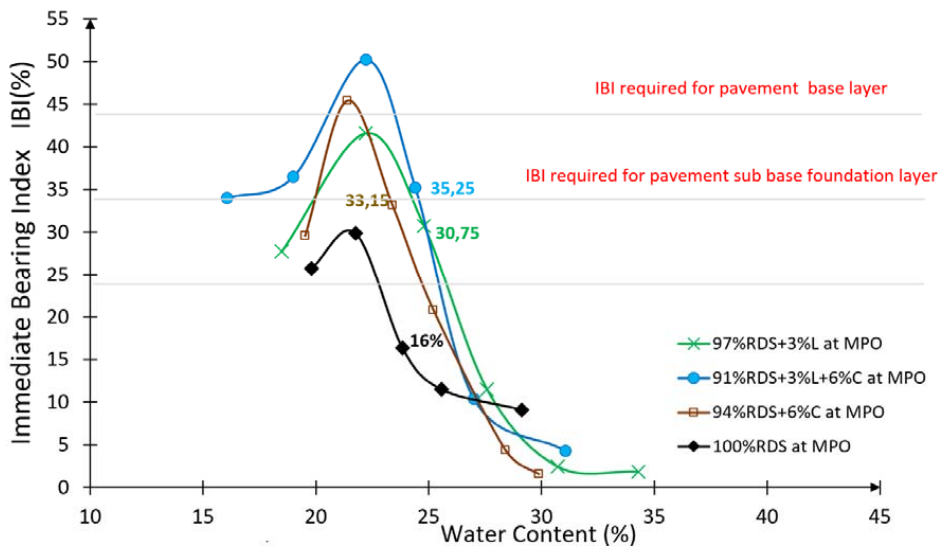and RDS + 3%L + 6%C at MPO



Fig. 10. Compaction-bearing curves (IBI) of the material after treatment with binder

Table 4. **Compaction parameters of the RDS and RDS treated with binders**

| Type | Compaction parameters | | IBI$_{MPO}$ | Correlation of Fleureau et al. (2002) | |
|---|---|---|---|---|---|
| Natural sediments (RDS) with LL = 55% | $\gamma_{dmax}$ (kN/m³) | W$_{MPO}$ (%) | (%) | $\gamma_{dmax}$ (kN/m³) | W$_{MPO}$ (%) |
| RDS at MPO | 16.33 | 23.5 | 16 | 16.95 | 18.20 |
| 97%RDS + 3%L at MPO | 15.74 | 24.79 | 30.74 | 16.8 | 18.91 |
| 94%RDS + 6%C at MPO | 15.95 | 23.38 | 33.15 | 16.56 | 18.51 |
| 91%RDS + 6%C + 3%L at MPO | 16.2 | 24.4 | 35.25 | 16.90 | 18.40 |
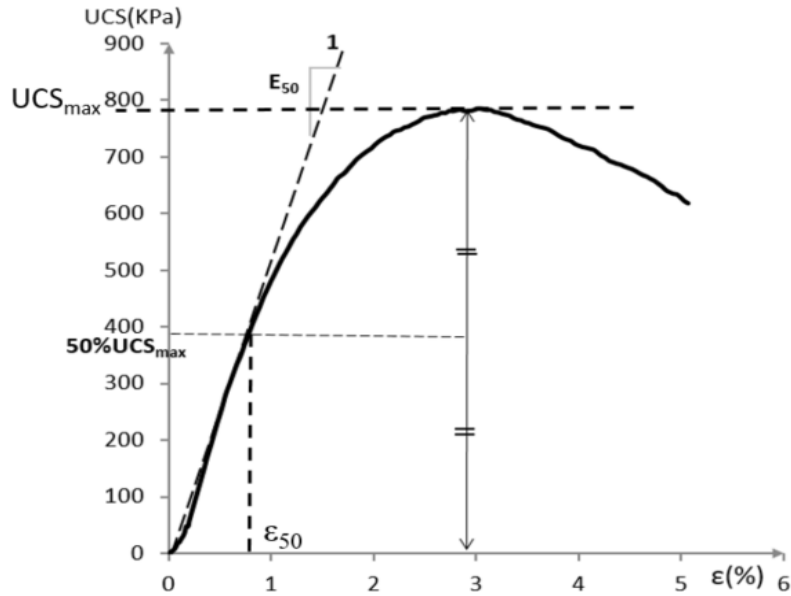


Fig. 11. Secant modulus E$_{50}$ versus strain ($\varepsilon$)

Table 5. **Results of the UCS and E$_{50}$ on the dredged sediments and sediments treated with binders**

| Mechanical parameters | RDS | Curing (days) | 97%RDS + 3%L | 94%RDS + 6%C | 91%RDS + 6%C + 3%L |
|---|---|---|---|---|---|
| UCS (MPa) | 0.688 | 7 | 1.687 | 1.565 | 1.841 |
| | | 14 | 2.516 | 3.279 | 2.838 |
| | | 28 | 2.644 | 3.724 | 3.84 |
| | | 90 | 3.19 | 4.128 | 4.057 |
| E$_{50}$ (MPa) | 0.10 | 7 | 0.30 | 0.26 | 0.21 |
| | | 14 | 0.37 | 0.44 | 0.39 |
| | | 28 | 0.39 | 0.49 | 0.54 |
| | | 90 | 0.60 | 0.54 | 0.63 |

*Tensile strength σ$_t$ and small strain modulus* E$_{SS}$

The tensile strength σ$_t$ was derived from the Brazilian splitting test (BST). The BST was carried out on cylindrical specimens, with diameter $\phi$ = 50 mm and a height h = 50 mm, according to NF EN 13286-42 (Association Francaise de Normalisation, 2003b). The tensile strength and modulus of elasticity at 360 days of curing (σ$_{t360}$ and E$_{SS360}$) were estimated according to NF EN 14227-1 (Association Française de Normalisation, 2013) and NF EN 13286-42 (Association Francaise de Normalisation, 2003b), using Eqs. 5, 6:

$$\sigma_{t360} = \sigma_{t28} / 0.60 \qquad (5)$$

$$E_{360} = E_{28} / 0.65 \qquad (6)$$

where σ$_{t28}$ and E$_{28}$ are the tensile strength and modulus of elasticity at 28 days of curing, respectively.

Furthermore, the modulus of elasticity at very small strains of the samples was measured using the ultrasonic wave propagation method. The velocity of sound wave propagation was used to estimate Young's modulus and Poisson's ratio of the material, according to the following Eq. 7:

$$E_{SS} = \frac{V^2 \times \rho \times (1+v) \times (1-2v)}{g(1-v) \times 10^6}, \qquad (7)$$

where V is the velocity [m/s], $\rho$ is the density [kN/m$^3$], g is the gravity [m/s$^2$], and v is Poisson's ratio.

The relationships ($\sigma_t$, $E_{SS}$) were plotted according to standards GTR 92 (LCPC, SETRA, 1992) and GTS 2000 (LCPC, SETRA, 2000), which exhibit five mechanical performance classes ranging from S1 to S5. The objective of the treatment was to achieve the highest possible mechanical class, i.e., the one closest to zone 3 (Fig. 13). The results show that the RDS samples belong to class S0, while the samples treated with 3%L and 6%C at 90d, 360d belong to class S2 and are suitable for use as a sub-base material for roads (Fig. 13). The samples at 28d belong to class S1 and can be used as road bed filling materials or subgrade layers for roads. The maximum mechanical performance was reached quickly between 28 and 90 days.

### Discussion
### Effect of curing time

Fig. 14 presents the ratio of tensile ($\sigma_t$) to compressive (UCS) strength as a function of curing time for the treated sediments, which ranges from 10–15% for all treated sediments. The objective of this report is to evaluate the effectiveness of lime and cement in soil stabilization by examining the mechanical properties of the treated sediments.

Specifically, the report presents the relationship between tensile and compressive strength as a function of curing time for the treated sediments and compares them with expected values for similar materials (Baldovino et al., 2018; Gajewska et al, 2017; Zentar et al., 2021). The findings indicate that the use of lime and cement significantly improved the mechanical properties of the treated sediments. However, it is worth noting that the specific values of $\sigma_t$/UCS may vary depending on such factors as the type of sediment, treatment method, and curing conditions. In addition, the report provides a linear equation that relates the two parameters, enabling the determination of one in terms of the other. The bar graphs in Fig. 15 show the relationship between curing time and the compressive strength UCS, mean modulus $E_{50}$, and small strain modulus $E_{SS}$, which increased with increasing curing time, indicating improved durability of the treated materials.

#### 1.1.1. Relationship between the UCS and modulus $E_{SS}$, $E_{50}$

Fig. 16 shows that there are linear and proportional relationships between the compressive strength (UCS) and the small and large strain moduli ($E_{SS}$, $E_{50}$) for all treated materials. It can be seen that there is a relatively good linear relationship between the UCS and $E_{SS}$, $E_{50}$ for all treated dredged sediment samples. The correlations between the small strain and large strain moduli and the compressive strength (UCS) are proposed in Table 6 as a way to reduce the time and cost of advanced laboratory experiments used to determine the modulus. It was observed that the moduli increased with the UCS.

Additionally, the use of binders (3%L and 6%C) had a positive effect on the UCS, IBI, $\sigma_t$, $E_{50}$, and $E_{SS}$ at all times.
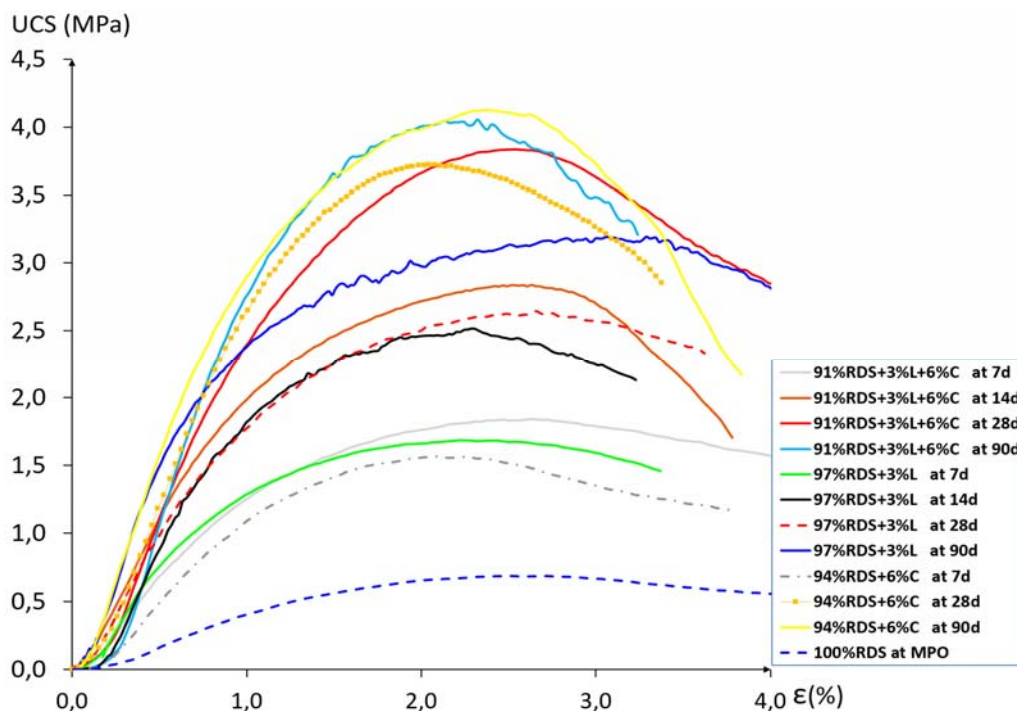


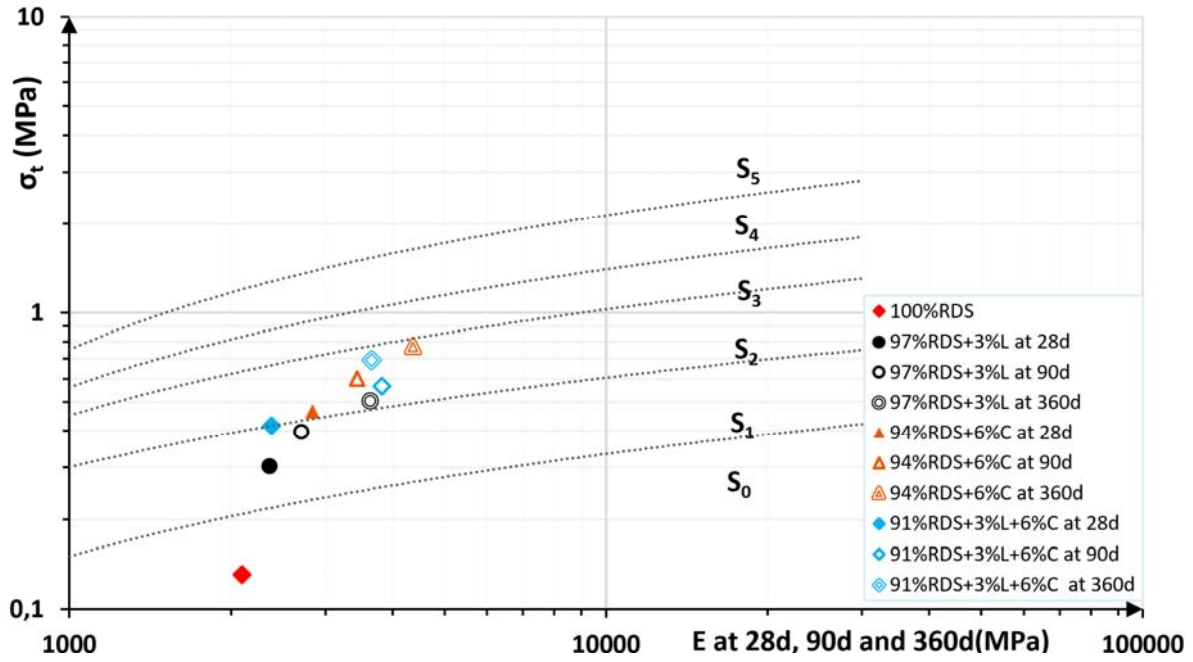Fig. 12. Evolution of the maximum UCS as a function of curing time for each mixture

Fig. 13. Positioning of the raw sediments and three formulations studied at 28, 90 and 360 days in the GTS classification chart
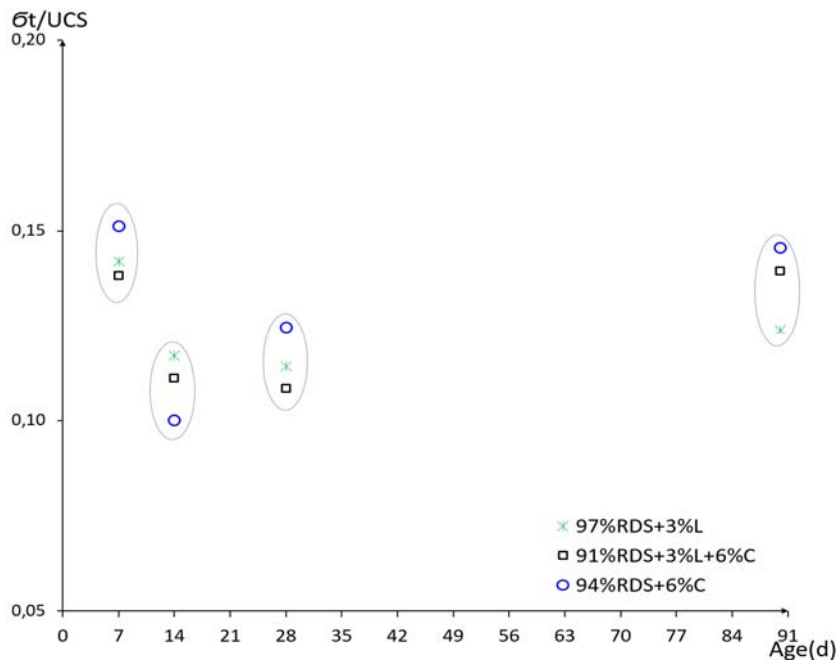


Fig. 14. Ratio of tensile ($\sigma_t$) to compressive (UCS) strength versus curing time
for the sediments treated with binders

## Conclusion

The valorization of the dam dredged sediments showed promising results for their use in road engineering. The addition of binders, specifically 3%L and 6%C, improves significantly the mechanical properties of the sediments, resulting in increased values of the UCS, IBI, $\sigma_t$, $E_{50}$, and $E_{ss}$. The use of treated sediments as a pavement layer is now feasible, with better durability and non-swelling properties. The addition of 3%L to 97%RDS led to the highest mechanical performance, with significant reduction in the plasticity index and swelling shrinkage. The formulations of 97%RDS + 3%L and 91%RDS + 3%L + 6%C were found to be suitable for use as a, subgrade layer, with maximum mechanical performance achieved between 28 and 90 days of curing. At 90 days, it was located in class S2, with high values of the IBI and $\sigma_t$. The addition of 6% cement to this formulation further improved its compressive strength, porosity,
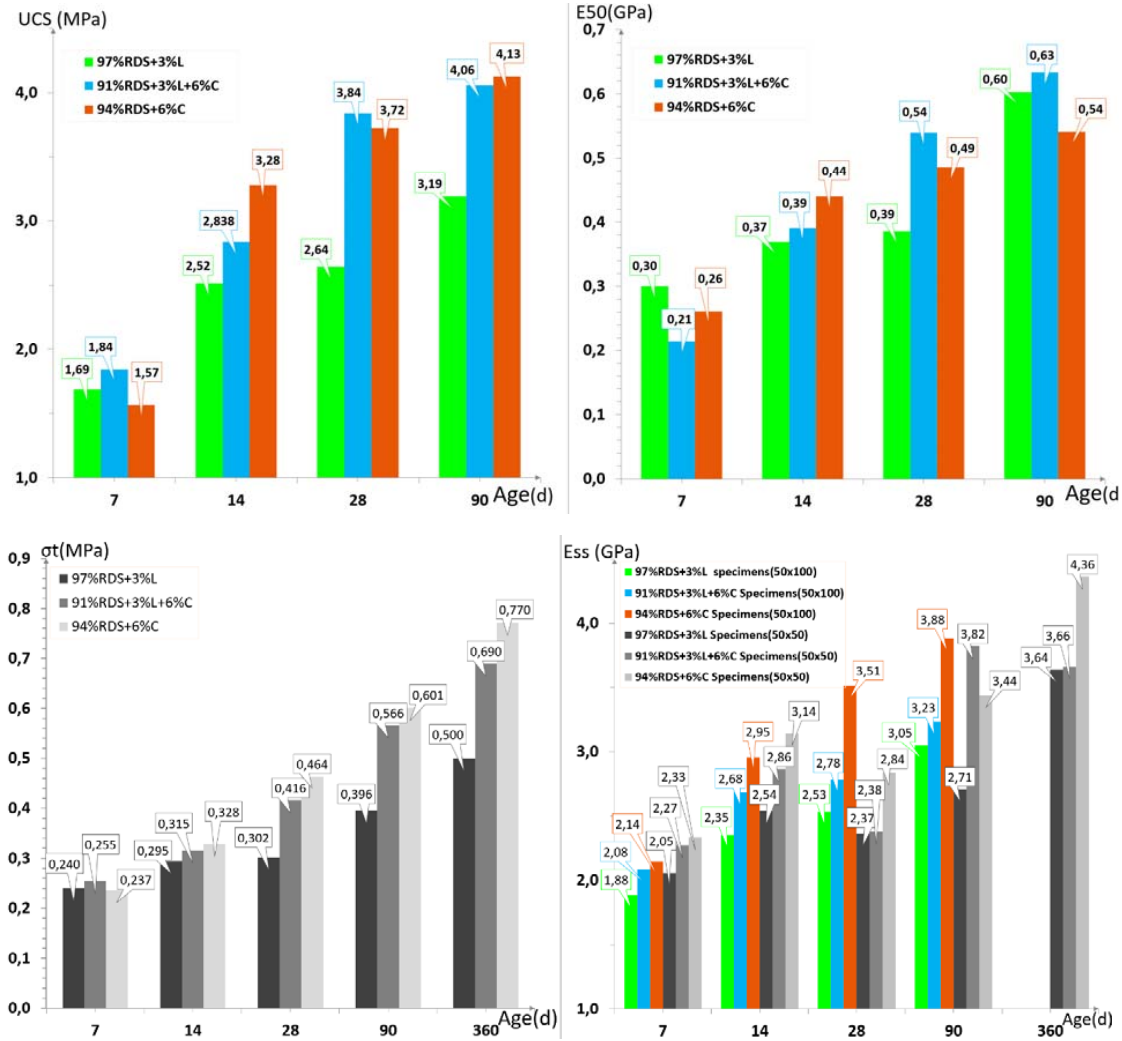
111

Fig. 15. Bar graphs of the relationship between curing time and the compressive strength UCS, modulus $E_{50}$, $E_{SS}$
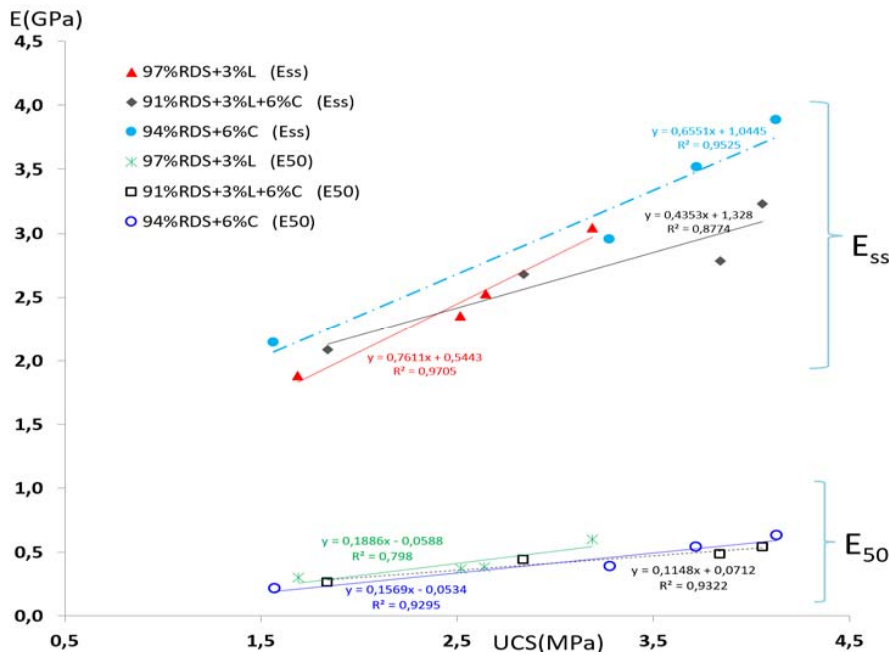


Fig. 16. Variation of the small strain modulus function of the UCS of the sediments
treated with binders

and tensile strength. Although the 94%RDS + 6%C formulation had good mechanical properties, it was located close to class S3 at 360 days. It is recommended to avoid using cement alone for the improvement of fine soils, according to the GTS 2000 standard. The study shows that adding lime to dredged sediments improves its compressive strength over time in samples containing 3%L. It can also help reduce the water content in dredged sediments by promoting the processes of hydration and contribution of dry matter, which can lead to increased strength and durability. Overall, the RDS treatment with binders is an effective method for improving mechanical properties and suitability for use as a pavement layer.

Table 6. **Correlations between the small strain and large strain moduli and the compressive strength (UCS) for the treated sediments**

| Formulations | Relationship between E and UCS | Coefficient of determination |
|---|---|---|
| 97%RDS + 3%L | $E_{SS} = 0.761\ UCS + 0.544$ | $R^2 = 0.97$ |
| | $E_{50} = 0.189\ UCS - 0.059$ | $R^2 = 0.80$ |
| 91%RDS + 3%L + 6%C | $E_{SS} = 0.435\ UCS + 1.328$ | $R^2 = 0.88$ |
| | $E_{50} = 0.115\ UCS + 0.071$ | $R^2 = 0.93$ |
| 94%RDS + 6%C | $E_{SS} = 0.655\ UCS + 1.045$ | $R^2 = 0.95$ |
| | $E_{50} = 0.157\ UCS - 0.053$ | $R^2 = 0.93$ |

**References**

Akula, P., Naik, S. R., and Little, D. N. (2021). Evaluating the durability of lime-stabilized soil mixtures using soil mineralogy and computational geochemistry. *Transportation Research Record: Journal of the Transportation Research Board*, Vol. 2675, Issue 9, pp. 1469–1481. DOI: 10.1177/03611981211007848.

NF EN ISO 10390:2022 French & European Standard, Soil, treated biowaste and sludge – Determination of pH, March 2022

Association Française de Normalisation (1991). *NF P94-054. Sols : reconnaissance et essais - Détermination de la masse volumique des particules solides des sols - Méthode du pycnomètre à eau*. Paris: Association Française de Normalisation, 6 p.

Association Française de Normalisation (1992a). *NF P11-300. Exécution des terrassements -Classification des matériaux utilisables dans la construction des remblais et des couches de forme d'infrastructures routières*. Paris: Association Française de Normalisation, 21 p.

Association Française de Normalisation (1992b). *NF P94-057. Sols : reconnaissance et essais - Analyse granulométrique des sols Méthode par sédimentation*. Paris: Association Française de Normalisation, 17 p.

Association Française de Normalisation (1993a). *NF P94-051. Sols : reconnaissance et essais - Détermination des limites d'Atterberg - Limite de liquidité à la coupelle - Limite de plasticité au rouleau*. Paris: Association Française de Normalisation, 15 p.

Association Française de Normalisation (1993b). *NF P94-055. Sols : reconnaissance et essais - Détermination de la teneur pondérale en matières organiques d'un sol - Méthode chimique*. Paris: Association Française de Normalisation, 7 p.

Association Française de Normalisation (1993c). *NF P94-068. Sols : Reconnaissance et essais - Mesure de la capacité d'adsorption de bleu de méthylène d'un sol ou d'un matériau rocheux - Détermination de la valeur de bleu de méthylène d'un sol ou d'un matériau rocheux par l'essai à la tache*. Paris: Association Française de Normalisation, 8 p.

Association Française de Normalisation (1993d). *NF P94-093. Sols : Reconnaissance et essais - Détermination des références de compactage d'un matériau - Essai Proctor Normal - Essai Proctor modifié*. Paris: Association Française de Normalisation, 28 p.

Association Française de Normalisation (1993e). *NF P98-230-2. Essais relatifs aux chaussées - Préparation des matériaux traités aux liants hydrauliques ou non traités - Partie 2 : fabrication des éprouvettes de sables ou de sols fins par compression statique*. Paris: Association Française de Normalisation, 10 p.

Association Française de Normalisation (1995). *XP-P94-041. Sols : reconnaissance et essais - Identification granulométrique. Méthode de tamisage par voie humide*. Paris: Association Française de Normalisation, 11 p.

Association Française de Normalisation (1996). *NF P94-048. Soil: investigation and testing - Determination of the carbonate content - Calcimeter method*. Paris: Association Française de Normalisation, 11 p.

Association Française de Normalisation (1997). *NF P94-078. Sols : Reconnaissance et essais. Indice CBR après immersion. Indice CBR immédiat. Indice Portant Immédiat - Mesure sur échantillon compacté dans le moule CBR*. Paris: Association Française de Normalisation, 12 p.

Association Française de Normalisation (1998). *XP-P94-047. Sols : reconnaissance et essais - Détermination de la teneur pondérale en matières organiques d'un matériau. Méthode par calcination*. Paris: Association Française de Normalisation, 6 p.

Association Française de Normalisation (2000). *NF EN-12879. Caractérisation des boues - Détermination de la perte au feu de la matière sèche*. Paris: Association Française de Normalisation, 11 p.

Association Française de Normalisation (2003a). *NF EN 13286-41. Unbound and hydraulically bound mixtures. Part 41: Test method for the determination of the compressive strength of hydraulically bound mixtures*. Paris: Association Française de Normalisation, 12 p.

Association Francaise de Normalisation (2003b). *NF EN 13286-42, Unbound and hydraulically bound mixtures. Part 42: Test method for the determination of the indirect tensile strength of hydraulically bound mixtures*. Paris: Association Francaise de Normalisation, 10 p.

Association Française de Normalisation (2012). *NF EN-13286-47. Mélanges traités et mélanges non traités aux liants hydrauliques - Partie 47 : Méthode d'essai pour la détermination de l'indice portant Californien (CBR), de l'indice de portance immédiate (IPI) et du gonflement linéaire*. Paris: Association Française de Normalisation, 13 p.

Association Française de Normalisation (2013). *NF EN-14227-1. Mélanges traités aux liants hydrauliques - Spécifications - Partie 1 : Mélanges granulaires traités au ciment*. Paris: Association Française de Normalisation, 32 p.

Association Française de Normalisation (2015). *NF P94-100. Sols : reconnaissance et essais - Matériaux traités à la chaux et/ou aux liants hydrauliques - Essais d'évaluation de l'aptitude d'un sol au traitement*. Paris: Association Française de Normalisation, 16 p.

ASTM (2006). *ASTM Standard D6276-99a. Standard test method for using pH to estimate the soil-lime proportion requirement for soil stabilization*. West Conshohocken: American Society for Testing and Materials, 4 p.

Baldovino, J. A., Moreira, E. B., Teixeira, W., Izzo, R. L. S., and Rose, J. L. (2018). Effects of lime addition on geotechnical properties of sedimentary soil in Curitiba, Brazil. *Journal of Rock Mechanics and Geotechnical Engineering*, Vol. 10, Issue 1, pp. 188–194. DOI: 10.1016/j.jrmge.2017.10.001.

Banoune, B., Melbouci, B., Rosquoët, F., and Langlet, T. (2016). Treatment of river sediments by hydraulic binders for valorization in road construction. *Bulletin of Engineering Geology and the Environment*, Vol. 75, Issue 4, pp. 1505–1517. DOI: 10.1007/s10064-015-0844-4.

Baston, G. M. N., Clacher, A. P., Heath, T. G., Hunter, F. M. I., Smith, V., and Swanton, S. W. (2012). Calcium silicate hydrate (C-S-H) gel dissolution and pH buffering in a cementitious near field. *Mineralogical Magazine*, Vol. 76, Issue 8, pp. 3045–3053. DOI: 10.1180/minmag.2012.076.8.20.

Bourabah, M. A., Serbah, B., Abou-Bekr, N., and Taibi, S. (2013). Geotechnical characterization of waste dredged sediments for Algerian dams. In: Manassero, M., Dominijanni, A., Foti, S., and Mussp, G. (eds.). *Coupled Phenomena in Environmental Geotechnics: From Theoretican and Experimental Research to Practical Applications*. London: CRC Press, pp. 299–305. DOI: 10.1201/b15004-34.

Cabalar, A. F., Karabash, Z., and Mustafa, W. S. (2014). Stabilising a clay using tyre buffings and lime. *Road Materials and Pavement Design*, Vol. 15, Issue 4, pp. 872–891. DOI: 10.1080/14680629.2014.939697.

Çokça, E. (1993). Prediction of swelling potential of Ankara soils by methylene blue test. *Doğa, Turkish Journal of Engineering & Environmental Sciences*, Vol. 17, No. 1, pp. 57–63.

Daheur, E. G., Li, Z.-S., Demdoum, A., Taibi, S., Goual, I. (2023). Valorisation of dune sand-tuff for Saharan pavement design. *Construction and Building Materials*, Vol. 366, 130239. DOI: 10.1016/j.conbuildmat.2022.130239.

Djelloul, R., Mrabent, S. A. B., Hachichi, A., and Fleureau, J.-M. (2017). Effect of cement on the drying–wetting paths and on some engineering properties of a compacted natural clay from Oran, Algeria. *Geotechnical and Geological Engineering*, Vol. 36, Issue 2, pp. 995–1010. DOI: 10.1007/s10706-017-0370-1.

Eades, J. L. and Grim, R. E. (1966). A quick test to determine lime requirements for lime stabilization. *Highway Research Record*, Issue 139, pp. 61–72.

Eid, J. (2017). New construction material based on raw earth: cracking mechanisms, corrosion phenomena and physico-chemical interactions. *European Journal of Environmental and Civil Engineering*, Vol. 22, Issue 12, pp. 1522–1537. DOI: 10.1080/19648189.2017.1373707.

Fleureau, J.-M., Verbrugge, J.-C., Huergo, P. J., Correia, A. G., and Kheirbek-Saoud, S. (2002). Aspects of the behaviour of compacted clayey soils on drying and wetting paths. *Canadian Geotechnical Journal*, Vol. 39, No. 6, pp. 1341–1357. DOI: 10.1139/t02-100.

Gajewska, B., Kraszewski, C., and Rafalski, L. (2017). Significance of cement-stabilised soil grain size distribution in determining the relationship between strength and resilient modulus. *Road Materials and Pavement Design*, Vol. 19, Issue 7, pp. 1692–1701. DOI: 10.1080/14680629.2017.1324808.

Hallouz, F., Meddi, M., Mahé, G., Toumi, S., and Rahmani, S. E. A. (2018). Erosion, suspended sediment transport and sedimentation on the Wadi Mina at the Sidi M'Hamed Ben Aouda Dam, Algeria. *Water*, Vol. 10, Issue 7, 85. DOI: 10.3390/w10070895.

Hamouche, F. and Zentar, R. (2018). Effects of organic matter on mechanical properties of dredged sediments for beneficial use in road construction. *Environmental Technology*, Vol. 41, Issue 3, pp. 296–308. DOI: 10.1080/09593330.2018.1497711.

Hilt, G. H. and Davidson, D. T. (1960). Lime fixation in clayey soils. *Highway Research Board Bulletin*, Issue 262, pp. 20–32.

Hussan, A., Levacher, D., Mezazigh, S., and Jardin, L. (2022). Valorization of a highly organic sediment: from conventional binders to a geopolymer approach. *Journal of Composites Science*, Vol. 6, Issue 5, 147. DOI: 10.3390/jcs6050147.

hydrodragage-c.t.systems (2005). *Rapport technique barrage BAKHADA Wilaya De Tiaret Levés Bathymétriques Des Barrages En Exploitation Lots II Et III  Echelon Cheliff Et Centre*.

Jamsawang, P., Charoensil, S., Namjan, T., Jongpradist, P., and Likitlersuang, S. (2021). Mechanical and microstructural properties of dredged sediments treated with cement and fly ash for use as road materials. *Road Materials and Pavement Design*, Vol. 22, Issue 11, pp. 2498–2522. DOI: 10.1080/14680629.2020.1772349.

Khattab, S. A., Al-Mukhtar, M., and Fleureau, J.-M. (2007). Long-term stability characteristics of a lime-treated plastic soil. *Journal of Materials in Civil Engineering*, Vol. 19, No. 4, pp. 358–366. DOI: 10.1061/(ASCE)0899-1561(2007)19:4(358).

Larouci, A., Senhadji, Y., Laoufi, L., and Benazzouk, A. (2021). Dredged dam raw sediments geotechnical characterization for beneficial use in road construction. *International Journal of Engineering Research in Africa*, Vol. 57, pp. 81–98. DOI: 10.4028/www.scientific.net/JERA.57.81.

LCPC, SETRA (1992). *Guide des Terrassements Routiers. Réalisation des remblais et des couches de forme*. Paris: LCPC, SETRA, 102 p.

LCPC, SETRA (2000). *Traitement des sols à la chaux et/ou aux liants hydrauliques. Application à la réalisation des remblais et des couches de forme. Guide technique*. Paris: LCPC, SETRA, 240 p.

Loudini, A., Ibnoussina, M., Witam, O., Limam, A., and Turchanina, O. (2020). Valorisation of dredged marine sediments for use as road material. *Case Studies in Construction Materials*, Vol. 13, e00455. DOI: 10.1016/j.cscm.2020.e00455.

Makki-Szymkiewicz, L., Hibouche, A., Taibi, S., Herrier, G., Lesueur, D., Fleureau, J.-M. (2015). Evolution of the properties of lime-treated silty soil in a small experimental embankment. *Engineering Geology*, Vol. 191, pp. 8–22. DOI: 10.1016/j.enggeo.2015.03.008.

Molnár, Z., Pekker, P., Dódony, I., and Pósfai, M. (2021). Clay minerals affect calcium (magnesium) carbonate precipitation and aging. Earth and Planetary Science Letters, Vol. 567, 116971. DOI: 10.1016/j.epsl.2021.116971.

Qureshi, M. U., Alsaidi, M., Aziz, M., Chang, I., Rasool, A. M., and Kazmi, Z. A. (2021). Use of reservoir sediments to improve engineering properties of dune sand in Oman. Applied Sciences, Vol. 11, Issue 4, 1620. DOI: 10.3390/app11041620.

Raouf Achour, Nor-Edine Abriak, Rachid Zentar, Patrice Rivard & Pascal Gregoire , Valorization of unauthorized sea disposal dredged sediments as a road foundation material, Environmental Technology Volume 35, 2014 - Issue 16, https://doi.org/10.1080/09593330. 2014.889758

Seed, H. B., Woodward, R. J., and Lundgren, R. (1962). Prediction of swelling potential for compacted clays. Journal of the Soil Mechanics and Foundations Division, Vol. 88, Issue 3, pp. 53–87. DOI: 10.1061/JSFEAQ.0000431.

Sivapullaiah, P. V., Sridharan, A., and Bhaskar Raju, K. V. (2000). Role of amount and type of clay in the lime stabilization of soils. *Ground Improvement*, Vol. 4, Issue 1, pp. 37–45. DOI: 10.1680/grim.2000.4.1.37.

Taibi, S., Duperret, A., and Fleureau, J.-M. (2009). The effect of suction on the hydro-mechanical behaviour of chalk rocks. *Engineering Geology*, Vol. 106, Issues 1–2, pp. 40–50. DOI: 10.1016/j.enggeo.2009.02.012.

Townsend, F. C. (1979). *Use of lime in levee restoration. Technical report GL-79-12*. Vicksburg: US Army Engineer Waterways Experiment Station, 110 p.

Tribout, C., Husson, B., and Nzihou, A. (2011). Use of treated dredged sediments as road base materials: environmental assessment. *Waste and Biomass Valorization*, Vol. 2, Issue 3, pp. 337–346. DOI: 10.1007/s12649-011-9068-4.

Venkatarama Reddy, B.V., & Gupta, A. Characteristics of soil-cement blocks using highly sandy soils. Mat. Struct. 38, 651–658 (2005). https://doi.org/10.1007/BF02481596

Wang, D., Abriak, N. E., Zentar, R., and Chen, W. (2013). Effect of lime treatment on geotechnical properties of Dunkirk sediments in France. *Road Materials and Pavement Design*, Vol. 14, Issue 3, pp. 485–503. DOI: 10.1080/14680629.2012.755935.

Wang, D., Zentar, R., Abriak, N. E., and Xu, W. (2012). Experimental investigation on consistency limits of cement and lime-stabilized marine sediments. *Environmental Technology*, Vol. 33, Issue 10, pp. 1197–1205. DOI: 10.1080/09593330.2011.633565.

Yukselen, Y. and Kaya, A. (2008). Suitability of the methylene blue test for surface area, cation exchange capacity and swell potential determination of clayey soils. *Engineering Geology*, Vol. 102, Issues 1–2, pp. 38–45. DOI: 10.1016/j.enggeo.2008.07.002.

Zentar, R., Wang, H., and Wang, D. (2021). Comparative study of stabilization/solidification of dredged sediments with ordinary Portland cement and calcium sulfo-aluminate cement in the framework of valorization in road construction material. *Construction and Building Materials*, Vol. 279, 122447. DOI: 10.1016/j.conbuildmat.2021.122447.

# ВАЛОРИЗАЦИЯ ИЗВЛЕЧЕННЫХ ОТЛОЖЕНИЙ ПЛОТИН ПРИ ПРОЕКТИРОВАНИИ ДОРОЖНОЙ ОДЕЖДЫ

Бумедьен Сербах[1,2]*, Магния Асмахане Бурабах[2], Джоанна Ид[3], Салима Бушмелла[4], Муссааб Хариче[5], Набиль Абу-Бекр[2], Саид Таиби[6]

[1]Университет Тиарета, Алжир
[2]Университет Тлемсена, Алжир
[3]Группа Ai Environnement FACÉA, Нуази-ле-Гран, Франция
[4]Университет Сук-Ахраса, Алжир
[5]Университет Джельфы, Алжир
[6]Университет Гавра, Франция

*E-mail: boumediene.serbah@univ-tiaret.dz

**Аннотация**
**Введение**: данная работа является частью исследования, направленного на валоризацию извлеченных отложений путем разработки составов для использования в дорожном строительстве. **Цель исследования** заключалась в том, чтобы определить, соответствуют ли материалы, отобранные для слоев дорожной одежды, стандартам проектирования, в частности, требованиям к плотности, гранулометрическому составу, пластичности, органическому веществу и механическим характеристикам. **Методы**: с тем чтобы определить физико-химические и механические характеристики извлеченных отложений, полученных из проб, отобранных на плотине Бахадда, расположенной в полузасушливом климате западного Алжира, отложения были обработаны вяжущими в небольших количествах (3% извести (L), 6% цемента (C)) для повторного использования в дорожном строительстве. В ходе исследования была изучена динамика физико-механических характеристик обработанных отложений, включая предел текучести (LL), показатель пластичности (PI), абсорбционную емкость по методу метиленового синего (VBS), индекс текущей нагрузки (IBI%), неограниченную прочность на сжатие (UCS), прочность на растяжение $σ_t$ и модуль упругости при малых деформациях $E_{ss}$ и больших деформациях $E_{50}$.
**Результаты** показали, что добавление извести и цемента в извлеченные отложения повышает их прочность, о чем свидетельствует увеличение прочности на сжатие (UCS) с течением времени для образцов, содержащих различные объемы вяжущего (3%L, 6%C и 3%L + 6%C). Кроме того, было продемонстрировано влияние содержания воды на механические свойства составов. Исследование показало, что прочность увеличивается при уменьшении содержания воды.

**Ключевые слова:** валоризация, извлеченные отложения, уплотнение, модуль упругости, неограниченная прочность на сжатие (UCS), прочность на растяжение, экогеоматериал, дорожное строительство.

# Guide for Authors
# for submitting a manuscript for publication in the «Architecture and Engineering»

The journal is an electronic media and accepts the manuscripts via the online submission. Please register on the website of the journal http://aej.spbgasu.ru/, log in and press "Submit article" button or send it via email aejeditorialoffice@gmail.com.

Please ensure that the submitted work has neither been previously published nor has been currently submitted for publication in another journal.

**Main topics of the journal:**

1. Architecture
2. Civil Engineering
3. Geotechnical Engineering and Engineering Geology
4. Urban Planning
5. Technique and Technology of Land Transport in Construction

**Title page**

The title page should include:

The title of the article in bold (max. 90 characters with spaces, only conventional abbreviations should be used); The name(s) of the author(s); Author's(s') affiliation(s); The name of the corresponding author.

**Abstract and keywords**

Please provide an abstract of 100 to 250 words. The abstract should not contain any undefined abbreviations or unspecified references. Use the IMRAD structure in the abstract (introduction, methods, results, discussion).

Please provide 4 to 6 keywords which can be used for indexing purposes. The keywords should be mentioned in order of relevance.

**Main text**

It should have the following structure:
1) Introduction,
2) Scope, Objectives and Methodology (with subparagraphs),
3) Results and Discussion (may also include subparagraphs, but should not repeat the previous section or numerical data already presented),
4) Conclusions,
5) Acknowledgements (the section is not obligatory, but should be included in case of participation of people, grants, funds, etc. in preparation of the article. The names of funding organizations should be written in full).

**General comments on formatting:**

- Subtitles should be printed in Bold,
- Use MathType for equations,
- Tables should be inserted in separate paragraphs. The consecutive number and title of the table should be placed before it in separate paragraphs. The references to the tables should be placed in parentheses (Table 1),
- Use "Top and Bottom" wrapping for figures. Figure captions should be placed in the main text after the image. Figures should be referred to as (Fig. 1) in the text.

**References**

The journal uses Harvard (author, date) style for references:
- The recent research (Kent and Park, 1990)...
- V. Zhukov (1999) stated that…

**Reference list**

The list of references should only include works that are cited in the text and that have been published or accepted for publication. Personal communications and unpublished works should only be mentioned in the text. Do not use footnotes or endnotes as a substitute for a proper reference list. All references must be listed in full at the end of the paper in alphabetical order, irrespective of where they are cited in the text. Reference made to sources published in languages other than English or Russian should contain English translation of the original title together with a note of the used language.

**Peer Review Process**

Articles submitted to the journal undergo a double blind peer-review procedure, which means that the reviewer is not informed about the identity of the author of the article, and the author is not given information about the reviewer.
On average, the review process takes from one to five months.